Behavior and Design of Cast-in-Place Anchors under Simulated Seismic Loading

Final Report (Volume III)

Headed Anchors in Plastic Hinge Zone of Reinforced Concrete Members

By

Zhibin Lin
Assistant Professor, North Dakota State University, Fargo, ND
(Formerly a Post-Doctoral Researcher at the University of Wisconsin, Milwaukee)

Luke Butler
Graduate Research Assistant, University of Cincinnati

Bahram Shahrooz
Professor and Co-Principle Investigator, University of Cincinnati

Jian Zhao
Associate Professor and Principle Investigator, University of Wisconsin, Milwaukee

Submitted to National Science Foundation for the NEESR Project Funded under Grant No. CMMI-990712342

Department of Civil Engineering and Mechanics
University of Wisconsin, Milwaukee, WI 53201

July 2013

Executive Summary

All experimental tests of the NEES-Anchor project were conducted in five phases. The volume of the project report focuses on the behavior of reinforced anchors in plastic hinge zones of reinforced concrete members. Note that the existing design specifications for headed anchors, such as those stipulated in ACI 318-11 and in CEB design guidelines, do not allow anchors in concrete that would be substantially damaged during an earthquake. All the test data can be found in NEES project warehouse at https://nees.org/warehouse/project/725.

The tests in Phase IV of the NEES-Anchor project was design to verify if the code-conforming anchor reinforcement is sufficient to support the anchor connections in plastic hinge zones of a reinforced concrete (RC) wall. Specifically, two 4-stud connections were installed in the boundary elements of a 1/2-scale concrete wall, likely to be used in 20-story buildings with RC core walls and steel frames. The concrete wall specimen was 10 ft tall and the cross section was 10 x 60 in. The anchor connections were within the plastic hinge zone of the concrete wall, which was expected to develop significant damage during the simulated seismic loading. The existing design code recommends U-shaped hairpins, therefore, closed ties and additional J-hooks were used as anchor reinforcement in the test. The wall was subjected to a axial compression, equivalent to 10 percent of its axial load capacity before being subjected to cyclic loading in displacement control on its top. The generated shear force (story shear) was applied to the anchor connections through two hydraulic actuators.

The connections in Phase IV tests did not reach their expected capacity. The two top anchors fractured in tension at early stage of loading. When the anchors fractured, the wall had not been able to experience the level of damage around the connections that would accurately mimic a severe earthquake event. Observation made during the test indicated that the thickness of the embedded plate (0.5 in.) was small such that the plate bent when the shear tab, located at the middle of the embedded plate, attempted to transfer the tensile force to the two bolts 2 in. away from the shear tab; The bent plate might have caused prying action, which increased the tensile loads on the anchors. More importantly, the connectors between the hydraulic actuators and the shear tabs were not properly fabricated such that the eccentricity of the vertical component of the applied load (shear) on the connection was significantly increased (from 2.5 in. (the design

eccentricity) to 13 in. (the actual eccentricity)). The increased eccentricity significantly increased the resulting moment, which in turn increased the tensile loads on the two top studs.

While the Phase IV test was not able to provide information on the seismic behavior of anchor connections in seismically damaged concrete, Phase V tests have shown that well-confined core concrete, even in plastic hinge zones, can support anchors in plastic hinge zones. The tests in Phases II and III of the NEES-Anchor project indicated that the key role of anchor reinforcement, in addition to carrying the forces from the anchors, is to protect concrete around the anchors from splitting, breaking out, and crushing. This better understanding of the behavior has led to alternative designs and detailing for anchor reinforcement. Therefore the Phase V tests were conducted to verify the implemented anchor reinforcement.

Phase V tests had six specimens: three for single anchors in tension and another three for single anchors in shear. The column specimen had a cross section of 12 x 12 in. and a height of 61 in. Nine No. 5 Grade 60 bars were provided as the longitudinal reinforcement. The test anchors, installed 8 in. from the base of the columns, were made from a 3/4 in. diameter ASTM A193 Grade B7 threaded rod, a plate washer (1.5x1.5 in.) and a hex nut welded to the end. The test anchor, if fully developed, will take an ultimate tension load of 43 kips. Two anchors are loaded in shear specimens, resulting in a similar ultimate load, which was designed within the loading capacity of the hydraulic actuator. The required anchor reinforcement for the 3/4-in. anchors was provided using four No. 4 bars, and implemented using two No. 4 closed stirrups in the column located 2-in. from the test anchor. In addition to the longitudinal bars in the column, three No. 4 U-shaped hairpins were placed near the anchor in the vertical plane. These hairpins were expected to prevent the concrete near the anchors from flexural cracking.

Despite large cracks and concrete spalling occurred to the concrete within the plastic hinge zones, ductile steel fracture was achieved in all six tests, in which the RC columns were subjected to cyclic lateral displacement up to eight times their yield displacement. The successful tests indicated that well confined core concrete, even within plastic hinge zones, can support anchors. The test also confirmed that the anchor reinforcement should confine concrete, restrain concrete from splitting and blowout, and distribute loads from anchor heads to the rest of the structure/structural element. Further studies are needed to quantify the confinement requirements.

Acknowledgements

The project was supported by the National Science Foundation (NSF) under Grant No. 0724097. The authors gratefully acknowledge the support of Dr. Joy Pauschke, who served as the program director for this grant. The authors also thank the colleagues in ACI committee 355 for their valuable inputs. Any opinions, findings, and recommendations or conclusions expressed in this material are those of the authors and do not necessarily reflect the views of NSF.

The Phase IV test was conducted at the NEES MUST-SIM facility at the University of Illinois, Urbana-Champaign (UIUC), where Dr. Amr Elnashai and Dr. Billie Spencer serve as the directors. The authors are grateful for the support NEES MUST-SIM facility staff provided throughout the experimental program. Specifically, Dr. Daniel Kuchma provided invaluable suggestions on laboratory tests using the NEES MUST-SIM facility; Mr. Michael Johnson coordinated the entire experiment program from specimen shipment to specimen disposal; Dr. Chia-Ming Chang and Mr. Michael Bletzinger operated the testing equipment; Mr. Tim Prunkard provided laboratory support, including the fabrication of the adapters between the actuators and the embedded connections; and Mr. Weslee Walton organized a group of UIUC undergraduate students to record the test progress and observations, along with a UWM student.

The Phase V tests were conducted at the Structures Laboratory at the University of Wisconsin, Milwaukee (UWM), where Dr. Al Ghorbanpoor serves as the director. The authors are grateful for the support Dr. Ghorbanpoor provided throughout the experimental program. The authors would also like to thank Rahim Rashadi for his technical support on the hydraulic system.

Many UWM undergraduate students participated in the project. Specifically, Jushua Ollson, Kevin O'Connor, and Brian Petrin helped with the specimen preparation and test setup. Brian Petrin also drafted the specimen fabrication and created related drawings. John Cain attended the tests at the University of Illinois, Urbana-Champaign. Some of these undergraduate students were partially funded by Summer Undergraduate Research Fellowship (SURF) at UWM College of Engineering and Applied Science. The project would not be finished without these UWM undergraduate students.

Table of Contents

List of Figures

List of Tables

NOMENCLATURE

A	=	Empirical constant
b	=	Equivalent width of bridge deck
ΔE	=	Activation energy of the reaction process
I_o	=	Electric current (amperes) at initial stage
$I_{i*\Delta t}$	=	Electric current (amperes) at $i*\Delta t$ min
k_b	=	Boltzmann's constant
L	=	Span length of a bridge
n	=	No. of interval over 6-hour period (n=360/Δ t)
P	=	Applied one axle load
Q	=	Total charge passed, in coulombs
R	=	Resistivity of the sample
t	=	Thickness of deck slab
Δt	=	Interval (min) used to record current
S	=	Girder spacing length
S_1, S_2, S_3	=	First, second, and third principal stresses
T	=	Absolute temperature
$\sigma(T)$	=	Conductivity of the sample (1/R)
σ_x, σ_y, σ_z	=	Transversal stress, stress along vertical and longitudinal stresses
σ_{z0}	=	Initial longitudinal stress

CHAPTER 1 Introduction

1.1 Overview of NEES-Anchor Project

There are knowledge gaps in the seismic design of headed anchors, both within a single anchor and a group of anchors as a connection: 1) there are no behavioral data on anchors embedded in concrete with substantial damage; thus, an anchor design may have uncontrollable performance; 2) the desired ductile anchor failure may become brittle fracture of anchors under cyclic shear or combined cyclic tension-shear, leading to an unsafe design; and 3) the potential benefits of adding supplementary reinforcement around anchors is overlooked, which may turn a brittle concrete failure into a more ductile behavior. To rectify these gaps in the existing knowledge base, the NEES-Anchor project is to:

- Obtain detailed experimental data for cast-in-place anchors/studs under simulated seismic loadings with a focus on combined tension-shear loading;
- Evaluate the limitations of current seismic design provisions (e.g., Appendix D of ACI 318-05), and develop improved design methodologies and equations; and
- Evaluate proposed design methods and details by testing connections between steel girders and concrete walls.

The experimental tests were conducted in five phases. The experimental tests include

- 61 tests of unreinforced single anchors subjected to cyclic loading (Phase I);
- 20 tests of reinforced single anchors subjected to shear (Phase II);
- 28 tests of reinforced single anchors subjected to tension (Phase III);
- 2 tests of anchor groups in plastic hinge zones of a concrete wall (Phase IV); and
- 6 tests of reinforced single anchors in plastic hinge zones of columns (Phase V).

Additional tests were conducted for anchor rods in shear with various exposed lengths (Phase O). The tests in Phase II and Phase III of the NEES-Anchor project indicated that the key role of reinforcement, in addition to carrying the forces from the anchors, is to protect concrete around the anchors from splitting, breaking out, and crushing. This understanding has led to alternative designs and detailing for the anchor reinforcement. The volume of the project report focused on

Phases IV and V tests. The test in Phase IV was to evaluate the performance of anchors with code-specified anchor reinforcement. Phase V tests were designed to evaluate the proposed anchor reinforcement schemes.

1.2 Concrete Anchoring System

The behavior of cast-in anchors and headed studs subjected to static loading has been extensively studied (CEB 1997; Cannon 1995; Cook et al. 1989; Klingner et al. 1982; Eligehausen et al. 2006), and the results have been implemented in design codes (ACI 318 2011; *fib* 2012). The behavior of anchors established with these tests was based on the conditions in which the concrete is not cracked and anchor reinforcement is not provided around the anchors. Experimental data regarding cyclic behavior of anchors used in cracked concrete are also very limited. The level of cracking and damage in the concrete around the connections depends on the location within the building height. For example, the loading in a typical outrigger beam–wall connection is cyclic axial force due to the floor diaphragm. As mentioned in the literature [Shahrooz et al. 2004a and 2004b], the concrete wall in the upper floors has moderate levels of cracking when it was subjected to earthquake, but the wall in the lower floors will likely undergo extensive damage. As a result, the structural behavior of anchor in such location, such as bracing system connected to the concrete or outrigger beam–wall connection as shown in Figure 1.1, is crucial to provide guidance to the anchor seismic design.

Figure 1.1: Anchors installed in typical plastic hinge zones

1.3 Anchor Connections in Plastic Hinge Zones

Modern design of concrete structures allow the development of plastic hinges at the end(s) of beams ends and the base of columns at moderate or high seismic risk zones [Ibarra and Krawinkler, 2005]. This requires carefully detailing reinforcement in concrete elements in the plastic hinge zones. The plastic hinge zones (roughly defined in Figure 1.2 by Hoehler, (2006)) are expected to experience extensive inelastic deformation, including reinforcing bar yielding and concrete cracking (see Figure 1.3), while the rest regions are expected to remain elastic throughout during an earthquake event.

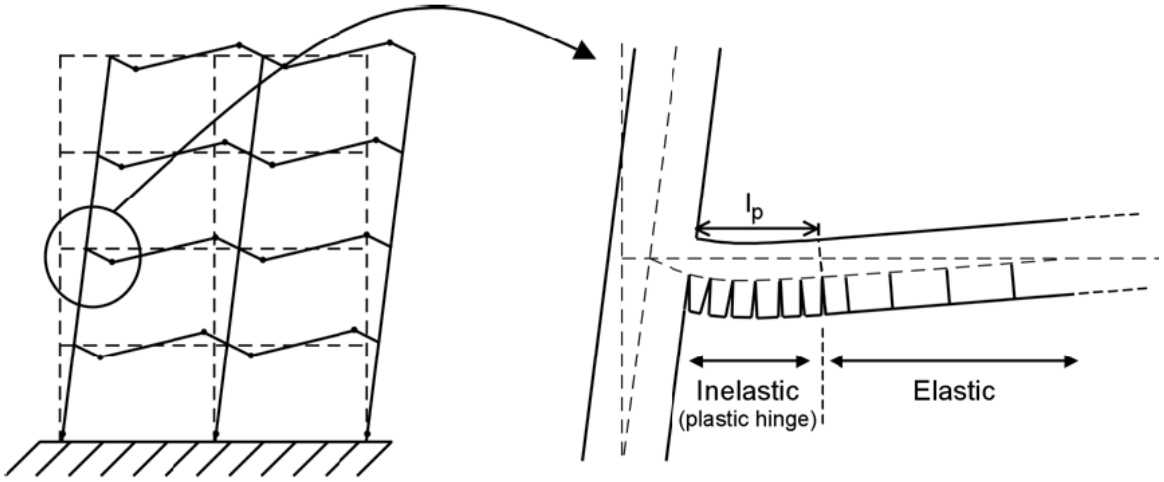

Figure 1.2: Plastic hinge zones (Hoehler, 2006)

Anchor connections are often time needed in the regions as shown in Figure 1.1, in which steel girders are connected to the concrete wall or braces are connected to beams and columns. On the other hand, the current building codes (e.g., Appendix D of ACI 318-11) and design guidelines [fib, 2008] are based on experimental tests of anchors cast/post-installed in concrete that experiences controlled minor damage (i.e., crack opening up to around 0.04 in.) [Eligehausen et al., 2006; Pallarés and Hajjar, 2009a, 2009b]. Therefore, engineers are left with no guidance when designing the embedded connections in concrete walls, where substantial concrete damage is expected, as the Appendix D of ACI 318-11 states, "The provisions of Appendix D do not apply to the design of anchors in plastic hinge zones of concrete structures under seismic loads."

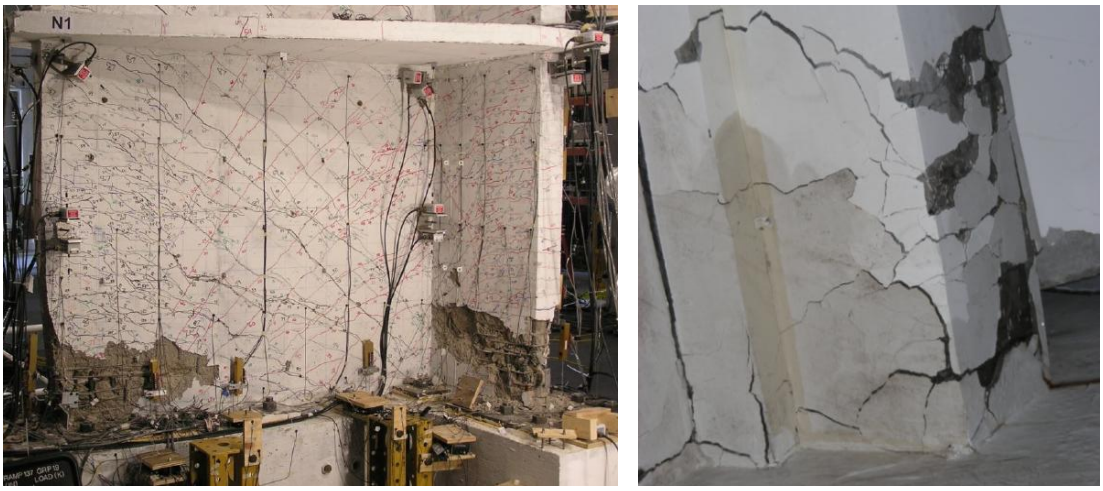

Figure 1.3: Expected damage in plastic hinge zones of reinforced concrete elements

The well-established design procedures for headed anchors, such as those stipulated in ACI 318-11 and in CEB design guidelines, do not apply to the anchors installed in concrete that likely be substantially damaged during an earthquake. It is recommended that the anchor reinforcement must be provided for the anchors installed in plastic hinge zones [ACI 318, 2008]. The tests in Phase II and Phase III of the NEES-Anchor project have provided some experimental information for solving the problem. The focus of the Phase V tests were to 1) identify the key parameters for the desired performance of anchors in plastic hinge zones; 2) observe the behavior of anchors in plastic hinge zones with local confinement; and 3) verify the implemented anchor reinforcement detailing.

1.4 Report Layout

The report is organized as follows: A literature review on the behavior of anchors in damaged concrete is provided in Chapter 2. Based on the research described in Volume II of the project report, a group of experimental tests were designed to evaluate the feasibility of installing headed anchors in damaged concrete. The experimental program is described in Chapter 3, and the test results are presented in Chapter 4. Chapter 5 described a large-scale test of anchor connections in a reinforced concrete wall was conducted at the NEES MUST-SIM facility at the University of Illinois at Urbana-Champaign. The research is summarized in Chapter 6 along with a list of subjects that should be investigated in the future.

CHAPTER 2 Literature Review

2.1 Introduction

The majority of anchor tests, including those conducted by manufactures, were conducted with unstressed and uncracked concrete [ACI 355, 1991; CEB, 1994]. Experimental tests of anchor used in damaged concrete in the literature are very limited. The existing studies, including those on post-installed anchors, are reviewed below. The seismic design guidelines for anchors in Appendix D of ACI 318-08 are only applicable to anchors located outside of plastic hinge zones (Section D.3.3.1). This is reasonable because spalling of the concrete cover and large crack widths inside of a plastic hinge will reduce the anchor capacity significantly and make anchoring impractical.

The behavior of anchor groups as a connection between steel members and concrete has been extensively studies as summarized in [Cook and Klingner, 1992; Lotze and Klingner, 1997; Grauvilardell et al., 2005]. Most studies have focused on the connections between steel columns and their concrete foundations as summarized by Grauvilardell et al. (2005). Foundation concrete itself is not usually supposed to develop damage in an earthquake; therefore the large amount of research is not reviewed here in this report. Very limited studies are available in the literature regarding the behavior of anchor connections in damaged concrete. These studies are summarized as follows.

2.2 Concrete Anchors in Damaged Concrete

Canon (1981)

Large safety factors were specified in seismic design regulations in 1980's [ACI 349, 1990]. Canon (1981) conducted 21 tension tests of expansion anchors in cracked concrete beams. The beams were 24-in. wide and 12-in. deep with spans ranging from 8 ft through 15 ft. The longitudinal reinforcement varied from three No.4 bars to three No. 8 bars to evaluate the impact of beam reinforcement (the transverse reinforcement was not reported). The applied loads varied in amplitudes and frequencies, and the peak loads were pretty close to the maximum allowable loads according to the aforementioned design guidelines. Compared with anchors installed in

uncracked concrete, the observed behavior of expansion anchors, represented by the number of load cycles, under which the anchor displaced significantly, and the maximum anchor displacements, was significantly affected by the flexural cracks in the beam intersecting the anchor. Although not reported, the different longitudinal reinforcement in the beams may have led to different crack sizes; however, the impact of longitudinal reinforcement seemed not significant.

Copley and Burdette (1985)

Copley and Burdette (1985) conducted 7 tests of anchor groups (each with 4 anchors) in high moment regions of reinforced concrete slabs. The test program included three tests of grouted A307 bolts, two tests of self-drilling anchors, and 2 tests of wedge anchors. The slabs with anchor groups installed at mid-span were simply supported and the loads were applied to the anchors also deformed and cracked the slabs. The support positions were designed to control the maximum moment (and therefore the maximum cracking) in the slabs at the designated loads. The applied loads represented those at serviceability limit states and ultimate limit states and an intermediate level. Other than one self-drilling anchor, all other tested anchors were able to resist the factored design loads. The anchor deformations were found directly related to the resulted moments (and thus the cracking) in the slab. The shear force was transferred from the concrete slab to the steel girder in a composite beam through headed studs. Duo to bending of the concrete slab in the perpendicular direction, longitudinal cracks may form and intersect with the shear studs.

Oehlers and Park (1992)

Cracks intersecting the shear studs may also form in concrete slabs from the wedging action of the studs in shear [Oehlers, 1989]. Oehlers and Park (1992) presented 25 push tests of shear studs in a series of studies of shear transfer in composite girders. At failure loads, concrete in front of the stud crushed, leading to combined bending and shear in the studs. Oehlers and Park concluded that the longitudinal cracks near the crush-prone region reduced the strength of concrete under tri-axial compression as illustrated in Figure 2.1, and the shear capacity is likely reduced by 10 percent. Transverse reinforcement near the shear studs were found beneficial to the strength of the shear studs because it confined the tri-axial compression zones. The benefit also came from the fact that the transverse reinforcement provided partial support to the shear stud; therefore the stiffness of the reinforcement, the distance of the reinforcement from the stud,

and the height affected the overall shear capacity of the studs (see Figure 2.1). Note that these observations are similar to those obtained in Phase II tests of the NEES-Anchor project.

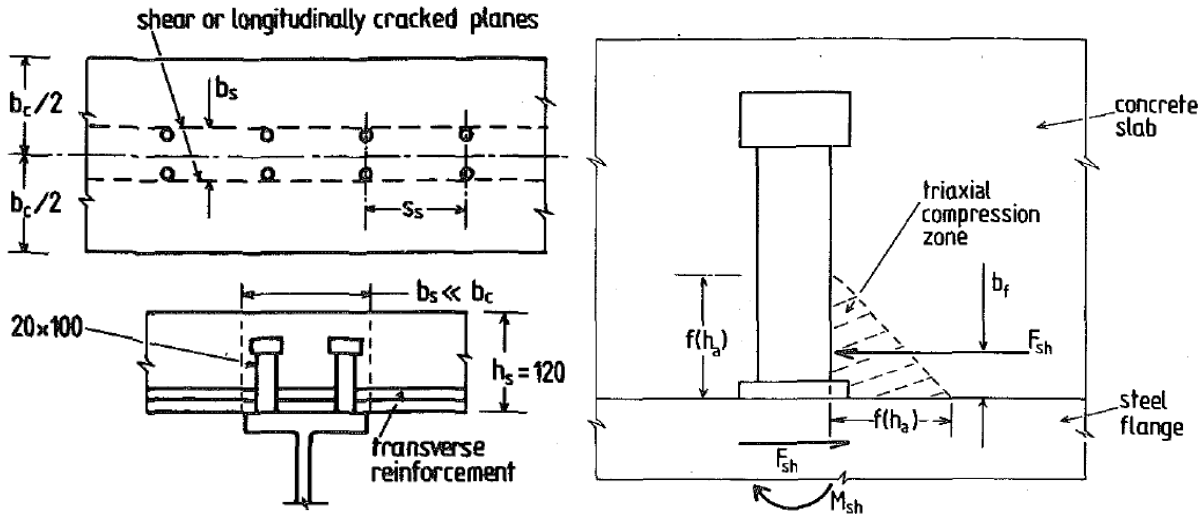

Figure 2.1: Failure mechanism of shear studs in concrete with longitudinal cracks (Oehlers and Park, 1992)

Eligehausen and Balogh (1995)

A series of tests were conducted for various types of anchors installed in cracked concrete in Europe, mostly led by Dr. Eligehausen at the University of Stuttgart, in 1980's. While the publications of the individual studies are in German and not easily accessible, their results have been summarized in Eligehausen and Balogh (1995). The results of headed studs and cast-in-place anchors are reviewed as follows. First of all, reinforced concrete memebers are assumed to develop cracks under service loading; thus Eligehausen (1984), Lotze (1987), and Eligehausen et al. (1986) investigated the probability of anchors being installed in to-be-cracked concrete. The studies found that it is very likely for anchors being installed in cracks because 1) cracks may form at many locations along a reinforced concrete member due to unpredictable loading conditions; 2) the force applied to the memeber therough the anchors may cause relatively large internal forces in the member, thus loeding to cracks (similar to that observed in Canon (1980)); and 3) the loaded anchors under shear or tension may create local splitting forces near the anchors (similar to that observed in Oehlers and Park (1992)). Therefore it is reasonable to assume that the structural concrete members are cracked, and the anchor capacities, largely established based on tests of anchors in uncracked and unstressed concrete, may need to be reduced.

Martin and Schwarzkopf (1984) conducted tension tests of headed studs in cracked concrete. Typical tension load vs. displacement curves for single studs in cracked and uncracked concrete are shown in Figure 2.2. In the presented tests, both studs had an embedment depth of 7.25 in., and the crack width through the depth of the concrete was held constant at 0.018 in. for the test in cracked concrete. Concrete breakout controlled the failure for both tests. The studs in cracked concrete had a smaller tension capacity – roughly 70% of the capacity of the stud in uncracked concrete. The stud in cracked concrete also showed a reduced stiffness and a larger displacement at breakout failure.

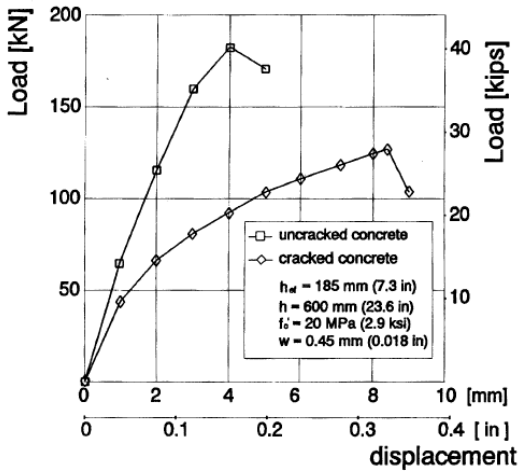

Figure 2.2: Typical load-displacement curves of headed studs in uncracked and cracked reinforced concrete (concrete cone failure)

A total of 43 tests of headed studs tested in cracked concrete were assembled and analyzed by Eligehausen and Balogh along with 362 undercut anchors. The results of 34 tests of headed studs were recovered and reproduced in Figure 2.3. Note that there are several ways to generate cracks in concrete through inducing bending moments or tension into the concrete. In most of the documented tests, cracks intersecting the studs were created (Eligehausen et al. 2004) and widened to the designated widths. The measured tension capacities were divided by the Code-predicted capacities for similar studs in uncracked concrete to obtain the capacity ratios shown in Figure 2.3 against the crack widths. The stud capacity reduces with an increase in the crack width. The capacity reduction is about 25 percent when the crack width is around 0.01 in., which was similar to the predicted reduction by Eligehausen and Ozbolt (1992) using finite element models. The finite element analyses indicated that the capacity reduction may be related the disturbed stress flows in cracked concrete when a headed anchor is subjected to tension. The

finite element analysis was not able to explain the further capacity reduction when the crack is wider as shown in Figure 2.3.

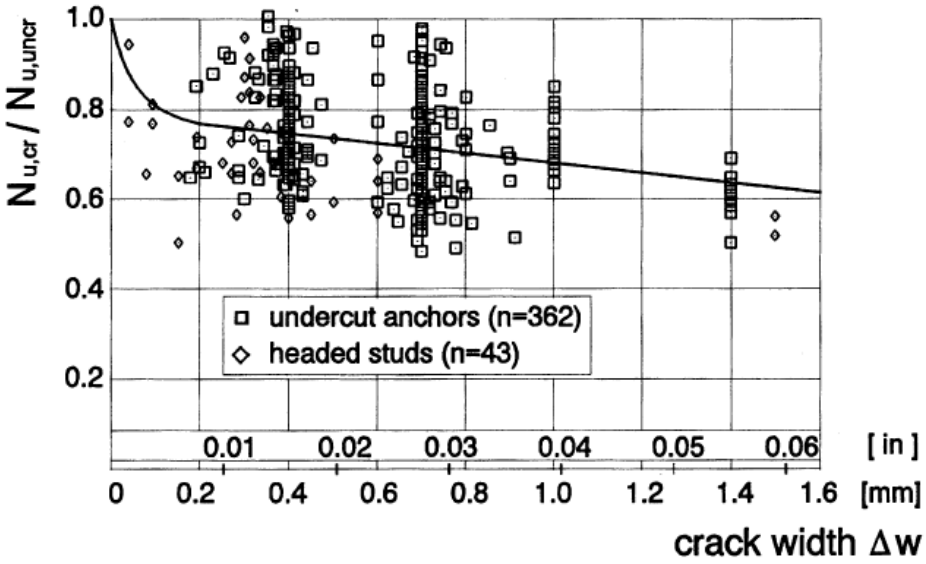

Figure 2.3: Typical load-displacement curves of headed studs in uncracked and cracked reinforced concrete (concrete cone failure)

Yoon, Kim, and Kim (2001)

Having recognized the above failure mechanisms for anchors in cracks, Yoon et al. (2001) conducted twelve tests of 7/8-in. headed studs in pre-cracked concrete and three tests with uncracked concrete. The concrete blocks were 28 x 28 x 8 in. with four types of cracks formed using wedge splitter before loading the studs in tension: two groups of three specimens with intersecting through depth cracks with 0.02-in. and 0.008-in. widths; one group of specimens with cracks through half depth of the concrete block; and the other group with through cracks 7 in. away from the stud. The stud embedment depth was 4 in. for all specimens. The results of these tests are shown in circles in Figure 2.4. Note that the capacity ratios were directly obtained by dividing the measured capacities because the Code-predicted capacities are 15% lower than the measured capacities for studs in uncracked concrete. On average, the studs in concrete with 0.008-in. cracks developed 7% more capacities compared with those with 0.02-in. cracks. The smaller crack width seemed to have similar impacts as shallower cracks as those studs developed roughly 7% more capacity. The off-center cracks (more than $1.5h_{ef}$ away from the stud) did cause a capacity reduction (14% on average). Overall, the measured stud capacities were 20 to 30

percent higher than the code predictions partially due to the conservative code equations for studs in uncracked concrete.

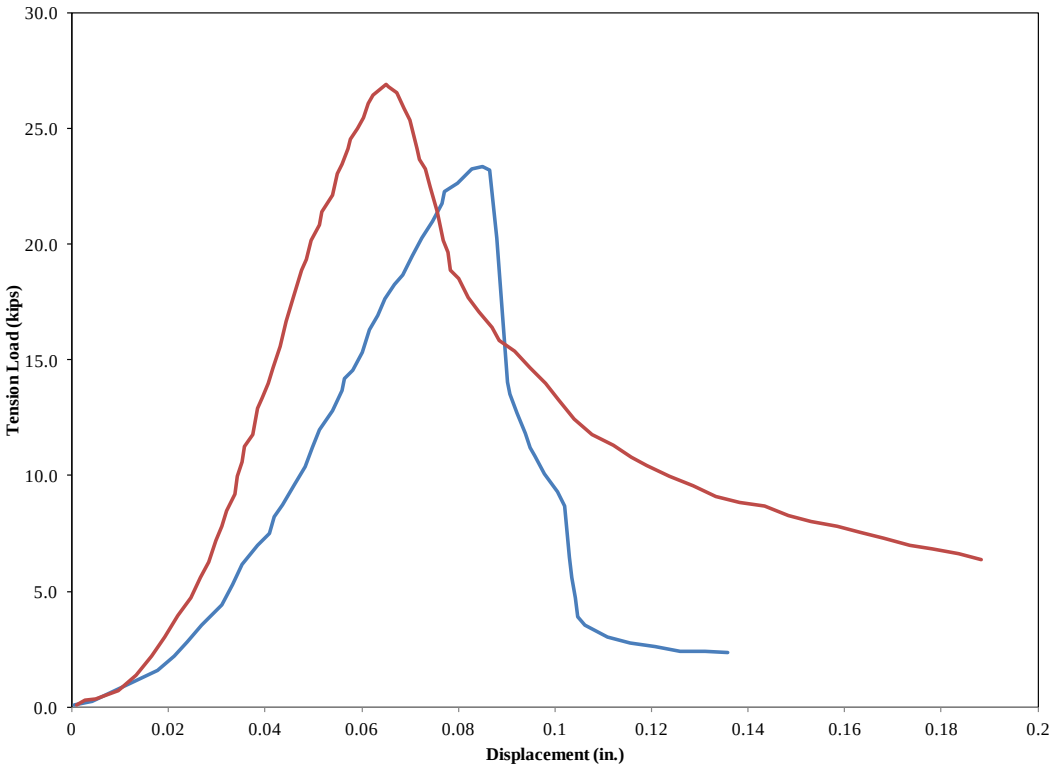

Figure 2.4: Typical load-displacement curves of headed anchors in uncracked and cracked concrete (concrete cone failure)

Jang and Suh (2006)

Further tests were conducted by Jang and Suh (2006) to provide further experimental data for the code specified capacity reduction factors for anchors in cracked concrete. Twenty groups of five tests were conducted for 1 in. diameter cast-in-place anchors in concrete with various types and extents of pre-formed cracks in the presented study. The main test variables were: 1) crack width (0.012, 0.031, and 0.059 in.); 2) crack depth (0.4, 2.0, and 4.0 in., which is the embedment depth of the test anchors); 3) crack position (intersecting the anchors and 3 in. from the anchors); and the number of cracks (one and two cracks). The cracks were created by inserting steel plates with designated crack widths before concrete was poured. The 1 in. diameter anchors had two threaded ends and a 3.875-in. squared plate at the embedded end. Because of the large head plate, the breakout cracks were initiated away from any intersecting cracks, and the measured breakout capacities were not affected by the intersecting cracks with various crack widths and depths. Specimens with cracks away from the test anchors showed 35% capacity reductions. This

reduction might have been due to unrealistic cracks used in the study: the cracked surfaces were smooth such that the shear transfer through aggregate interlock in actually cracks was eliminated. As a result, the amount of the concrete cracks needed to cause breakout failure was greatly reduced, and so did the breakout capacities.

Hoehler and Eligehausen (2008a)

Hoehler (2008a) conducted tests of post-installed anchors (expansion anchors and screw anchors) for use in cracked concrete to fasten nonstructural components and systems. During an earthquake these anchors may be subjected to repeated loads from component oscillation, and the seismic loads likely exceed the static loads. Therefore the anchors in their study were subjected to up to thirty cycles of tensile forces ranging from 50 and 100% of the measured average ultimate loads at a frequency between 0.1 to 2 Hz (ACI 355.2). Note that the measured ultimate loads are usually higher than the design capacities; therefore testing of anchors at this load levels may provide information on the reliability of these post-installed anchors for seismic applications. The anchors were installed in hairline cracks generated using a wedge splitter, and the cracks were widened to 0.03 in. (0.8 mm) [Eligehausen et al., 2004] before the anchor was loaded in tension. An analysis was performed [Hoehler, 2006] to verify that this crack width (0.03 in.) is likely the maximum crack width experienced by reinforced concrete members outside the plastic hinge zones. The test results indicated that the expansion anchors and the screw anchors behaved well under cyclic loading compared with those subjected to monotonic loading. Multiple failure modes were achieved including, concrete breakout, anchor pull through, and anchor fracture. The authors did not compare the measured anchor behavior with the code predicted capacities such that the impact of cracking on anchor behavior was not demonstrated.

Hoehler (2006)

As another part of the study by Hoehler (2006), tests were also conducted to investigate the impact of crack opening-closing as a result of seismic action on concrete members. Four types of anchors were used including headed studs, undercut anchors, expansion anchors, and screw anchors. The anchors were embedded in cracks preformed using a wedge splitter, and loaded to 40% of the average measured tensile capacity. This tensile load was maintained during the crack moving process to simulate the loads on the anchors caused by non-structural components. The increase in such loads on anchors due to earthquake induced vibration was ignored in this part of the tests. The pre-cracked concrete slab was then loaded in tension to open the cracks up to 0.03

in. (0.8 mm). Again this maximum crack width was obtained from the analyses of typical reinforced concrete members outside their plastic hinge zones. While the tensile load was maintained, the cracks were repeatedly opened (to 0.03 in.) and closed for 10 cycles. The number of crack cycles was obtained from seismic analyses of reinforced concrete structures and intended to represent the worst group of deformations due to an earthquake.

The repeated crack opening-closing (moving cracks) did not cause reduction in the tensile capacities of anchors failed by concrete breakout. The anchor displacement increased significantly compared with the anchors subjected to monotonic loading in cracked concrete. This might have been caused by crushing of concrete above the anchor head when the crack closed (The closing of the initial cracks caused large compression force around anchors). Meanwhile, the resulted decrease in the embedment depth of the anchor is insignificant; thus the ultimate tensile capacities were not affected by the moving cracks. On the other hand, moving cracks did cause much larger slip of expansion anchors and screw anchors, and some capacity reductions.

Zhang, Klingner, and Graves (2001)

Zhang et al. (2001) summarized the results of a comprehensive study of anchors in cracked and uncracked concrete led by Dr. Klingner at the University of Taxes, Austin in 1990's. While most existing tests of anchors in cracked concrete focused on evaluating the capability of anchors to resist design service loads or factored ultimate loads, a group of tests by Zhang (1997) first evaluated the seismic behavior of anchor connections in cracked concrete. The tests focused on expansion anchors and undercut anchors that are of interest by nuclear industries. The test setup is shown in Figure 2.5. The four-anchor groups were subjected to cyclic moments at a rate similar to that in an earthquake. The tests indicated that the cracks (0.01 in. wide) did not affect the capacity of tested undercut anchors but caused larger displacements at failure. Meanwhile, the expansion anchors in cracks developed low capacity and in some cases the failure modes changed from concrete breakout (for anchors in uncracked concrete) to pull-out (for anchors in cracked concrete). These observations confirmed those by Eligehausen and Balogh for anchors subjected to static loading.

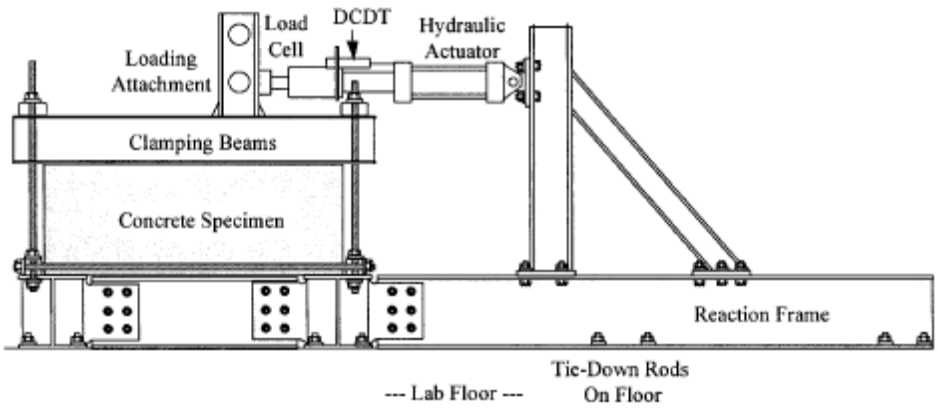

Figure 2.5: Test setup in the tests by Zhang et al. (2001)

Shahrooz, Tunc, and Deason (2004)

In the second phase of a research led by Dr. Shahrooz at the University of Cincinnati, two test anchor connections were placed in the boundary elements of reinforced concrete walls, which experienced substantial damage (cracking and spalling). The specimens were designed to simulate the connections between outrigger beams and reinforced concrete core walls in a high rise building. The prototype structure is shown in Figure 2.6 and the test structure was roughly ¼ scale. The wall specimen had a cross section of 4.5 x 36 in.; therefore the plastic hinges are expected to extend at least 3 ft from the foundation. Two anchor connections were installed in each of the two test walls, and the lower connection is at 2 ft above the foundation and thus within the expected plastic hinge zones as shown in Figure 2.7. The wall specimens were subjected to an axial compressive force equivalent to 10 percent of their axial capacities followed by reversed cyclic displacements at the top of the wall. In the meantime, the each of the two anchor connections was subjected to 50% of the measured shear force as illustrated in Figure 2.8.

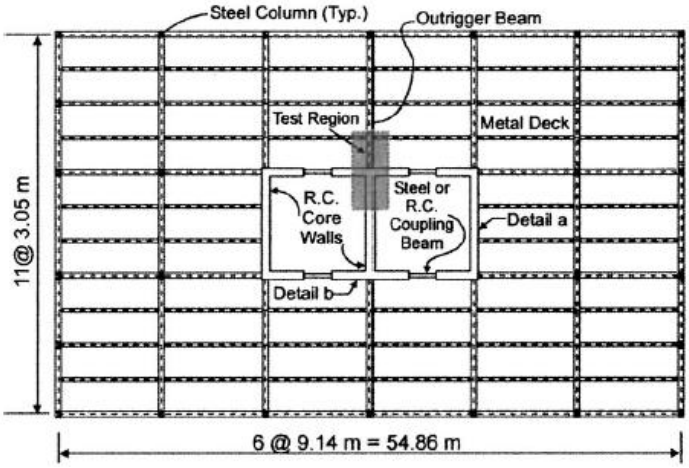

Figure 2.6: Prototype structure of the tested girder-wall connections (Shahrooz et al. 2004)

The plastic hinge zone formed during the test of specimen 1 (a rectangular wall) and the rebar yielding and cracking extended near 6 ft above the foundation. This is roughly two times the section height, which is similar to the code-specified plastic hinge zone in the commentary of provision D3.3.2 (ACI 318-11). Meanwhile the lateral loads applied though the anchor connection in addition to the shear at the wall top as illustrated in Figure 2.8 changed the damage pattern of the wall such that the majority of concrete crushing occurred below the lower connection at 2 ft above the foundation. The bottom connection, which was subjected to cyclic tension, developed ductile behavior despite the damage in concrete around the connection. This may have been attributed to the dense grid of reinforcement at the wall boundary elements as shown in Figure 2.7. The top connection, on the other hand failed by concrete breakout though the concrete developed less damage compared with the bottom connection. Note that the breakout cracks started behind the heads of the studs. This may have been due to the fact the amount of the horizontal reinforcement (6 No. 2 bars) behind the anchor connection was not sufficient such that forced applied to the wall through the anchor connections failed to be further transferred to the rest of the wall.

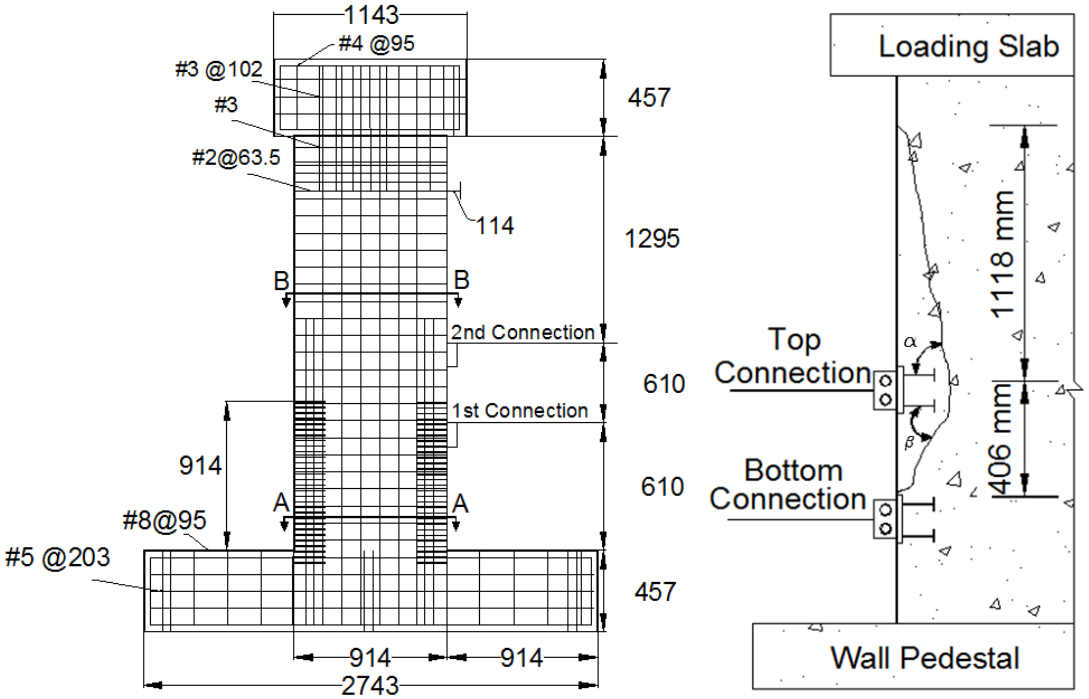

Figure 2.7: Specimen design and failure modes of anchor connections in RC walls (Shahrooz et al. 2004)

The second specimen (a T-shaped wall) did to experience large damage because the loading to the wall had to be terminated at 0.5 percent drift due to equipment limitations. The anchor connections were subjected to cyclic tension along. Both connections failed by anchor fracture. In this case the unlimited concrete around the anchor connection, in addition to confinement to the concrete, may have helped in preventing the concrete breakout failure.

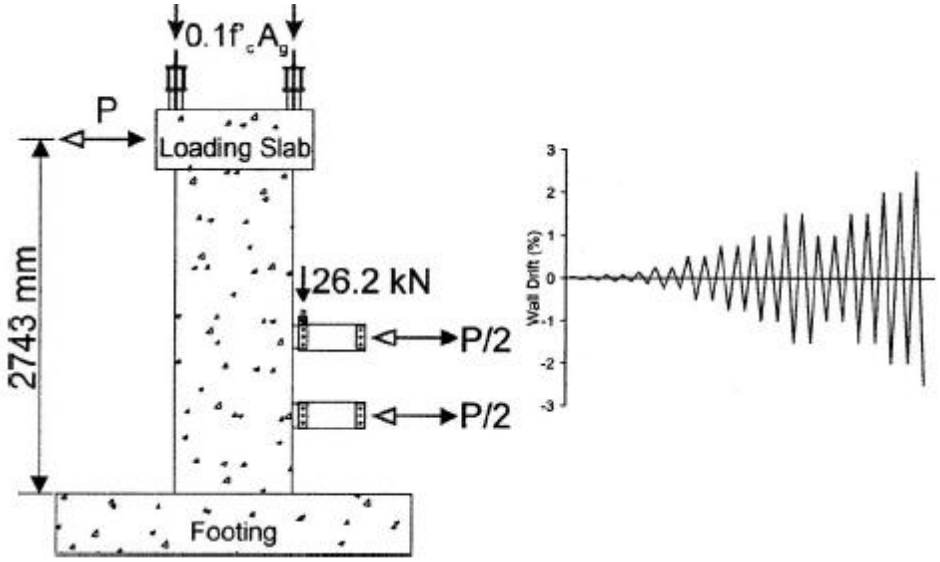

Figure 2.8: Loading protocol for the anchor connections in RC walls (Shahrooz et al. 2004)

Summary of anchor tests in damaged concrete

The behavior of anchors mounted on the plastic hinge zones that are commonly formed under earthquake loading has not been investigated in previous studies. Concrete in most existing studies had cracks up to 0.03 in., which is representative for concrete outside plastic hinge zones. Most existing tests were conducted for post-installed anchors in tension. The adverse impact of cracks on anchor behavior observed in these previous studies has led to the views that the potential spalling of the concrete cover and large cracks inside of plastic hinge zones will significantly reduce the anchor capacities.

2.3 Design Regulations

The seismic design procedures for concrete anchors, such as those stipulated in ACI 318-11 and in CEB design guidelines, do not apply to those installed in concrete that may be substantially damaged during an earthquake. For example, ACI 318-11 D.3.3.2 specifies:

The provisions of Appendix D do not apply to the design of anchors in plastic hinge zones of concrete structures under earthquake forces.

This strategy is explained in the commentary that "the possible higher levels of cracking and spalling in plastic hinge zones are beyond the conditions for which the nominal concrete-governed strength values in Appendix D are applicable." It should be noted that steel reinforcement is usually needed and provided in plastic hinge zones. Concrete encased in such reinforcement transfer anchor forces differently from plain concrete, which has been used in most of the previous tests.

For anchors that must be installed in damaged concrete such as plastic hinge zones, ACI 318-11 allow engineers the reason their own design in the commentary by stating "where anchors must be located in plastic hinge regions, they should be detailed so that the anchor forces are transferred directly to anchor reinforcement that is specifically designed to carry the anchor forces into the body of the member beyond the anchorage region." The anchor reinforcement stipulated by ACI 318-11 in Appendix D is not entirely reasonable as discovered by the study (see Volume II of the project report). In addition, dedicated anchor reinforcement may cause rebar congestions.

The European codes (CEB 2011) for seismic design of anchorage similarly stipulate that the provisions for anchors used in uncracked or cracked concrete do not apply to the design of anchorages in critical regions of concrete elements where concrete spalling or excessive cracking may occur. The common accepted crack widths outside of the plastic hinge zone are less than 0.8 mm for column and 1.05 mm for beam [Hoehler, 2006], or ranges from 0.01 inches to 0.06 inches [Fogstad et al., 2006] based on German nuclear qualification requirements for anchor design.

CHAPTER 3 Test Program for Single Anchors in RC Columns

3.1 Introduction

The specimen used in Phase IV study of the NEES-Anchor project, targeting the anchor connections in concrete walls, was designed and fabricated before the Phase II and Phase III tests. The connection design thus did not reflect the knowledge obtained from the Phase II and Phase III tests. Therefore, a group of tests were designed to evaluate the proposed anchor reinforcement for use in the anchor connections located in plastic hinge zones. These tests are called Phase V tests, which were actually completed before the Phase IV test. Due to the limited testing capacity at UWM Structures Laboratory, single anchors were used these tests.

Phase V tests have six beam-column specimens: three for single anchors in tension and the other three for two single anchors in shear, as shown in Figure 3.1. Two single anchors are used in the shear specimens, resulting in a symmetric loading to minimize torsion. Because the purpose of the tests is to verify the concept of anchor reinforcement, the reinforced concrete column and the test anchors were selected to fit within the loading capacity of the available hydraulic actuator.

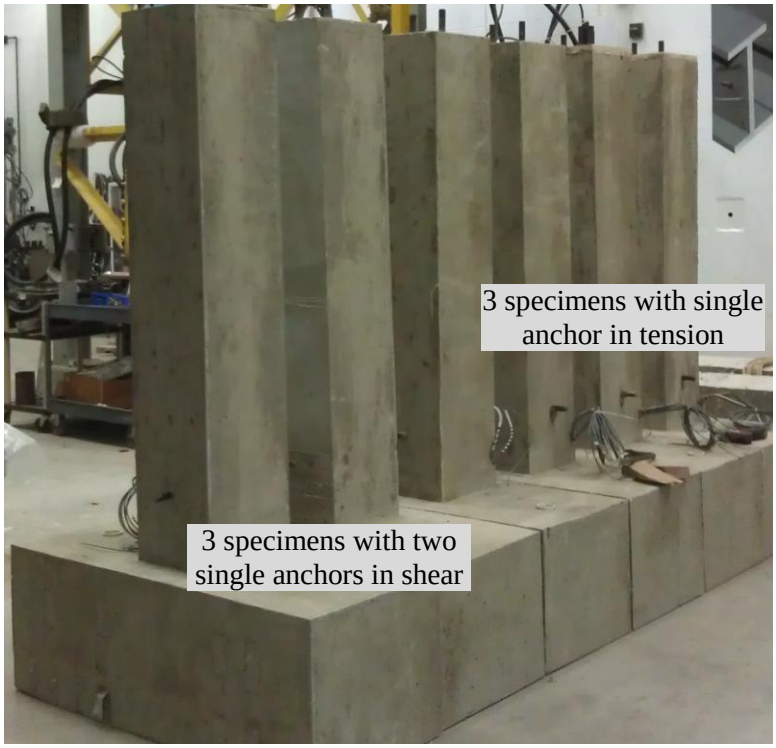

Figure 3.1: Six specimens in Phase V study

3.2 Specimen Design

3.2.1 Reinforced concrete column

The column was designed considering a typical case where anchor connections are needed, as shown in Figure 3.2. The damping devices create tension forces on the anchor connections installed on the columns and shear forces on the anchor connection installed on the beam. Both connections are located in the plastic hinge zone of the reinforced concrete (RC) elements. Considering that the RC columns would develop extensive cracks with the plastic hinge zones, and the cracked concrete may not be able to provide sufficient resistance for the anchors, three specimens were prepared for the anchor tests in tension and in shear. The initial plan was to deform the RC column to certain performance level, such as a displacement equal to four, six, and eight times its yield displacement, before the anchors were to be loaded.

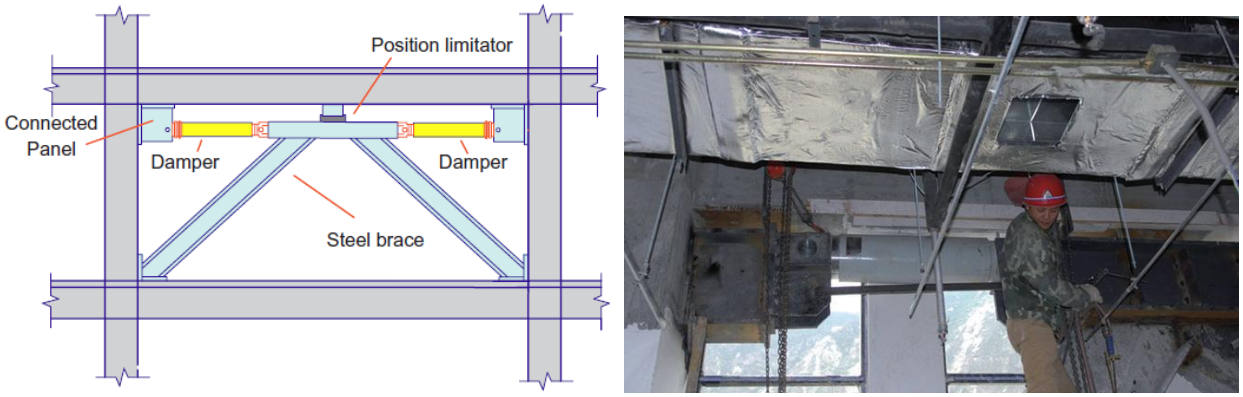

Figure 3.2: Anchor connections placed in plastic hinge zones subjected to tension/shear

The dimension of the RC test column is shown in Figure 3.3. The specimen design did not rigorously follow a scaling process. Again the purpose of the tests was to verify whether, with the proposed anchor reinforcement, anchor connections can be placed within plastic hinge zones. One anchor was placed in each tension specimen and two single anchors were placed in each shear specimen, as shown in Figure 3.1; therefore, the column size was selected as 12 x 12 in. This way, when the anchor was placed in the middle of the column (to create symmetric loading and to avoid torsion in the RC column), as illustrated in Figure 3.3, the anchor had a small side edge distance. The small side edge distances guaranteed that concrete breakout capacity according to ACI 318-11, would be smaller than the ultimate tensile capacity of the test anchor such that anchor reinforcement were needed. Similarly, the edge distances would be sufficiently small such that the concrete breakout failure would dominate the behavior if the anchor

reinforcement were not provided. The column height was designed as 5 ft. from the top face of the base block, which is close to that of a half story height. The construction has a mistake such that the final column height was 61 in. The column base block had a dimension of 48 x 20 in. and a height of 17 in. as shown in Figure 3.3. Two tie-down holes were created using embedded PVC tubes. The tie down points were 3 ft apart following the hole pattern in the strong floor of the UWM Structures Laboratory.

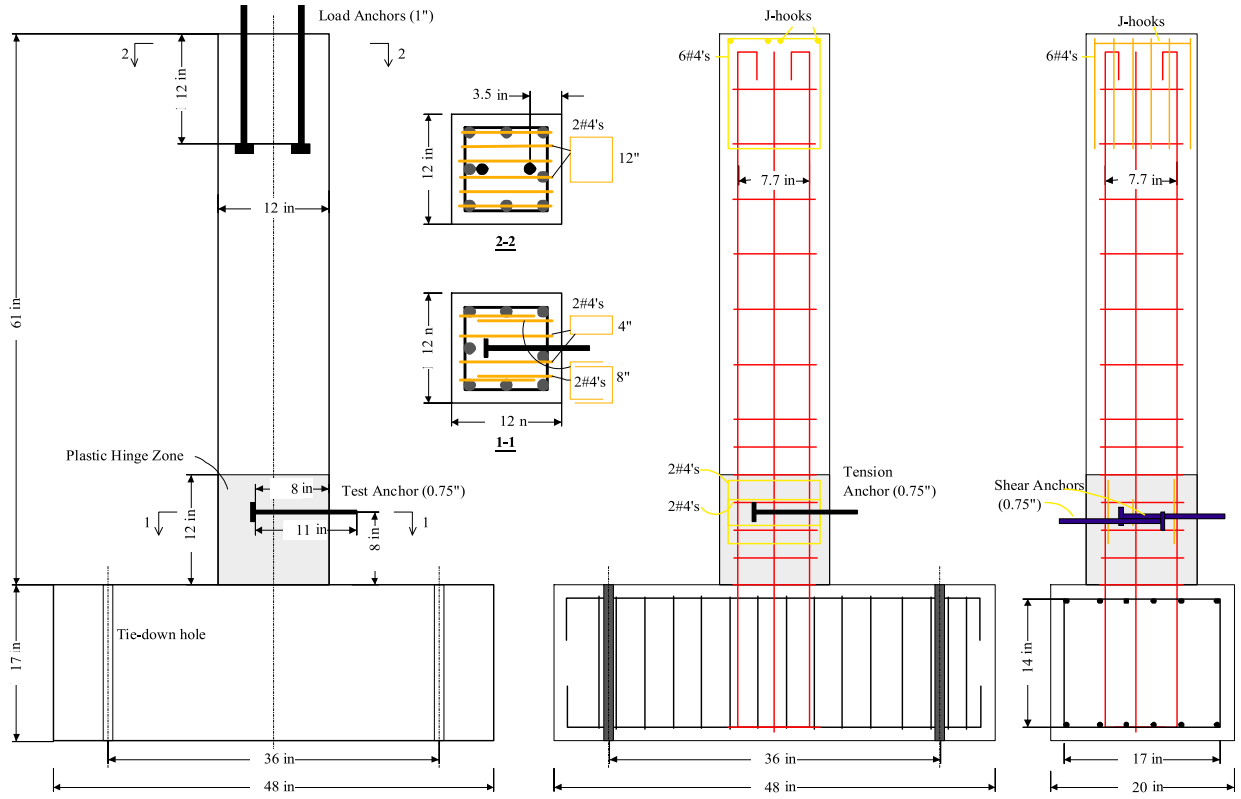

Figure 3.3: Dimension and reinforcement of Phase V sepcimens

Eight No. 5 bars (ASTM Grade 60) were provided as the longitudinal reinforcement for the columns. The reinforcement ratio was 1.72 percent, within the common range (1 to 8 percent). The concrete cover was 1.5 in., typical for RC members. The center-on-center spacing was near 3.7 in for the three bars on each face. The actual bar spacing was slightly different because the center bas needed to be offset to avoid the test anchor. A strain compatibility analysis indicated that the cross section had a nominal moment capacity about 60 k-ft. This corresponded to about 12 kips at the top of the column. Considering the maximum shear forces to be developed at 8 in. above the base block, the maximum load needed for the top actuator was less than 20 kips, within the capacity of the MTS Model 244.31, 55-kip actuator used in the study. The shear

design for the column for this load led to No. 4 ties at a spacing of 6 in., as illustrated in Figure 3.3. Additional ties were provided within the plastic hinge zone (the length of the plastic hinge zone l_p=1.5h=18 in.) as described below.

3.2.2 Test anchors

The test anchors were made from 3/4 in. diameter ASTM A193 Grade B7 threaded rods (f_{ya}=105 ksi and f_{uta}=131 ksi). The net tensile area ($A_{sa,N}$) and the net shear area ($A_{sa,V}$) for the 3/4-in threaded rods are 0.334 in.^{2}. The test anchor, if fully developed, would take an ultimate tension load of 43.8 kips, which is within the capacity of the MTS Model 244.31, 55-kip actuator used in the study. A plate washer (1.5 x 1.5 in.) and a hex nut were welded to the end. The net bearing area (A_{brg}) was 1.8 in.^{2}, sufficient to carry the tensile load without causing pulling out failure as observed in Phase III tests. The concrete compressive strength (f_c') was assumed as 4000 psi and the maximum bearing strength was assumed as 6.0f_c', similar to that assumed in Type G specimens in Phase III tests.

Two anchors are loaded in shear specimens. Each anchor, if its full shear capacity could be developed, would take 26.3 kips. Therefore, the actuator needed to provide a load of 52.6 kips, which is within the capacity of the MTS Model 244.31, 55-kip actuator. In reality, concrete cover may crush in front of the anchor shafts, resulting in significant reduction in the needed loading capacity.

The required anchor reinforcement for the 3/4-in. anchors in tension was found to be 0.73 in.^{2} Two additional No. 4 ties were used, and located 2-in. from the test anchor, as shown in Figure 3.4. The needed anchor shear reinforcement was found to be 0.44 in.^{2} The two No. 4 ties were deemed sufficient, considering other ties within the plastic hinge zone.

The column would develop flexural cracks under lateral loads. The crack location may be predicted if the bond-slip relationship is accurately known. One the other hand, the cracks could propagate rather arbitrarily, especially when the column develop inelastic behavior. Knowing that the concrete bearing strength can be significantly less than the design assumption (8f_c'), three No. 4 U-shaped hairpins were placed near the anchor in the vertical plane, as shown in Figure 3.4. These hairpins are expected to confine the concrete from flexural cracking near the anchor heads.

Figure 3.4: Reinforcing steel cage of Phase V sepcimens

The lateral loading was applied through two 1-in. anchors as illustrated in Figure 3.3 instead of a concrete loading block. Two 1-in. anchors were used to avoid the rotation of the loading plate due to accidental misalignment between the column and the actuator. The 1-in. anchors had limited side edge distances (6 in.); therefore anchor shear reinforcement (four No. 4 U-shaped hairpins) was provided as illustrated in Figure 3.3 and shown in Figure 3.4. The reinforcing bars were placed just below the concrete top surface to avoid the crushing of concrete cover (close to a zero-in. cover on the top), as observed in Phase II tests.

3.2.3 Materials

Ready mixed concrete with Wisconsin Department of Transportation Type A-FA mixture was used. The mixture design of the concrete is shown in Table 3.1. The water-cementitious material ratio was 0.4, and the amount of fly ash by weight of total cementitious materials was 30 percent. The maximum size of coarse aggregate was 3/4 in. The target concrete compressive strengths for the normal strength concrete was 4000 psi.

The measured air content of fresh concrete was 6.4 percent and the measured slump was 4 in. Compression tests of hardened concrete cylinders were conducted following ASTM C39. The rate of loading was kept at 250 lb/s to 630 lb/s in accordance with ASTM C39. The hardened

concrete had a compressive strength of 5800 psi at 28 days, and the compressive strength went up 6900 psi at about 84 days (during most of Phase V tests), as listed in Table 3.2.

Table 3.1: Mixture of WisDOT Type A-FA Concrete

Materials	Mixture Designation (lbs/yard^3)*
Cement	395
Coarse Aggregate	2002
Fine Aggregate (35%)	1075
Design Water	27 gals
Maximum Water	32 gals
Silica Fume	0
Fly Ash	170

Note: Water / (cement + fly ash) = 0.4. The slump of the mixing is 4 in.

Table 3.2: Compressive Tests of Cylinders (4 x 8 in.)

Concrete age	Test 1	Test 2	Test 3	Average
28 days	5650	5930	5790	5790
84 days	6410	7150	7170	6910

The No. 5 reinforcing steel with a nominal yield strength of 60 ksi were used as longitudinal reinforcement. Full-size bars were tested with a gauge length of 8 in. following ASTM A370. The tests were conducted under monotonic displacement control using a MTS loading frame with a 100-kip capacity. Two strain gauges were used in addition to the bar elongation to measure the bar deformation. The obtained stress-strain curves are shown in Figure 3.5.

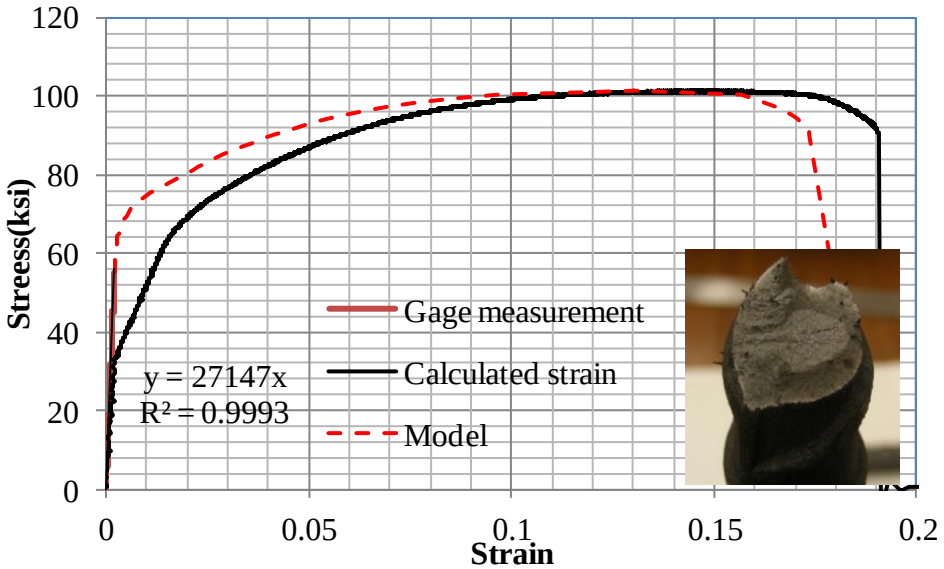

Figure 3.5: Stress-strain behavior of No. 5 steel reinforcing bars

The black solid lines shows the calculated strains from measured bar elongation, which includes full range of behavior. The test bar slipped when the bar stress was beyond 30 ksi. The strain gage measurements up to bar yielding were used to calculate the difference between the calculated strain and the projected strain. The modified stress-strain behavior is shown in red dashed lines in Figure 3.5. The test bar exhibited the local necking and the cup-cone tensile fracture surfaces, as shown in the inserted picture, which is typical for ductile metals. The yield strength, as determined by the 0.2% offset method, was about 65 ksi, and the ultimate strength was 101 ksi. The modified behavior, shown in red dashed lines in Figure 3.5, was used in the prediction of column behavior, which was used to determine the cyclic loading protocol.

3.2.4 Predicted column behavior

The behavior of the columns was predicted using fiber-based analysis in OpenSees V.2.41. The test columns were modeled using six displacement based beam-column elements. Concrete01 was used for confined concrete core and cover concrete with the measured concrete strength. instead of existing steel models in OpenSees, Bond_SP01 with the following parameters (f_y (bar yield strength) = 55 ksi; s_y (bar yield strain) = 0.0019; f_u (bar ultimate strength) = 101 ksi; s_u (bar ultimate strain) = 0.13; b (post-yield slope ratio) = 0.2; R (reloading parameter) = 0.8) were used for the rebars because it best fit the measured behavior as shown in Figure 3.6a. Strain penetration effects were also considered [Zhao and Sritharan, 2007] using the following parameters (f_y (bar yield strength) = 55 ksi; s_y (bar yield strain) = 0.0153 in.; f_u (bar ultimate strength) = 101 ksi; s_u (bar ultimate strain) = 0.534 in.; b (post-yield slope ratio) = 0.45; R (reloading parameter) = 1.0). The strain penetration model is shown in Figure 3.6b. The simulated behavior fits well the measured behavior.

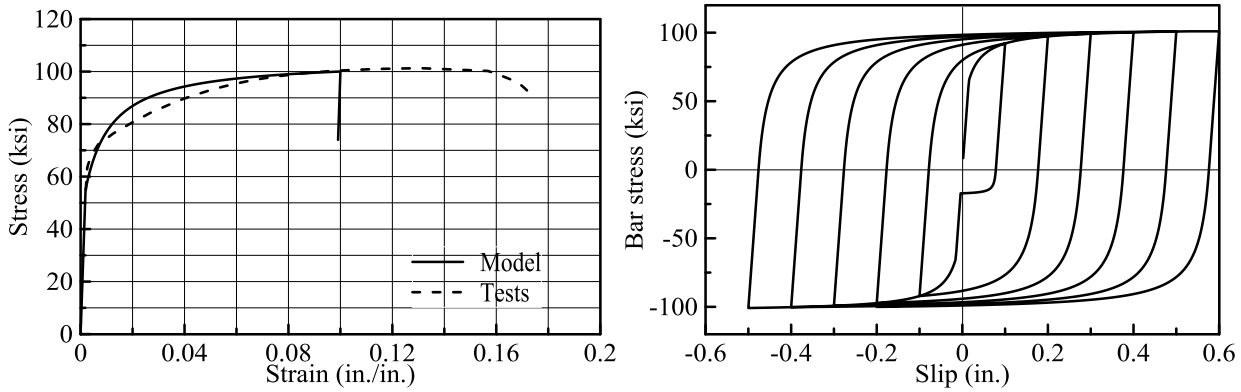

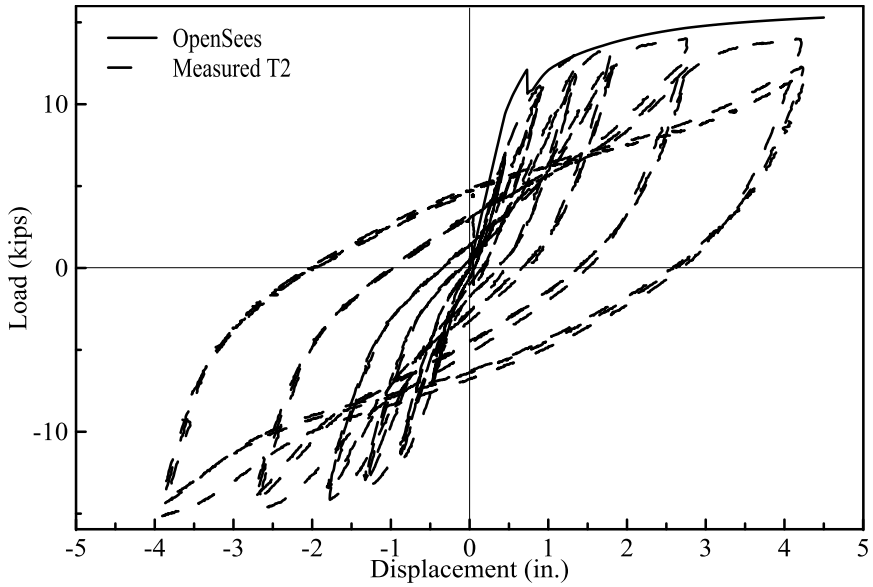

Figure 3.6: Predicted behavior of the column in Phase V tests

3.3 Test setup

The test setup is schematically shown in Figure 3.7, and the actual setup is shown in Figure 3.8. The specimen was fixed to eh strong floor of the testing laboratory using two high-strength threaded rods. One MTS Model 244.31, 55-kip actuator was used to apply a reversed cyclic displacement at the top of the column. A T-shaped loading plate (shown in shaded part at the top of the column) was used to connect the two 1-in. loading anchors with the swivel head of the actuator. A steel channel was welded to the loading plate to increase the stiffness of the loading plate (Note that the specimen T1 was tested with a different loading plate, and the loading plate was bent permanently; therefore the test of Specimen T1 is not presented in this report). The center line of the actuator piston was aligned with the top face of the 1-in. thick loading plate; therefore the lateral load was applied at 62 in. above the base block. Another MTS Model 244.31, 55-kip actuator was used to apply tensile forces to the anchor shown in Figure 3.7. The centerline of this actuator was located at the height of the test anchor. Both actuators were supported by the same loading frame. In order to minimize the relative displacement between the reaction frame and the specimen, a shoring frame was placed in between the reaction frame and the specimen. A hydraulic jack was used to create pre-compression before the test.

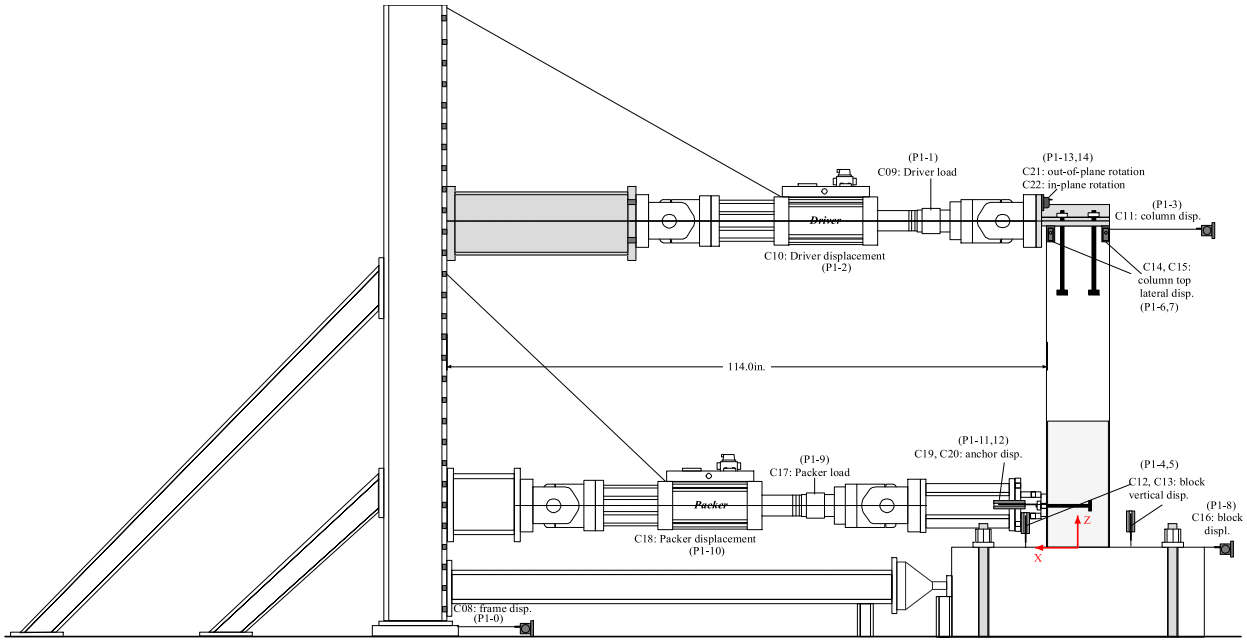

Figure 3.7: Schematics of the test setup in Phase V tests

Figure 3.8: Picture of the test setup in Phase V tests

The test setup for shear tests is same as that for the tension tests, except the adapting device for the anchor bolts. The shear setup is shown in Figure 3.9.

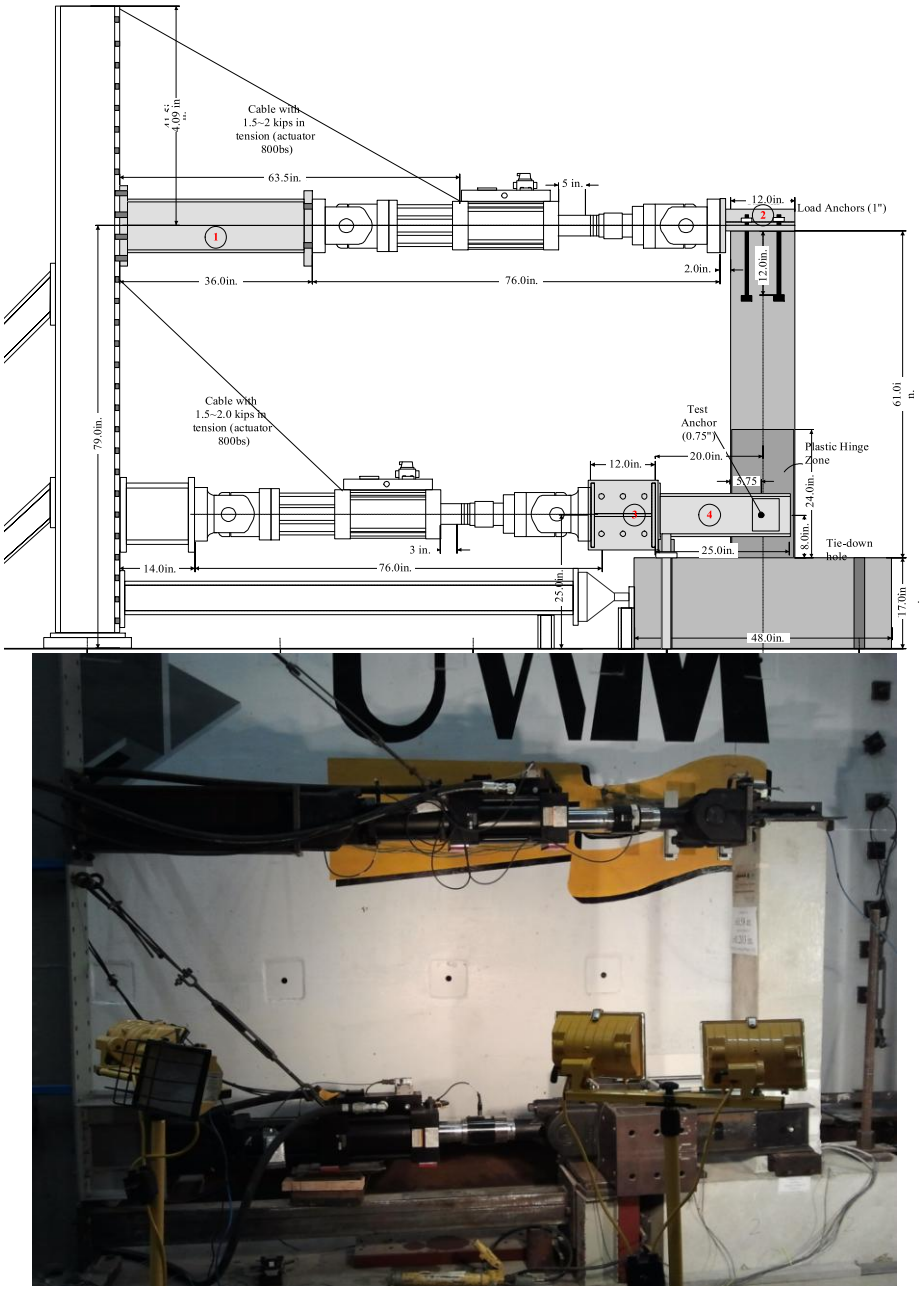

Figure 3.9: Picture of the test setup for anchors in shear in Phase V tests

3.4 Loading protocol

Specimen T1 was loaded to near eight times the yield displacement before the anchor was loaded in tension. This deformation represented the worst scenario plotted during the test design. The test of Specimen T1 indicated that column core was able to support the anchor bolt till it

developed its full tensile capacity. Therefore the testing plan was slightly changed, and two types of loading were used in the following tests.

The columns were subjected to reversed cyclic displacements. The displacement history included groups of three cycles with the following peak displacements: ±0.58, ±1.12, ±1.66, ±2.20, ±3.28, and ±4.9 in. These peak displacements were selected after the results of T1 test. The column top rotated during the loading, and the specimen slightly moved relative to the reaction frame. After all these effects, the column bars would yield at the first peak displacement (Δy). The following peak displacements thus represented ±2Δy, ±3Δy, ±4Δy, ±6Δy, and beyond ±9Δy. The detailed calculation behind these peak displacements are shown in Appendix A. The last peak displacement was also limited by the travel limit of the hydraulic actuator (±5 in.). Loading rates for displacement cycles were kept at 0.24 in./min throughout the tests.

The anchor in Specimen T2 was loaded in monotonic tension till failure after the column was subjected to the predefined loading history described above. The anchor in Specimen T3 was loaded following a cyclic tensile loading history. Unidirectional (tension only) cyclic displacement-controlled loading was trialed first and the test stopped inexpertly. this was due to fact that the anchor was subjected unidirectional cyclic loading while the column is subjected to reversed cyclic loading. The unsynchronized loading caused relatively large compression that often time triggered the interlock, and stopped the tests. Therefore, the cyclic loading on the anchors was applied in load-control, and the peak loads are 21, 42, 43, and 44 kips. The anchor was then loaded monotonically in tension till failure. The loading rate was 200 lb/s. The bottom actuator was applying much larger loads than the top actuator; therefore it took the bottom actuator a bit longer to achieve the predefined peak displacement. The column loading was suspended for one minute at the zero displacement at the end of each cycle group to synchronize the loading.

The anchors in Specimen S1 were loaded in monotonic shear till failure after the column was subjected to the predefined loading history described above. The anchors in Specimen S2 were loaded in reversed cyclic loading, and the peak displacements were determined based upon the results of the Specimen S1. Both test stopped before the expected load/displacement was achieved because the anchors failed due to combined bending and shear as described later in this report.

3.5 Instrumentation Plan

The instrumentation plan was schematically shown in Figure 3.7. Most sensors are listed in Table 3.3. Four strain gages were used to verify the shear load applied to each anchor in Specimen S2. Eight additional strain gages were used in Specimen S3 to capture the load transferring within the FRP strips. Details about these additional sensors are described in the discussion of individual tests.

Table 3.3: list of sensors used in Phase V tests

#	Channel name	Conversion	Sensor description	Sensor type	Excitation
1	SG-00in	4807.69231	Gage at column base	Strain gage	2V
2	SG-04in	4807.69231	Gage 4 in. form column base	Strain gage	2V
3	SG-08in	4807.69231	Gage 8 in. form column base	Strain gage	2V
4	SG-12in	4807.69231	Gage 12 in. form column base	Strain gage	2V
5	SG-24in	4807.69231	Gage 24 in. form column base	Strain gage	2V
6	SG-48in	4807.69231	Gage 48 in. form column base	Strain gage	2V
7	SG-A08	4807.69231	Gage on one confining reinforcement	Strain gage	2V
8	Frame-X	0.25	Displacement of reaction frame	Celesco 2-in. string pot	28V
9	Column-load	5.5	Top acuator (Driver) load	Actuator inside	10V
10	Column-disp	1	Top acuator (Driver) displacement	Actuator inside	10V
11	Column-X	1	Column top in-plane displacement	Celesco 10-in string pot	28V
12	Base-Z(x-9in)	0.18186	Base block uplifting at x=-9 in.	LVDT, 2 in.	15V
13	Base-Z(x+9in)	0.18394	Base block uplifting at x=+9 in.	LVDT, 2 in.	15V
14	Top-Y(x+6in)	0.2	Column top out-of-plane displacement	Celesco 2-in. string pot	28V
15	Top-Y(x-6in)	0.2	Column top out-of-plane displacement	Celesco 2-in. string pot	28V
16	Base-X	0.2	Base block displacement	Celesco 2-in. string pot	28V
17	Anchor-load	5.5	Bottom actuator (Packer) load	Actuator inside	10V
18	Anchor-disp	0.5	Bottom actuator (Packer) displacement	Actuator inside	10V
19	Anchor-X (Y=+6in.)	1.25638	Anchor displacement @ y=6 in.	Sensotec LVDT	6V
20	Anchor-X (Y=-6in.)	1.11935	Anchor displacement @ y=-6 in.	Sensotec LVDT	6V
21	Tilt-X	1	X-axis rotation from the tilt meter	Applied Geo tilt meter	+-12V
22	Tilt-Y	1	X-axis rotation from the tilt meter	Applied Geo tilt meter	+-12V

Strain gages were installed on the column longitudinal bars to monitor the column behavior. The location of strain gages is shown in Figure 3.10. The numbers in the sensor name shown in Table 3.3 indicate the height of the strain gage in inches (e.g., SG-08 is a strain gage installed on the middle bar 8 in. above the base block). The strain measurements also confirmed the range of

plastic hinge zones. Additional No. 4 U-shaped hairpins were used to confine the concrete around the anchor head to prevent the flexural cracks from passing the anchor bolts. One additional strain gage was installed on a U-shaped hairpin to monitor the demands on such confining reinforcement.

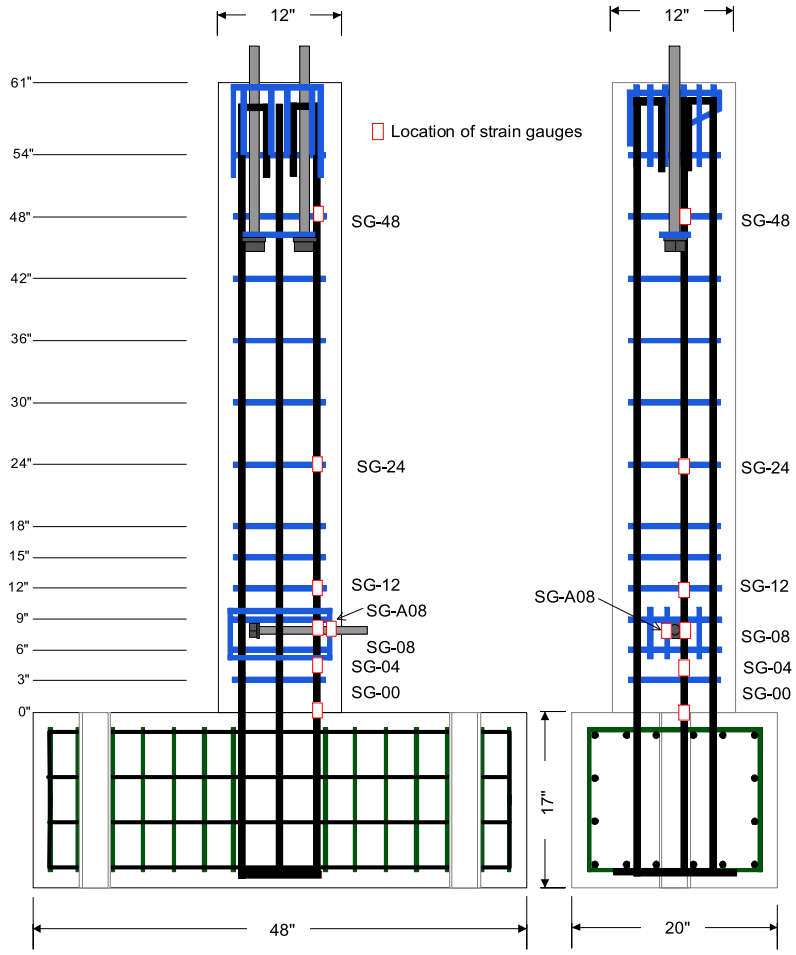

Figure 3.10: Strain gage locations in Phase V tests

The column displacements was measured using a sting pot attached to a reference column that was fixed to the strong floor (Figure 3.11a). The base block movement was captured using another string pot as shown in Figure 3.11b, The potential rotation of the column was captured using two additional string pots at the north and south corners of the test column (Figure 3.11c). The uplifting of the base block was monitored using two 2-in. LVDT's as shown in Figure 3.11d. The LVDT's were supported on a cantilever beam fixed to the reference column. The horizontal movement of the reaction frame (braced column at the south side) was also monitored using a

string pot. The two actuators provided measured displacements and loads at both the column top and at the anchor location.

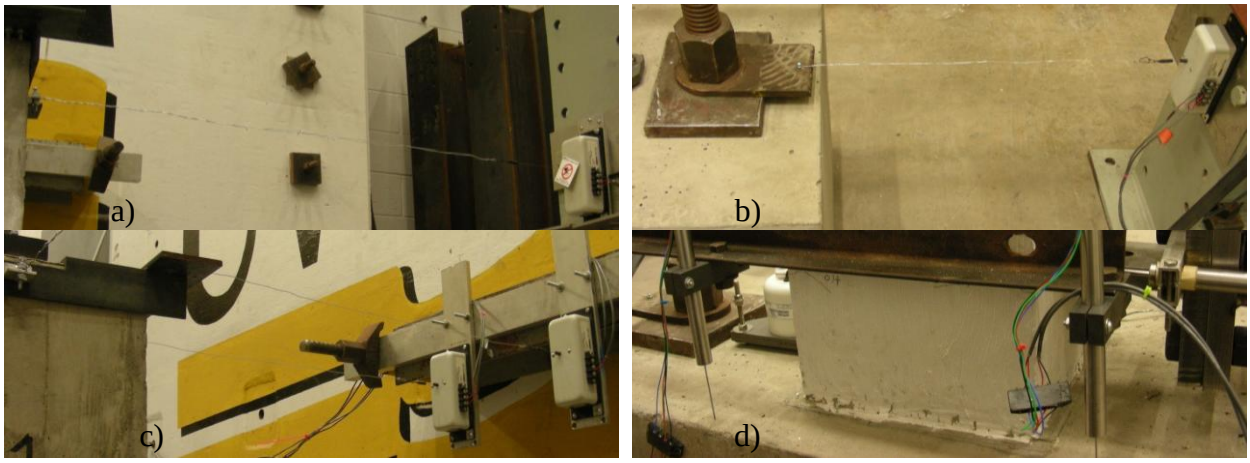

Figure 3.11: Instrumentation locations in Phase V tests

The anchor displacements relative to the concrete surface were measured using two 6-in. spring-loaded LVDT's mounted on the loading plate at both east and west sides, as shown in Figure 3.12. The magnetic cores of the LVDT's were just about 6 in. away from of the center of the test column. The LVDT's were 8 in. above the base block for the tension anchors while the LVDT's had to be place at 18 in. above the base block for the shear anchors. Figure 3.12 also shows the adapting devices for the anchors in tension and for the anchors in shear.

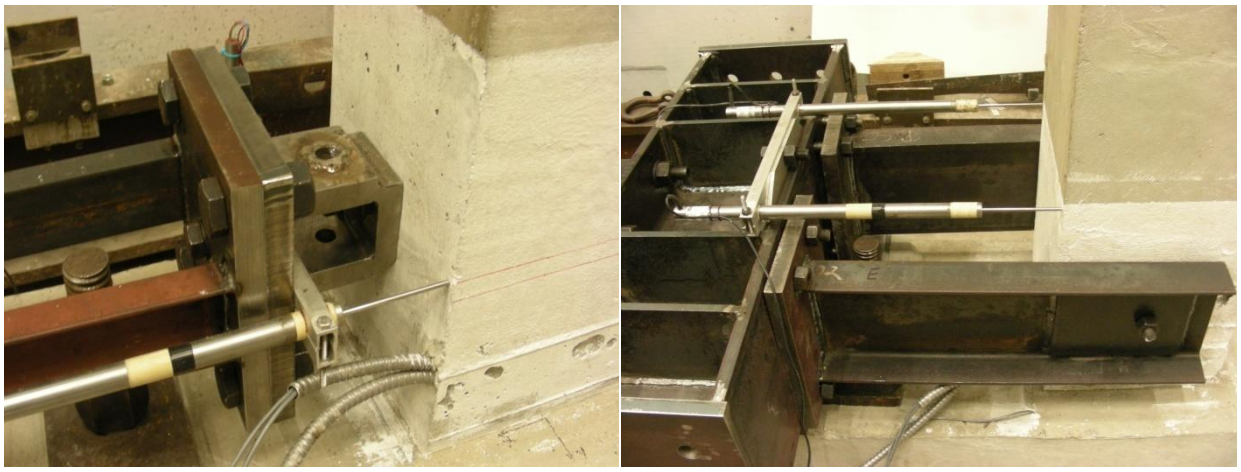

(a) One anchor in tension **(b) Two anchors in shear**

Figure 3.12: LVDT's for anchor displacements

An IO Tech DaqBook 2000 was used to collect data from all sensors listed in Table 3.3. The sampling frequency was 2 Hz for all tests. The collected data was filtered using an in-house program with a cutoff frequency of 0.1 Hz.

3.6 Potential Failure Modes

The test specimen could fail with a number of possible failure modes under the complex combination of column loading and anchor loading. Design checks were conducted for a variety of failure modes to ensure that specimen would not fail before the testing anchor reached at its full design capacity.

3.6.1 Column flexural failure

The specimen was treated as a simply supported beam with a span of L (61 in.) after the plastic hinge was developed. The beam was supported at the column base and the column top by the actuator. The anchor load was a point load P_u placed at h=8 in. from the support at the column base. The member had three No. 5 bars, thus its nominal moment capacity, M_b, was calculated as 506 kips-in. In order to cause flexural failure, the point load to be applied to the test anchor would satisfy

$$M_b = P_u h\ (L-h)/L. \quad (3.1)$$

The calculated point load was 72.8 kips, which is larger than the anchor capacities.

3.6.2 Column shear failure

The shear capacity of the member (V_b), considering the tie (No.4) spacing of 3 in., was calculated as the summation of concrete contribution (V_c = 18.2 kips) and tie contribution (V_s = 77.6 kips). In order to cause shear failure, the point load to be applied to the test anchor would satisfy

$$V_b = P_u + P_{@\ top}. \quad (3.2)$$

The load on the column top was estimated as 12 kips from the design check shown above. The calculated point load was 83.8 kips, which is larger than the anchor capacities.

3.6.3 Anchor pullout failure

The net bearing area, A_{brg}, was 1.8 $in.^2$ as shown in the section of specimen design. In order to cause shear failure, the point load to be applied to the test anchor would satisfy

$$P_u = 8\ f_c'\ A_{brg}. \quad (3.3)$$

The compressive strength of the concrete, f_c' was assumed as 4000 psi. The calculated point load was 57.6 kips, which is larger than the anchor capacities. Note that the concrete had a higher

compressive strength. This failure mode would not control if the confining reinforcement could prevent cracking near the anchor head.

3.6.4 Shear friction along the flexural cracks

The normal force (N) on the potential shear friction plane was calculated as 148.8 kips. In order to cause shear failure, the point load to be applied to the test anchor would satisfy

$$P_u = \mu N. \tag{3.4}$$

The dry friction coefficient μ=0.4 from the PCI design handbook. The calculated point load was 59.8 kips, which is larger than the anchor capacities.

3.6.5 Concrete breakout

With stirrups and anchor reinforcement, the concrete breakout cone may develop from the outside of the stirrups toward to the base and top column (another boundary supported by the top actuator). Rather the cracking development along the 35 degree as specified in ACI-318-11 appendix D, it is likely that the developed flexural cracks may provide the shortcut for the breakout path and thus the concrete breakout results in the dry friction, as specified in Case 4 above.

3.6.7 Anchor fracture in tension

The tensile capacity of the anchors was calculated from the measured ultimate strength (131 ksi) and the net tensile area (0.334 in.^{2}),

$$P_u = f_{uta} A_{se,N} \tag{3.5}$$

The calculated point load was 43 kips.

3.6.7 Anchor fracture in shear

The shear capacity of the anchors was calculated from

$$V_u = 0.6 f_{uta} A_{se,V} \tag{3.6}$$

The calculated point load was two times the shear capacity, 53.5 kips if concrete cover would not be pushed off. If the cover concrete was lost during the test, the anchors in shear would have an exposed length *l*, and the shear capacity can be calculated based on Lin et al. (2011). Specifically, The shear capacity of anchor bolts with an exposed length *l* can be calculated as

$$V_{se} = f_{ya} A_{se,v} \sin(\beta) + \frac{f_{ya} \cos(\beta)}{\frac{1}{0.9 A_{se,v}} + \frac{l}{3.4 S}}, \tag{3.7}$$

where the rotation angle of the exposed anchor is $\beta = \theta + l_p \tan^{-1} \frac{\varepsilon_{max}}{d_a}$,

in which the maximum tensile strain (ε_{max}) and the anchor diameter (d_a) can be obtained from the anchor material; θ is the initial end rotation allowed by the oversized holes and/or concrete deformation, l_p is the length of plastic hinge and may be taken as d_a, and should not be larger than $l/2$ for shorter exposed lengths (i.e., $l < 2d_a$).

To avoid friction between load plate and concrete surface during the test, a 1/8 in gap was controlled between the loading plate and the concrete surface. Therefore, the exposed length could be either 1/8 in. or with additional 1.5 in., which was the concrete cover depth. The calculated point load had an upper bound at 54.9 kips and a lower bound at 28.7 kips

3.7 Summary

Six column specimens were prepared to verify the effectiveness of the proposed anchor reinforcement for anchor bolts placed within the plastic hinge zones. The anchor fracture was expected to control the failure of the specimen. In addition to the anchor behavior, the column tests also provides information of crack widths at a variety of performance levels. The recorded information is shown below.

CHAPTER 4 Test Results of Single Anchors in RC Columns

4.1 Test of Specimen T2

4.1.1 Behavior of Column T2 and Crack patterns under Cyclic Loading

The crack map of Specimen T2 is shown in Figure 4.1. The development process of these cracks is shown in figures in Appendix A. The concrete flexural cracks near the base were firstly observed and then another two cracks at both sides of the location of the anchor through the height when the column was subjected to the first group of displacements at 0.58 in. Another three flexural cracks developed at higher location away from the base with the further increase of the loading. In particular, the crack width at the base reached up to 1.0 mm at both north and south sides when the commanded displacement increased to the maximum ±1.12 in. During this loading cycle, flexural cracks developed in the base block at the location of the bars. The flexural cracks did not widen during the following loading cycles due to 1) the stresses in the longitudinal bars of the column did not further increase after the bars got into strain hardening range of behavior; and 2) the longitudinal bars in the base block controlled the cracking. At

More cracks developed during the loading level at 1.66 in. The flexural cracks in column T2 reached up to 45 inches above the base block. Due to the extensive development of plastic hinge zone, in which the reinforcing bars passing yielding, no further flexural cracks developed above this height in the later loading cycles. Instead, more x-shaped cracks developed in the plastic hinge zone. A few major cracks further opened up at the loading cycles at 3.28 in.

Further damage in the plastic hinge zone as well as concrete cover spalling was observed at both sides of the column, when the column was subjected to the group of displacement at 4.9 in. The crack widths are shown in Figure 4.1 after all loading steps are complete for the column. By plotting the crack pattern and crack width developed after the loading cycles 4.9 in., the variation of the crack width from bottom to top through the height of the column was observed as crack cycling proceeded. The crack width at the base rose up to 9.0 mm at both north and south sides. A couple of other major cracks are observed within the plastic hinge zone. However, it was believed that the crack did not pass through the core concrete around the anchor head. The cracks are distributed evenly and the largest crack width was 0.4 mm outside the plastic hinge zone. .

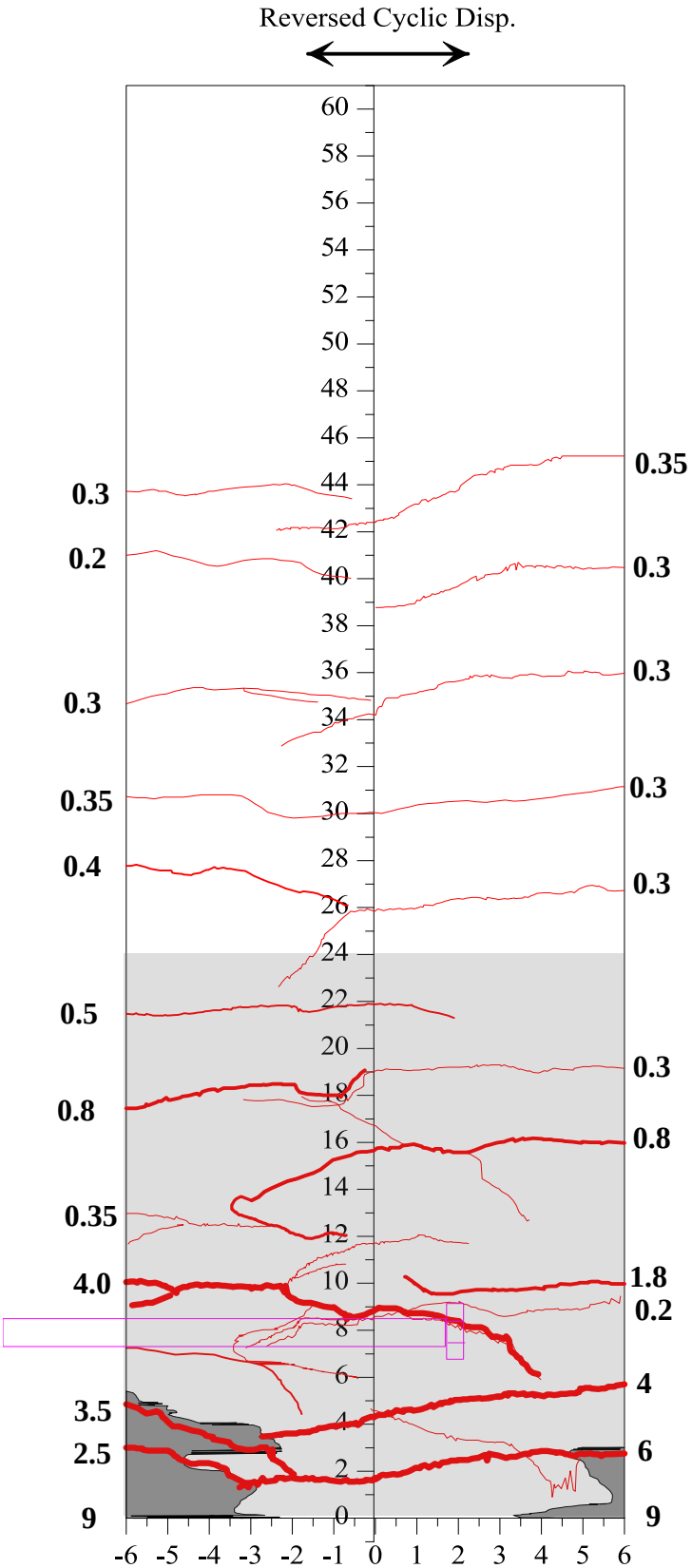

Figure 4.1: Crack patterns and measured crack widths in T2 after ±4.9 in loading cycles

The cyclic behavior of column T2 is shown in Figures 4.2 and 4.3. The column had a typical hysteretic behavior, similar to others in the literature. The load vs. actuator displacement curves indicated that the actuator was able to follow the predefined loading history. However, the reaction frame was not rigidly tied with the specimen; therefore the actuator displacements were somewhat different from the true column displacement measured using a string pot. The true column behavior indicates a 0.8 in. difference between the two displacement measurements. This difference may have been attributed to 1) the specimen was not rigidly fixed with the reaction frame; 2) the reaction frame allowed additional movement; 3) the oversized holes on the loading plate allowed 1/8 in. difference.

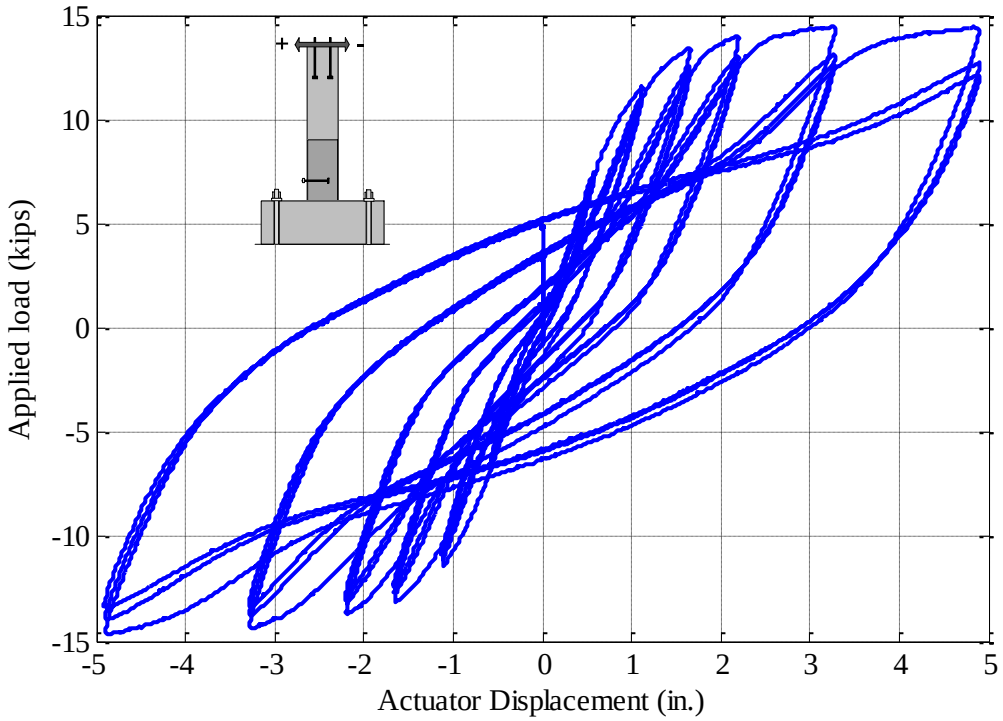

Figure 4.2: Load vs. actuator displacement curves of column T2

The column displacement vs. the strain reading at the column base is shown in Figure 4.4. The strain gage reading had large noise signals. However, a closer look at the strains during the first displacement loading cycle (0.58 in.), shown in Figure 4.5, indicated that the longitudinal bars first yielded at a displacement of 0.5 in. (Δy). Hence, the column T2 was loaded close to $8\Delta y$. The achieved displacement in the positive direction was about 0.3 in. higher than that in the negative direction. This was due to the fact that the reaction frame was wedged against the specimen, thus allowing less relative movement.

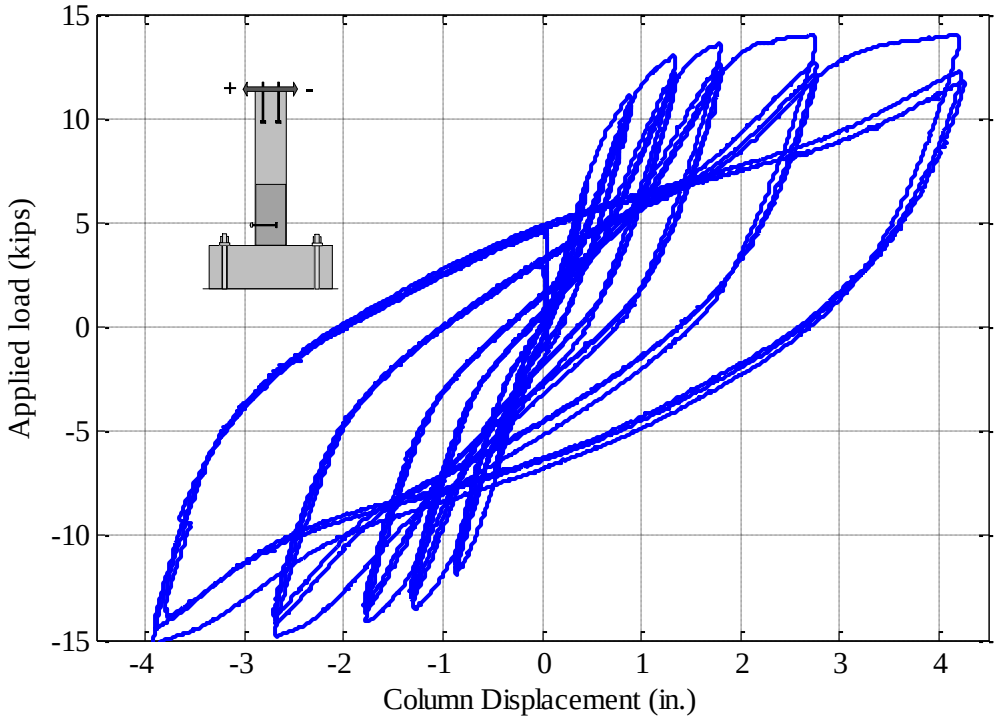

Figure 4.3: Load vs. column displacement curves of Specimen T2

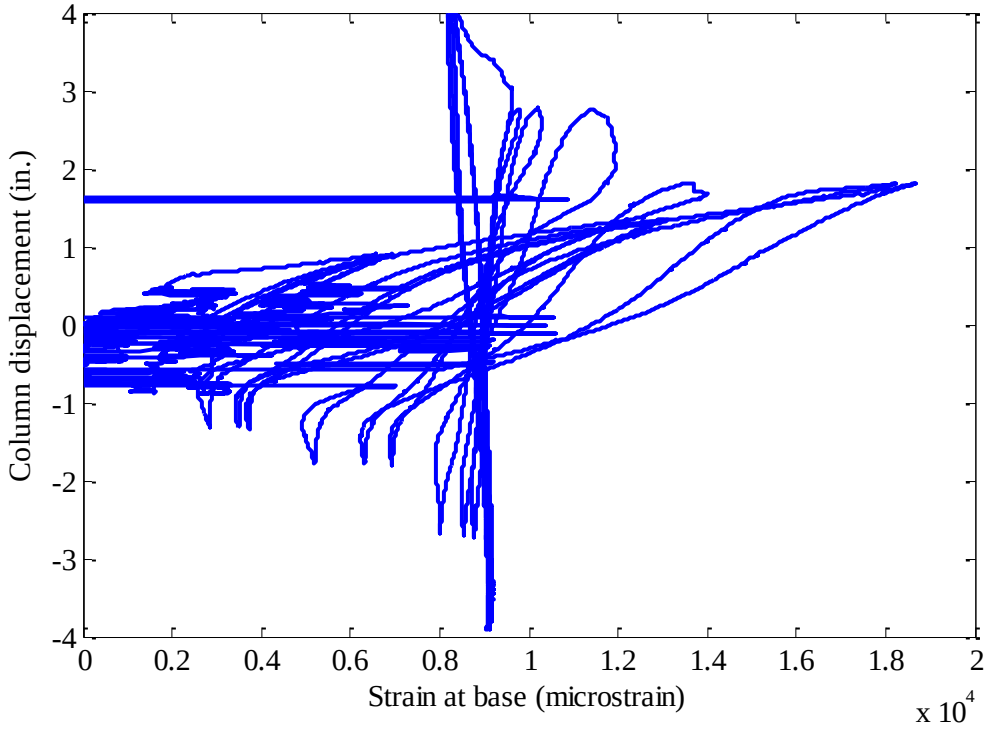

Figure 4.4: Bar strain vs. column displacement curves of Specimen T2

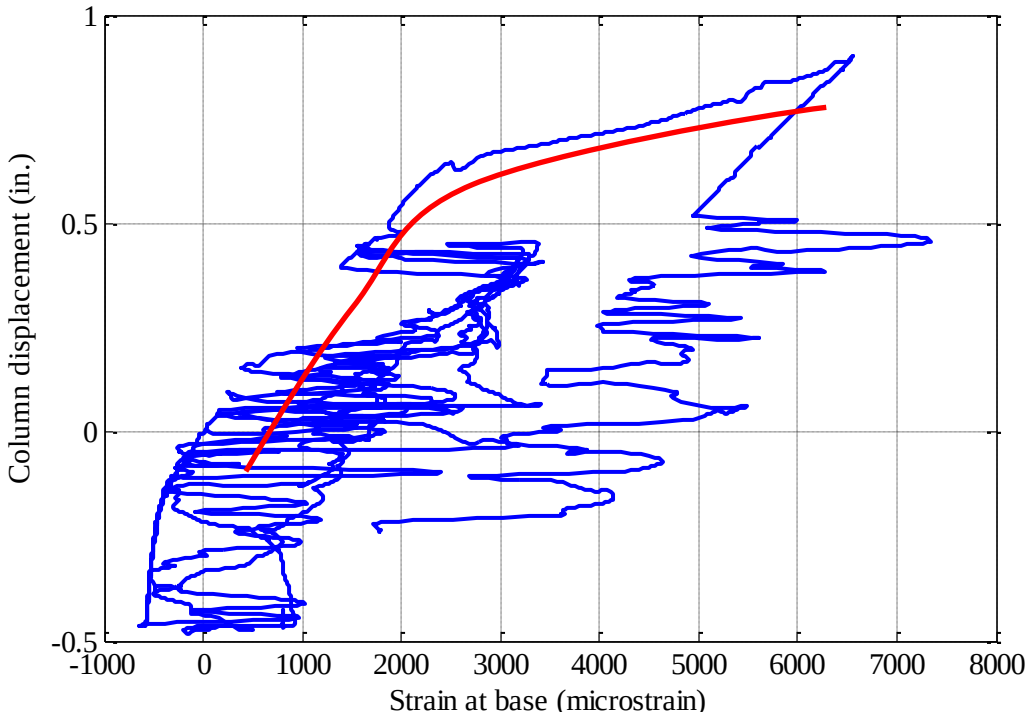

Figure 4.5: Bar strain vs. column displacement curves of Specimen T2 (0.58 cycles)

The column developed stable and ductile hysteretic behavior, as indicated in Figure 4.3. However, it was expected that the column capacity would start dropping if the column were loaded beyond the current maximum displacement. This was because concrete cover started crushing at both sides of the column during the last loading cycle.

Both strain gages at 4 and 8 in. above the base developed inelastic strain larger than 20 thousand micro-strain, indicating the large demands within the plastic hinge zone. The strain gage at 12 in. above the base malfunctioned. Nevertheless, the strain gage at 24 in. above the base detected strains larger than the yield strain, indicating that the plastic hinge zone may extend to two times the section height.

4.1.2 Behavior of Anchors in Tension

The load vs. displacement behavior of the anchor bolt, as plotted in Figure 4.6, demonstrated that the steel ductile failure was achieved. This observation also confirmed that the anchors can be installed in the plastic hinge zone if the suitable anchor reinforcement is provided, as stated in Phase III of the NEES-Anchor project. Unlike normal sharp drop after peak load, the anchor steel had a relative long descending range. It may have been attributed to slow energy release

rather than sudden energy release in a typical coupon tests, in which rigid loading devices are typically used.

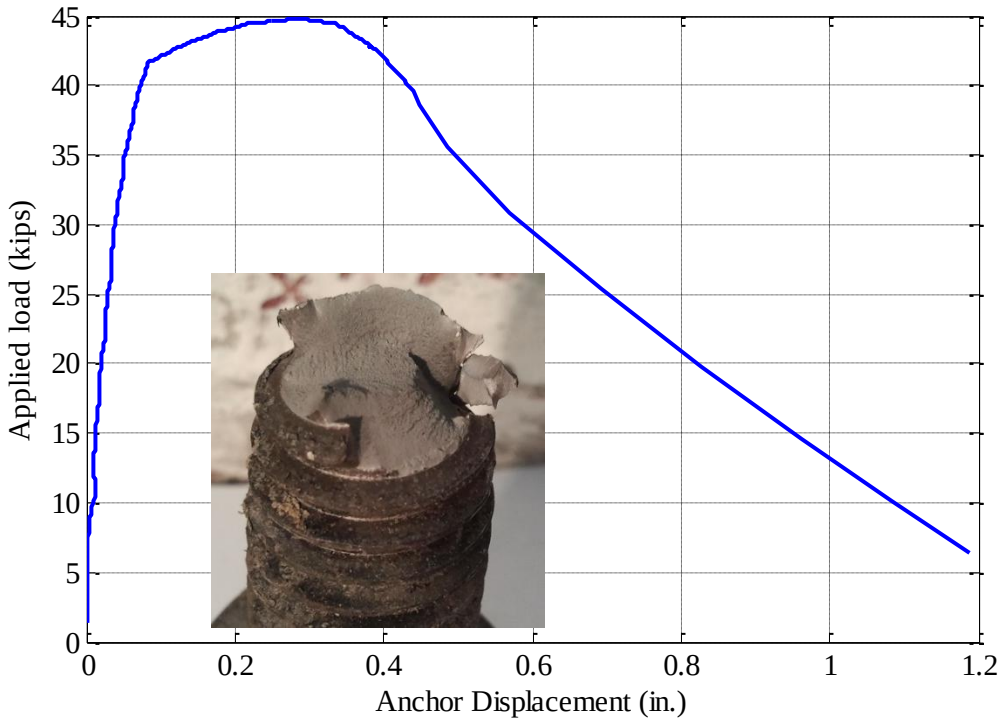

Figure 4.6: Load vs. displacement of anchor in tension (T2) after cyclic loading

Concrete within the plastic hinge zones was extensively cracked as shown in Figure 4.7 before the anchor was subjected to tensile loading. These existing cracks before anchor loading changed the development of a breakout cracks: instead of a concrete breakout cone as usual in un-reinforcement concrete, the crack surfaced out to the side faces due to a limited side edge distance as shown in Figure 4.7. The inclined cracks were soon arrested by a flexural crack in the column outside the local confined concrete as shown in Figure 4.8. The flexural crack, which was likely through the entire column section, became the weakest link in the loading resisting system. The concrete column attempted to shift out when the anchor load was at its peak. The dry friction provided higher capacity than the anchor fracture in tension as shown in Chapter 3; therefore the file failure mode was anchor bolt fracture as indicated by the load vs. displacement curve in Figure 4.6.

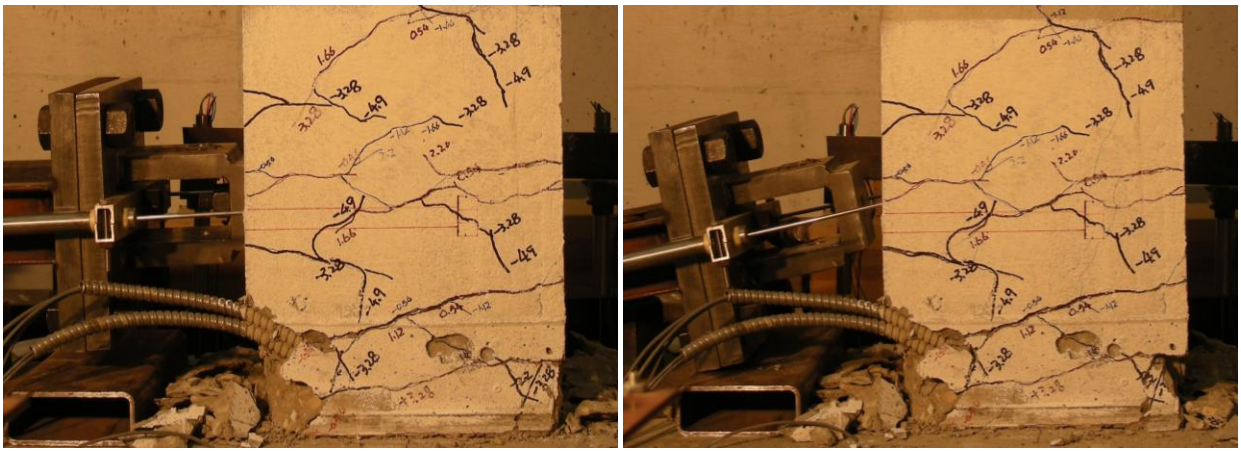

Before the anchor failure **After the anchor failure**

Figure 4.7: Comparison of concrete cracking patterns

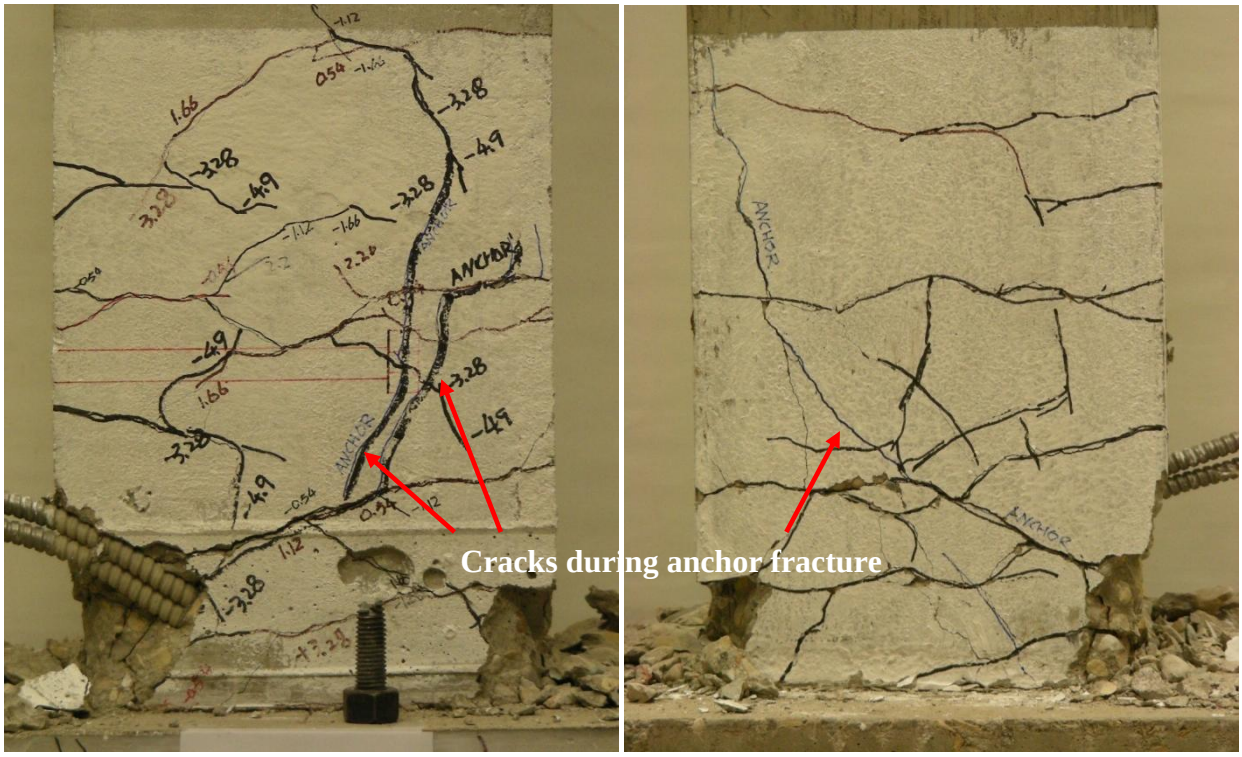

(a) East side **(b) West side**

Figure 4.8: Breakout cracks arrested by a flexural crack

This observed failure mode was possible because the concrete near the anchor head was well confined by the anchor reinforcement (i.e., additional closed ties) and the local confining steel that prevent flexural cracks from passing through the anchor bolt. The strain gage installed on one of the U-shaped hairpin indicates that the hairpins were not subjected to high demand, as shown in Figure 4.9. Further study is needed to provide information such that a design methodology can be developed.

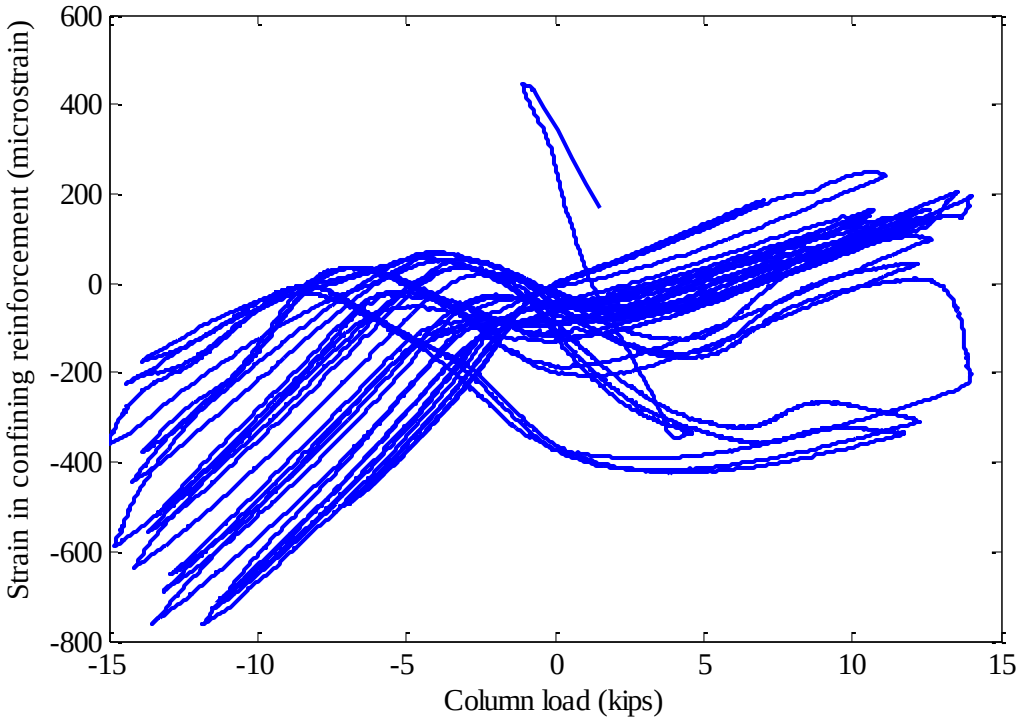

Figure 4.9: Strain in the confining reinforcement (T2)

4.2 Test of Specimen T3

4.2.1 Behavior of Column T3 and Crack patterns under Cyclic Loading

The column was subjected to the same loading as that in the test of Specimen T2. The anchor bolt, on the other hand was subjected to cyclic loading. the cyclic loading of the anchor was controlled by the applied load at the following levels: 21 kips, 42 kips, 43 kips and 44 kips based on the results of T2 test. The anchor was then load in monotonic tension till failure. One other thing that was different from the test of T2 is that the monotonic loading was applied when the column was loaded to 4.9 in. in the negative direction. The reason for trying this different situation was that the cracks in the plastic hinge zone would open wide in this case, creating the worst situation for the anchor bolt. The load vs. actual anchor displacement was plotted in Figure 4.10. The detailed column behavior is described below. The development of the cracking pattern is shown in Appendix A.

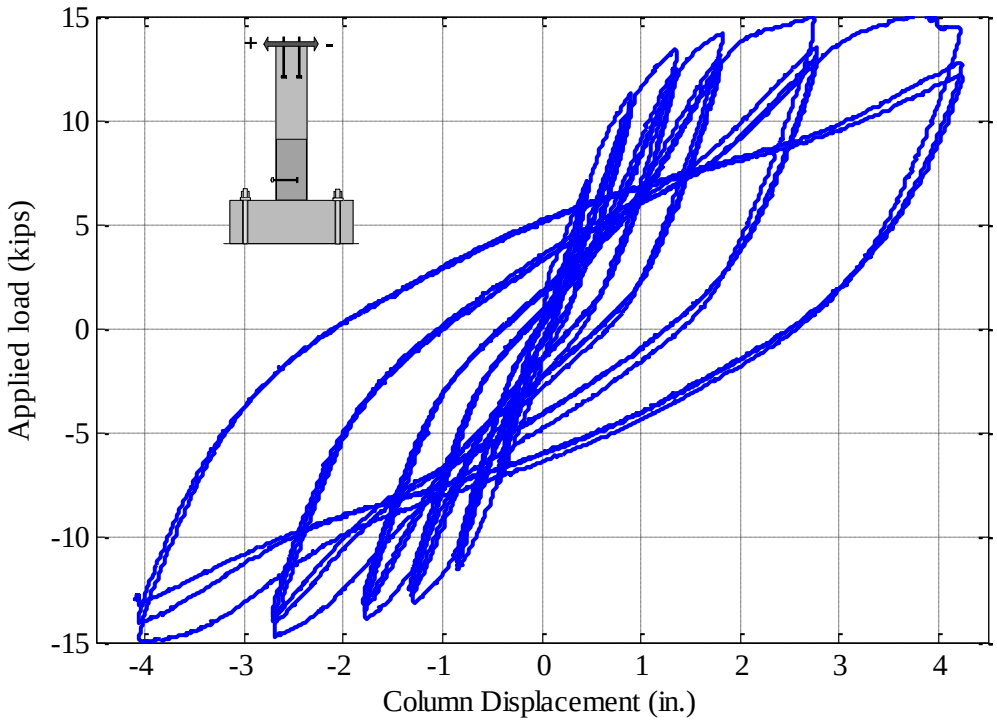

Figure 4.10: Load vs. column displacement of the column T3

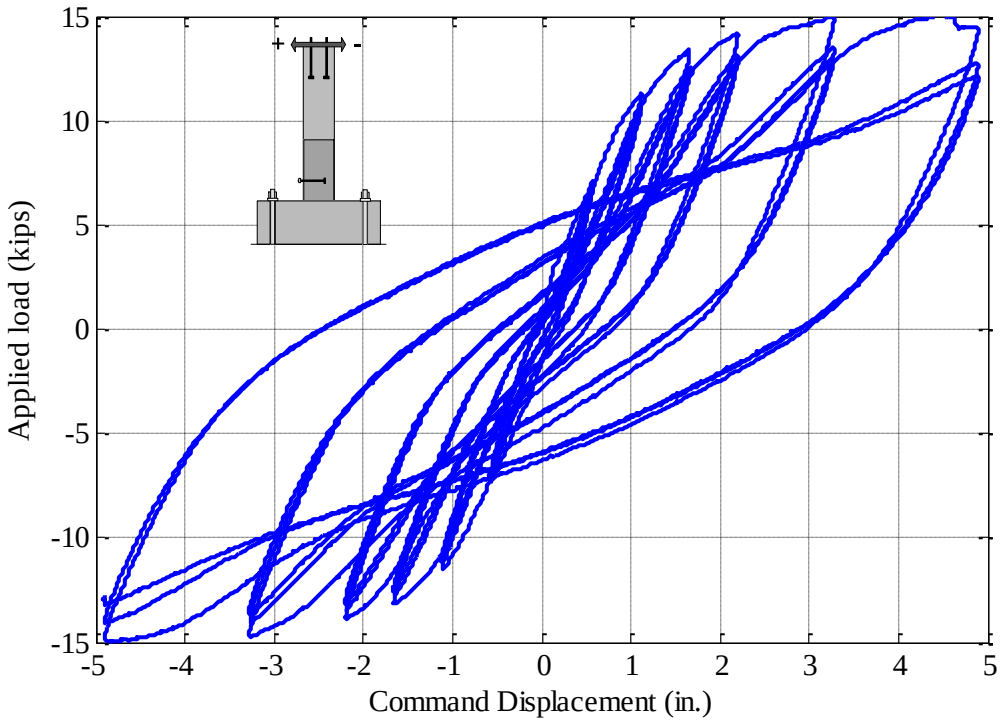

Figure 4.11: Load vs. command displacement of the column T3

±0.58 in. cyclic displacement

The column had its first crack near 3 kips. Cracks showed up at the location of 0.0 in. and 4.0 in. above the concrete base almost simultaneously, as shown in Figure A.8. After the cracks, the column stiffness reduced to about 1/3 of its initial uncracked stiffness. The cracking load is similar to the predicted cracking load with ACI design equation (9-9). New cracks developed upon further loading at 12 in. above the concrete base, which corresponded to a plateau near 6 kips of the load on the curve in Figure A.8. In addition, some smaller cracks occurred at maximum load level near 7.13 kips.

At the targeted displacement, the strain gage at the column base detected a strain increase of 3000 micro-strains, slightly larger than the yield strain of No. 5 bars. The increase in the strain may have been attributed to the interface crack developed in this step. This indicates that the yield displacement was likely slightly less than 0.5 in.

The load vs. displacement curve had positive slope after the first crack till the command displacement of 0.58 in. The actual column displacement was 0.52 in. The unloading curve from the targeted yield displacement had a slope in between the uncracked column and the cracked column. This was comparable to the experimental observation in the literature [Kreller, 1989]. The load vs. displacement curve in the negative-displacement direction (pushing column away from the top actuator) had a positive slope till the targeted negative command displacement of 0.58 in. the zigzag with short plateau on the load vs. displacement curve attribute to the new cracks developed at the south side of the column. The peak load reached up to -7.52 kips at the maximum negative targeted displacement, which is slightly higher than the positive peak load when the column was toward the positive displacement (pulling column toward the top actuator). The actual column displacement rose up to -0.5 in, which had a 14 percent decrease as compared to the commanded displacement. It confirmed the previous observation in T2 test that pulling column toward the actuator may more likely reach targeted displacement than pushing column away from the actuator, which is because the potential rigid movement of the test block may be restrained by the wedged beam underneath of the actuator when the column was subjected to pulling.

Reloading curve in the positive direction at the second cycle did not follow the original loading curve because of the existing cracks after the first loading cycle. The reloading to the targeted

yield displacement Δ_y did not achieve the peak load of 7.13 kips, as shown in the first cycle. However, such small degradation about 1 percent should be explained as the difference between the cracked column and the uncracked column.

After the three cycles in the first group, the observation demonstrated that the cracks was roughly symmetric distributed through the column. Also, the cracks were measured for both sides of the column and the crack width at the 4 in. above the base reached 0.6 mm.

±1.12 in. cyclic displacement

New flexural cracks were observed, as shown in Figures A.7, when the applied load was 8 kips toward the targeted positive displacement of 1.12 in. for the second group loading. Such cracks also corresponded to the zigzag points in the load vs. displacement curve. An obvious sharp change of the column stiffness due to the first cracking at the first group cycles, the column stiffness gradually decreased toward the targeted displacement. New smaller cracks developed up to 46 in. above the concrete base. Maximum load reading had a level of 11.2 kips when the column reached the positive displacement of 1.12 in.

The actual column displacement was 1.03 in., which is 8 percent less than the commanded displacement. Obviously, as mentioned before, such variation was caused by rigid movement of the reaction frame and the specimen, which was limited by the shoring system. Loading toward the negative displacement presented the similar trend. New flexural cracks were observed at south side when the column was subjected to pushing away from the actuator, thereby leading to the further degradation of the column stiffness. The only 3 percent difference of the peak load (-11.62 kips) at the maximum negative displacement as compared to the peak load in the positive displacement demonstrated the column had a symmetric geometry, also as indicated in symmetric cracking distribution throughout the column shown in Figure A.8.

Reloading curves in either the positive or negative direction at the second and third cycles, due to the column stiffness degradation, did not follow the original loading curve but less than 4.5 percent difference in peak loads demonstrated the behavior of the column was steadily stable. Moreover, the unloading curves closely followed the former unloading curves in either positive or negative direction further confirmed the column had a stable performance under the loading.

After this group of cycle loading, the cracks steadily opened, in particular at the interface and 4 in. above the base. The crack width at the interface reached 1 mm while the two major cracks distributed at both side of the embedded anchor had a width of 0.8 mm.

±1.66 in. cyclic displacement

The first loading curve was *concave upward* at very low stress levels by following the last reloading curve and then loading curve was actually characterized by a concave downward behavior when the column passed the 1.12 in. displacement toward the new targeted displacement. Correspondingly, new flexural cracks as well as the further opening of the original cracks near base were observed, as shown in Figure A.9, when the column was subjected to the targeted positive displacement of 1.66 in. Flexural crack was observed in the base block at the north side when the load was 12 kips and such crack also corresponded to the short plateau in the load vs. displacement curve in Figures 4.10 and 4.11. The column stiffness further decreased with the development of the cracks. Maximum load reading had a level of 13.5 kips when the column rose up to the positive displacement of 1.66 in.

Several short plateaus, due to the new flexural cracks, exhibited in the load vs. displacement curve during the column toward the negative targeted displacement. The peak load reached at -13.28 kips when the column was at the -1.66 in. displacement, which is compatible to the 13.5 kips in the positive displacement.

The column stiffness degradation was more obvious than the last group of the loading. The peak loads at 12.49 and -12.8 kips were not reached as the same level as the first cycle during the second cycle of loading in the either positive or negative direction. The difference between the first cycle and second or third cycle reached up to 7.8 and 9.6 percent in the positive direction while 3.5 and 5.1 percent in the negative direction, respectively. However, the unloading curves closely followed the last unloading curve, indicating that the column behavior was stable and, in particular, the shape of the hysteretic loops of the column appeared to be healthy without apparent pinching.

Again the reloading curve is characterized by a concave upward behavior as compared with the concave downward behavior in first loading curve. For example at a displacement of 1 in., the load was near 10 kips during the first loading while the load was only 7.5 kips during the reloading. A splitting crack occurred at the top of the column on the East face. The inspection

after the test demonstrated that such crack was caused due to not flat concrete top, which in turn caused the load plat pushing out the northeast corner because of the local elevation. Three scratches on the load plate responded on the uneven surface on the top of the column. Also, from this cycle, the loading plate started sliding on the top of the column top, correspondingly leading to clicking sounds during the test. The sliding can be seen from a sudden increase in the difference between the actuator displacement and the actual column displacement.

After three cycles in this group, the cracking continued propagation and opened. The crack width at the interface reached 1.5 mm while the two major cracks distributed at both side of the embedded anchor had a width of 1.25 mm. The smallest cracks at the 48 in. above the base had a width of 0.3 mm.

±2.2 in. cyclic displacement

Some diagonal or branches of the cracks started propagated from the original flexural cracks, as shown in Figure A.10. The loading capacity, due to the yielding of longitudinal reinforcement, did not increase dramatically, which in turn did not cause further flexural cracks through the height. Identical to previous observation, the loading curve followed the reloading curve of last load cycles. Beyond the 1.66 in. of the last targeted displacement the load-disp. curve became concave downward till 2.2 in. The unloading curve first had a decreasing slope of 11.8 kips/in. till 1.0 in., below which the load became negative (though the displacement was still in the positive region). At zero displacement, the column top rotation was 0.2 degree along counter-clockwise direction, indicating that the column was slightly twisted due to the cracking propagation in the concrete unevenly. The smaller slope for both unloading and the following reloading path near the neutral position were observed as compared to the reloading curve at higher stress level. The peak load in the negative direction was -13.99 kips. The unloading curve followed a slope of about 3.0 kips/in till -1.0 in., beyond which the unloading slope reduced and the load changed the sign similar to the positive-direction unloading. The reloading curve started following the loading curve at 0.5 in. rather than a concave downward shape, the reloading curve was concave upward till the targeted displacement at 2.2 in. The reloading curve again changed its slope at about -1.0 in. The peak load at the third cycle in the positive direction was 12.9 kips, with a 7.0 percent drop compared with the first loading and 2.4 percent drop from the second loading while 13.3 kips in the negative direction compared with 3.7 percent with the first loading and 1.6 percent drop from the second loading.

The measurement of the crack growth for the whole column was conducted when the column reached the maximum displacement in the either positive or negative direction after the three cycles. The crack width at the interface reached 3 mm while the major crack below the embedded anchor had a width of about 3 mm, by which the load transfer at the anchor in tension stage may find a shortcut.

±3.28 in. cyclic displacement

Crack further opened concentrated in plastic hinge zone with the increase of the loading level, in Figure A.12. The loading started with slipping of the loading plate near 0.7 kips in tension. Such slip was signaled by a series of clicking sounds when the displacement was below 0.8 in. The slip of the loading plate did not occur in previous cycles most likely because by now the shim plates inside the bolt hole of the loading plate has already been damaged, thus allowing relative movement of the loading anchors and the bolt holes. Unlike the T2 test where relative movement was partially restrained by two nuts when they were pushed up to grinding concrete surface, such relative movement, however, may have directly contributed to relatively larger difference between the commanded displacement and actual column displacement because there was always an opening gap between nuts and concrete surface through the test to restrain the movement. The concrete surface started spalling near the base. Such concrete cover spalling was signaled by a series of crushing sounds when the loading was up to 14 kips. One piece of concrete cover was crushed and spalled out at the southwest corner at the base, which was responded to the sharp drop at the load curve at 14.9 kips. The load was 14.87 kips at the peak when the column reached positive displacement 3.28 in.

The unloading curve again was parallel to other unloading branches till 2.0 in. near the zero load. The reloading curve started at about 2.0 in. following a smaller slope. The reloading path in the positive direction, as identical to previous statement, was concave upward and the difference between the load path and reloading path at about 2.0 in. was as large as 4.5kips. The reloading slope started increasing beyond 2.0 in. until the peak load was 13.5 kips. Such difference between the loading path and the reloading path was mainly because of concrete crushing: concrete crushed as load increased during the loading process; the crushed concrete did not recover after the loading came back from the opposite direction, thus causing relatively higher column rotation, which in turn reduced the moment arm permanently and finally resulting in the smaller loads corresponding to the same displacement. Such difference toward the achieved

loads was smaller in the negative direction as compared to the positive direction. This might have been due to the fact the tension force (pulling the column), along with a downward (counter clockwise) rotation caused a resulting compression force at the south side of the column, thereby causing more concrete crushing, identical to the similar observation in T2 test. When the load was applied in the negative direction (pushing the column) the upward (clockwise) rotation caused a resulting small tension that reduces the net compression at the north side of the column, thus resulting in less crushing of concrete. Therefore, the load difference was mainly caused by the crushed concrete that was vulnerable to allow more rotation and thus reduced the moment arm. Note that such load difference in both directions in the applied horizontal loads may not show up in the actual RC columns or beams, which may deform evenly in both directions along with the rigid floor. The reloading path in the positive direction was slightly lower than the first reloading. This was attributed to the fact that the peak load during the first reloading was lower than the first peak load, thus causing insignificant increase in concrete crushing. The unloading path followed the first unloading path closely.

±4.9 in. cyclic displacement

The loading in the positive direction followed the reloading curve of the last cycle till 3.28 in. beyond which the loading curve turned concave downward. The peak load occurred before the targeted displacement at 14.9kips. The load dropped suddenly after the peak point, which corresponded to roughly 0.75 in. thick concrete cover crushed and separated from the column. The load drop was about 0.6 kips, indicating that the neutral axis shifted in by 1/4 in. from the initial axis. Such load drop did not show up in T2 test. This is mainly because the crushed concrete covers were removed during the test, thus leading to a smooth stiffness degradation curve rather than sharp drop. Unlike the positive direction, the peak load in the negative direction did not drop notably, even though the load increased near the targeted displacement fluctuated and picked up 15 kips in the end. This peak load was only by 0.1 kips higher than that in the positive direction. To place the load on the anchor in cyclic tension by following details in the next section, the column remained at the negative maximum displacement.

Comparison of the crack growth and crack density under various cyclic loading levels was plotted in Figure A.14. Most cracks concentrated in the plastic hinge zone at the end of the last cyclic loading. The crack width at the base opened up to 9 mm while the major crack below the embedded anchor had a width of about 8 mm, as shown in Figure 4.12.

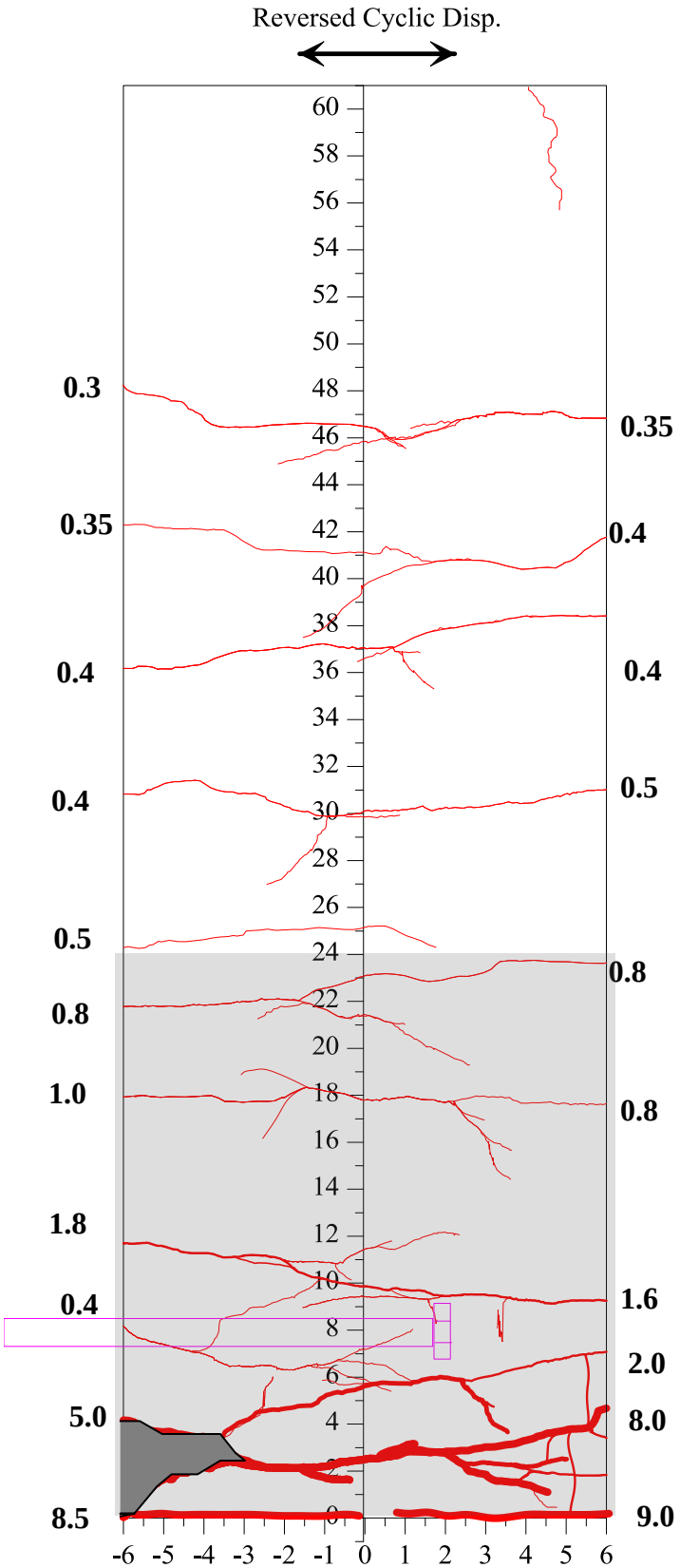

Figure 4.12: Crack patterns in Column T3 and measured crack widths after cyclic loading

4.2.2 Behavior of anchor in T3 under Cyclic Loading

The load vs. displacement behavior for the anchor in Specimen T3 is shown in Figure 4.13. The cyclic behavior is plotted along with the monotonic behavior of the anchor in Specimen T2 for comparison purposes.

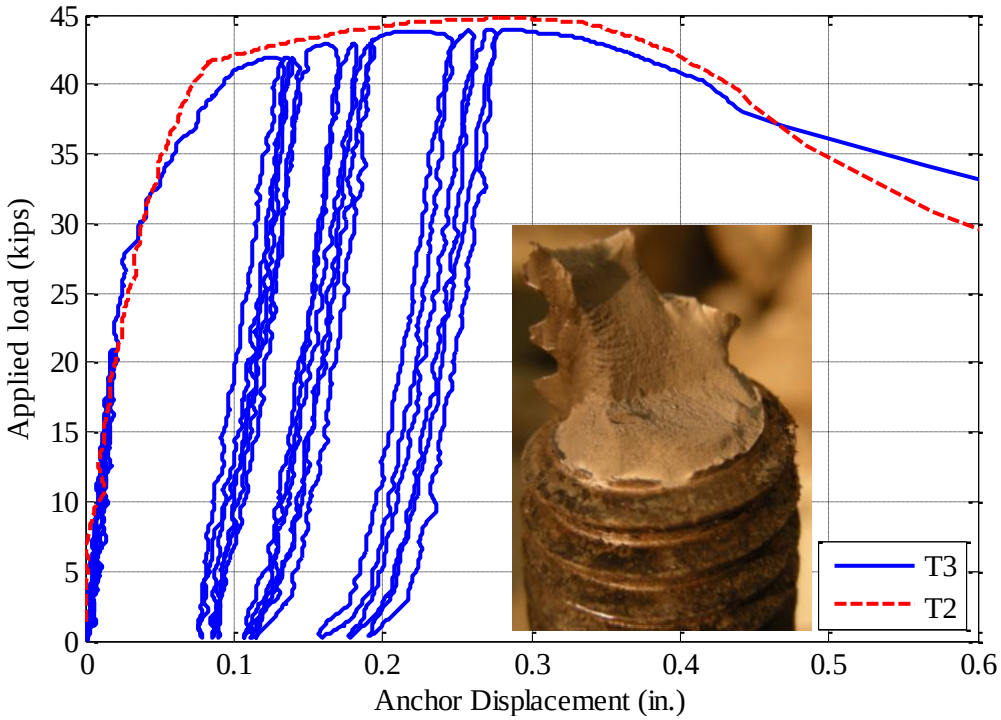

Figure 4.13: Behavior of anchor is Specimen T3 under cyclic loading

The anchor behaved elastically in the first group toward the loading of 21 kips. A large diagonal crack, as observed in Figure 4.14a, occurred during the first round toward 42 kips. This was similar to that observed in T2 test. Such diagonal crack was mainly because the force placed on the embedded anchor was transferred into the concrete cone that was confined by anchor reinforcement toward the lower support at the base and the upper support by the top actuator. The tensile load on the anchor in turn caused a bending moment in the column, which led to concrete cover cracks along outside of the anchor. Such additional bending (Figure 4.14b), due to forces from both top and bottom actuators, resulted in such high compressive force on the north surface of the column outside of the anchor head that finally caused the large piece cracked concrete crushed and separated away from the column, as illustrated in Figures 4.14b and 4.14c.

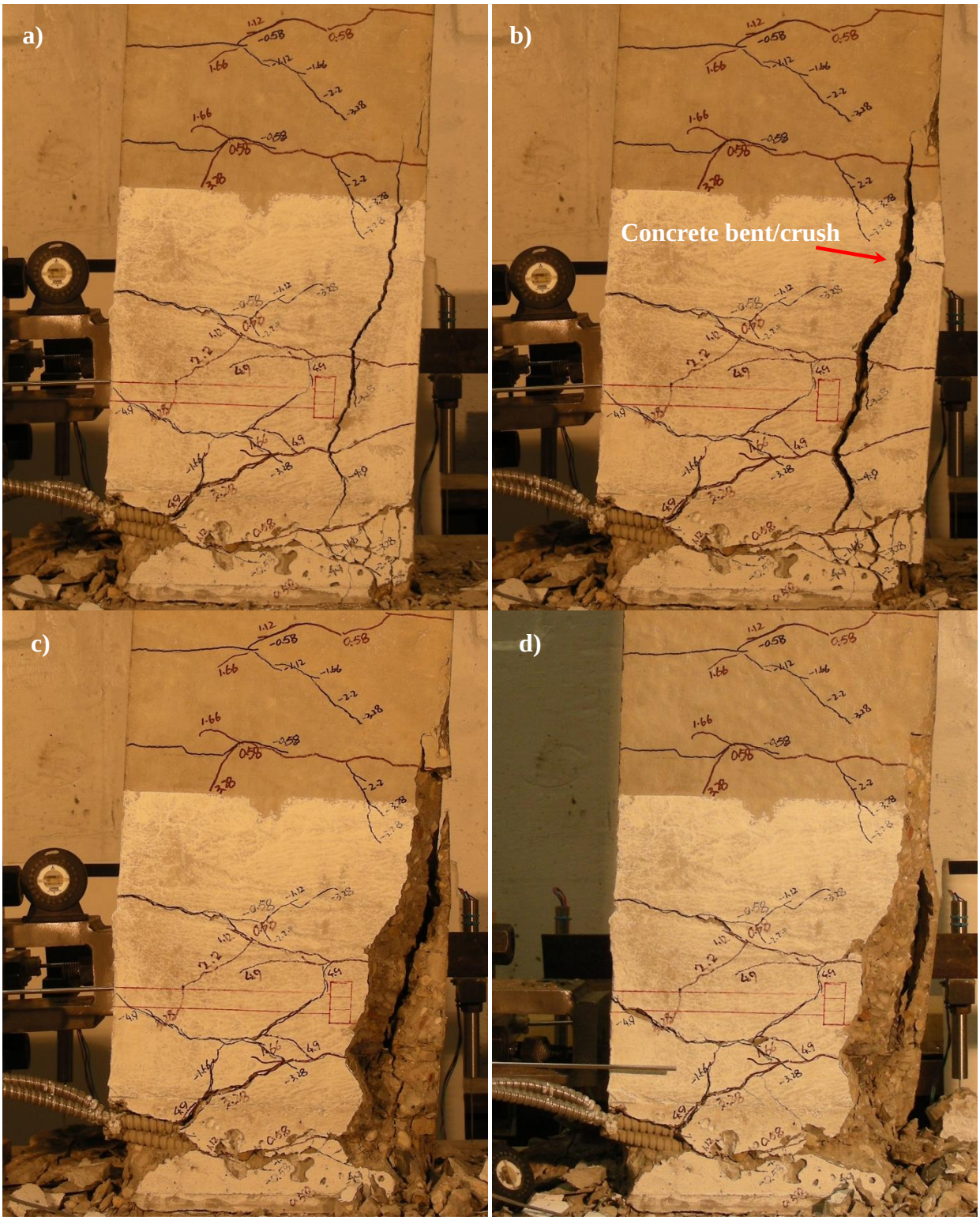

Figure 4.14: Cracking in column whne the anchor subjected to cyclic tension (T3)

The comparison of the load vs. displacement curve at the monotonic loading (T2 test) and cyclic loading in this case (T3 test) in Figure 4.13 indicated that the load curve followed the monotonic

path closely till the failure. The small difference was mainly caused by upward orientation of the anchor in this case (T3) that may cause an additional small bending as well as governing tension on the anchor shaft when the anchor was subjected to tension, thus leading to the slightly low load path and final capacity. The difference may also have come from variations built in experimental tests.

The anchor remained steady at the load level of 44 kips without too much additional displacement. According to potential failure modes calculation in Chapter 3, the column will be able to take 61.8 kips before a flexural failure occurs. With the diagonal cracks path, the anchor tension force was now transferred to the rest of the column through the dry friction (as schematically shown in Figure 4.15a and grinding powder found at the entrance of friction surface in Figures 4.15b and 4.15c). The sliding surface was along a flexural crack above the base, which was opened before the tension force was applied to the anchor. This was slightly different from the monotonic loading in T2. According to the monotonic loading curve in T2, the anchor at a commanded displacement of 0.58 in. at 43 kips, however, was compatible to that of 0.6 in. at the same loading level. This means that the column was stable without obvious degradation under cyclic loading and can still carry more loads.

At 44-kip targeted load, the actuator did not reach the 44 kips, instead, it went unloading at about 43.6 kips. The actuator displacement increased notably, indicating that the anchor steel was yielded, as shown in Figure 4.13. The third cycle of loading showed that the anchor was able to achieve 43.9 kips. In this group of loading, the displacement increase (from actuator reading) was higher than the last two groups. Monotonic tension was applied after the cyclic loading. The anchor bolt was able to carry a tension load of 43.99 kips, which is slightly smaller than the capacity of the anchor subjected to monotonic loading. The similar behavior indicated that the concrete core was well protected by anchor reinforcement, as shown Figure 4.15c.

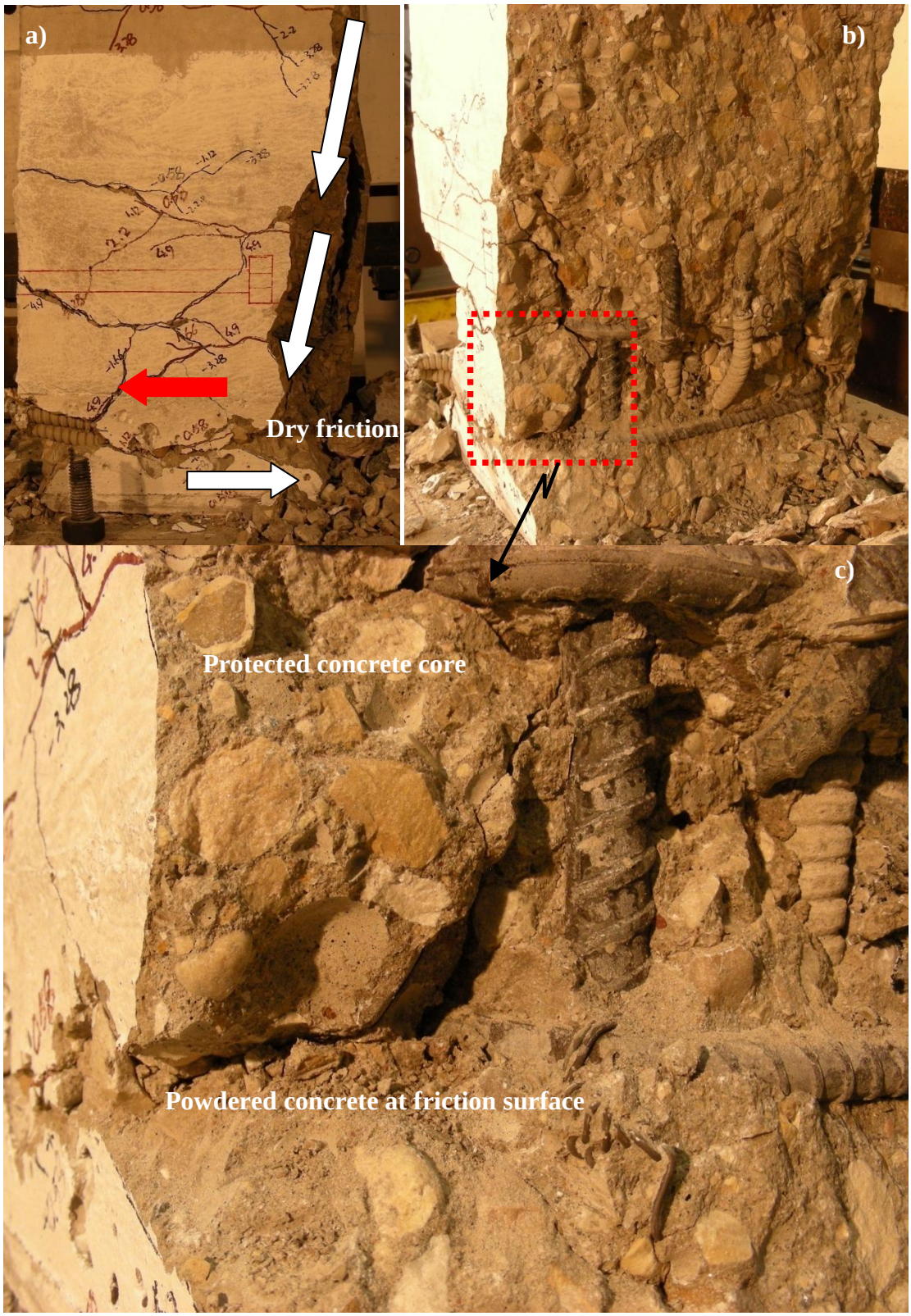

Figure 4.15: Evidence of final failure and load transfer path (T3)

The load vs. anchor displacement for both T2 and T3, as plotted in Figure 4.13, demonstrated that the steel ductile tension failure was achieved for anchors installed in plastic hinge zones under both monotonic and cyclic loading. It confirmed that the proposed anchor reinforcement and the needed local confining reinforcement are effective. Additional study is needed to fully develop a design method.

4.3 Test of Specimen S1

Anchor connection, in particular in bracing and damping system, may be installed in side wall or sides of the columns. As such, anchors may be subjected to shear force. The second group of tests of two single anchors in shear were dedicated to provide related information.

4.3.1 Behavior of Column S1 and Crack patterns under Cyclic Loading

This was the first shear test. The column was subjected to cyclic loading before the two single anchors were loaded in monotonic shear. The column behavior is shown below: the load vs. actuator displacement curves in Figure 4.16 and the load vs. column displacement curves in Figure 4.17. The column had a initial offset (3/4 in. away from the actuators), therefore the load vs. displacement curves are not symmetric and the maximum displacement was ±4.8 in.

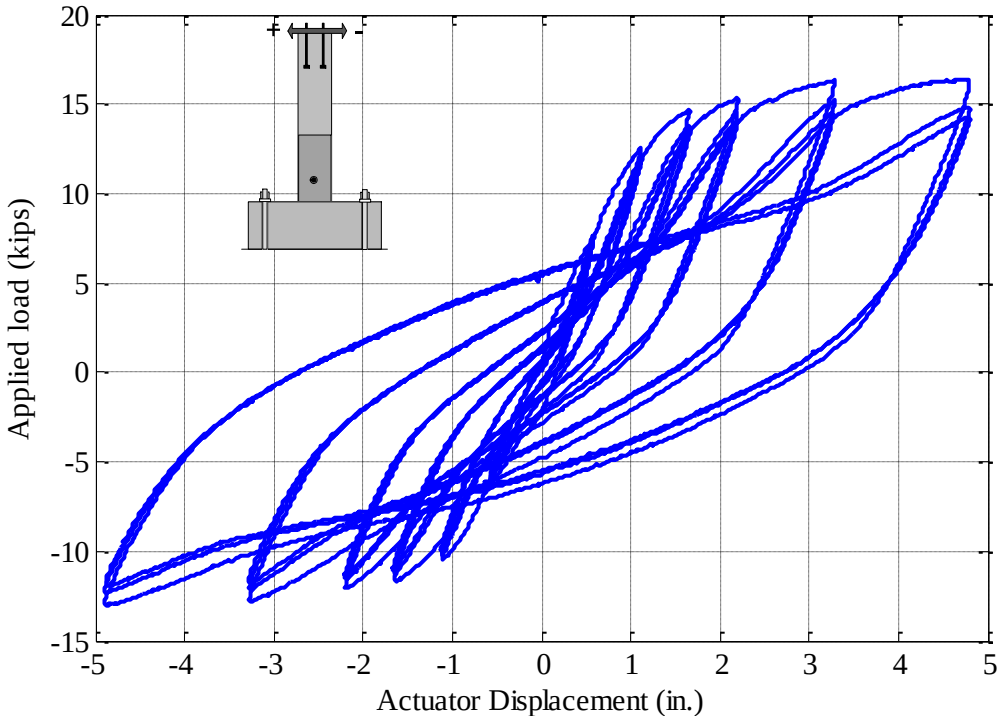

Figure 4.16: Load vs. actuator displacement for Specimen S1

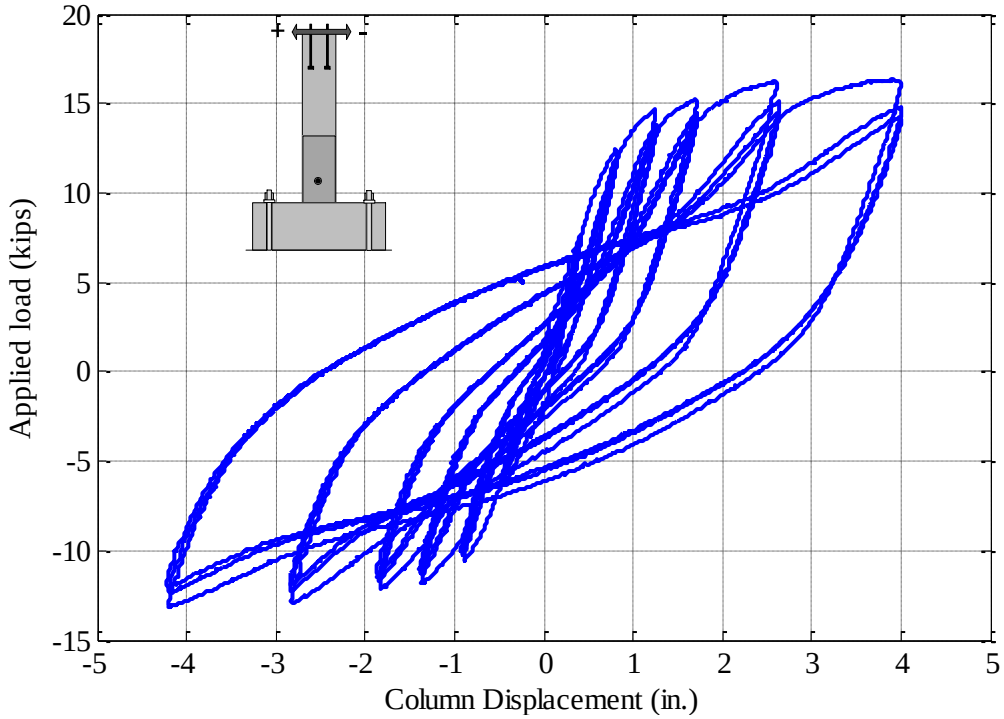

Figure 4.17: Load vs. column displacement for Specimen S1

±0.58 in. cyclic displacement

The load curve had a first short plateau near 3.5 kips, indicating the first crack. Cracks developed at 0.0 in., 6 in. and 12.0 in. above the concrete base almost simultaneously, as shown in Figure A.15. After the cracks, the column stiffness, similar to the column T3, reduced to about 1/3 of its initial uncracked stiffness, as observed in Figure A.15c. New cracks developed at 16 in. above the concrete base with further loading, which corresponded to a plateau near 4 kips of the load on the curve in Figure A.15c. Some smaller cracks then developed, which are related to several zigzag points shown in loading curve at maximum load level near 7.5 kips.

The load vs. displacement curve had a positive slope after the first crack till the targeted displacement of 0.58 in. The actual column displacement was near 0.50 in., which is 14 percent less than the commanded displacement of 0.58 in. Such variation, as described in previous tests was mainly because of the rigid movement of the uplift of the actuator, test block, and the frame.

The unloading curve from the targeted yield displacement, identical to the previous observation in S1 test, had a roughly constant slope in between the uncracked column and the cracked column. The load curve in the negative-displacement direction had a similar characteristic as that in positive direction. A positive slope was hold till the targeted negative displacement of

0.58 in. First short plateau on the load curve at about -3 kips in negative direction attributed to the new cracks at the south side of the column. After that, the stiffness slope decreased to 1/3 of the original loading slope. The peak load only had a level of -6.6 kips at the maximum negative targeted displacement, which is 13 percent smaller than that in the positive peak load. The actual column displacement was -0.51 in.

Reloading curve in the positive direction at the second and third cycles did not follow the original loading curve but presented the concave upward behavior because of the existing cracks after the first loading cycle. The reloading to the targeted yield displacement resulted in a load of 7.5 kips (7.4 kips in the third cycle), within 3 percent difference between the cracked column and the uncracked column. Concrete compressive damage was not prominent at this stage.

After the three cycles, the cracks were measured through the column. Among them the major cracks distributed at the both sides of the anchor near the base had a width of 0.4 mm at south side and 0.3 mm at north side, which is slightly smaller than that in the same loading level in previous tests in T2 and T3.

±1.12 in. cyclic displacement

The loading curve followed the reloading curve of last load cycles, as shown in Figure 4.17. Beyond the 0.58 in. of the last targeted displacement the load vs. displacement curve became concave downward. New flexural cracks were detected, as shown in Figures A.16, when the applied load was 8.5 kips. Such cracks corresponded to a short plateau in the load vs. displacement curve and similar zigzag points exhibited at 10.4 and 11 kips, respectively. The column stiffness degraded further due to yielding of bars. Some small cracks developed up to 42 in. above the concrete base. The peak load was 12.49 kips when the column reached the maximum positive displacement, which was 12 percent higher than that in the same displacement level in previous tests in T2 or T3. Correspondingly, the load was -10.5 kips at the peak when the column was loaded till the negative maximum displacement, which was 10 percent smaller than that in the same displacement level in previous tests in T2 or T3 and almost 2 kips difference between positive and negative directions. This may have been related to the initial crookedness of S1. This column an in-plane offset of 3/4 in. and an out-of-plane offset of 1.0 in., measured from the top face. This in-plane offset caused a shift of the column reinforcing cage in the form. An after-test survey indicated that the longitudinal bars had a concrete cover of

2.5 in. at south side, while the concrete cover at north side was only 1.5 in. This indicated that the column reinforcement shifted about 0.5 in. toward the north side (negative direction). This would cause a higher moment capacity in the positive direction, as shown in Figure 4.17, when the actuator was pulling the column.

Reloading curves in either the positive or negative direction at the second and third cycles, as shown in Figure A.16c, due to the column stiffness degradation, did not follow the original loading curve. The column had a less than 6 percent difference in peak loads (even smaller than 3 percent in the negative direction), and the unloading curves closely followed the former unloading curves in either positive or negative direction however. These observations demonstrated the behavior of the column was stable at this stage of loading

The actual column displacement at the first loading cycle in either positive or negative direction was 1.00 in., with an 11 percent less than the commanded displacement of 1.12 in. Even though such difference may respond to rigid movement of the loading system and test specimens, partial movement from the frame movement was recognized from the dial gage reading of a 0.05 in. during the test. With the increase of the cracking growth and propagation, the crack width at south side near the base increase to 1 mm from 0.4 (at last loading level) while correspondingly the crack width at north side, due to slightly lower loading level, was only 0.6 mm. One major through-crack distributed at 4 in. above the base had a width of 0.5 mm.

±1.66 in. cyclic displacement

Similar to the observation in previous tests, the first loading curve (Figure 6.10) was concave up following the last reloading curve and then loading curve, but concave down when the column passed the displacement 1.12 in. toward the new targeted displacement. Further opening of the existing cracks near base were observed, as shown in Figures A.17, when the column was subjected to the targeted positive displacement of 1.66 in. Flexural cracks were observed at the north side in the base when the load was 13.4 kips and such crack also corresponded to the apparent plateau in the load vs. displacement curve in Figure A.17c. The column stiffness further decreased with the development of the cracks. The maximum load was 14.58 kips when the column was 1.66 in.

Several short plateaus, due to the new flexural cracks, exhibited in the load vs. displacement curve in Figure 4.17 when the column was loaded back toward the targeted negative

displacement. The peak load was -11.82 kips when the column was at the -1.66 in. displacement, with roughly 3 kips difference (by 19 percent) to that in the positive displacement. Such difference was again due to the shift of reinforcement as mentioned above.

The first reloading in the positive/negative direction had an apparent drop from the loading curve, as indicated by the shaded area in Figure A.17c. For example, the loading level in the positive direction had a roughly 3-kip load drop at a displacement of 1 in as compared to the loading curve. The peak load was 13.73 kips, which was almost 1 kip difference from the first loading. The following unloading curve was thus lower than the first unloading by roughly 1 kip. The column may have been shifted towards the strong wall (west) such that one of the LVDT's for the anchors, resting on the column at 16 in. above the foundation beam, had a ¼ in. offset and the spring loaded core fell out of the column face. Note that this may also have been caused by the lateral movement of the actuator piston not connected to the column. The lateral movement may have been caused by the shake from the top of the column where the loading plate adjusted its position constantly due to the gap between the loading anchors and the bolt hole in the loading plate. This was confirmed later by observing the position of the foundation beam. Near the zero position, the second round unloading had more pinching. The reloading in the negative direction reached -14.4 kips, a smaller drop in the load compared with the positive direction. The following unloading curve was thus slightly lower than the first unloading from the negative peak. The second reloading in the positive direction reached 13.5 kips while the unloading curve followed closely the second unloading path.

±2.2 in. cyclic displacement

The loading capacity, due to the yielding of longitudinal reinforcement, did not increase much in this group of loading, which in turn did not cause further flexural cracks in the column (Figure A.18). Identical to previous observation, the loading curve followed the reloading curve of the last load cycles, as shown in Figure 4.17. Beyond the 1.66 in. of the last targeted displacement the load-disp. curve became concave down till 2.2 in. The peak load was 15.21 kips when the column was loaded to 2.2 in. Concrete cover near the base at the south side was crushed and separated away from the column, causing a reduction in the internal moment arm, which in turn affected the reloading capacity. At zero displacement, the column top rotation, as revealed in Figure 6.16, was 0.4 degree along counter-clockwise direction, indicating that the column was

slightly twisted due to the cracking propagation in the concrete unevenly. The smaller slope for both unloading and the following reloading path near the neutral position were observed as compared to the reloading curve at higher stress level. The peak load in the negative direction was -12.18 kips and thus the difference of the peak load between positive and negative direction reached up to more than 3 kips as anticipated.

The difference between the loading and reloading curve further increased with an increase of the loading level. This difference in the positive direction, due to having a relatively higher loading level, was more pronounced than that in the negative direction, as shown in shaded area in Figure A.18c. The unloading curve, followed a constant slope till -1.0 in., beyond which the unloading slope reduced and the load changed the sign similar to the positive-direction unloading. The reloading curve started following the loading curve at 0.5 in., the reloading curve was concave upward till the targeted displacement at 2.2 in. The reloading curve again changed its slope at about -1.0 in. The peak load at the third cycle in the positive direction was 14.07 kips, with a 7.5 percent drop compared with the first loading and 2.4 percent drop from the second loading. The peak load was -11.5 kips in the negative direction, with a 5.6 percent drop compared with the first loading and a 1.6 percent drop from the second loading.

The measurement of the crack growth for the whole column was conducted when the column reached the maximum displacement in the either positive or negative direction after the three cycles. The crack width at the interface reached 2.5 mm while the major crack below the embedded anchor had a width of about 2 mm.

±3.28 in. cyclic displacement

The first loading curve again followed the reloading curve of last load cycles till the last targeted displacement, as shown in Figure 4.17. Several pieces of concrete cover were crushed and separated from the south surface near the base, as shown in Figure A.19. The peak load was 16.1 kips when the column was loaded to 3.28 in. A dial gage indicated that the reaction frame had a 0.05 in. movement.

The unloading curve again was parallel to other unloading branches till 2.0 in. near the zero load. The reloading curve started at about 2.0 in. with a small slope. The reloading path in the positive direction was concave up and the difference between the load path and reloading path at about 2.0 in. was as large as 4.0 kips. The reloading slope started increasing beyond 2.0 in. until the

peak load reached at 15.1 kips. Such difference between the loading path and the reloading path was mainly because of concrete crushing. Similarly, the reloading path in the positive direction at the third cycle was slightly lower than the first and the second reloading cycle. The unloading path followed the first unloading path closely.

±4.8 in. cyclic displacement

Rather than a 4.9-in. target displacement in previous tests, the actuator actually was only able to apply 4.8 in. on the column because the column leaned towards the actuator by 3/4 in.. The peak load occurred at the targeted displacement of 16.3 kips in the positive direction while -13.1 kips in the negative direction. The first loading in the positive direction followed the reloading curve of the last cycle till 3.28 in. beyond which the loading curve turned concave down, as shown in Figure 4.17. The reloading at the second or third cycle curve, however, displayed different concave upward behavior, as indicated in Figure A.20. The area between the loading path and the reloading path thus corresponded to the peak load drop during the reloading cycles, as shown in shaded area in Figure A.20c. It also demonstrated that the south side (positive direction), due to the relatively higher loading level, underwent much severer damage than the north side (negative direction), thus causing larger loading drop during the reloading paths.

At the first targeted displacement, the strain gage at the column base picked a reading about 3500 micro-strain as shown in Figure 4.18. This indicates that the yield displacement was again a bit less than 0.5 in. Actually the longitudinal bars developed higher than yielding strain beyond 24 in. above the column base as indicated by the measured strain in Figure 4.19.

Comparison of the crack growth and crack density under various cyclic loading levels was plotted in Figure A.21. The flexural cracks firstly developed at the base and within the plastic hinge zone. Small flexural cracks were then observed at higher location with the increase of the loading level. The cracks widened and propagated upon further loading, in particular, at the plastic hinge zone. Most cracks concentrated in the plastic hinge zone at the end of the last cyclic loading. The crack width at the base opened up to 8 mm while the major crack at 4 in. above the base had a width of about 7 mm, as shown in Figure 4.20. Outside the plastic hinge zone, the flexural cracks were evenly distributed and the maximum crack width, measured at the surface of concrete, was 0.4 mm.

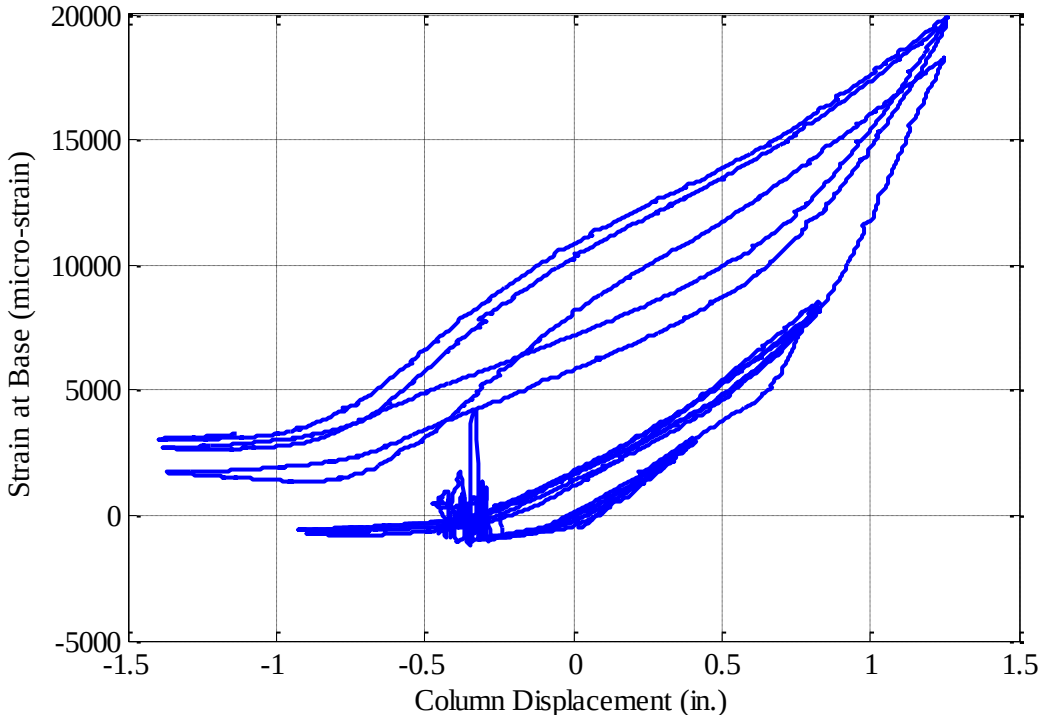

Figure 4.18: Strain development at column base in Specimen S1

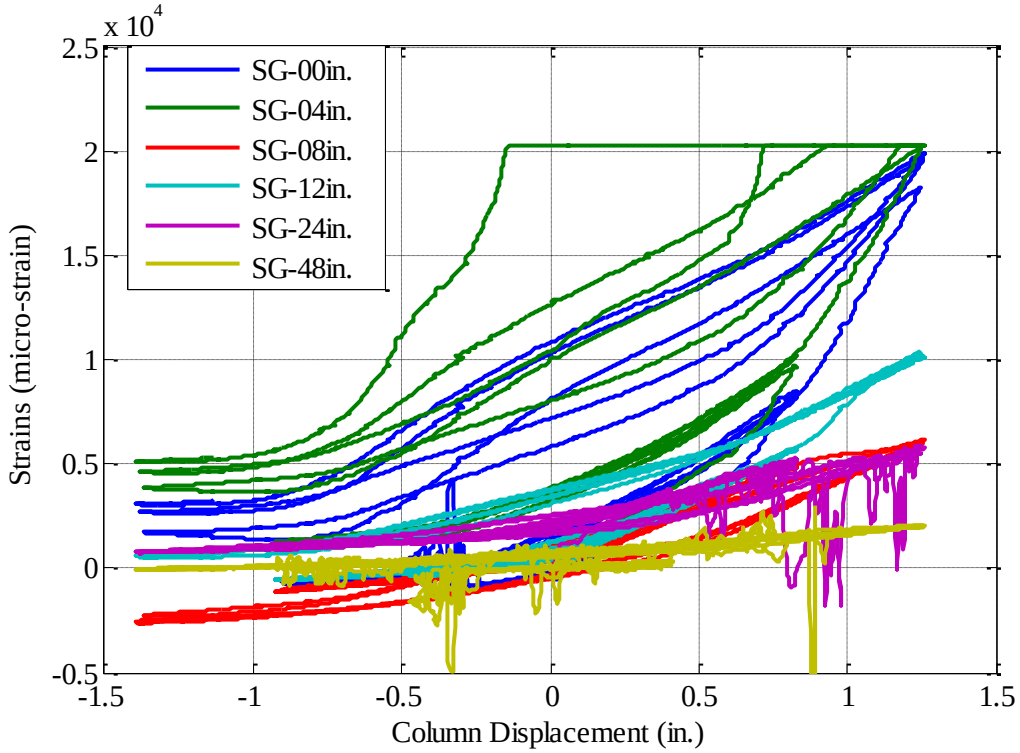

Figure 4.19: Strain development at column bars in Specimen S1

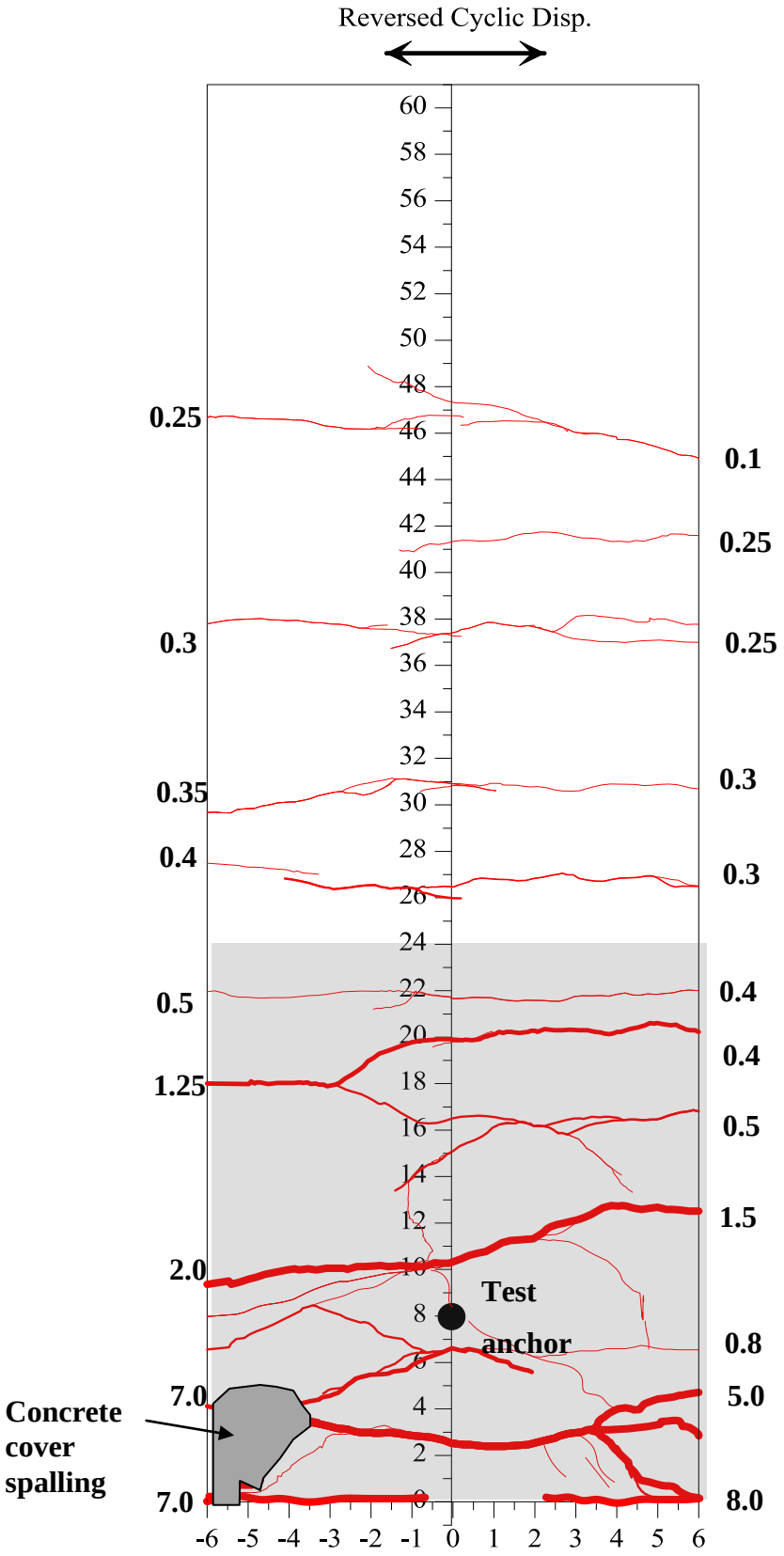

Figure 4.20: Crack patterns and measured crack widths after ±4.8 in loading (S1)

4.3.2 Behavior of two single anchors in monotonic shear

If the two single anchors could develop their full shear capacities, the final failure of the specimen would be similar to that observed in Specimens T2 and T3. A breakout crack (shown in red lines in Figure 4.21) might form, and the crack propagation would be arrested by the existing flexural cracks at about 4 in. above the base. On the other hand, it was also possible that the concrete in front of the anchor crushes, resulting in an exposed length of 1.5 in. (or $2d_a$). The exposed length will greatly reduce the anchor shear capacity such that the anchor bolt will break at about half of pure shear capacity due to combined tension and shear.

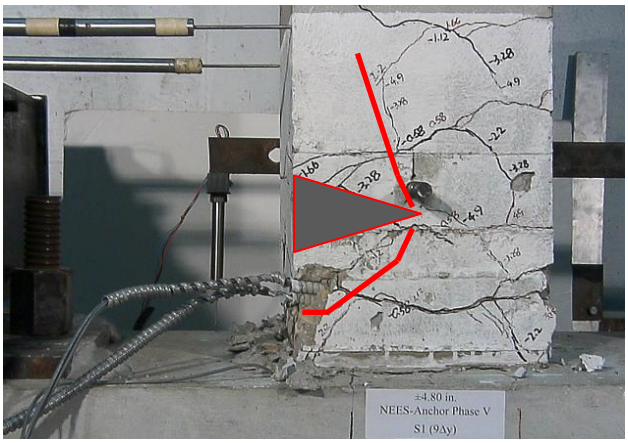

Figure 4.21: Prediction of concrete breakout before the anchor test (east surface)

The observation of the crack growth and crack propagation near the anchors was not available because of the loading plate. The observation of concrete (cover) breakout cracks was only available after they extended outside of the load plate, as shown in Figure 4.22.

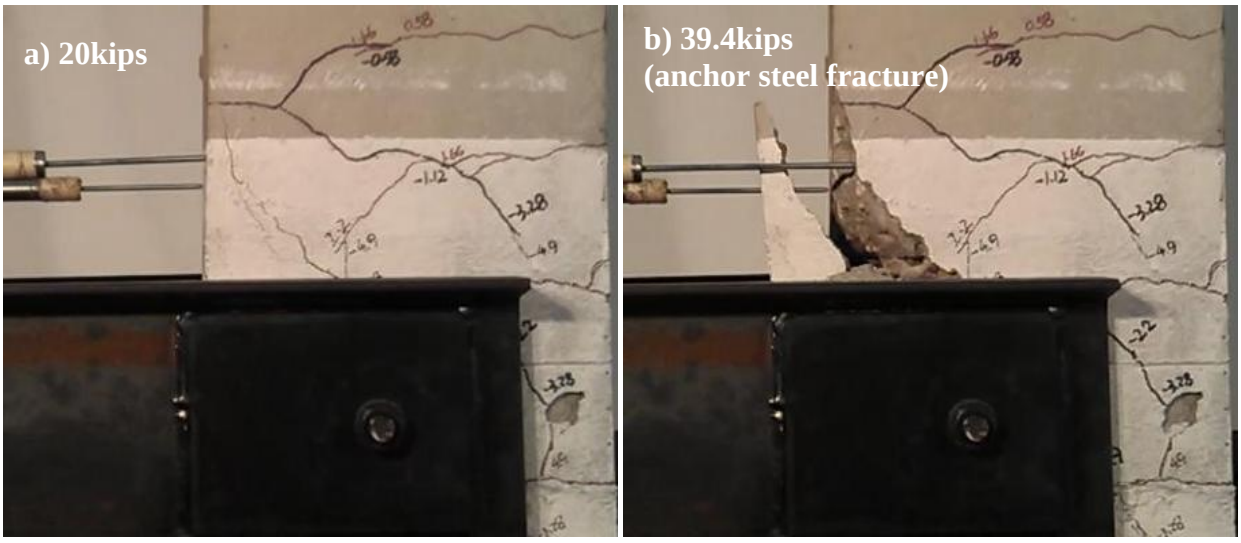

Figure 4.22: Crack pattern during the process of anchor loading (S1)

The behavior of the two single anchors subjected to monotonic shear is shown in Figure 4.23. The plot contains the combine behavior from the two single anchors. The anchors behaved elastically till about 7.5 kips, beyond which the slope reduced significantly, indicating the first cracks and crush of concrete in front of the anchors. The concrete breakout crack showed up at east surface of the column, when the anchors were loaded at 20 kips, as shown in Figure 4.22a. An after-test inspection indicated that the concrete cover on the east side was pushed out starting from an existing vertical cracks, and then the cover cracks bent out at an angle about 35 degree, as shown in Figure 4.24a. At the same time, the concrete cover cracks were arrested by the existing flexural cracks and the cracked concrete pieces were not significantly crushed, as shown in Figure 4.24b. This created a higher stiffness for the west anchor. The west anchor might have been subjected to a larger shear compared with the east side anchor, which experienced much bending deformation.

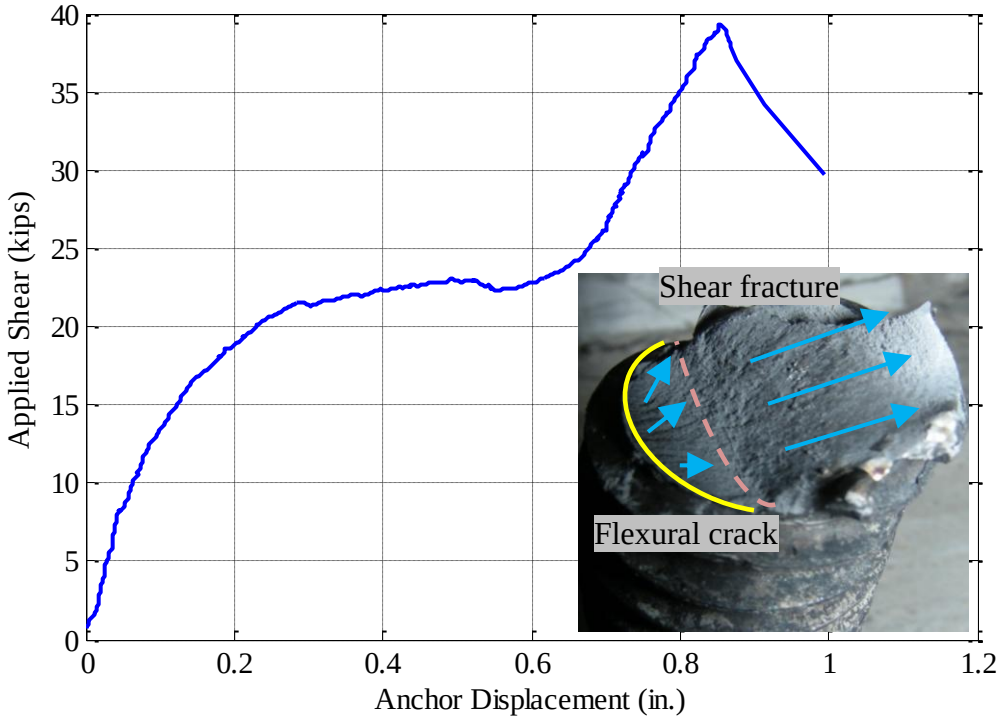

Figure 4.23: Behavior of two single anchors in monotonic shear (S1)

After the cracks, the loading level did not pick up too much as shown by a long plateau in the load vs. displacement curve in Figure 4.23. One piece of concrete cover was pushed out on top of load plate, which was responded to the sharp drop at the load curve at 23.1 kips, as shown in Figure 4.23. Such load drop may also indicate that the concrete cover was pushed out and

crushed into the pieces, which may leave the anchor shaft exposed and allow the anchor to rotation with less support, thus causing loading drop with large deformation.

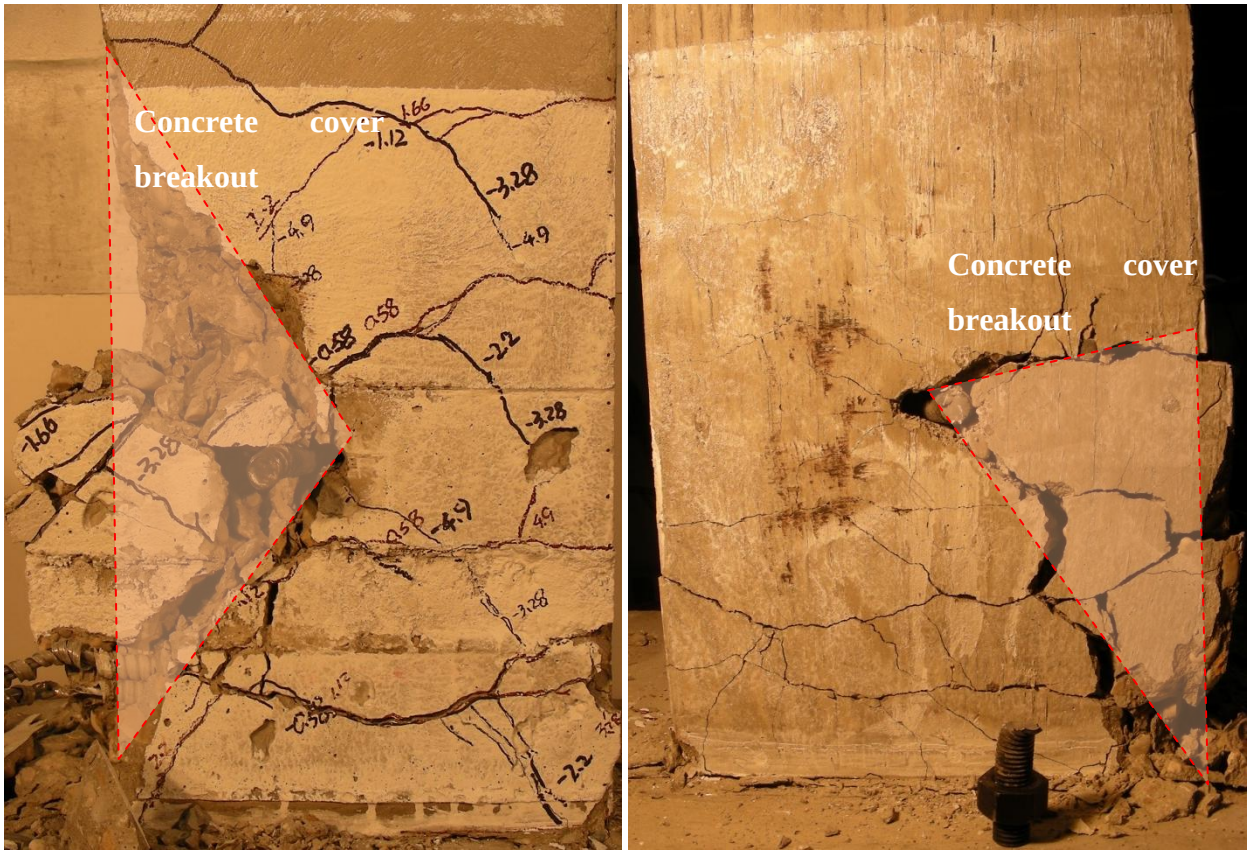

(a) East side **(b) West side (anchor fracture at this side)**

Figure 4.24: Cover crack pattern after anchor fracture in shear (S1)

The load increased with a relatively high slope when the loading was at 25 kips, suggesting that the anchor shaft carried the load till the failure by fracture. Anchor rods failed at the west side by fracture in shear while the other rod at the east side was also bent, when they were subjected to the loading level of 39.4 kips. Concrete cover at the east side, as observed in Figure 4.24a, was totally pushed away during the anchor fracture toward 39.4 kips. A close inspection showed that the concrete breakout cone at the west side started from the initial flexural cracks at roughly 2 in. above the anchor and then were pushed out toward the south, which was identical to the second potential failure mode as predicted in Figure 4.21.

Anchor rods had a peak load of 39.4 kips, which fell within the range of predicted upper limit and lower limited: (28.7 kips, 54.9 kips). The exposed length of the anchor shafts were 1.5 in. at the east and 1.0 in. at the west, which were measured after the crushed concrete were removed.

The predicted shear capacities were supposed to be 28.7 and 28.9 kips, respectively. However, the measured peak load was 39.4 kips, a bit lower than the predicted loads. Such difference may be likely caused due to partial support from the cracked concrete in front of anchor. Concrete breakout cones at both sides were not totally pushed away from the column. Instead, the concrete breakout cones were crushed into the pieces during the test, as indicated by the grinding powder due to the crushing.

In general, the load vs. anchor displacement, as plotted in Figure 4.23, demonstrated that the steel ductile failure by shear was achieved under the proposed concept, as indicated in steel fracture by the inserted picture in Figure 4.23. Such sound concrete core was able to protected under the proposed anchor reinforcement that it allowed embedded anchor to fully develop capacity, even though concrete in plastic hinge zone was suffered from severe damaged and most concrete cover was crushed and totally separated from the column.

4.4 Test of Specimen S2

The anchor in Specimen S1 failed in shaft fracture after the concrete cover was pushed away. This is similar to the observations may in the Phase II tests. Therefore the test of Specimen S2 was slightly modified. Instead of loading the anchor after the column was subjected to cyclic loading, both the column and the anchors were loaded simultaneously.

The behavior of Column S2 is plotted in Figures 4.25 and 4.26. The values in the load vs. actuator displacement curves will be referenced in the following discussion while the load vs. column displacement shows the actual behavior. Note that the anchors were simultaneously loaded with the column, therefore, the loads detected by the top actuator were affected by the force applied to the anchors. One the other hand, because the displacements of the anchors were directly monitored using two LVDT's, the anchor behavior was deemed not affected by the column loading. The behavior of the two single anchors in shear is plotted in Figures 4.27 and 4.28. Again the values in the load vs. anchor command displacement curves will be cited in the discussion.

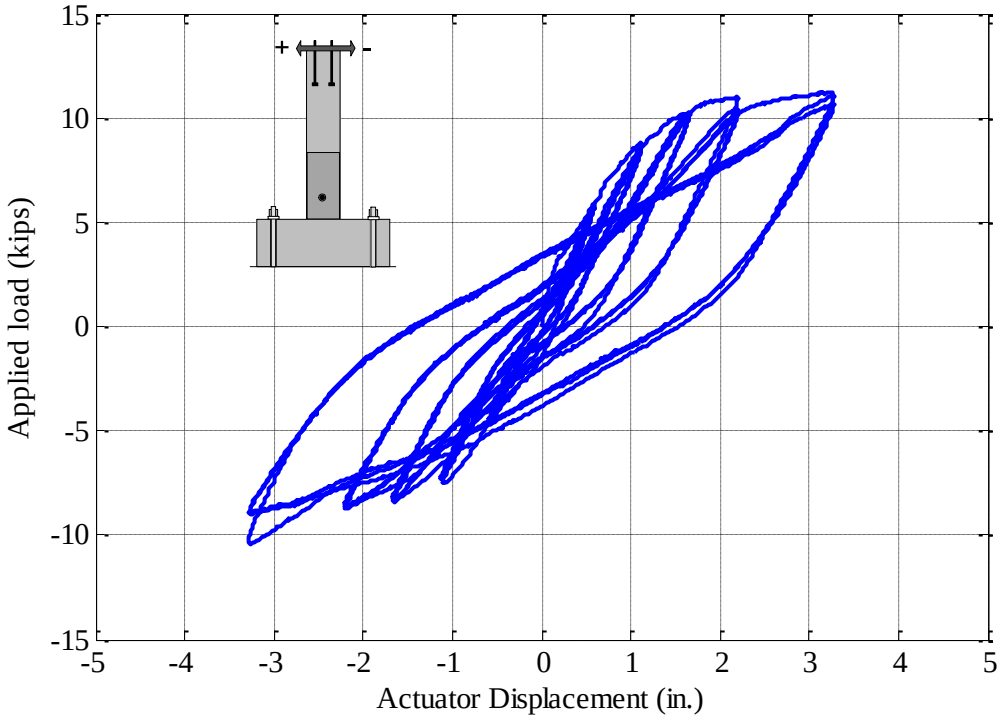

Figure 4.25: Load vs. actuator displacement for Specimen S2

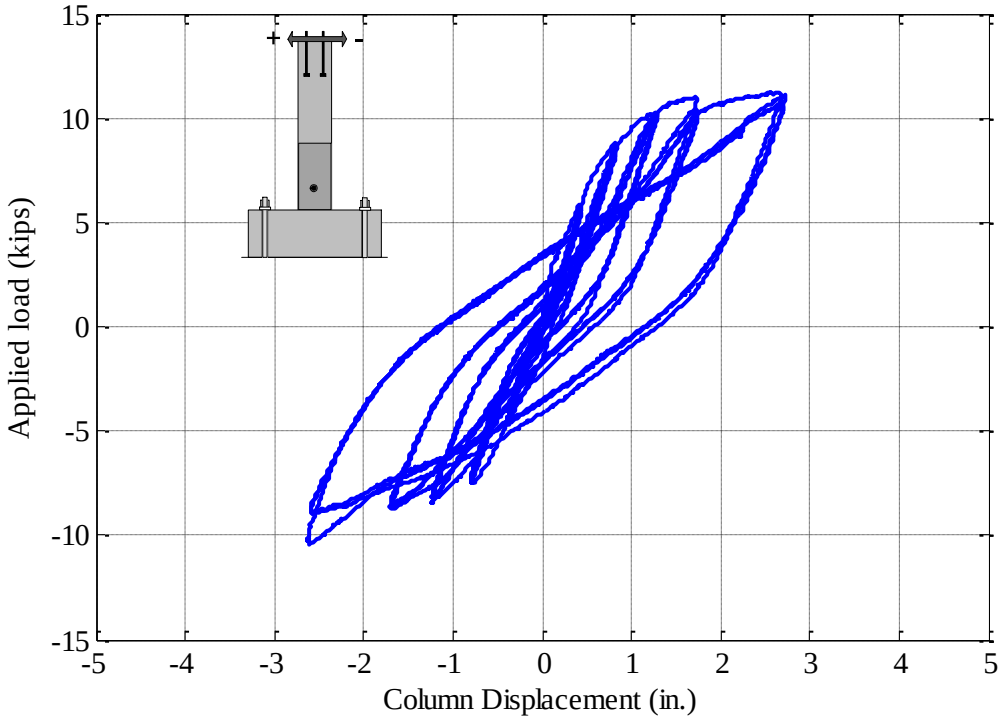

Figure 4.26: Load vs. column displacement for Specimen S2

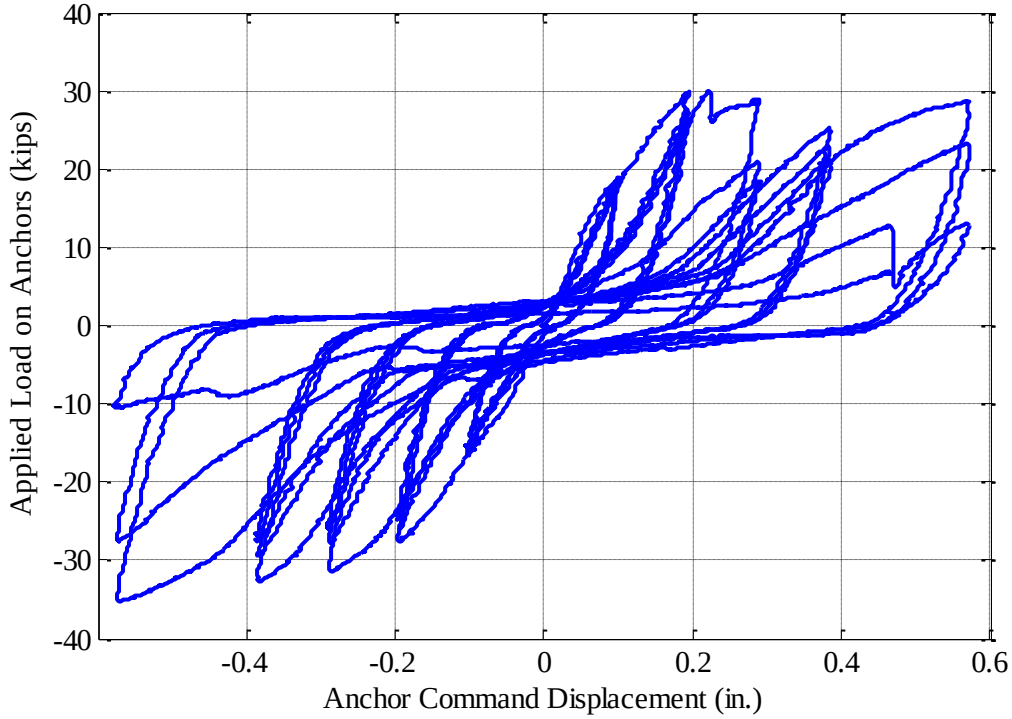

Figure 4.27: Load vs. anchor command displacement for Specimen S2

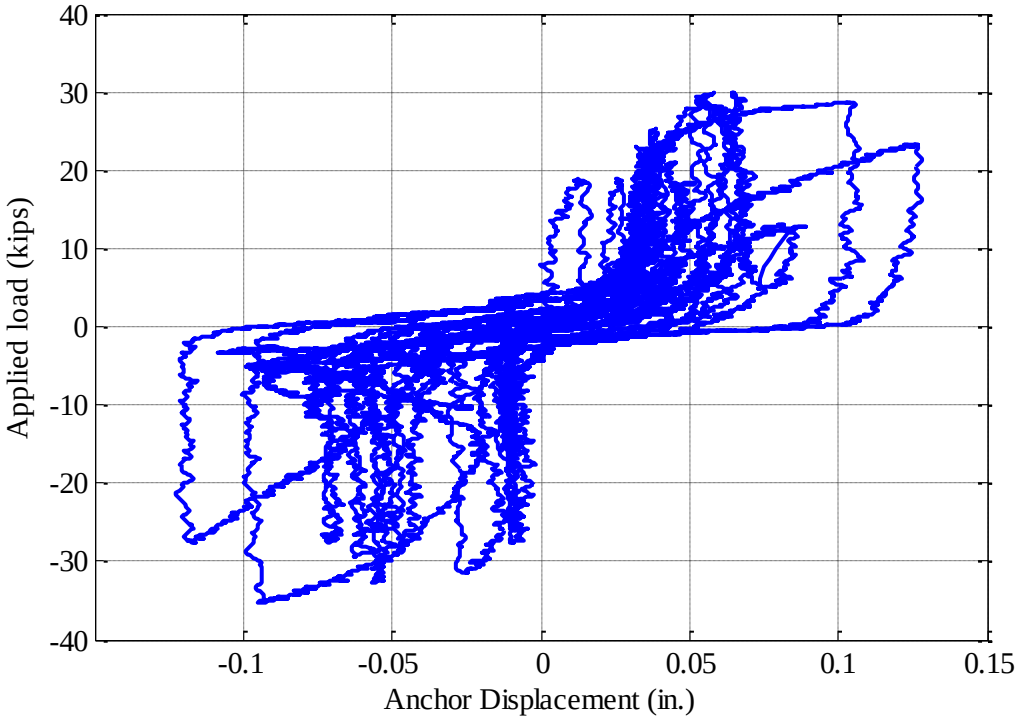

Figure 4.28: Load vs. anchor displacement for Specimen S2

±0.58 in. (column) and ±0.203 in. (anchors) displacement

The onset of cracks and crack pattern may not be easily observed due to the presence of the loading plate as shown in Figure A.22. Similar to most previous tests, the load curve had a first crack near 3.0 kips, which responded to a transition point in load curve. Beyond this loading, the column stiffness reduced to about 1/3 of its initial uncracked stiffness. Smaller cracks developed after the first cracks and the peak load was only 5.8 kips, about 23 percent less than those in the most previous column tests. This was mainly caused by the large force applied to the anchors by the bottom actuator. The load vs. displacement curve at anchor, as indicated in Figure 7.3d, initially displayed a slag till 0.01 in, beyond which the anchor picked up the load sharply up to the maximum of 18.7 kips, when both column and anchors were loaded to their first targeted displacement.

The unloading curve of the column from the first target displacement, identical to the previous observation in column tests, had a roughly constant slope in between the uncracked column and the cracked column. Reloading curve of the column toward the positive direction at the second and third cycles did not follow the original loading curve but presented the concave up behavior because of the existing cracks after the first loading cycle. Similarly, reloading curve of the anchor obviously experienced relatively larger displacement at the second and third cycles before the peak load was picked up. Such behavior may have been caused by concrete damage in front of anchor during the previous loading cycle. Unlike the large deformation at the reloading curves in the positive direction, reloading curves in the negative direction demonstrated that concrete behaved elastically, which in turn did not cause relative displacement between anchor and column. Embedded anchors with initial offsets of the 0.75 in. at east side and 0.25 in. at west side away from the column centroid line toward the south (positive direction) may explain such relatively higher stiffness at negative direction as compared to positive direction. Also, the longitudinal reinforcement at the location of centroid of the column will restrain the deformation of the anchor in the negative direction and provide more support on the anchor, thereby leading to higher stiffness at this direction.

±1.12 in. (column) and ±0.392 in. (anchors) cyclic displacement

The loading curve displayed the identical characteristics as observed in most previous experimental tests. The loading curve initially followed the reloading curve of last load cycles. Beyond the last targeted displacement the load vs. displacement curve became concave down till

the peak. New flexural cracks developed in the column when the applied load was 7.0 kips. Such cracks corresponded to a short plateau in the load vs. displacement curve in Figure 4.25. The column stiffness degraded further due to concrete crack growth and crack propagation during the loading cycles. The peak load was 8.8 kips when the column reached the target positive displacement, with over 20 percent lower than that in the same displacement level in previous tests in T2 or T3 (over 30 percent lower than in S1). Such large deviation, as addressed above, is likely caused by the anchor force from the bottom actuator. Correspondingly, the load vs. displacement curve of the anchors exhibited a plateau up to 0.3 in. displacement, suggesting that the anchor has rarely relative movement against the column at initial stage, beyond which the anchors picked up the loading sharply up to the peak load of 30 kips.

The load was -7.5 kips at the negative peak. Reloading curve of the column toward the positive direction at the second and third cycles was slightly lower than the original loading curve but presented the concave upward behavior because of the existing cracks after the first loading cycle. Similarly, reloading curve of the anchor obviously experienced relatively larger displacement at the second and third cycles before the peak load was picked up. Such variation may likely be caused by concrete cracks in front of anchor at the first loading cycle. Unlike the large deformation at the reloading curves in the positive direction, reloading curves in the negative direction demonstrated that concrete behaved elastically and no obvious plastic deformation was observed at the second and third cycles. With the increase of the cracking growth and propagation, the crack width at both north and south sides near the base increase to 1 mm.

±1.66 in. and ±0.581 in. cyclic displacement

The beginning part of the loading curve was concave up following the last reloading curve and then loading curve was characterized by a concave down when the column was loaded beyond the displacement 1.12 in. toward the new target displacement. A breakout crack was formed at east surface near 9 kips. Cracks showed up at the location of anchor. After the cracks, the column stiffness reduced to about another 1/2 of its initial stiffness, which corresponded to a sharp drop of the anchor loading from 29.59 to 27 kips, as indicated at anchor loading curve. Further opening of the breakout cone at east side was observed when the column was subjected to the targeted positive displacement of 1.66 in. Flexural cracks were observed at the north side at the base when the load was 9.2 kips and such crack also corresponded to the apparent plateau

in the load vs. displacement curve. The column stiffness further decreased with the development of these cracks. Maximum load reading had a level of 10.2 kips when the column was loaded to 1.66 in.

The first reloading in the positive/negative direction, due to the concave up characteristics, had an apparent loading drop from the loading curve, as indicated by the shaded area in Figure A.25c. Concrete cover breakout cracks opened further during the second and third cycles while the corresponding anchor load dropped to 20.9 kips with 23 percent decreasing at the second cycle compared to that in the first cycle. The reloading of the column in the negative direction reached -8.5 kips, a smaller drop in the load compared with the positive direction. The following unloading curve was thus slightly lower than the first unloading from the negative peak. The second reloading in the positive direction reached 10.0 kips while the unloading curve followed closely the second unloading path.

±2.2 in. and ±0.77 in. cyclic displacement

Identical to previous loading cycles, the loading curve followed the reloading curve of last load cycles, as shown in Figure 4.25. Beyond the 1.66 in. of the last target displacement, the load-disp. curve became concave down. The peak load was 10.93 kips when the column was loaded to 2.2 in. Concrete cover near the base at both north and south side, due to relative low column bending, did not display any concrete crushing. The peak load in the negative direction was -8.7 kips and thus the difference of the peak load between positive and negative direction reached up to more than 2 kips.

The loading curve of anchor displayed obvious pinching effects, suggesting that the no relative movement occurred when the column was loaded in the position/negative direction. With the presence of the concrete cover breakout, the peak load was 24.93 kips at the first cycle in positive direction. By contrast, the load in the negative direction was picked up to -32.6 kips, with a 31 percent higher than that in the positive direction. The behavior of the anchor loaded in either positive direction or negative direction displayed a linear manner, although local crushed concrete caused relatively larger anchor deformation. During the third loading cycle, the concrete cover breakout cone was pushed out and separated from the column at front of anchor at east side. In order to protect sensors, the broken concrete piece was taken away.

±3.28 in. and ±1.148 in. cyclic displacement

The loading curve grew in concave downward behavior till 3.28 in. after following the reloading curve of last load cycles till the last targeted displacement. The peak load was 16.09 kips when the column was loaded to 3.28 in. The reloading path in the positive direction at the third cycle was slightly lower than the first reloading (at the second cycle). The unloading path followed the first unloading path closely. The reloading at the second or third cycle curve displayed close concave upward behavior. Area between the concave downward in the loading path and the concave upward in the reloading path thus responded to the loading drop during the reloading cycles, as shown in shaded area in Figure A.26c. It also demonstrated that the south side (positive direction) underwent much severer damage than the north side. Comparison of the crack growth and crack density under various cyclic loading levels was plotted in Figure A.28. The flexural cracks were not developed as much as previous tests. Small flexural cracks were observed through higher location with the increase of the loading level. More branched cracks were propagated from the original cracks, in the plastic hinge zone.

As mentioned before, the anchors displayed pinching effects and underwent a large movement with the column before they picked up the load. The behavior of the anchor behaved linearly at the initial loading stage while its loading curve sharply increased when the load increased. Comparison of the actuator commanded displacement and actual anchor displacement in Figures 4.27, and 4.28 demonstrated that the actuator displacement increased dramatically at the load at 29 kips, indicating that the column was having additional bending moment and deflection at the location of the anchor bolt. The anchor remained steady at the load level of 29 kips without much additional displacement.

As compared to the peak value of 39.4 kips in monotonic loading, anchor rods failed at the east side by fracture in shear under a loading of 30 kips. The other rod at the east side was also bent at the same time. Concrete breakout cone at the east side, as observed in Figure A.27, was totally pushed away during the anchor fracture toward the peak load. The well confined concrete core with the proposed anchor reinforcement allowed the embedded anchors to fully develop their capacity, even though concrete in plastic hinge zone was suffered from damaged and most. It confirmed that the anchor can be installed in the plastic hinge zone or similar situation where concrete was suffered from severe damaged if the suitable anchor reinforcement has been introduced as stated in Phase II and III.

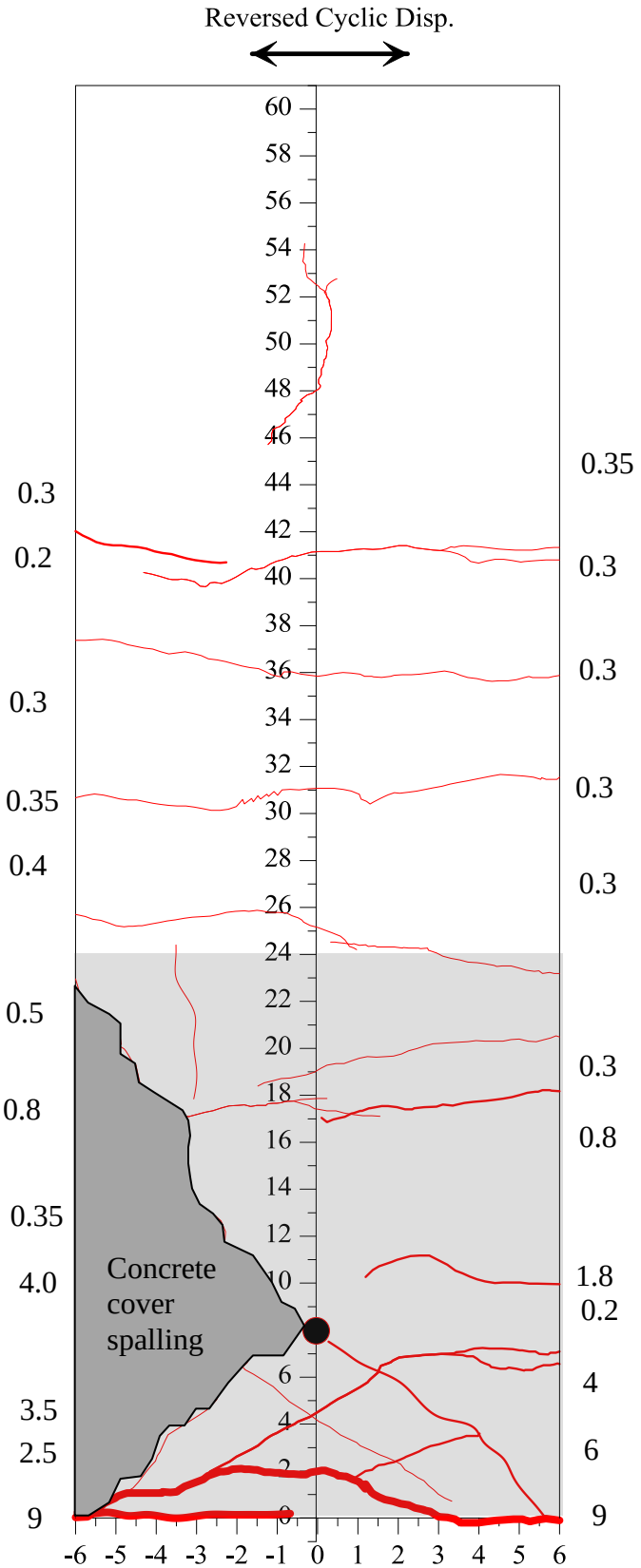

Figure 4.29: Crack patterns of column S2 and measured crack widths

(a) East side (anchor fracture at this side) **(b) West side**

Figure 4.30: Crack pattern after anchor fracture by shear (S2)

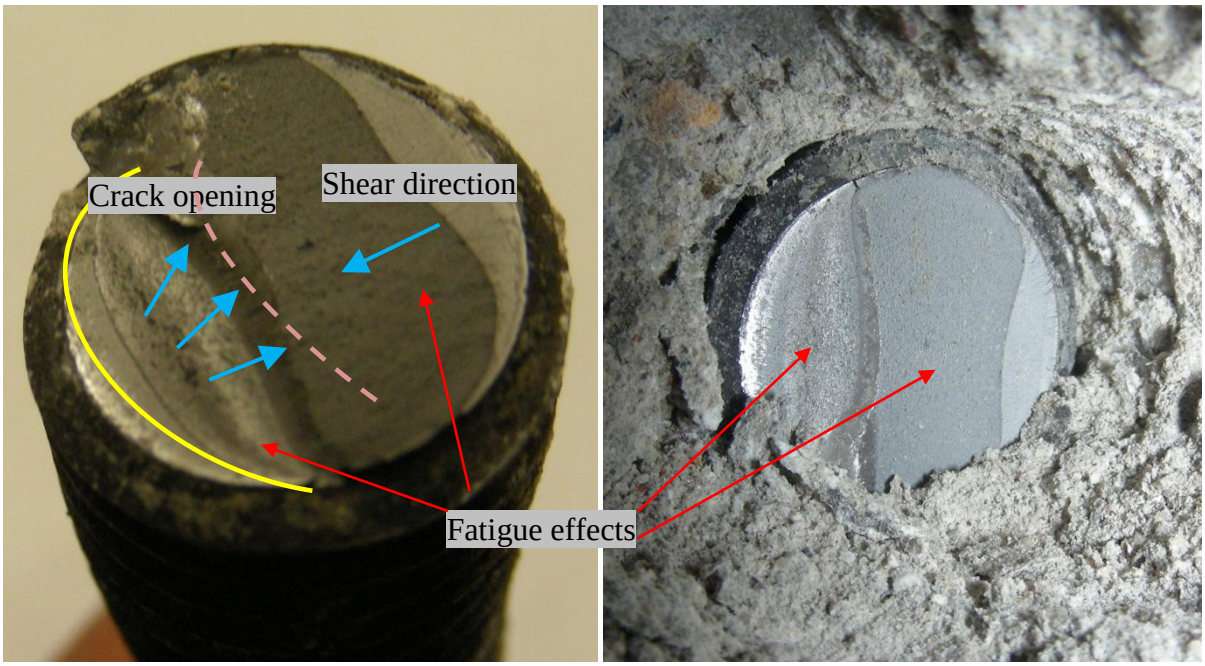

Figure 4.31: Fracture of the anchor rod in Specimen S2

4.5 Test of Specimen S3

4.5.1 Introduction

The anchors in Specimens S1 and S2 were not able to develop their full shear capacity through steel fracture dominated the failure. The main reason was that the concrete cover was damaged and spalled under the combined action of column flexural deformation and anchor deformation. The anchor shaft thus lost lateral support, which led to combined loading on the test anchors. This is similar to the observations may in the Phase II tests. The last specimen was then dedicated to identification of a solution.

The explored solution was to use external protection for the concrete cover using fiber reinforced polymer (FRP) wrapping. The test was conducted in a similar way to Specimen T2 with a slightly modified loading protocol. With concrete cover being protected, it was impossible to predefine a displacement history suitable for the test. Considering that in the target structure application, the anchor connections are used for connection damping devices to the structural elements; Therefore instead of controlling the actuator with displacement-control, a predefined load history was used similar to the test of T3. Both the column and the anchors were loaded simultaneously.

4.5.2 Design of FRP wrapping.

The FRP wrapping was achieved using QuakeWrap™ TU27C carbon fabric from QuakeWrap, Inc. The carbon fabric was attached to the pretreated column using QuakeBond J300SR saturating resin. The FRP sheet has a tensile capacity (breaking force) of 6.8 kips/in. If the anchors in shear fully develop their shear capacity, each anchor would carry a shear force of 26.3 kips. The width of the FRP sheet was then proportioned for this design force, resulting in a total width of 3.9 in. A 2-in. strip was placed on top of the anchor bolts and another 2-in. strip was placed below the anchor bolts as shown in Figure 4.32.

The QuakeWrap product is developed mainly for structural strengthening. The FRP strips were wrapped around the column and overlapped by 12 in. on the North side of the column. The bond property between the concrete and the FRP strips was not known; therefore the overlapping was expect to hold the concrete cover from spalling. This test was in exploratory nature, and further studies are needed to fully develop the external reinforcement for anchor systems.

Figure 4.32: FRP wrapping of Specimen S3

4.5.3 Behavior of Specimen S3.

The behavior of Column S3 is plotted in Figures 4.33 and 4.34. The cyclic behavior of the two single anchors is shown in Figure 4.35. The loads applied to the anchors were controlled using load-control schemes, as a result, the loads on anchors significantly affect the measured hysteretic behavior of the column. The ductile behavior of the column was not reflected in the measured load vs. displacement curves. Hence, it is not meaningful to analyze in details the measured behavior. Most damage to the plastic hinge zone occurred to the concrete below the FRP strips, as shown in Figure 4.36.

With the loads from the anchors at 8 in. above the base, the peak loads captured by the top actuator were lower than the actual loading capacity, which is similar to the test of Column S2. In addition, the high load applied to the anchors actually caused apparent degrading behavior. Additional study is needed to confirm this observed behavior, especially for those structures that incorporate damping devices.

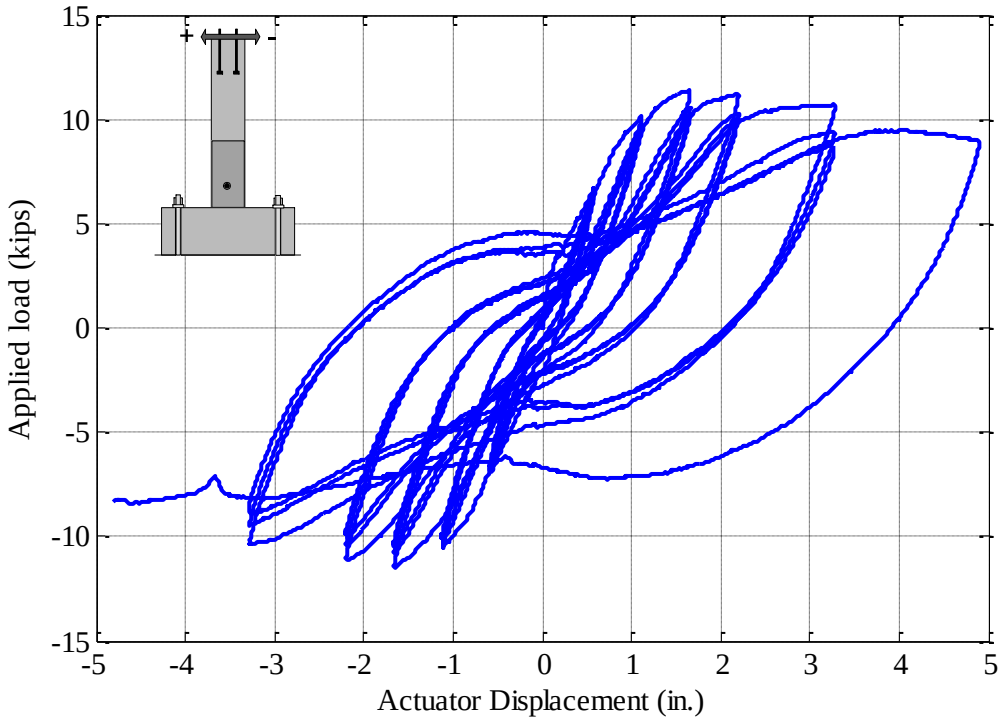

Figure 4.33: Load vs. command displacment for Specimen S3

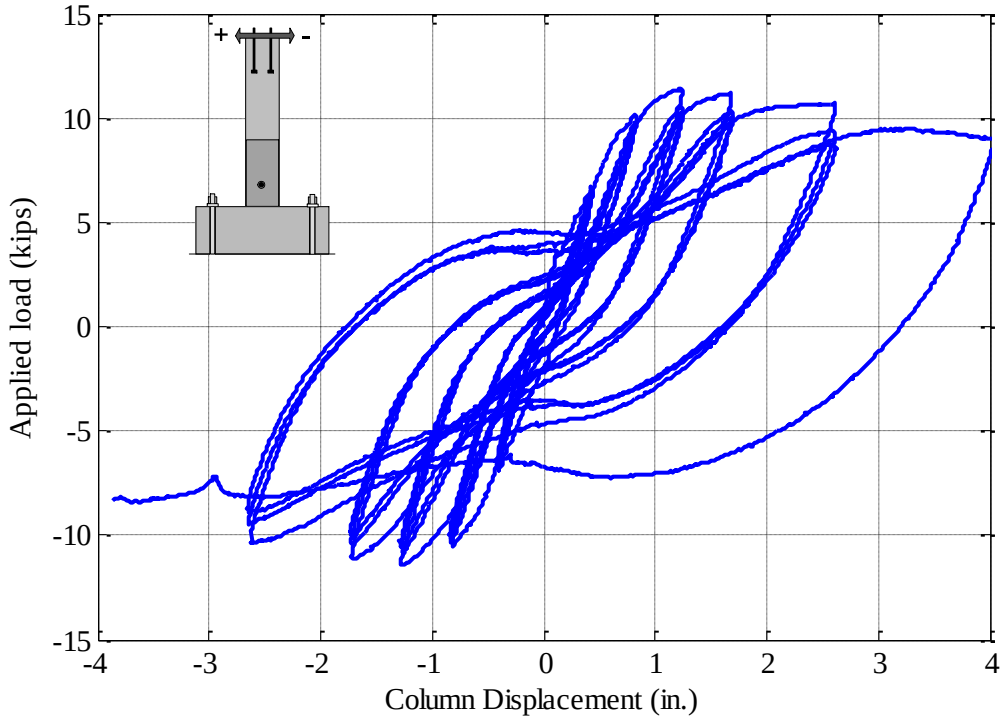

Figure 4.34: Load vs. column displacment for Specimen S3

The anchor bolts had high stiffness as shown in Figure 4.35. In this case the load on the top of the column in turn affected the measured anchor behavior, especially during the unloading

stages. With a load smaller than the peak load the anchor just experienced, the anchor deformation should have reduced along with the reduced load; however, because the column at the same time experienced unloading. The column unloading may have been at a faster pace than the anchor unloading. Therefore the anchors experienced increasing deformation during the unloading stage. This unusual behavior may have also been related to the location of the LVDT's, which were used to measured the anchor displacements, was 10 inches higher than the actual anchor location (at 8 in. above the column base).

In general, the anchors had an increased displacement during the second and third cycles compared with the first loading cycle. This indicated that concrete experienced damage, specifically concrete in front of the anchors crushed as shown in Figure 4.36. The anchors were able to carry 49 kips in the first cycle of 49 kips, which however had created damage to the anchor bolts. This large load likely initiated flexural cracks, which reduced the area of the anchor shafts. When the anchors were loaded in the negative direction, the reduced cross section caused fracture to the east side anchor, and shown in Figure 4.36.

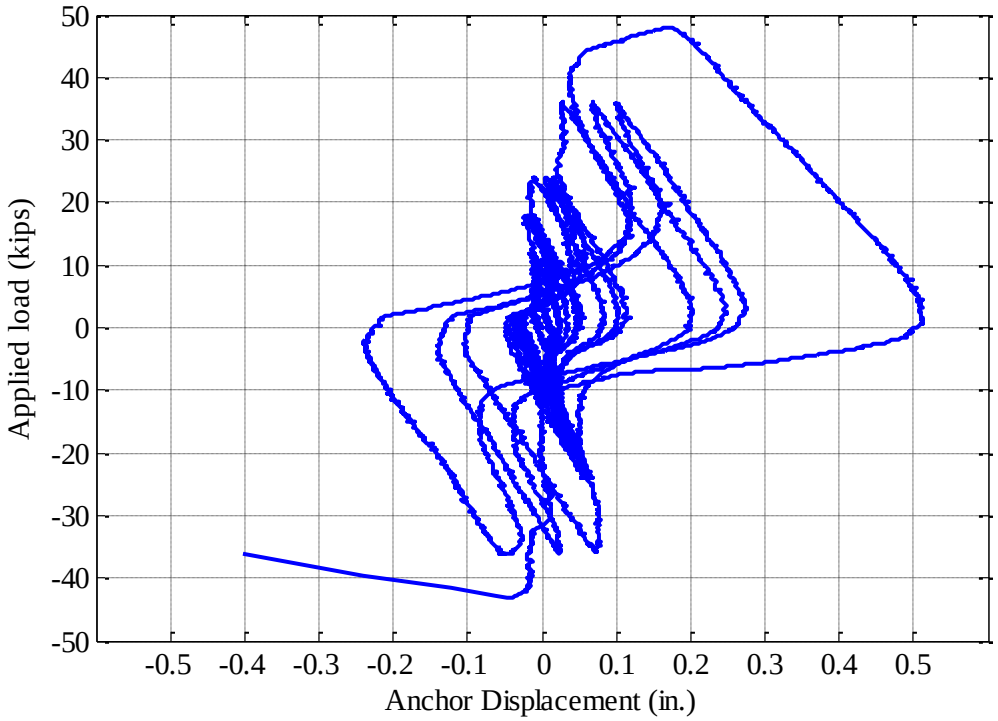

Figure 4.35: Load vs. column displacment for Specimen S3

East side **West side**

Figure 4.36: Damaged column in Specimen S3

Strain gages were installed on the second bundle of fibers from the anchor bolts, as shown in Figure 4.36. These strain gages may not be able to reflect the deformation in the entire FRP strip because the FRP strips were unidirectional and the cross links were weak. The strain measurements were used to examine one hypothesis: the force that caused concrete cover spalling in Specimens S1 and S2 would be transferred to FRP strips through bond between the concrete and FRP strips; or the force was transferred to the FRP strips through the 90-degree bent at the ends and the bond action can be ignored.

The strains in the east side FRP strip are shown in Figure 4.37. The strain gages were designated with their horizontal distance from the anchor bolt. For example SG-0in. was the strain gage just below the anchor bolt on the second fiber bundle (the first fiber bundle may be crooked). In general, the strain measurements increased with an increase in the shear force applied to the anchors. When the shear force on the anchors was positive, the actuator applied a tensile force to the anchors; as a results, all the strain gages detected tensile strains, which is as expected. When the shear force on the anchors was negative, the actuator applied a compressive force to the anchors. In this case the strain gages, which are not in front of the anchor, again detected tensile strains, indicating that bond action was small . This is further confirmed with the strains: the strain gages at 0, 1, 2, and 3 in. away from the anchor detected similar strains. Without further study, it can be concluded that the 90-degree bent is needed if outside confinement is to be used.

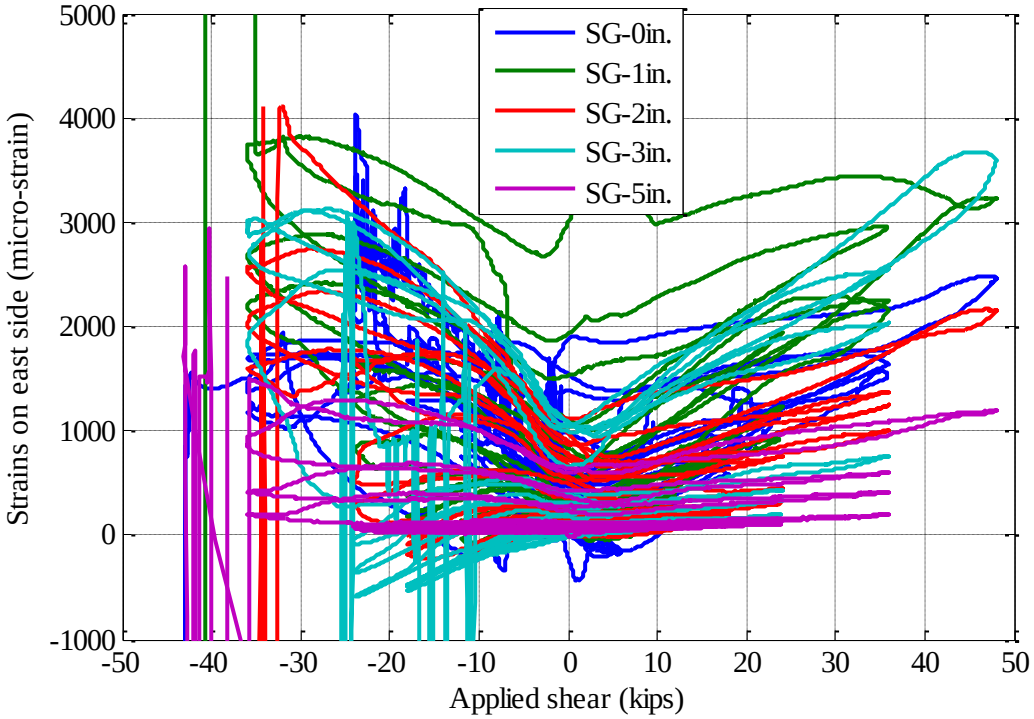

Figure 4.37: Measured strains on east side FRP in Specimen S3

4.6 Summary of Phase V tests

The NEES-Anchor project has provided some experimental information for solving the problem. Six tests were conducted for single anchors embedded in the plastic hinge zone of columns. The test anchors consisted of a 3/4-in. diameter ASTM A193 Grade B7 threaded rod and a plate washer and a hex nut welded to the end. Additional stirrups were used near the headed anchors to serve as the anchor reinforcement, and three U-shaped hairpins were placed in the vertical plane to restrain the concrete around the anchors from cracking. The anchor tension tests indicated that well-confined core concrete could support anchors located in plastic hinge zones. The confining reinforcement, especially for anchor groups, should be further studied.

Concrete cover spalling is also critical for the behavior of embedded connections, especially those subjected to shear forces. The headed anchors/bars lose lateral support after the concrete cover spalls below the embedded connections. In this case the headed anchors/bars will fail at a much lower capacity as a result of combined shear, bending, and tension [Lin et al., 2011]. In the three shear tests shown in Figure 4.38, the concrete cover was not protected and it spalled during the first two tests, resulting in a large reduction in the shear capacity and stiffness. On the

other hand, carbon fiber reinforced polymer (CFRP) sheets used in the last test protected the concrete cover. The steel fracture in shear was observed, and the measured shear capacity was similar to the code predicted steel capacity.

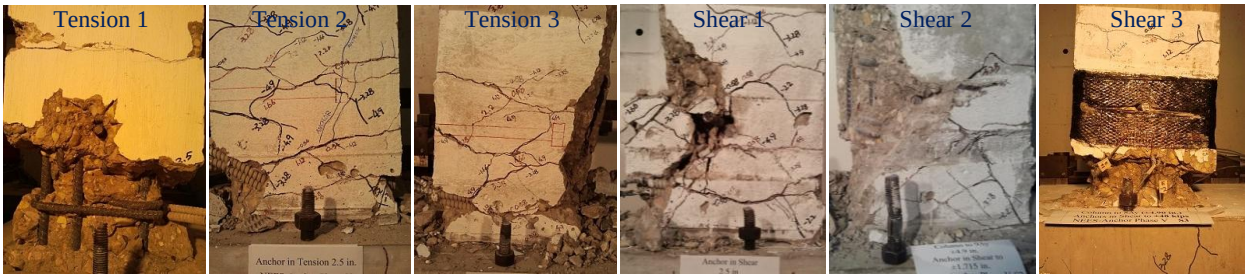

Figure 4.38: **Summary of NEES-Anchor tests of reinforced anchors in plastic hinge zones**

CHAPTER 5 Test of Anchor Groups in RC Walls

5.1 Introduction

For low-to-moderate rise buildings up to 25 to 30 stories, core walls are commonly used to resist nearly all of the lateral forces due to a seismic or wind loading event [Shahrooz et al., 2004]. Often, these lateral loads are transferred to the structural walls through a series of steel outrigger beams that bridge the perimeter framing to the core walls. The outrigger beams and the structural diaphragm transfer the lateral and gravity loads to the core wall typically through embedded anchor connections. A common outrigger beam-wall connection detail involves a shear tab welded onto a plate which is anchored to the wall by headed studs or threaded rods with nuts [Shahrooz et al., 2004]. This type of "shear connection" relies heavily on adequate performance of headed studs under combined actions of gravity load and cyclic tensile load perpendicular to the connection [Shahrooz et al., 2004]. A previous research was expanded in order to better understand the behavior of cast-in-place anchors under combined cyclic shear and tensile loading.

The tests in Phase IV study was a direct extension of a previous research conducted at the University of Cincinnati [Shahrooz et al., 2004]. Is this earlier research, two ½-scale wall specimens were tested to investigate (a) the effect of damage on the performance of outrigger beam-wall connections, (b) the effect of the boundary element on the performance of outrigger beam-wall connections, and (c) the presence of floor diaphragm and its role in transferring forces into the core wall. As part of the research reported herein, a ½-scale test specimen was designed and fabricated similar to the rectangular tested previously (labeled "R-wall" in Shahrooz at al. (2004)). The effect of the damage around the connection (concrete spalling and yielding of wall reinforcement) and the effect of the boundary reinforcement on the performance of the connection were examined. However, because Shahrooz et al. (2004) had concluded that outrigger beams transfer the majority of lateral forces to the core wall with negligible participation by the floor diaphragm, the test specimen did not have a slab similar to what had been done previously.

The focus of the presented research was to further understand the behavior of cast-in-place anchors under cyclic tension-shear loading with wall boundary reinforcement confining the

anchors. The current codes, namely Appendix D of ACI 318-08, are limited in terms of design of anchored connections for use in moderate to high seismic regions. Due to lack of sufficient test data, ACI simply mandates that anchors be designed such that anchor fracture is the governing failure mode. In addition, ACI Appendix D.3.3.1 states that the provisions laid out in Appendix D do not apply to the design of anchors in plastic hinge zones of concrete structures under earthquake forces. Therefore, the behavior of cast-in-place anchors in plastic hinge zones, where a high level of cracking and spalling takes place around the anchor, was also investigated as part of this research; similar to that experienced by a lower-story outrigger beam-wall connection during a severe seismic event.

5.2 Previous Relevant Research

Hawkins, N. M., Mitchell, D., and Roeder, C. (1980)

Hawkins et al. (1980) conducted 22 tests of stud connections between steel girders and concrete columns for use in mixed construction. The tests were conducted in two groups: the first group of 12 tests used 4-in. long studs and the second group of 10 tests used 6-in. long studs. The stud groups connected two steel sections to a concrete block with minimum reinforcement. The specimens were supported on the steel beams with a variety of distances from the concrete. The concrete block was then loaded both monotonically and cyclically. The tests showed that the connections were able to carry combined tension and shear; however their moment resisting capacities were limited by the tensile behavior of the studs. The specimens subjected to relatively larger moments failed by brittle concrete failure. The tests also showed that cyclic loading can cause reduction in both the ultimate capacity and the stiffness.

Shahrooz, B.M.; Deason, J.T.; and G. Tunc (2004a)

Cyclic behavior of headed stud groups under combined action of gravity shear and cyclic diaphragm force was studied. The test results suggest that the connection reaches the design loads, but the mode of failure is stud pullout, which does not have any ductility and lacks energy dissipation. Furthermore, their findings suggest that the design methodologies fail to capture the increase in strength due to the wall boundary reinforcement encasing the studs. The boundary element also alters the mode of failure from stud pullout to stud fracture. New design equations were proposed to account for the effects of confinement around the studs..

Shahrooz, B.M.; Tunc, G.; and Deason, J.T. (2004b)

This research was undertaken to evaluate the design equations developed as part of the study reported above, and to examine the effects of cracking, damage, and yielding of reinforcement on the strength of studs. In this study, two cantilever wall assemblies were tested: one contained an outrigger beam-wall connection with a floor diaphragm, and the other contained an outrigger beam-wall connection without a floor diaphragm. Both specimens were subjected to cyclic diaphragm loading, and a constant gravity shear was applied to the connections. The experimental results showed that for the outrigger beam-wall connection, the outrigger beam transferred the majority of the diaphragm tensile forces directly to the wall with negligible participation of the floor slab. Consequently, floor slab-wall connections can be designed solely to resist gravity loads unless the connections are specifically designed to transfer diaphragm forces into the core wall.

Peterson, D.; Johnston, J.; Zhao, J.; Shahrooz, B. M.; and Tong, X. (2008)

This paper is largely a compilation of past research focused on cyclic testing of cast-in-place anchors to examine the effects of seismic loading. In addition, this paper is a review of various design codes used around the world for anchor design, and tries to show the lack of uniformity in the codes as well as the lack of research in regards to seismic design. Cyclic tensile loading of headed anchors was investigated extensively (Peterson et. al). "Cyclic tension has been shown to have a negligible effect on anchor strength compared to monotonic loading" (Rodriguez et al. (2001)). Moreover, the "current strength reduction factor of 25 percent for seismic design of anchors subjected to cyclic tension may be overly conservative". Cyclic shear loading of headed anchors showed steel fracture due to low-cycle fatigue to be the typical failure mode (Peterson et. al). Single anchor tests conducted by Klingner et al. (1982) demonstrated that anchor bolts under cyclic shear would fail at much lower loads than monotonically loaded anchor bolts due to the effects of low-cycle fatigue. Very little research has been is available for anchors under combined cyclic tension-shear because of the complexities associated with buckling under compressive loads. Lastly, the paper stresses the importance of not only strength but also for ductility for semis design of connections using anchors. "The largest factor ensuring structural stability during an earthquake is to allow the building to endure large deflections without collapsing." The authors are interested in furthering their research efforts of establishing a seismic tension-shear interaction model for concrete anchors.

Zhang, Y.; Klinger, R.; and Graves, H. L. (2001)

The static and dynamic behavior of undercut and expansion anchors (post-installed anchors) in concrete was investigated. The objective of this research was to gather data in an attempt to understand the differences between static and seismic behavior of anchors in concrete under various conditions, including anchor types, hairpins, concrete cracking, and proximity to member edges. Part of the research program was focused on multiple-anchor connections. The load-displacement curves for both the dynamic and static tests were nearly the same except for some differences near the ultimate load. The most significant outcome of the dynamic tests was the need to increase the base plate displacement to offset the negative influence of spalling of concrete in front of the anchors. The effects of cracks on load-displacement behavior of multiple anchor connections were also examined. Tests showed that the maximum load was nearly the same in cracked and uncracked concrete under dynamic tests. However, displacements were larger for the anchors in cracked concrete as compared to the uncracked concrete.

The results seemed to suggest that the multiple anchor tests under all conditions behaved consistently to previous single anchor tests. The conditions include cracked or uncracked concrete, with or without edge effects, with or without hairpins loaded under dynamic loading conditions. The authors claim that multiple anchors designed for ductile behavior in uncracked concrete will most likely still behave in a ductile manner under dynamic loading. Hairpins increased the ultimate capacity toward the edge of near-edge, multiple anchor connections . No cast-in-place anchors were tested in this program. In addition, the added confinement effects from boundary reinforcement on the anchors were not addressed.

5.3 Specimen Selection and Design of Test Specimen

5.3.1 Prototype Structure

The test specimen was designed as a ½-scale specimen derived from a 15-story prototype structure with the floor plan shown in Figure 5.1. The prototype building was also used in a previous study conducted at the University of Cincinnati [Shahrooz et al., 2002]. The prototype building served two purposes. It was used to determine the loads for design of the test specimen. In addition, the web of the center I-shaped wall was used as the basis for the geometric design of the embedded connections and wall in the test specimen.

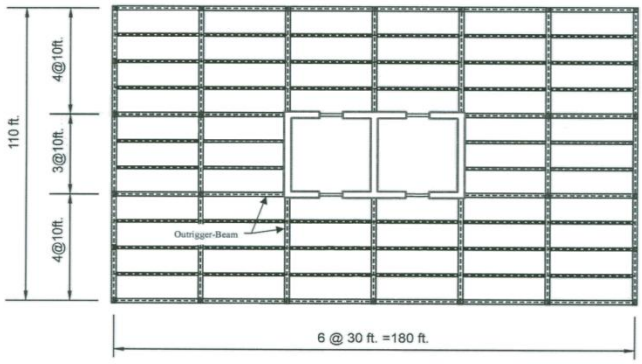

Figure 5.1: Plan view of prototype structure (Shahrooz et al., 2002)

To maximize the lease space, a central core is a preferred lateral resistance system in moderate-rise office buildings [Shahrooz et al., 2002]. Thus, the main lateral load resistance system is the two C-shaped walls and the central I-shaped wall that are linked to form the central core. The selected building has 6 spans in the E-W direction at 30 feet and 3 bays in the N-S direction with joists at 10 feet on center. The gravity load resisting system is comprised of the steel frames with shear connections. The floor system is a steel-deck reinforced concrete diaphragm with lightweight concrete. The height of the first floor is 16 feet, and the remaining of the floors are 12 feet high. Table B.1 and B.2 in the Appendix B give a summary of the steel shapes used in the prototype structure, The concrete core walls were 18" thick and the dimensions are shown in Figure 5.2. For the prototype structure, the dead and live load for floors 1 – 14 were determined to be 81 psf and 50 psf, respectively; and roof dead load and live load were determined to be 21.3 psf and 20 psf, respectively.

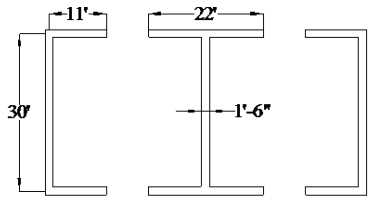

Figure 5.2: Core wall dimensions in the prototype structure

5.3.2 Modeling of Prototype Structure

The prototype building was modeled in the structural analysis software ETABS in order to obtain the seismic forces used for the design of the test specimen [Shahrooz et al., 2004]. The following parameters were assumed for the analysis of the ETABS model: The 0.2 second and 1 second spectral response acceleration (%5 of Critical Damping) values were: S_s = 2.29 g and S_1

= 0.869 g, respectively; T_L=12 seconds; and a soil site class D (ASCE 7-05, 2005). The response modification factor for the prototype structure was R=8. Because the research focused on seismic application of anchored connections, wind loading was not investigated. In addition, because the focus was only on the N-S outrigger beam-wall connection, the seismic loading in the E-W direction was not considered either. The seismic story shear force and story deflection were generated by the ETABS model, see Table 5.1.

Table 1: Seismic Shear Force in N-S Direction Based on ASCE 7-05

Floor	Shear Force (kips)	Story Def. (in)
Roof	83	2.53
14	541	2.33
13	493	2.12
12	446	1.91
11	401	1.70
10	356	1.49
9	313	1.28
8	271	1.08
7	231	0.89
6	191	0.70
5	154	0.53
4	118	0.38
3	85	0.25
2	54	0.14
1	27	0.06
Base Shear	3765	-

In order to determine the percentage of the story shear force being resisted by each of the three core walls, the floor diaphragm and the core walls were modeled as a rigid beam and springs respectively, see Figure 5.3. The story shear force from ETABS was uniformly distributed across the width of the diaphragm. This load, designated as w1, was taken as the total shear force at that particular story divided by the width of the diaphragm. Because the floor diaphragm was assumed to be rigid in the ETABS model, the lateral load would be distributed to the lateral resisting elements according to their relative stiffness. The analytical model also took into account 5% accidental torsion, which was modeled as a linearly distributed torque. The stiffness of each wall was determined from Eq. 5.1, which accounts for flexural as well as shearing deformations,

$$k = \frac{P}{\Delta} = \frac{1}{\frac{L^3}{3EI} + \frac{L}{AG}}, \quad (5.1)$$

where:

E = Modulus of elasticity of the concrete wall

G = Modulus of rigidity of the concrete wall

A = Shear area of wall cross-section

L = Length from ground to story height

I = In-plane moment of inertia of wall

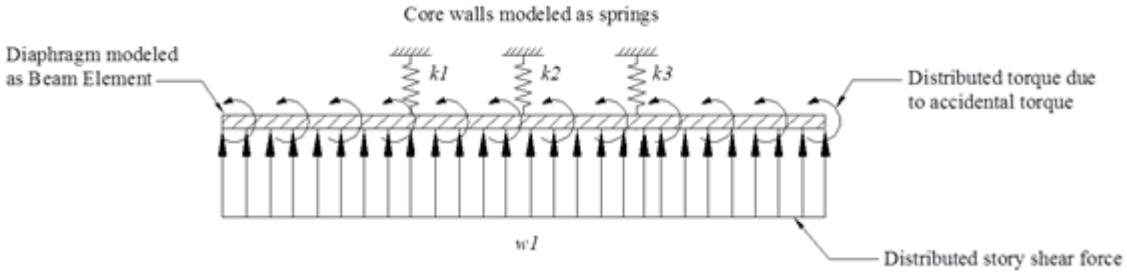

Figure 5.3: Analytical modeling of diaphragm and core walls

The calculated results are as shown in Table 5.2.

Table 5.2: Calculated forces in wall piers

	F1 (kips)	F2 (kips)	F3 (kips)
Roof	11.3	38	33.5
14	75.0	**246**	219
13	69.6	223	201
12	63.9	199	183
11	58.6	177	166
10	53.0	155	148
9	47.7	134	131
8	42.6	114	115
7	37.2	94.5	98.7
6	31.8	76.1	82.9
5	26.9	59.8	68
4	21.5	44.3	53
3	15.8	30.4	38.4
2	10.4	18.8	24.8
1	5.3	9.1	12.6
Floor	**Wall 1**	**Wall 2**	**Wall 3**

5.3.3 Connection Design

The loads resisted by wall 2, i.e., the center I-shaped wall, in floor 14 was chosen as the design loads for the connection in the test specimen. The test specimen was designed as a ½ -scale of the prototype structure; hence, the design forces will be a quarter of those in the prototype. The loads used for the design of the connections were determined using the governing load case of 1.2D +1.0L +1.0E. A 600ft^2 floor was taken as the tributary area for the gravity loads of the connection.

$$V_{prototype} = [(1.2(81psf) + 1.0(50psf))[600\,ft^2][\frac{1kip}{1000lbs}] + 1.0(0) = 88.3kips$$

$$V_{ua} = [\frac{88.3kips}{4}] = 22.1kips$$

$$N_{prototype} = 1.2(0) + 1.0(0) + 1.0(246) = 246kips$$

$$N_{ua} = [\frac{246kips}{4}] = 61.5kips$$

The provisions of ACI 318-08 Appendix D were followed to design the embedded anchor connections. The dimensions of the final designed embed plate, anchors (threaded rods), and shear tab are summarized in Table 5.3. In addition, the connection details are shown in Figure 5.4.

Table 5.3: Summary of connection geometry and properties

	Dimensions	Grade Steel
Embed Plate	6”Wx10”H	A36
Anchors	½” Dia. x 6” embed	A193-B7
Shear Tab	5”Wx9 1/8”H	A36

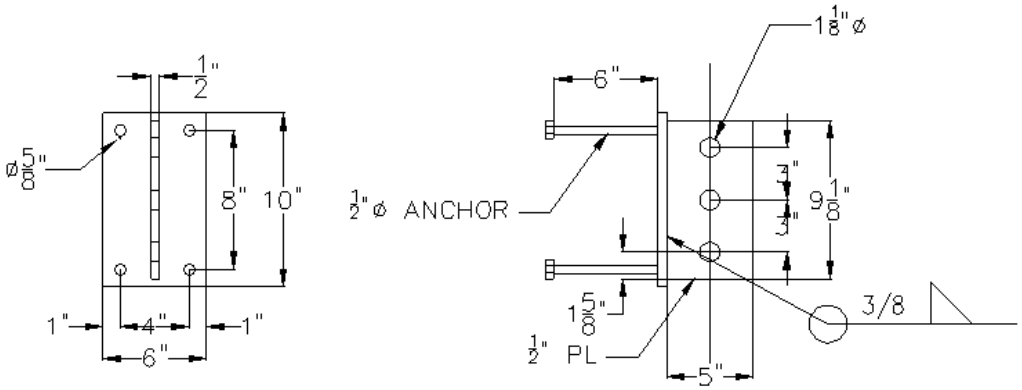

Figure 5.4: Dimensions of embed plate, anchors, and shear tab

The limit states for the anchors in tension and in shear are summarized in Table 5.4. The anticipated capacity of the connections were:

$$\phi N_{sa} = \phi n A_{se,N} f_{uta}$$

$$\phi N_{sa} = \phi n A_{se,N} f_{uta} = 1.1(4)(.142in^2)(125ksi) = 78.1kips$$

$$\phi V_{sa} = \phi n 0.6 A_{se,V} f_{uta} = 1.1(4)(0.6)(.142in^2)(125ksi) = 46.9kips$$

Where ϕ is an over-strength factor taken as 1.1. For combined tension and shear, ACI 318-08 D.7 requires the use of an interaction equation to predict the capacity of a group of anchors.

$$\left(\frac{N_{ua}}{\phi N_n}\right)^{5/3} + \left(\frac{V_{ua}}{\phi V_n}\right)^{5/3} \le 1.0 \qquad \left(\frac{61.5kips}{78.1kips}\right)^{5/3} + \left(\frac{22.1kips}{46.9kips}\right)^{5/3} = .957 \le 1.0$$

Therefore, the two connections on the test specimen were designed to fail slightly above the calculated design loads, assuming an over-strength factor of the anchor material equal to 1.1.

Table 5.4: ACI 318-08 Appendix D anchor design

Anchor Limit States (ACI section)	Governing ACI Equation	Value (kips)	Failure Mode Applicable
Steel strength of anchor in tension (D.5.1)	$N_{sa} = nA_{se,N}f_{uta}$	**71.0**	YES
Concrete breakout strength in tension (D.5.2)	$N_{cbg} = \frac{A_{Nc}}{A_{Nco}}\psi_{ec,N}\psi_{ed,N}\psi_{c,N}\psi_{cp,N}N_b$	15.3	NO, see D.4.2.1
Pullout strength of anchor in tension (D.5.3)	$N_{pn} = \psi_{c,P}N_p$	72.6	YES
Concrete side-face blow strength of anchor in tension (D.5.4)	$N_{sbg} = \left(1 + \frac{s}{6c_{a1}}\right)N_{sb}$	14.1	NO, see RD.5.4.2
Steel strength of anchor in shear (D.6.1)	$V_{sa} = n0.6A_{se,V}f_{uta}$	**42.6**	YES
Concrete breakout strength of anchor in shear (D.6.2)	$V_{cbg} = \frac{A_{Vc}}{A_{Vco}}\psi_{ec,V}\psi_{ed,V}\psi_{c,V}\psi_{h,V}V_b$	12.6	NO, see D.4.2.1
Concrete pryout strength of anchor in shear (D.6.3)	$V_{cpg} = k_{cp}N_{cbg}$	28.2	NO

5.3.4 Wall Specimen Design

After proportioning the anchors, the wall reinforcing steel was designed using the provisions from Chapter 14 and Chapter 21 of ACI 318-08 (see Appendix B for wall design calculations). To design the wall reinforcing, it was assumed that the location of the centerline of the anchor

connections would be at 2’-0” above the base of the foundation and that there would be an applied shear and axial load at the top of the wall. These forces were calculated to simulate the forces experienced in the prototype building. Two actuators would replicate the connection forces, and a Loading and Boundary Condition Box (LBCB) would be used to simulate the applied shear and axial load. The 2’-0” height for the anchor connection was chosen so that the anchors would be within the plastic hinge region of the wall taken as $0.5l_w$ from the base, where l_w is the in-plane length of the wall. For the test specimen, l_w is 60” and therefore the plastic hinge region is expected occur up to 30” vertically from the wall base. The capacity of the wall was selected such that the base of the wall would form a plastic hinge when the anchors would reach their design capacity. Hence, a sufficient level of damage occurs around the connection. The moment capacity of the wall was determined by using the software XTRACT (2002). According to XTRACT, the outermost longitudinal #4 bars were to yield at 12780 k-in and the failure moment capacity was at a moment of 16035 k-in. This is made clear by examining Figure B.1 in Appendix B titled "Expected wall moment vs. steel strain."

Knowing the capacity of the connections and the moment capacity of the wall from XTRACT, a free body diagram was constructed to determine the maximum forces that the wall could resist at connection failure. These forces were used to design the wall reinforcing as well as to perform checks to ensure the wall would not fail in shear before the connections would fail. The final wall reinforcement design consisted of #4 longitudinal bars, and #3 stirrups and #3 ties spaced at 3” on center to form a boundary element at each end of the wall. See Figure 5.5 for the wall reinforcing.

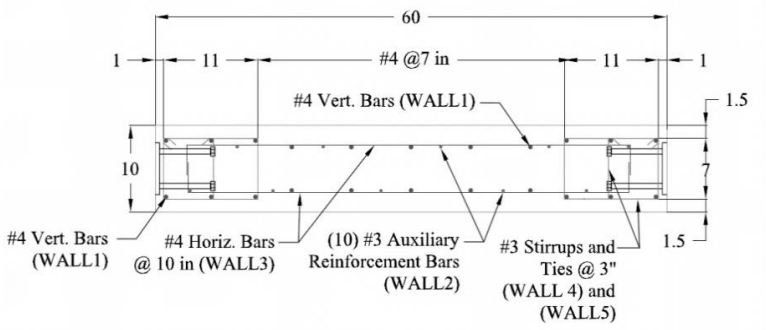

SECTION A-A

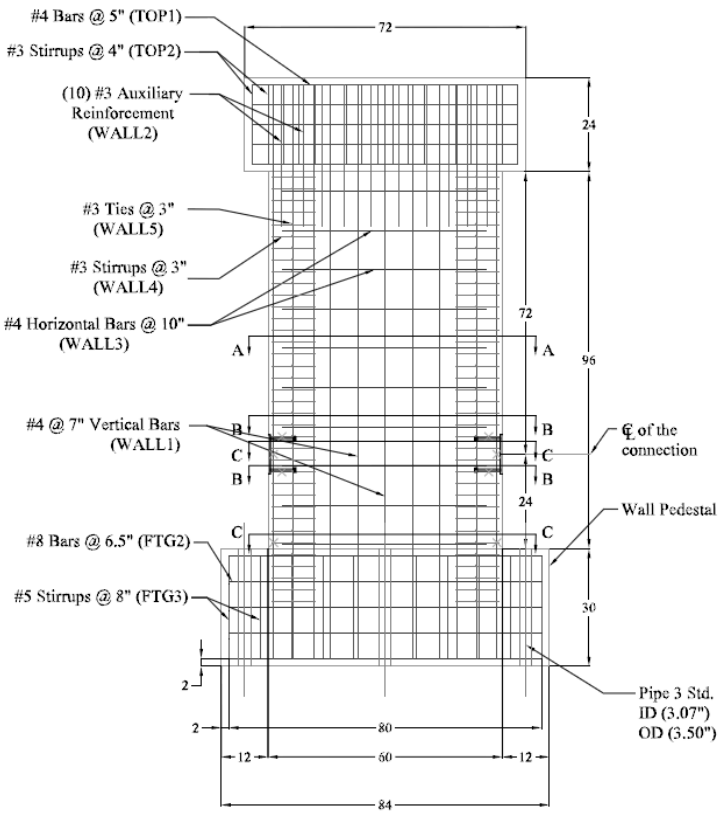

SIDE VIEW OF THE RECTANGULAR WALL

Figure 5.5: Wall Reinforcement Detail

5.3.5 Expected Capacity of Test Specimen

In the prototype structure, the connection shear force is due to gravity load that is constant. On the other hand, the tensile force applied to the connection is due to diaphragm action; hence, the tensile force would be cyclic. Two actuators are needed to simulate a constant shear and a cyclic tensile force. For ease of testing, it was decided to use a single actuator placed at an angle. As a result, both the tensile and shear forced would be cyclic. Maintaining the calculated shear to tensile forces, the angle of the actuator is $q = \tan^{-1}(\frac{V_{ua}}{N_{ua}}) = \tan^{-1}(\frac{22.1}{61.5}) = 19.8°$ from the horizontal. Due to the test facility's strong floor configuration, an angle of 23^{o} from the horizontal was selected. With the actuators placed at 23^{o} to the horizontal, the force applied to the connection (by the angled actuator) is 41.6 kips at the onset of yielding of the longitudinal wall reinforcement. The corresponding horizontal lateral load at the top of the wall (applied by the LBCB) is 76.8 kips. When the wall reaches its expected ultimate moment capacity of 16035 k-in, the actuator force and LBCB forces should be 52.2 kips and 96.2 kips respectively.

The force (P) in the actuator corresponding to the anchor failure can be calculated by manipulating the ACI interaction equation $\left(\frac{N_{ua}}{\phi N_n}\right)^{5/3}+\left(\frac{V_{ua}}{\phi V_n}\right)^{5/3}\le 1.0$. The actuator has an angle θ = 23° from the horizontal; hence, N_{ua} = Pcos(θ) and V_{ua} = Psin(θ). Using the values of ϕN_n and ϕV_n from Table 5.4, the magnitude of P is computed to be 59.0 kips from the following equation.

$$\left(\frac{N_{ua}}{\phi N_n}\right)^{5/3}+\left(\frac{V_{ua}}{\phi V_n}\right)^{5/3}\le 1.0$$

$$\left(\frac{P\cos(\theta)}{\phi N_n}\right)^{5/3}+\left(\frac{P\sin(\theta)}{\phi V_n}\right)^{5/3}\le 1.0 \quad where\ \phi N_n = 71\,kips;\ \phi V_n = 42.6\,kips;\quad \theta = 23^{o}$$

Therefore, the expected force in the angled actuator ranges between 41.6 kips and 59.0 kips depending on the selected limit state. The calculations indicate that the wall will have developed its flexural capacity when the anchors develop their capacities.

5.4 Test Specimen Details and Experimental Program

5.4.1 Test Specimen

One ½-scale specimen was tested. The test specimen was cast on its side for simplicity; see the figures in Appendix C. Samples of the ASTM A615 Grade 75 #4 vertical reinforcing bars and ASTM A193-B7 threaded rod, used for the embedded anchors, were tested for their tensile strengths. The average tensile strengths of the #4 bars and the threaded rods were 102.8 ksi and 128.1 ksi respectively. The stress-strain diagrams for the #4 bars and the threaded rods can be found in Appendix C. The average 36-day compressive strength of the concrete cylinders was 4,344 psi. A number of strain gages were installed to monitor strains at the following locations.

- The connection centerline of the outermost #4 longitudinal rebar
- The stirrups above the centerline of the connection
- The stirrups below the centerline of the connection
- The wall of the outermost #4 longitudinal rebar

Two strain gages were installed at each location, and both connections were instrumented. Figure C.8 in Appendix C shows the locations of the strain gages. In addition, concrete strain

gages were placed around the connection and at various locations around to wall, refer to Figure C.7 in Appendix C.

5.4.2 Materials

The material properties are shown in the following figures.

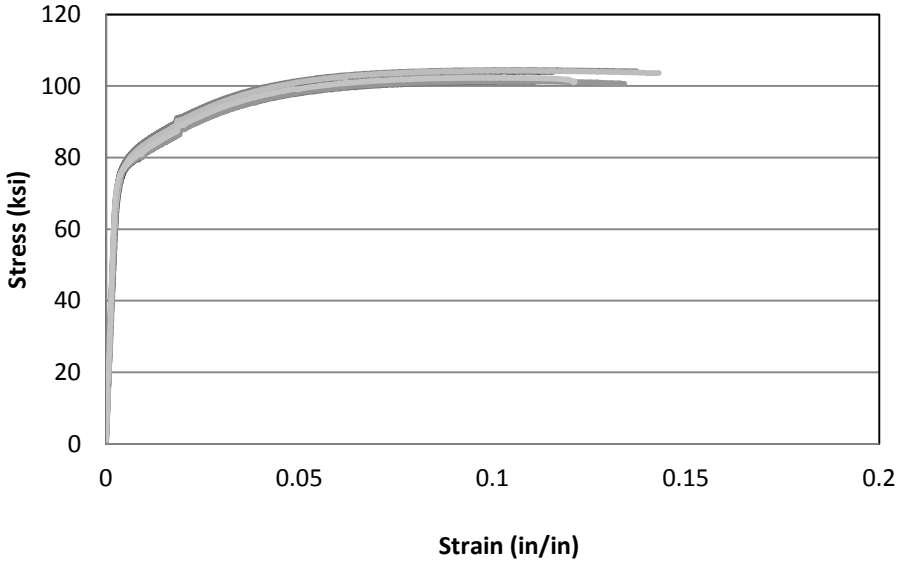

Figure 5.6: ASTM A615 Grade 75 #4 Rebar used in wall

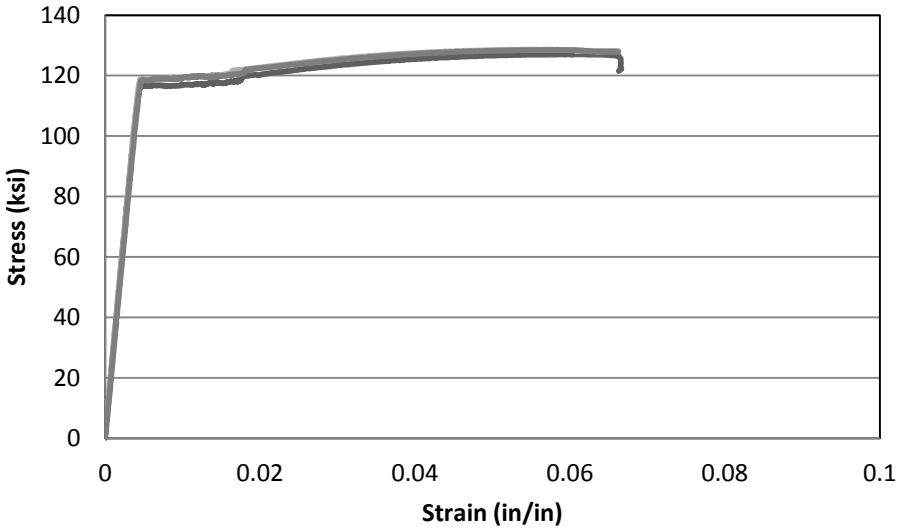

Figure 5.7: ASTM A193-B7 Threaded Rod Used as Anchors

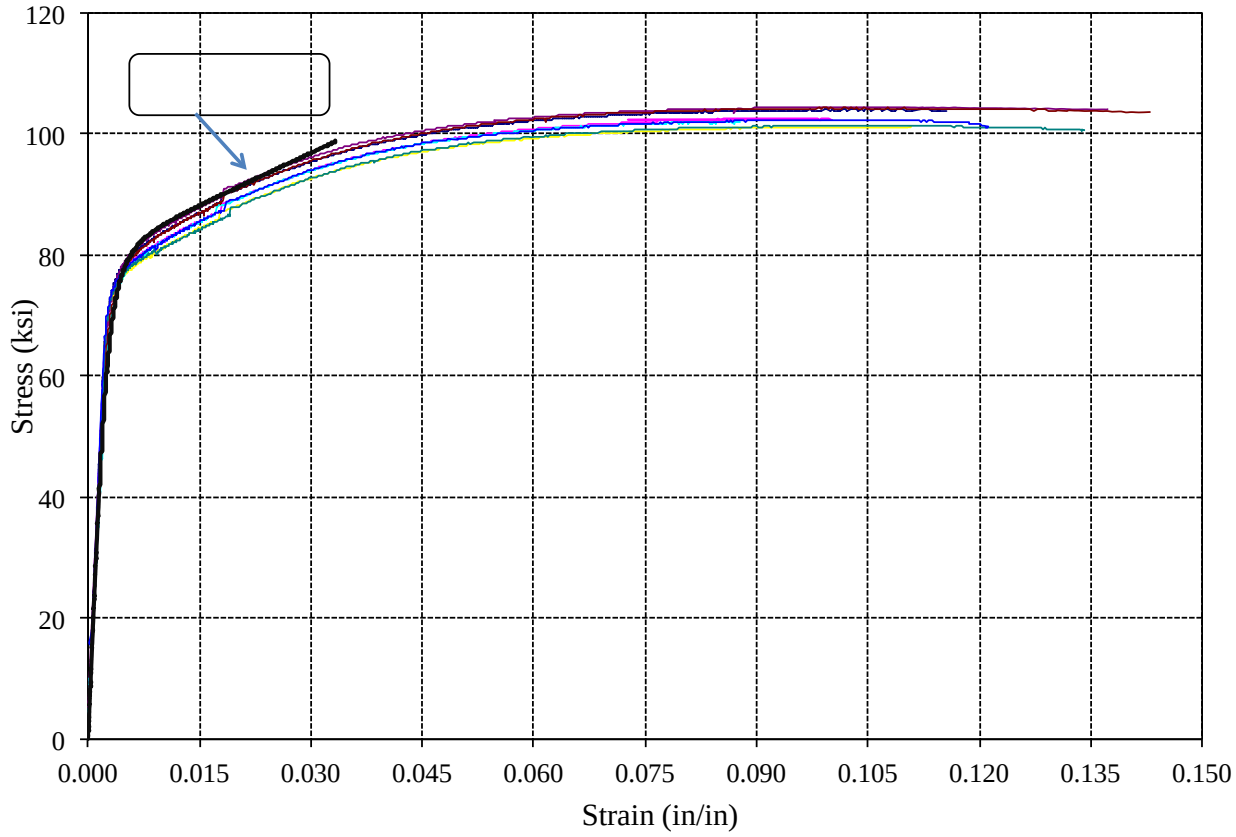

Figure 5.8: Correlation of measured stress-strain diagrams by a Ramberg-Osgood function

5.4.3 Experimental Program

The test was performed in an upright position at the NEES facility at the University of Illinois at Urbana-Champaign. The specimen was loaded using one loading and boundary condition box (LBCB) and two actuators angled at 23 degrees from the horizontal, one attached to each embedded anchor connection on the left and right sides of the wall. The LBCB, attached to the top of the wall, applied a constant axial compressive load equal to $0.10f_c'Ag$ or 300 kips throughout the duration of the test as well as a cyclic lateral load as shown in the schematic in Figure 5.9. The actuators were loaded laterally with a 1:2 ratio to that of the LBCB. The loading protocol consisted of three cycles with the same displacement amplitudes followed by one cycle with smaller displacement amplitude corresponding to the preceding cycle. Figure 5.10 shows representative cycles for the actuators and LBCB. The test specimen was designed such that the wall would have developed its flexural capacity at the base when the anchors reached their expected capacity. Loading the wall up to its expected capacity was intended to ensure that

heavy cracking and possibly spalling of the concrete would take place near the connection so that the behavior of the anchors near or in a plastic hinge zone could be evaluated.

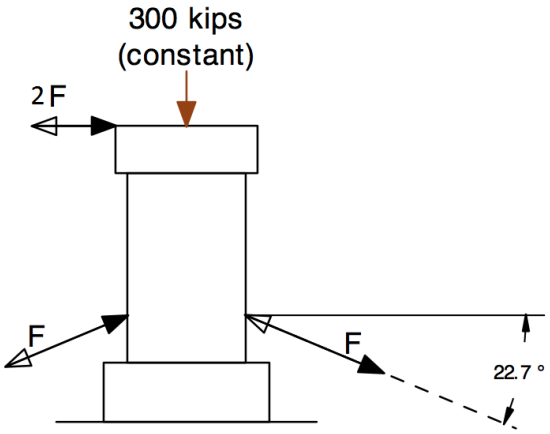

Figure 5.9: Loading Schematic (Phase IV)

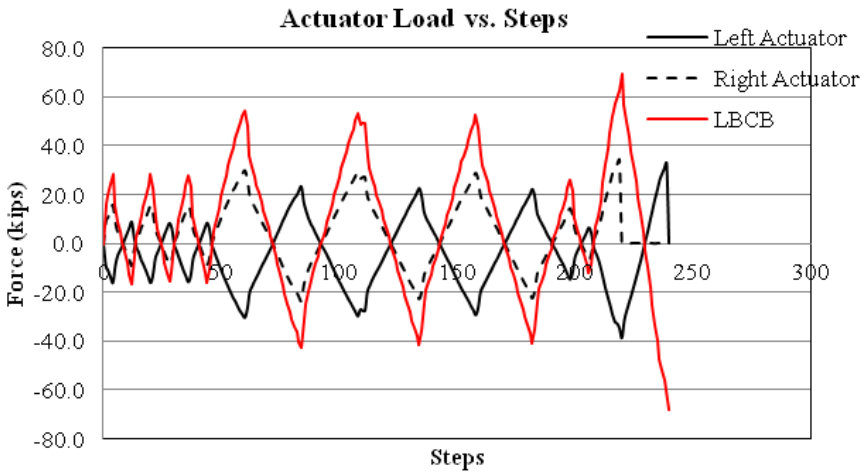

Figure 5.10: Actuator loading on anchor connections

5.5 Test Results and Discussion

5.5.1 Connection Capacity

As shown in Figures 5.11 and 5.12, both the left and right anchor connections failed due to steel fracture. The same failure mode is expected per ACI 318-08 Appendix D provisions. The right anchor was the first connection to fail at a load of 37.9 kips followed by the left anchor at 36.0 kips. Up to failure of the first connection, both the left and right anchors were loaded simultaneously. The actuator connected to the right anchor was removed after failure of this connection, and only the left anchor was loaded. The axial loading and lateral loading of the

wall were not altered after failure of the first anchor. The hysteresis response of the wall is shown in Figure 5.13. The right connection failed when the wall lateral load (i.e., base shear) was 105 kips with a corresponding lateral drift of 0.178 in. or 0.15%. Failure of the left connection occurred at 90.6 kips. The hysteresis response indicates the wall had experienced a significant level of inelasticity by the time the connections failed.

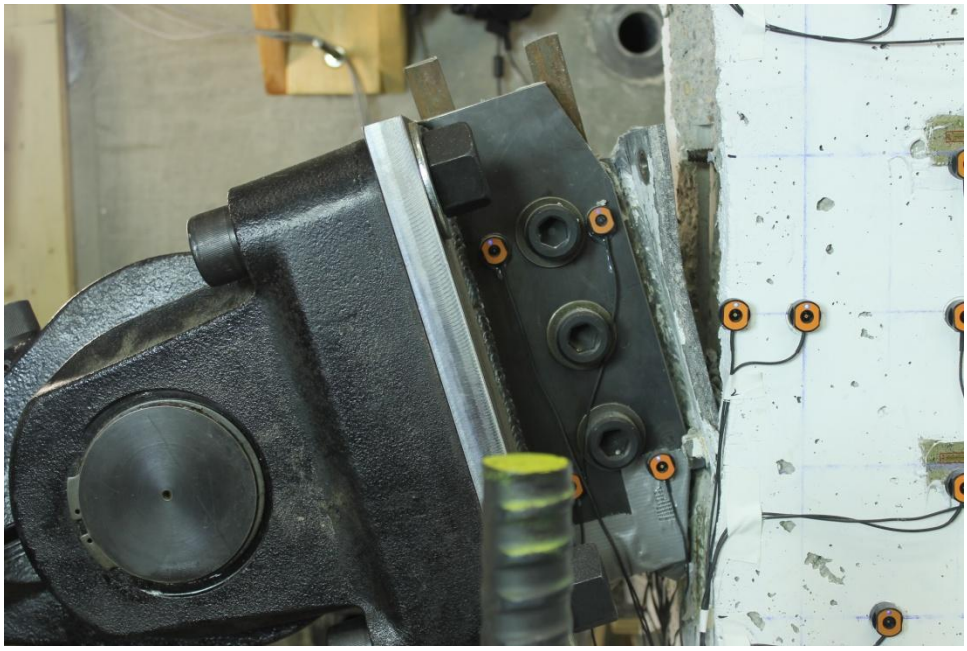

Figure 5.11: Photo of left anchor connection at failure

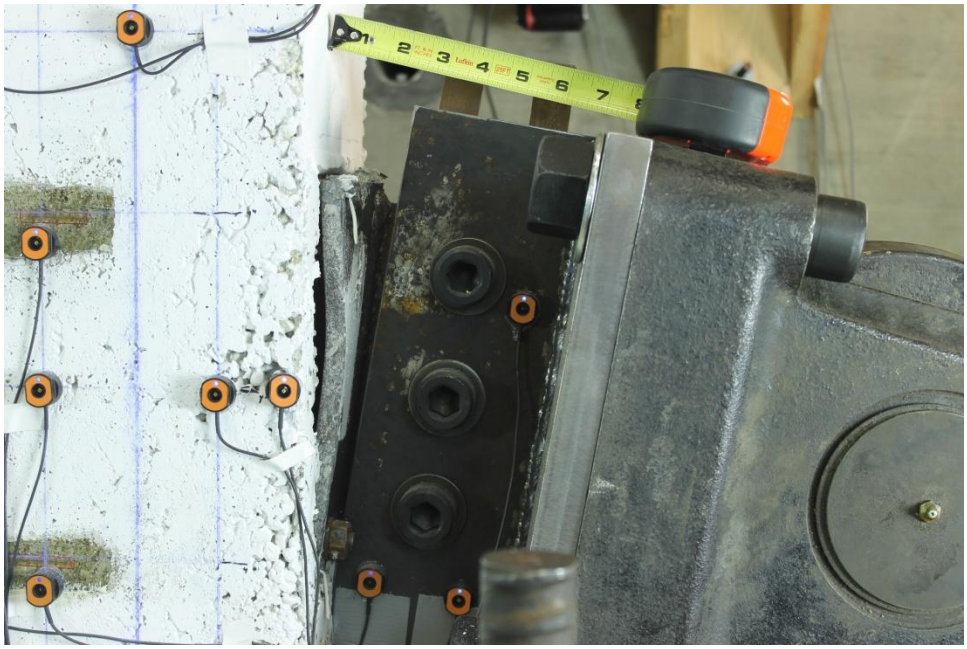

Figure 5.12: Photo of right anchor connection at failure

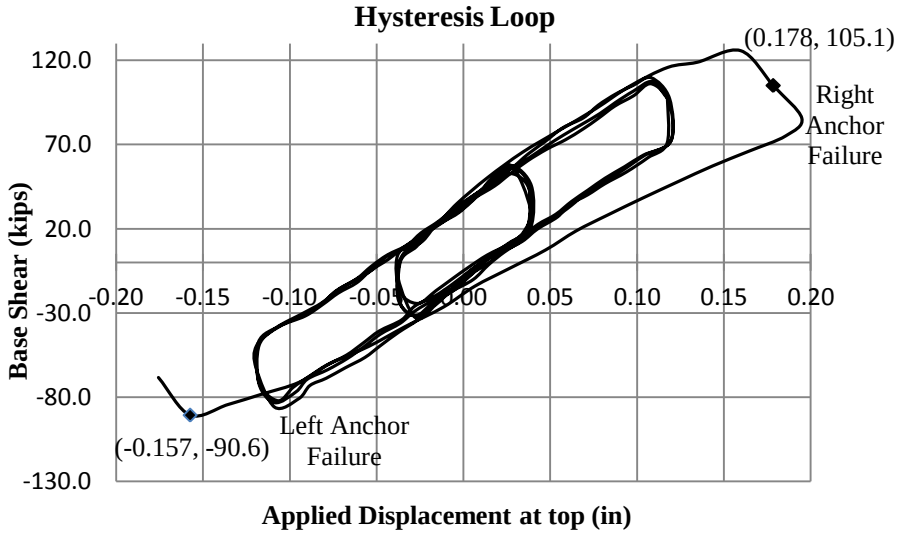

Figure 5.13: Wall hysteresis response

5.5.2 Evaluation of Connection Performance

As discussed in Section 5.3, the expected capacity of the anchor connections was 59.0 kips. However, the connections failed at approximately 63% of the calculated capacity. In an attempt to understand the discrepancy between the expected and measured capacities, a parametric study involving 7 cases was conducted.

5.5.2.1 Parameters

The main variables for the parametric study were (a) the eccentricity shear in the connection, (b) the distribution of the tensile force between the top and bottom anchors, (c) the threaded rods' tensile strength, and (d) the ratio between the shear and tensile strengths of the threaded rods. Different distribution of tension force between the top and bottom anchors was intended to simulate the effects of localized cracking and damage that affect the distribution of the total tension force among the anchors that are in tension or in compression. In design calculations, the small eccentricity of the shear force is neglected. The eccentric shear will, however, produce a moment that affects the distribution of tensile force in the top and bottom anchors. For all cases the applied shear was distributed equally among the four anchors. That is, the shear in each threaded anchor is 25% of the total applied shear force. The influence of the aforementioned variables was examined with reference to the model shown in Figure 5.14.

The range of these variables is summarized in Table 5.5. Case 1 in this table is the control case, i.e., the model used in the design calculations shown in Section 5.3.3.

Table 5: Variables for Parametric Study

Case No.	1	2	3	4	5	6	7
Threaded rod tensile strength, f_u (ksi)	125	125	125	120	120	118	118
Threaded rod shear capacity/tensile strength	0.6	0.6	0.577	0.577	0.577	0.577	0.577
Shear eccentricity, (in)	0	2.5	2.5	2.5	3.0	2.5	3.0
%Tension to top bolts	50	50	50	60	60	60	60
%Tension to bottom bolts	50	50	50	40	40	40	40

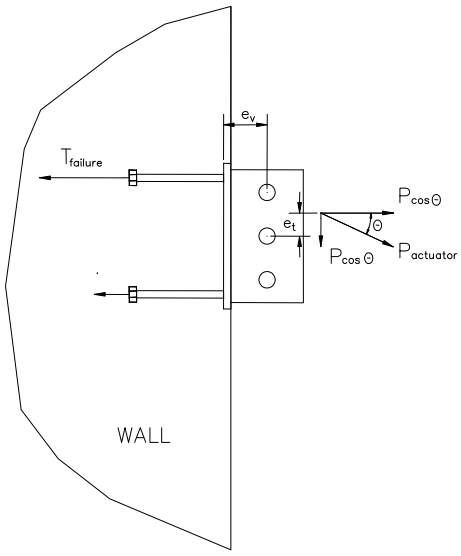

Figure 5.14: Free body model of anchor connection

The shear force eccentricity (e_v) was taken as 0", 2.5", and 3.0". The small shear eccentricity is commonly ignored in design, and the value of zero for case 1 corresponds to this practice. The distribution of the total applied tensile force was changed from 50%, i.e., an equal distribution among the top and bottom anchors, to 60%, i.e., a larger tensile force in the top anchors. The actual eccentricity was greatly increased because the connection between the hydraulic actuators and the anchor connections were made such that the actual shear force was applied at the swivel head of the actuators, as shown in Figure 5.11 and 5.12. The increased eccentricity caused additional tension on the top two anchors, which had contributed to the unexpected early failure.

Although the tensile strength of the threaded rods was established, material variability is expected. The use of resistance factors for LRFD or safety factors for ASD design account for such a variability. The tensile strength of the threaded rods was measured to be 125 ksi, which was used for cases 1, 2, and 3. In case of the remaining 4 cases, the tensile strength was taken as 118 or 120 ksi, i.e., 5.6% or 4% smaller than the measured value.

Using Von Mises yield criterion, the shear strength is $1/\sqrt{3}$ of the tensile strength. This value, which is 0.577, is commonly rounded up to 0.6. For example, ACI D.6.1 uses the equation $V_{sa} = n0.6A_{se,V}f_{uta}$ to compute the shear strength of anchors. The rounding of 0.577 to 0.60 is minor, but it was, nevertheless, selected as a variable.

5.5.2.2 Results and Discussions

Consistent with the observed mode of failure (Figures 5.11 and 5.12), the top anchors, which are subjected to a tensile force, are more critical than the bottom anchors. Hence, the calculations were focused on the capacity of the top anchors. Two shear-tensile load interaction relationships were considered: (a) a trilinear equation, and (b) the traditional power equation. These two interaction relationships are compared in Figure 5.15.

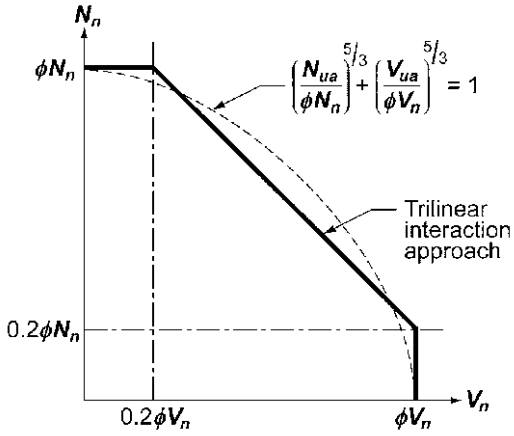

Figure 5.15: Design Interaction Diagram (Source: ACI 318-08)

The following equations define the trilinear interaction diagram.

If $V_{ua} \le 0.2\phi V_n$ the full strength in tension is permitted, i.e., $fN_n \ge N_{ua}$ or $\frac{fN_n}{N_{ua}} \ge 1.0$

If $N_{ua} \le 0.2\phi N_n$ the full strength in shear shall be permitted, i.e., $fV_n \ge V_{ua}$ or $\frac{fV_n}{V_{ua}} \ge 1.0$

If $V_{ua} > 0.2\phi V_n$ and $N_{ua} > 0.2\phi N_n$, the interaction equation is $\left(\frac{N_{ua}}{\phi N_n}\right) + \left(\frac{V_{ua}}{\phi V_n}\right) \le 1.2$

or $\left(\frac{N_{ua}}{1.2\phi N_n}\right) + \left(\frac{V_{ua}}{1.2\phi V_n}\right) \le 1.0$

As indicated in Figure 5.15, the power interaction equation is $\left(\frac{N_{ua}}{\phi N_n}\right)^{5/3} + \left(\frac{V_{ua}}{\phi V_n}\right)^{5/3} \le 1.0$

A value of one from any of the above equations indicates that the predicted strength is equal to the actual strength. When the value is below unity, the predicted strength is underestimated; and when the value is above unity, the predicted strength is overestimated.

The interaction values were computed for each case shown in Table 5.5. The values are shown in Table 5.6 separately for the trilinear and power interaction equations. The results are also shown graphically in Figure 5.16.

Table 5.6: Values for interaction equations

(a) Right Connection							
Case No.*	1	2	3	4	5	6	7
N_{ua} (kips)	8.7	11.0	11.0	12.8	13.2	12.8	13.2
V_{ua} (kips)	3.7	3.7	3.7	3.7	3.7	3.7	3.7
ϕN_n (kips)	17.7	17.7	17.7	17.0	17.0	16.7	16.7
ϕV_n (kips)	10.6	10.6	10.2	9.8	9.8	9.7	9.7
Power Interaction Eq.	0.48	0.63	0.64	0.82	0.85	0.84	0.88
Tilinear Interaction Eq.	0.70	0.81	0.82	0.94	0.96	0.96	0.98
(b) Left Connection							
Case No.*	1	2	3	4	5	6	7
N_{ua} (kips)	8.3	10.5	10.5	12.1	12.6	12.1	12.6
V_{ua} (kips)	3.5	3.5	3.5	3.5	3.5	3.5	3.5
ϕN_n (kips)	17.7	17.7	17.7	17.0	17.0	16.7	16.7
ϕV_n (kips)	10.6	10.6	10.2	9.8	9.8	9.7	9.7
Power Interaction Eq.	0.44	0.57	0.58	0.75	0.78	0.77	0.81
Tilinear Interaction Eq.	0.66	0.77	0.78	0.89	0.91	0.91	0.93

* See Table 5.5 for case numbers.

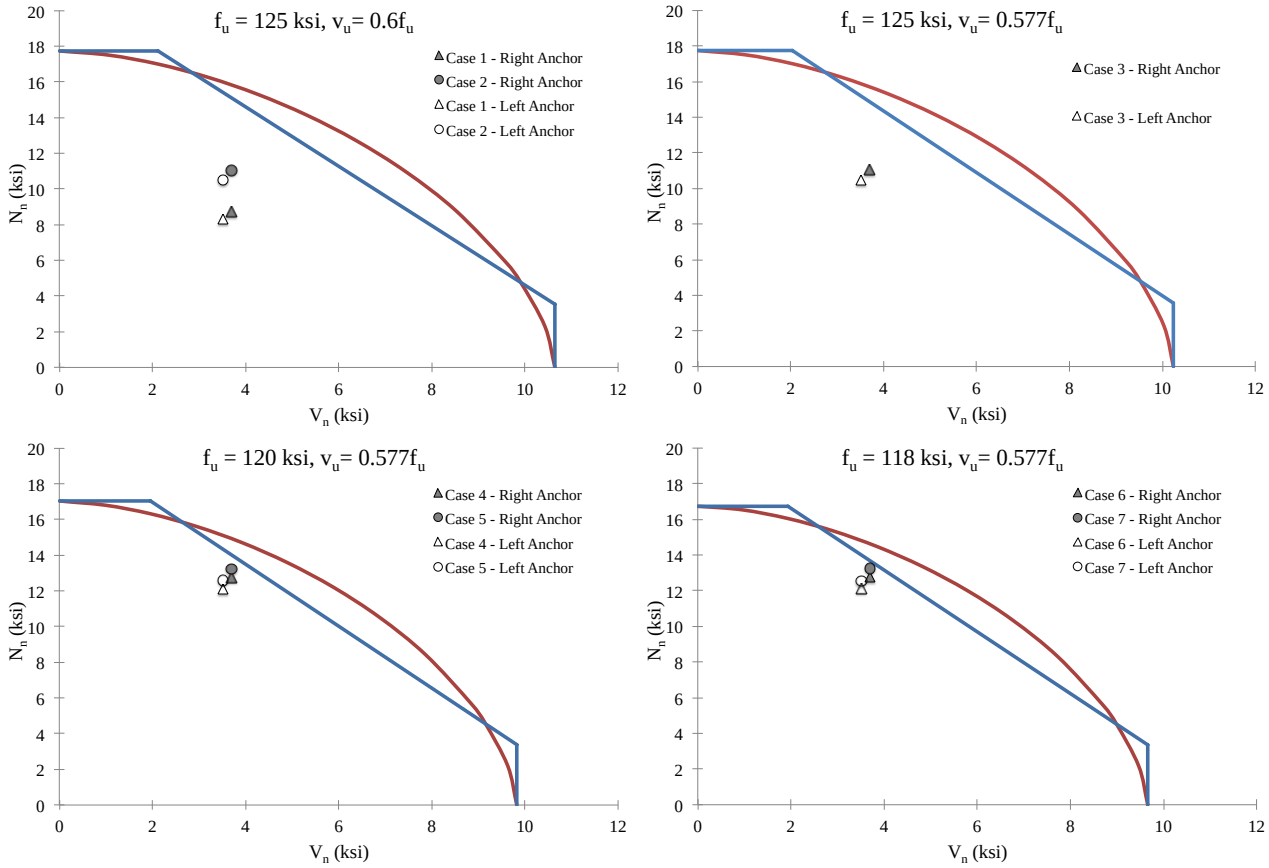

Figure 5.16: Interaction Diagrams for Various Cases and Load Demands

For the test specimen, $V_{ua} > 0.2\phi V_n$ and $N_{ua} > 0.2\phi N_n$; hence, the trilinear interaction equation is more conservative than the traditional power interaction equation, as evident by larger interaction values shown in Table 6 or the closeness of the demands to the interaction diagrams illustrated in Figure 5.16. Using the parameters selected for Case 7 in conjunction with trilinear interaction equation, the interaction values are nearly equal to unity (0.98 and 0.93 for the right connection and left connection, respectively). Although it is unlikely that all of the selected parameters would have synergistically reduced the connection capacity, the sensitivity of the calculated capacity due to small variations in design parameters is evident. The effect of a small shear eccentricity of 2.5 in., which is typically ignored in design, is appreciable. The only difference between cases 1 and 2 is the shear eccentricity, zero for Case 1 and 2.5 in. for Case 2; nevertheless, the value of interaction equation increases by a factor of 1.16 (for the trilinear interaction equation) and 1.31 (for the power interaction equation). In other words, the connection shear capacity is appreciably reduced when the small shear eccentricity is taken into account.

5.5.3 Evaluation of Wall Performance

Strain gages were bonded onto the longitudinal bars and on the transverse reinforcement (ties) above and below the connection. The exact locations of these gages are shown in Figure C-5 in Appendix C. The measured stress-strain diagrams for the wall longitudinal transverse reinforcement were consolidated into a single set of values through the use of a Ramberg-Osgood (R-O) (Collins and Mitchell 1991) function shown below

$$f_{ss} = E_s \varepsilon \left(A + \frac{1 - A}{\left[1 + (B\varepsilon)^C\right]^{1/C}} \right) \le f_{pu}$$

As shown in Appendix C, the R-O function with A = 0.02, B=350, C=3, and E = 28500 matches well with the measured stress-strain diagrams. The stress corresponding to a measured value of strain was obtained from the Ramberg-Osgood relationship. The strains and stresses at various locations corresponding to the right and left anchor failure are summarized in Table 5.6. A positive value indicates tensile strain/stress, and compressive strain/stress is denoted by a negative number.

The maximum value of overturning moment is at the based of the wall. As a result, the wall longitudinal bars at the base were the most highly stressed with the largest value being 40.2 ksi on the right side of the wall when the left anchor failed. This value corresponds approximately to $0.57f_y$, where f_y is the measured yield strength. The longitudinal bars at the elevation of the connection centerline developed a maximum stress of $0.36f_y$, which also occurred when the left anchor failed. At right anchor failure, the wall boundary element tie below the connection reached a peak stress of 19 ksi. The low level of stress in the transverse reinforcement is expected considering that the wall did not undergo major damage. The specimen had been designed such that the wall would have experienced inelastic deformations when the anchors failed. However, the anchors failed at loads lower than expected, and the design objective was not achieved.

In addition to steel strain gages, concrete strain gages were placed at various locations on the wall surface, especially around the anchors; refer to Appendix C. The strains can be found in the appendix in Table C-1.

Table 5.6: Measured strains and stresses at various locations

(a) Right Side of the Wall					
Location	**Label**	**Right Anchor Failure**		**Left Anchor Failure**	
		Strain (in/in)	**Stress (ksi)**	**Strain (in/in)**	**Stress (ksi)**
Wall longitudinal bar @ the base	Strain gage 1 (BA-S-SG-C4-1)	-1.066E-03	-30.90	1.266E-03	35.10
	Strain gage 2: (BA-S-SG-C4-2)	-1.055E-03	-30.60	1.471E-03	40.20
Transverse bar (tie) below the connection	Strain gage 3: (BA-S-SG-C4-3)	1.270E-04	3.60	5.070E-05	1.40
	Strain gage 4: (BA-S-SG-C4-4)	2.640E-05	0.75	1.080E-04	3.10
Wall longitudinal bar @ the connection C.L.	Strain gage 5: (OA-S-SG-C4-5)	-4.590E-04	-13.10	8.807E-04	24.90
	Strain gage 6: (OA-S-SG-C4-6)	-3.360E-04	-9.60	8.777E-04	24.80
Transverse bar (tie) above the connection	Strain gage 7: (OA-S-SG-C4-7)	8.630E-05	2.50	3.250E-05	0.90
	Strain gage 8: (OA-S-SG-C4-8)	1.940E-04	5.50	7.500E-05	2.10
(b) Left Side of the Wall					
Location	**Label**	**Right Anchor Failure**		**Left Anchor Failure**	
		Strain (in/in)	**Stress (ksi)**	**Strain (in/in)**	**Stress (ksi)**
Wall longitudinal bar @ the base	Strain gage 9: (BA-N-SG-C4-9)	9.450E-04	26.60	-8.639E-04	-24.80
	Strain gage 10: Malfunctioned	N/A	N/A	N/A	N/A
Transverse bar (tie) below the connection	Strain gage 11: (BA-N-SG-C4-11)	6.070E-04	17.20	2.842E-04	8.10
	Strain gage 12: (BA-N-SG-C4-12)	7.370E-04	20.90	2.187E-04	6.20
Wall longitudinal bar @ the connection C.L.	Strain gage 13: (OA-N-SG-C4-13)	7.280E-04	20.60	-4.692E-04	-13.40
	Strain gage 14: (OA-N-SG-C4-14)	1.008E-03	28.30	-2.988E-04	-8.50
Transverse bar (tie) above the connection	Strain gage 15: (OA-N-SG-C4-15)	-1.700E-05	-0.50	2.785E-04	7.90
	Strain gage 16: (OA-N-SG-C4-16)	-1.390E-04	-4.00	4.170E-04	11.90

5.6 Summary

The ½-scale specimen tested was an extension of a previous study done. Key objectives of the test were to further the understand the behavior of cast-in-place anchors under cyclic tension-shear loading located in the plastic hinge zone of a reinforced concrete shear wall. Currently, ACI Appendix D states that its provisions do not apply to the design of anchors in plastic hinge zones where a high level of cracking, spalling, and wall inelasticity would take place during a severe seismic event. Therefore it was of great interest to observe this type of behavior in order to further research in this area. Most of the key project objectives could not be fully met, due to the fact that the connections failed much earlier than anticipated. Because the connections did not reach their expected capacity, the wall was not able to experience the level of damage around the connection that would accurately mimic a severe earthquake event.

CHAPTER 6 Summary and Conclusions

6.1 Summary

The well-established design procedures for headed anchors, such as those stipulated in ACI 318-08 and in CEB design guidelines, do not allow the anchors to be installed in concrete that would be substantially damaged during an earthquake. For anchor that must be installed in such concrete as that in the plastic hinge zones of RC columns and walls, the current design codes recommend that the anchor reinforcement be provided. However, the codes are not clear about the anchor reinforcement design due to lack of experimental data.

The tests in Phase IV of the NEES-Anchor project was to verify if the code-conforming anchor reinforcement is sufficient to support the anchor connections in the plastic hinge zones. Phase IV tests included two 4-stud connections installed in the boundary element of a 1/2 concrete wall. The concrete wall was 10 ft tall and the cross section was 10 x 60 in. The anchor connections were within the plastic hinge zone of the concrete wall, which was expected to develop significant damage during the simulated seismic loading. The wall was subjected to a axial compression, equivalent to 10 percent of its axial load capacity. The wall was then subjected to cyclic loading in displacement control on its top. The generated shear force (story shear) was split into to two, and half of the measured shear force was applied to one anchor connection and the other half was applied to the other connection using two hydraulic actuators.

Meanwhile, the tests in Phases II and III of the NEES-Anchor project indicated that the key role of anchor reinforcement, in addition to carrying the forces from the anchors, is to protect concrete around the anchors from splitting, breaking out, and crushing. This better understanding of the behavior has led to alternative designs and detailing for anchor reinforcement. The focus of the Phase V tests were to 1) identify the key parameters for the desired performance of anchors in plastic hinge zones; 2) observe the behavior of anchors in plastic hinge zones with local confinement; and 3) verify the implemented anchor reinforcement detailing.

Phase V tests had six specimens: three for single anchors in tension and another three for single anchors in shear. The column specimen has a cross section of 12 x 12 in. and a height of 61 in. Nine No. 5 bars (Grade 60) are provided as the longitudinal reinforcement. The test anchors,

installed 8 in. from the base of the columns, are 3/4 in. diameter ASTM A193 Grade B7 threaded rod (f_y=105 ksi and f_{ut}=131 ksi) and a plate washer (1.5x1.5 in.) and a hex nut welded to the end.

The test anchor, if fully developed, will take an ultimate tension load of 43 kips. Two anchors are loaded in shear specimens, resulting in a similar ultimate load, which was designed within the loading capacity of the hydraulic actuator. The required anchor reinforcement for the 3/4-in. anchors was provided using four No. 4 bars, and implemented using two No. 4 closed stirrups in the column located 2-in. from the test anchor. In addition to the longitudinal bars in the column, four No. 4 U-shaped hairpins were placed near the anchor in the vertical plane. These hairpins were expected to confine the concrete from flexural cracking.

6.2 Conclusions

The connections in Phase IV tests did not reach their expected capacity. The top two headed anchors fractured in tension at early stage of loading. The failure loads were smaller than the design capacity because 1) the thickness of the embedded plate (0.5 in.) was small such that the plate bent when the shear tab, located at the middle of the embedded plate, attempted to transfer the tensile force to the two bolts 2 in. away from the shear tab; and 2) the connector between the hydraulic actuator and the shear tab was not properly fabricated such that the eccentricity of the vertical component of the applied load (shear) on the connection was significantly increased (from 2.5 in. (the design eccentricity) to 13 in. (the actual eccentricity)). The increased eccentricity significantly increased the tensile load on the top two anchors.

When the anchor fractured, the wall was not able to experience the level of damage around the connection that would accurately mimic a severe earthquake event The following conclusions could be drawn from the data that was received from the test. Note that these conclusions needs further justification using tests of anchor connections in damaged concrete.

- ACI Appendix D provisions correctly predicted the governing failure mode of the connections to be steel fracture. Thus the provisions of ACI D.4.2.1 appear to be justified. A practical way for designers to ensure a ductile failure by way of steel fracture of embedded outrigger beam-wall connections would be to design shear walls with boundary element reinforcement.

- The failure loads of both anchor connections showed that a large shear eccentricities should be considered when determining the failure loads of anchors in combined shear and tension loading, even if the eccentricities are small. This was confirmed by the parametric study which showed that even a small eccentricity of 2.5 in. made the value of the interaction equation increase approximately 31% towards unity, or the connections expected failure load

While Phase IV test was not able to provide information on the seismic behavior of anchor connections in plastic hinge zones, Phase V tests have shown that well-confined core concrete can support anchors in plastic hinge zones. Due to limited testing capacity, single anchors were tested in the part of the project. The successful tests reinstated that anchor reinforcement should confine concrete, restrain concrete from splitting and blowout, and distribute loads from anchor heads to the rest of the structure/structural element. In addition, pull-out failure should be considered in the design of reinforced anchors in tension. Concrete cover spalled during the shear tests, resulting in large reduction in anchor shear capacity. Cover spalling leads to exposed anchor shaft such that the anchors are subjected to combined shear, bending, and tension. Further studies are needed to quantify the confinement requirement.

6.3 Recommendations of Future Research

The Phase IV specimen did not meet the key research objectives, namely to achieve the level of damage around the connection that would adequately allow an assessment of the behavior of anchors in a plastic hinge zone, the lessons learned from this test will allow future research endeavors in this area to:

- Design a wall with less flexural capacity to try an ensure a high level of damage in the plastic hinge zone of the wall before anchor failure.
- Account for the eccentricity of the shear when computing predicted anchor failures to prevent the connection from failing more prematurely than expected.
- Design a proper connection, including the embedded plate, anchor bolts, and the anchor reinforcement to provide satisfactory seismic performance.

References

1. American Concrete Institute (ACI), "Building Code Requirements for Structural Concrete (ACI 318-11)." Farmington Hills, MI, 2011.
2. ACI Committee 349, 1990, "Code Requirements for Nuclear Safety Related Concrete Structures (349-90)," American Concrete Institute, Farmington Hills, Mich., 33 pp.
3. American Concrete Institute (ACI), "State-of-the-Art Report on Anchorage to Concrete, ACI 355.1R-91 (reapproved in 1997), American Concrete Institute, Farmington Hills. MI.
4. Cannon, R., (1981) "Expansion Anchor Performance in Cracked Concrete," *ACI Journal, Proceeding*, vol. 78, no. 6, pp. 471-479.
5. Cannon, R., (1995) "Straight Talk about Anchorage to Concrete, Part II." *ACI Structural Journal*, vol. 92, no. 6, pp. 1-11.
6. Comité Euro-International du Béton (CEB), (1997) "Fastenings to Concrete and Masonry Structures: State of the Art Report." Thomas Telford Service Ltd., London.
7. Cook, R. A. and Klinger, R. E. (1991). "Behavior of ductile multiple anchor steel-to-concrete connections with surface-mounted baseplates." *Anchors in Concrete–Design and Behavior, SP-130*, G. A. Senkiw and B. Lancelot, III, eds., American Concrete Institute, Farmington Hills, MI.
8. Cook, R. A., and Klingner, R. E. (1992). ''Ductile multiple-anchor steel to-concrete connections.'' Journal of Structural Engineering, vol. 118 no. 6, pp.1645–1665.
9. Copley, J. D., and Burdette, E. G., (1985) "Behavior of Steel-to-Concrete Anchorage in High Moment Regions," *ACI JOURNAL, Proceedings*, vol. 82, no. 2, pp. 180-187.
10. Eligehausen, R.; Mallée, R.; and Silva, J., (2006) "Anchorage in Concrete Construction." Wilhelm Ernst & Sohn, Berlin, Germany.
11. Eligehausen, R., and Balogh, T. (1995) "Behavior of Fasteners Loaded in Tension in Cracked Reinforced Concrete," *ACI Structural Journal*, vol. 92. no. 3, 29-35.
12. Eligehausen, R.; Mattis, L. (2004) Wollmershauser, R.; and Hoehler, M. S., "Testing Anchors in Cracked Concrete—Guidance for Testing Laboratories: How to Generate Cracks," *Concrete International*, vol. 26, no. 7, pp. 66-71.

13. Federation Internationale du Beton (*fib*), "Fastenings to Concrete and Masonry Structures." Special Activity Groups (SAG) 4 draft report, 2008, Obtained from Dr. Eligehausen.

14. Fogstad, C., Sailer, M., and Marxer, G. (2001) "Anchoring in Cracked Concrete." Hilti Technical Publication. A web document accessed in July 2013 at http://www.us.hilti.com/data/techlib/docs/technical publications/anchoring/.
15. Grauvilardell, J., Lee, D., Hajjar, J., and Dexter, R. (2005). "Synthesis of design, testing and analysis research on steel column base plate connections in high-seismic zones." *Structural Engineering Report no. ST-04-02*, University of Minnesota, Minneapolis, MN.
16. Hawkins, N. M., Mitchell, D., and Roeder, C. W. (1980). ''Moment resisting connections for mixed construction.'' Engineering Journal, vol. 17, no. 1, pp. 1–10.
17. Hoehler, M. and Eligehausen, R. (2008), "Behavior of anchors in cracked concrete under tension cycling at near-ultimate loads." *ACI Structural Journal*, vol. 105, No.5, pp. 601-608.
18. Hoehler, M., (2006) "Behavior and Testing of Fastenings to Concrete for Use in Seismic Applications, PhD dissertation, Universität Stuttgart, Stuttgart, Germany, 2006, 261 pp.
19. Ibarra L. F., and Krawinkler, H. (2005). "Global collapse of frame structures under seismic excitations", Rep. no. TB 152, The John A. Blume Earthquake Engineering Center, Stanford University, Stanford, CA.
20. Jang, J. and Suh, Y. (2006), "The experimental investigation of a crack's influence on the concrete breakout strength of a cast-in-place anchor." *Nuclear Engineering and Design*, vol. 236, no. 9, pp. 948-953.
21. Klingner, R.; Mendonca, J.; and Malik J., (1982). "Effect of Reinforcing Details on the Shear Resistance of Anchor Bolts under Reversed Cyclic Loading," *ACI Journal*, vol. 79 , no. 1, pp. 471-479.
22. Lin, Z., Petersen, D. Zhao, J., and Tian, Y. (2011) Simulation and design of exposed anchor bolts in shear. *International Journal of Theoretical and Applied Multiscale Mechanics*. vol. 2, pp. 111-119.
23. Lotze, E., and Klingner, R. (1997). "Behavior of multiple-anchor connections to concrete from the perspective of plastic theory." *PMFSEL Report no. 96-4*, University of Texas at Austin, TX.

24. Martin, H., and Schwarzkopf, M., "Versuche mit Kopfbolzen im gerissenen Beton (Tests with Headed Studs in Cracked Concrete)," Institut fur Betonstahl und Stahlbeton, Report no. 578/84, Munchen, 1984. (in German in Eligehausen and Balogh ,1995)
25. Oehlers, D. J. (1989). "Splitting induced by shear connectors in composite beams." J. Struct. Engrg., ASCE, 115(2), 341-362.
26. Oehlers, D.J. (1990). "Deterioration in strength of stud connectors in composite bridge beams." J. Struct. Engrg., ASCE, 116(12), 3417-3431.
27. Oehlers, D. J., and Coughlan, C. G. (1986). "The shear stiffness of stud shear connections in composite beams." J. Constr. Steel Res., 6(4), 273-284.
28. Oehlers, D. J., and Johnson, R. P. (1981). "The splitting strength of concrete prisms subjected to surface strip or patch loads." Mag. Concr. Res., 33(116), 171-179.
29. Oehlers, D. J., and Johnson, R. P. (1987). "The strength of stud shear connections in composite beams." Struct. Engr., 65B(2), 44-48.
30. Oehlers, D. and Park, S. (1992), "Shear connectors in composite beams with longitudinally cracked slabs." *Journal of the Structural Engineering*," vol. 118, no. 8, pp. 2004-2022.
31. Pallarés, L. and Hajjar, J. (2010a). "Headed steel stud anchors in composite structures, Part I: Shear." *Journal of Constructional Steel Research*, vol. 66, no. 2, pp.198-212.
32. Pallarés, L. and Hajjar, J. (2010b). "Headed steel stud anchors in composite structures, Part II: Tension," *Journal of Constructional Steel Research*, vol. 66, no. 2, pp. 213-228.
33. Roeder, C. W., and Hawkins, N. M. (1981). ''Connections between steel frames and concrete walls.'' Engineering Journal, vol. 18, no. 1, pp. 22–29.
34. Shahrooz, B.; Deason, J.; and Tunc, G., (2004) "Outrigger Beam–Wall Connections. I: Component Testing and Development of Design Model," *Journal of Structural Engineering*, vol. 130, no. 2, pp. 253-261.
35. Shahrooz, B.; Tunc, G.; and Deason, J., (2004) "Outrigger Beam–Wall Connections. II: Subassembly Testing and Further Modeling Enhancements," *Journal of Structural Engineering*, vol. 130, no. 2, pp. 262-270.
36. Shahrooz, B.M., Tunc., G., Deason, J. T. (2002), "RC/Composite Wall-Steel Frame Hybrid Buildings: Connections and System Behavior," Report no. UC-CII 02/01
37. XTRACT-Cross Sectional X Structural Analysis of Components version 2.6.2, copyright (2002). Imbsen and Associates, Inc. Computer Program.

38. Yoon, Y., Kim, H., and Kim, S. (2001), "Assessment of Fracture behavior for CIP anchors fastened to cracked and uncracked concrete." *KCI structural Journal*, vol. 13, no. 3, pp. 33-41.
39. Zhang, Y., Klingner, R. E. and Graves, III, H. L., "Seismic Response of Multiple-Anchor Connections to Concrete," Structures Journal, American Concrete Institute, Farmington Hills, Michigan, vol. 98, no. 6, pp. 811-822.
40. Zhao, J, Shahrooz, B. and Tong, X. (2008). Seismic Behavior and Design of Cast-in-Place Anchors/Headed Studs, 14th World Conference on Earthquake Engineering, October 12-17 2008, Beijing, China
41. Zhao, J. and Sritharan, S. (2007) Modeling of Strain Penetration Effects in Fiber-Based Analysis of Reinforced Concrete Structures. *ACI Structural Journal*, V. 104, no. 2, 1-7.

APPENDIX A Records of Crack Development in Phase V tests

A.1 Crack patterns of Specimen T2 under Cyclic Loading

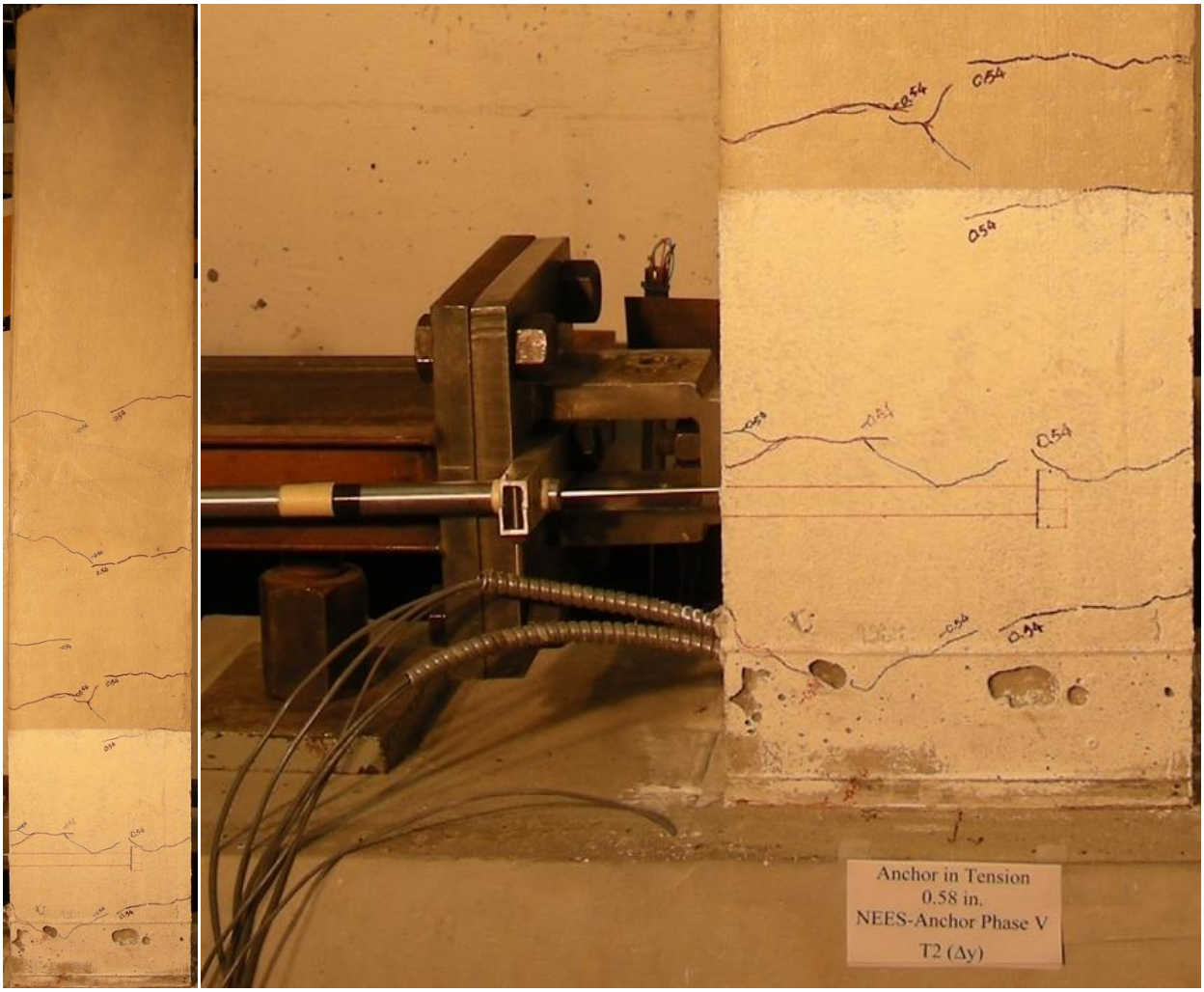

(a) Column crack pattern **(b) local cracking pattern**

Figure A.1-T2 after loading at ±0.58 in.

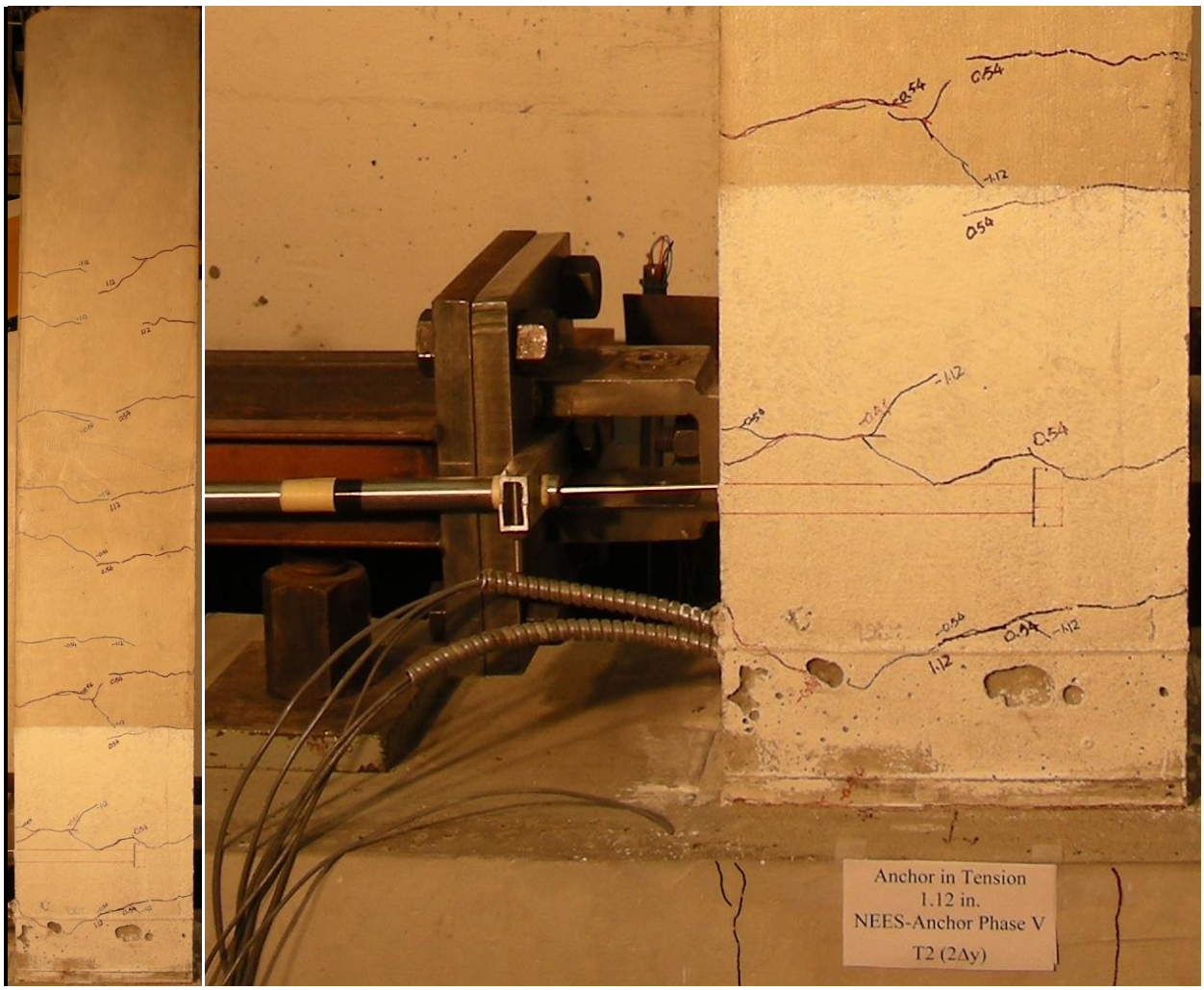

(a) Column crack pattern **(b) local cracking pattern**

Figure A.2-T2 after loading at ±1.12 in.

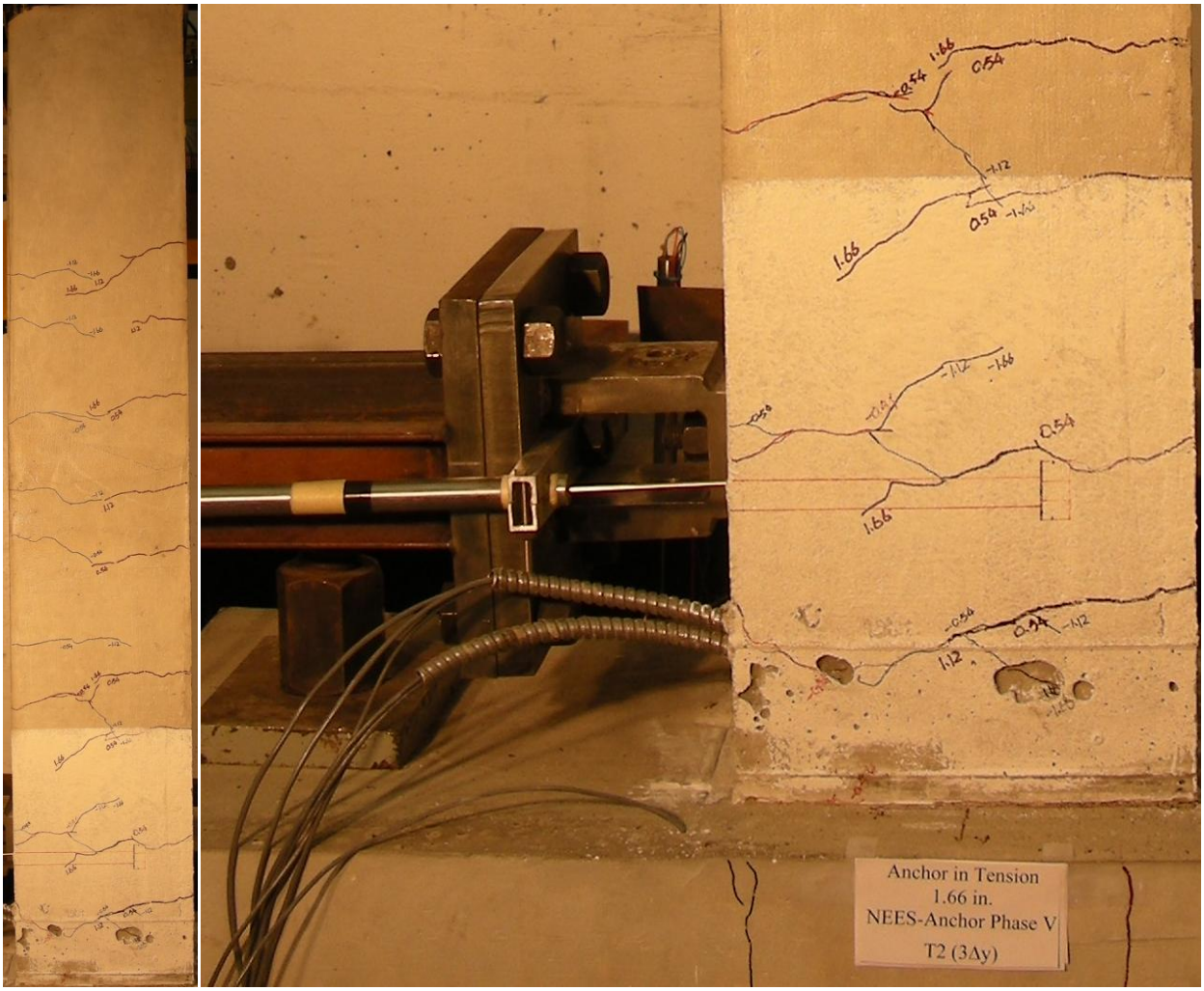

(a) Column crack pattern **(b) local cracking pattern**

Figure A.3-T2 after loading at ±1.66 in.

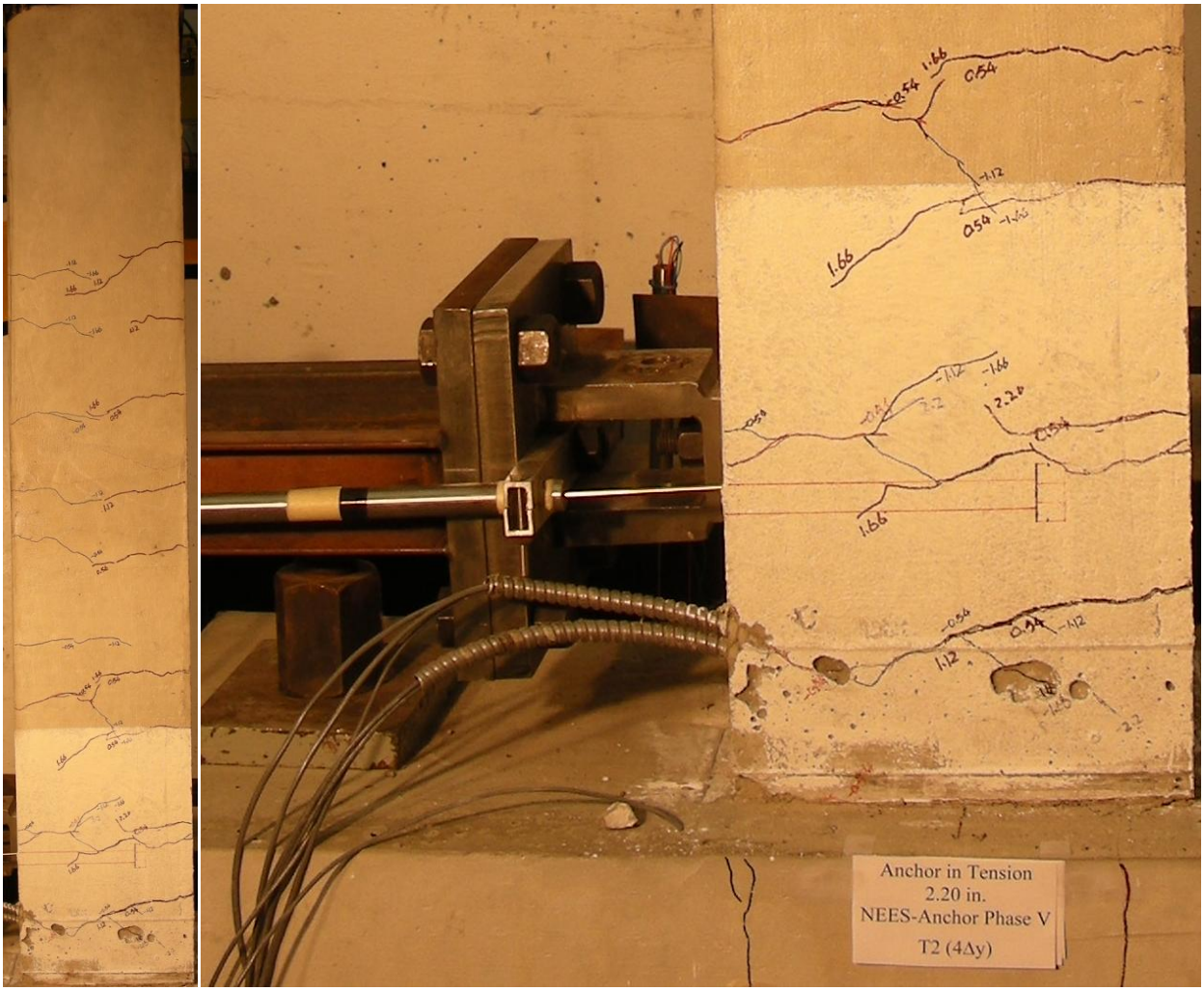

(a) Column crack pattern **(b) local cracking pattern**

Figure A.4-T2 after loading at ±2.2 in.

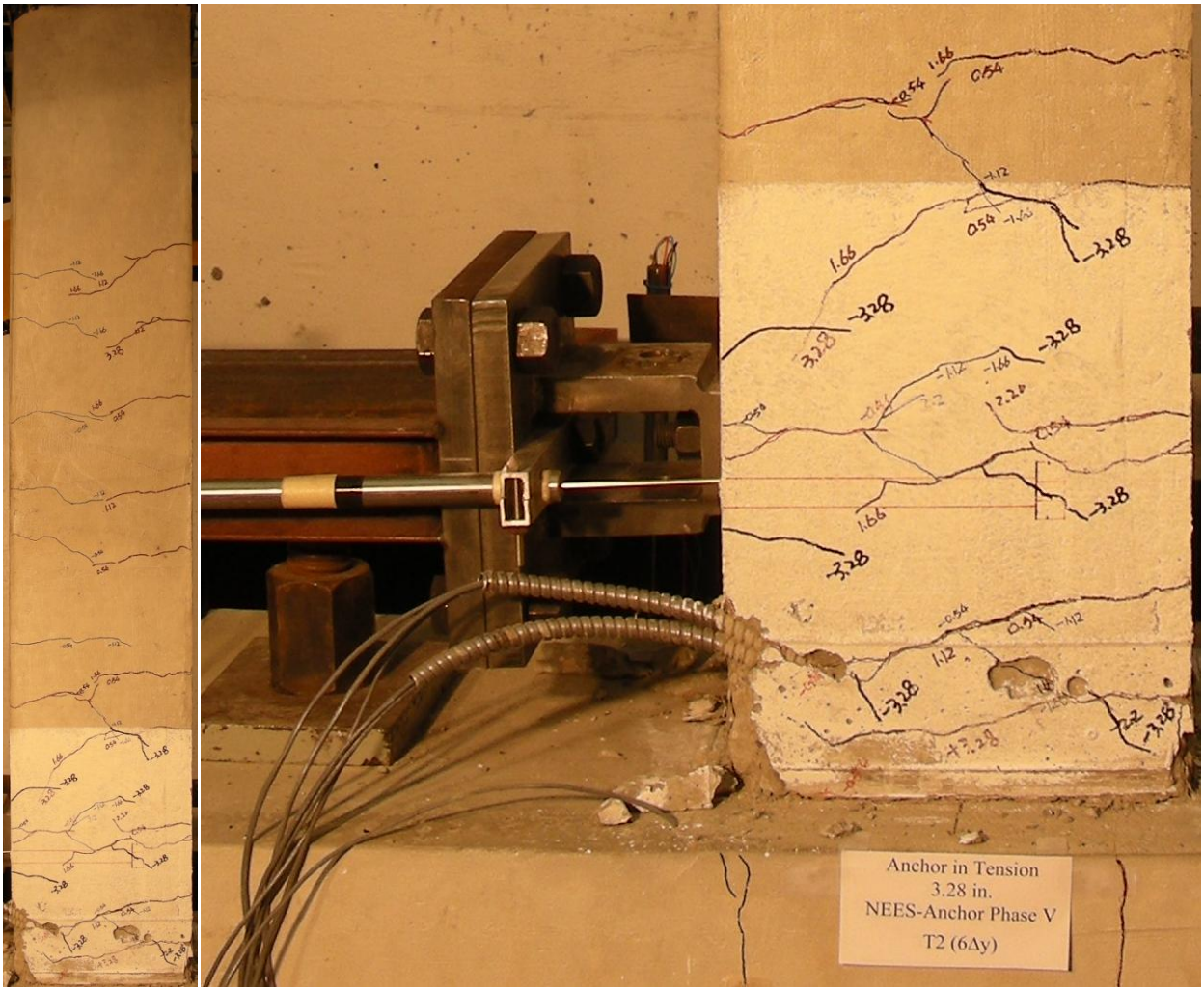

(a) Column crack pattern **(b) local cracking pattern**

Figure A.5-T2 after loading at ±3.28 in.

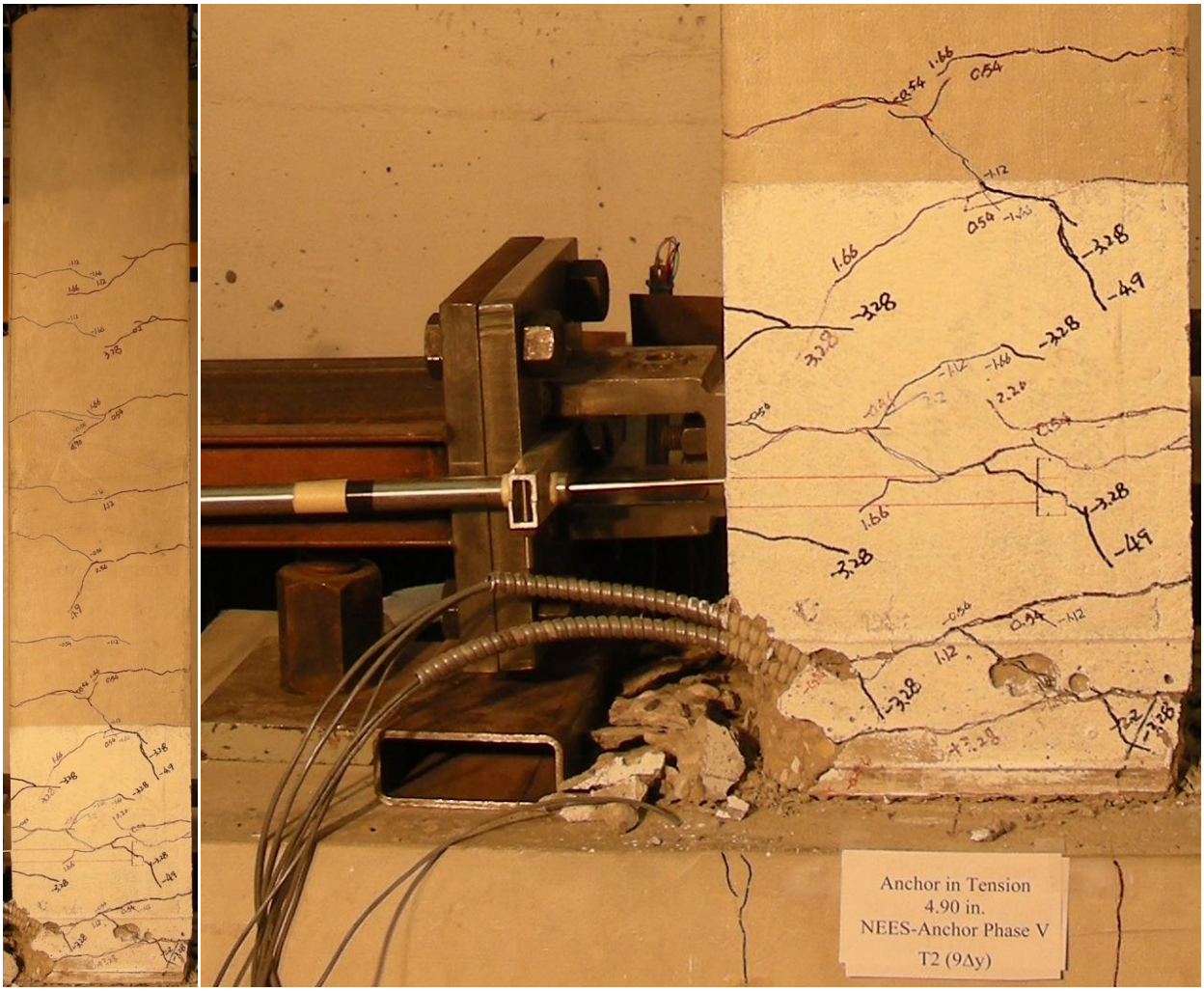

(a) Column crack pattern **(b) local cracking pattern**

Figure A.6-T2 after loading at ±4.9 in.

(a) ±0.58 in. (b) ±1.12 in. (c) ±1.66 in. (d) ±2.20 in. (e) ±3.28 in. (f) ±4.9 in.

Figure A.7-Crack development after all loading cycles (T2)

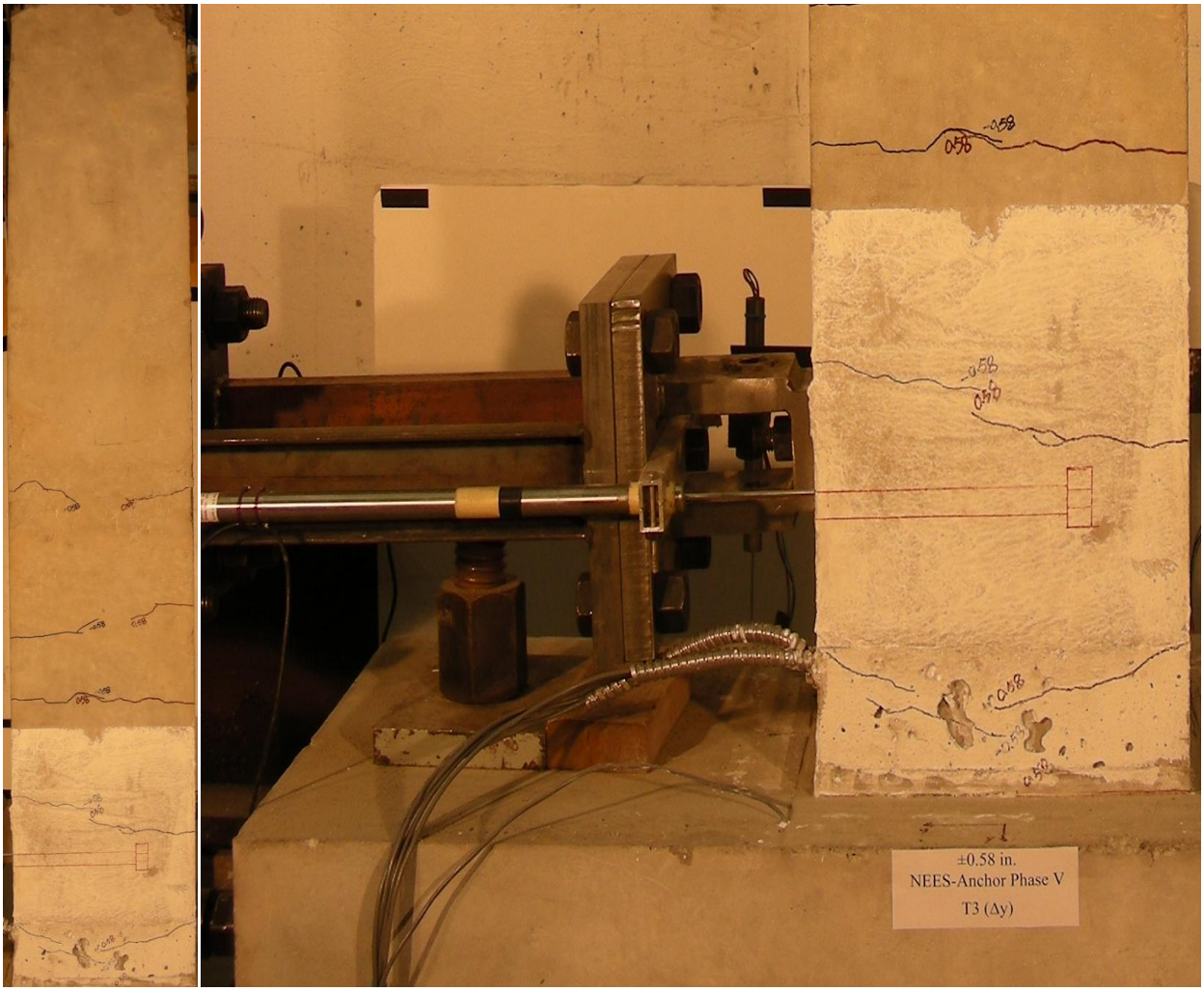

(a) Column crack pattern **(b) local cracking pattern**

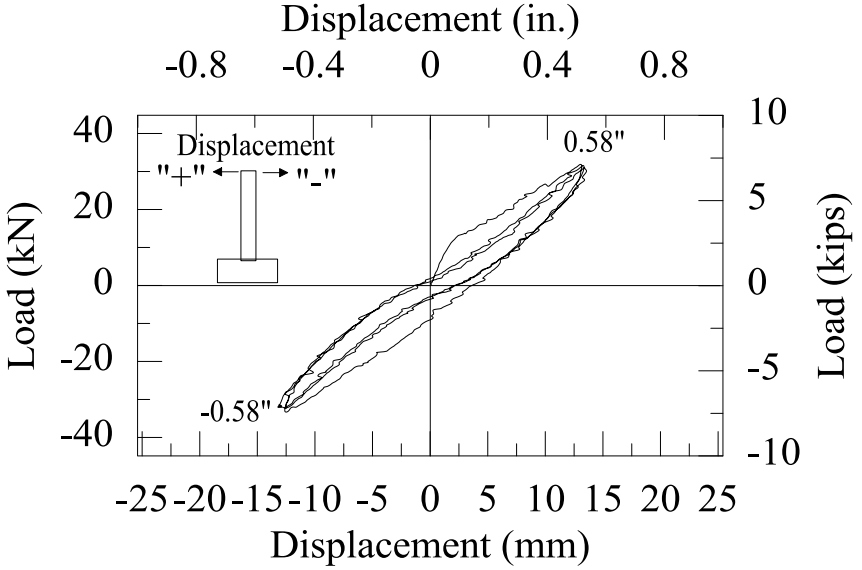

(c) Load vs. displacement

Figure A.8-T3 after loading at ±0.58 in.

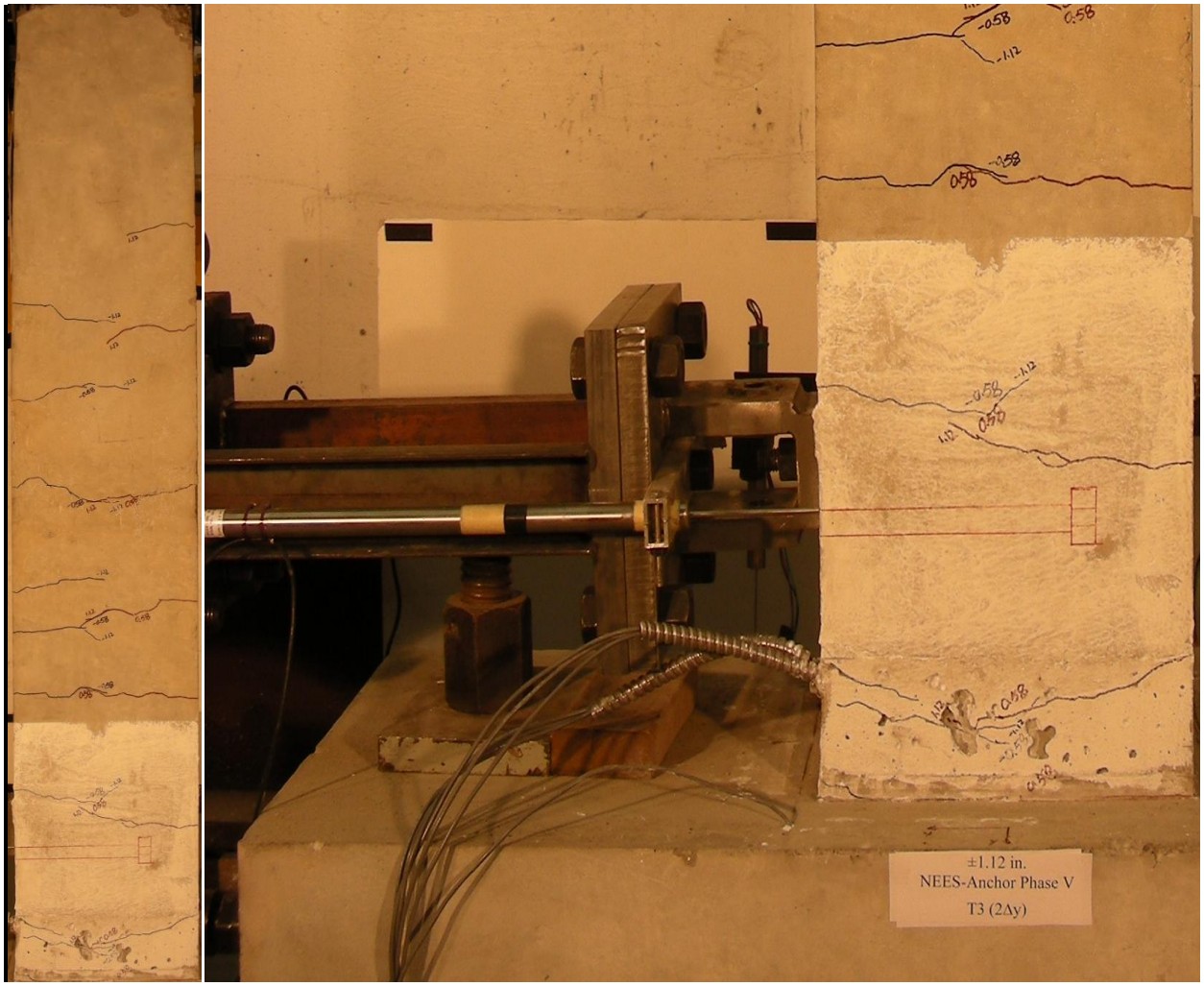

(a) Column crack pattern **(b) local cracking pattern**

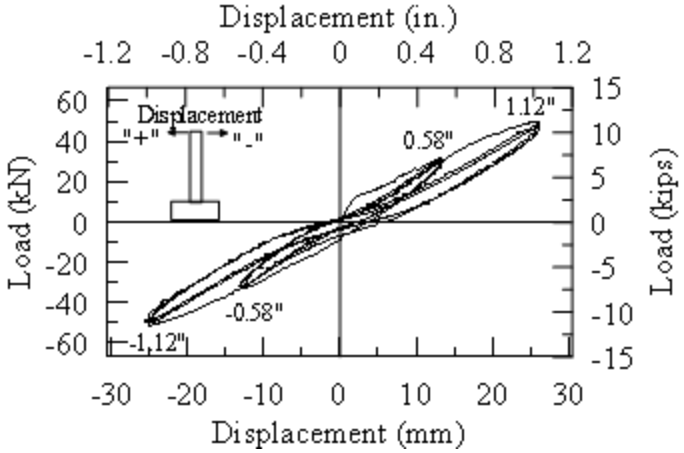

(c) Load vs. displacement

Figure A.9-T3 after loading at ±1.12 in.

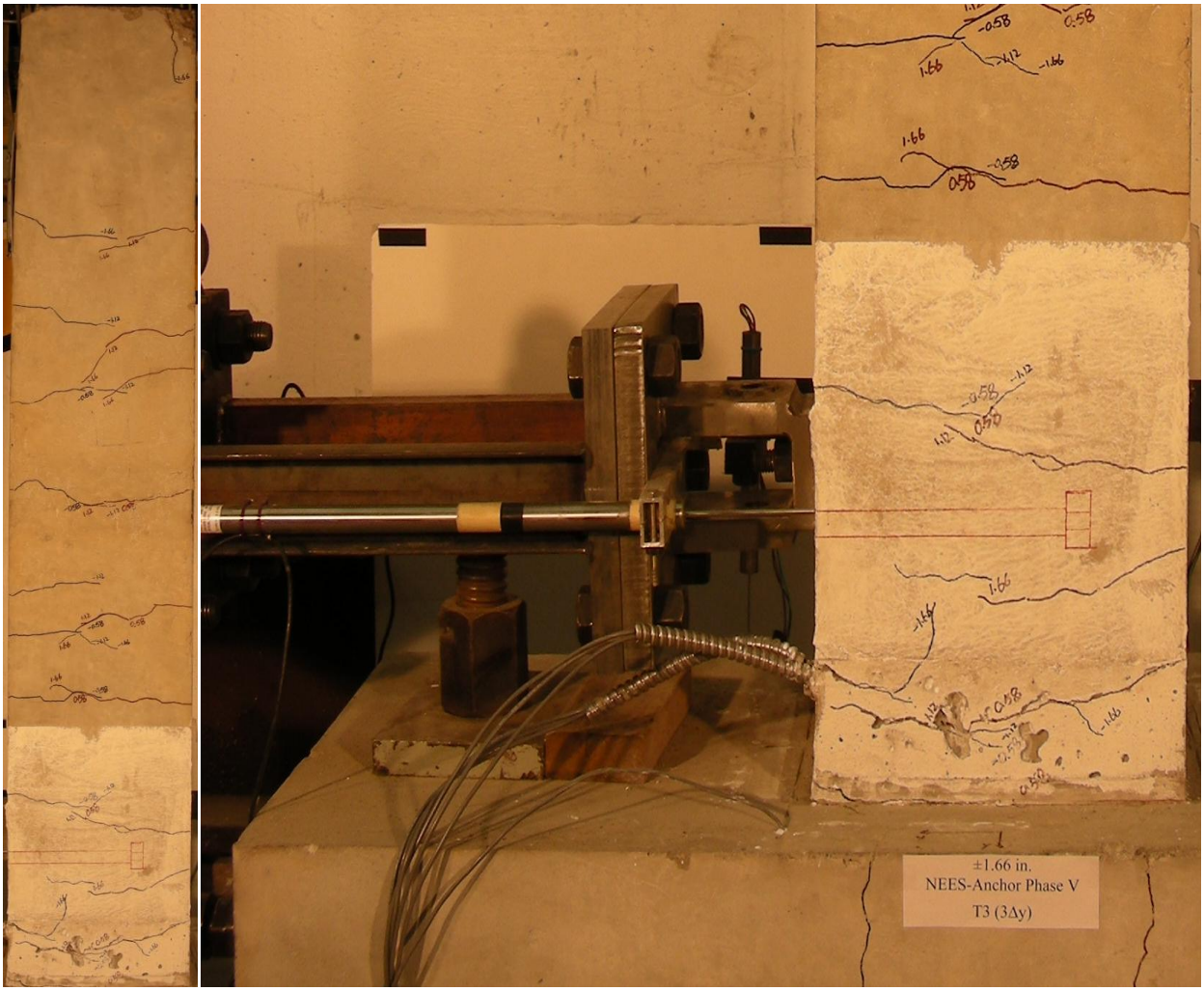

(a) Column crack pattern **(b) local cracking pattern**

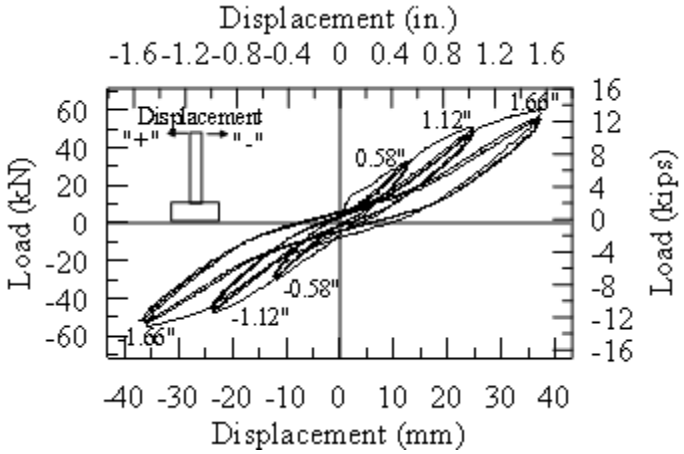

(c) Load vs. displacement

Figure A.10-T3 after loading at ±1.66 in.

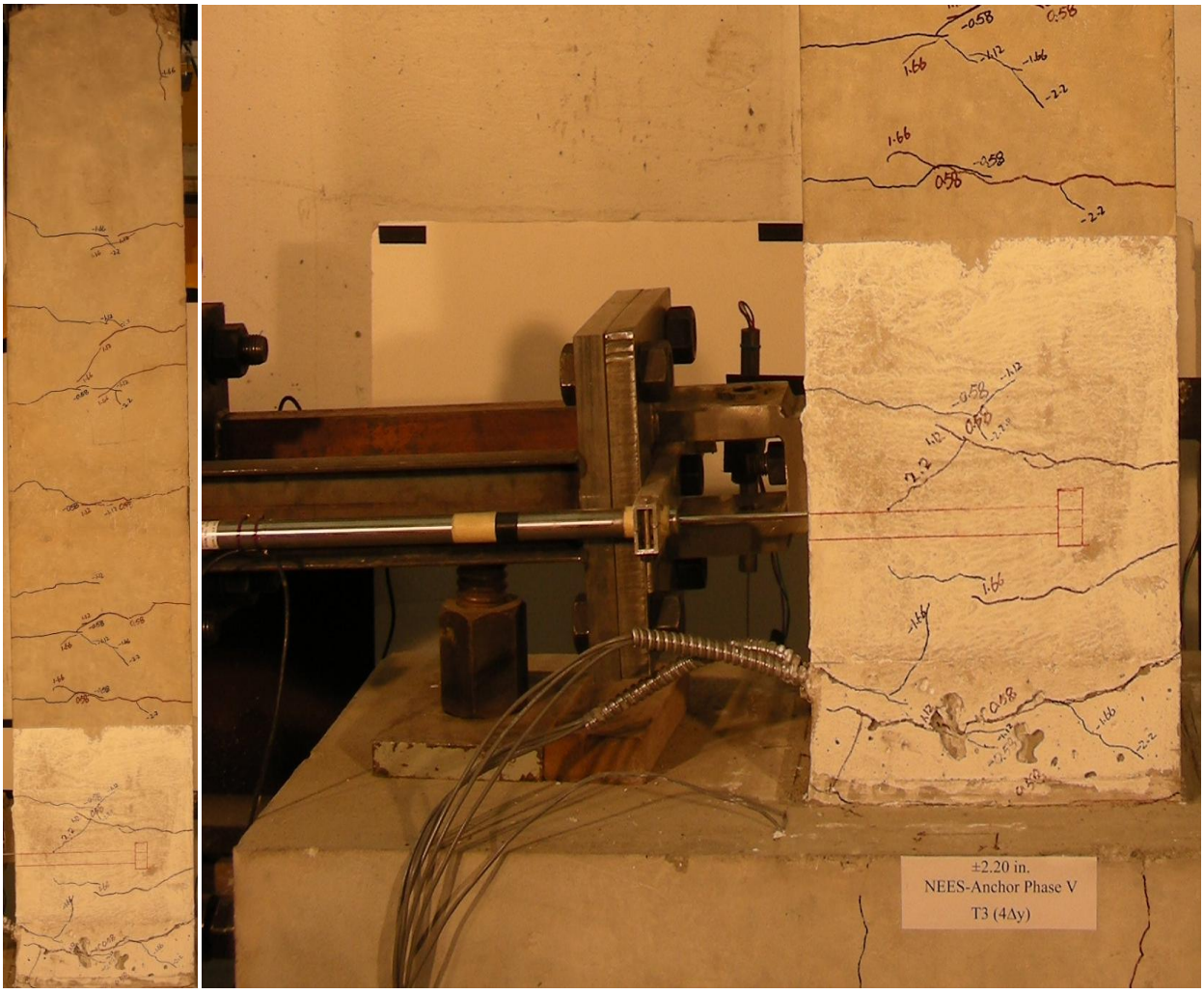

(a) Column crack pattern **(b) local cracking pattern**

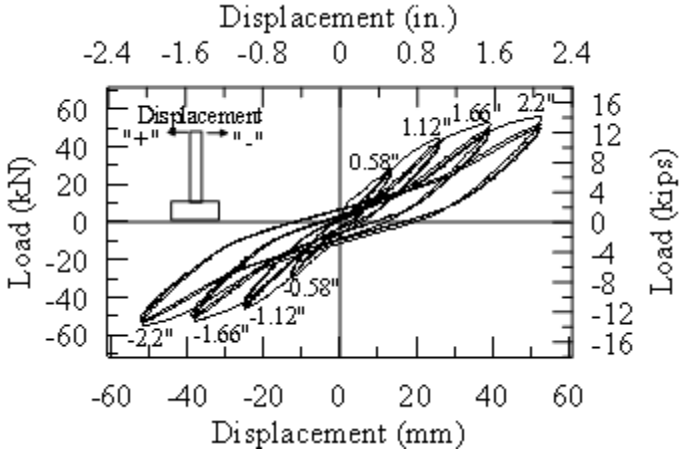

(c) Load vs. displacement

Figure A.11-T3 after loading at ±2.20 in.

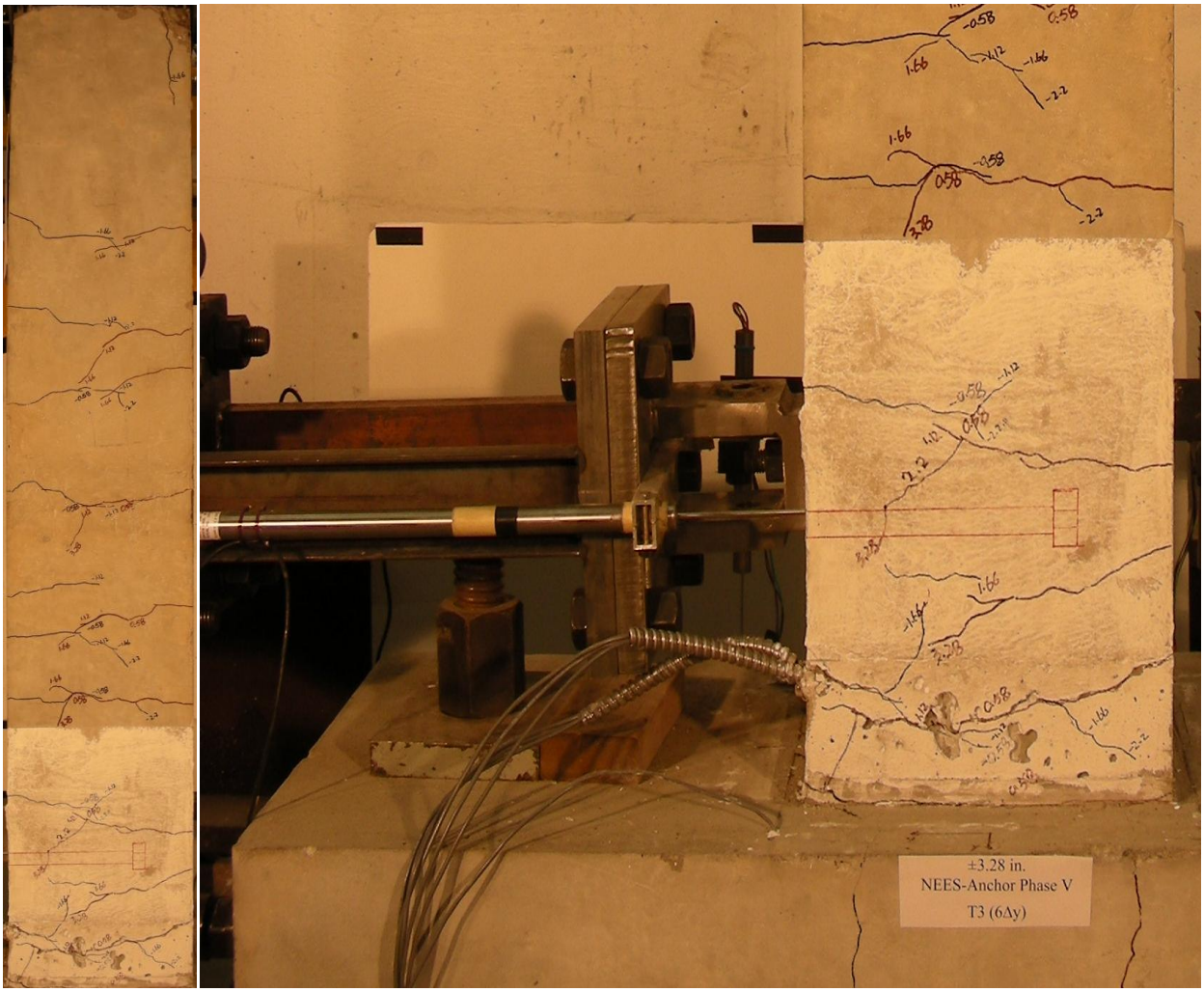

(a) Column crack pattern **(b) local cracking pattern**

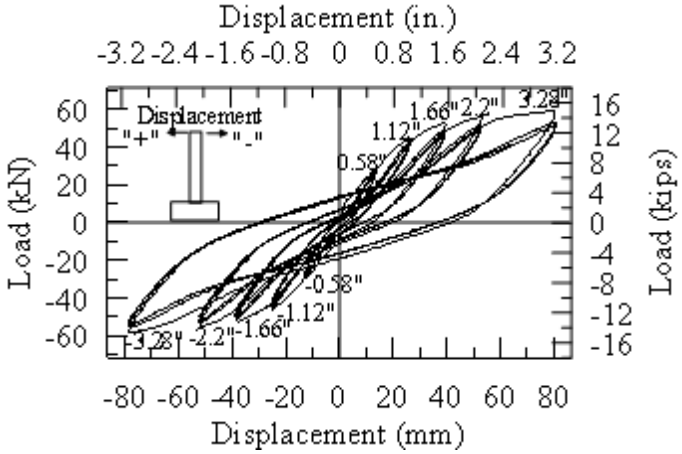

(c) Load vs. displacement

Figure A.12-T3 after loading at ±3.28 in.

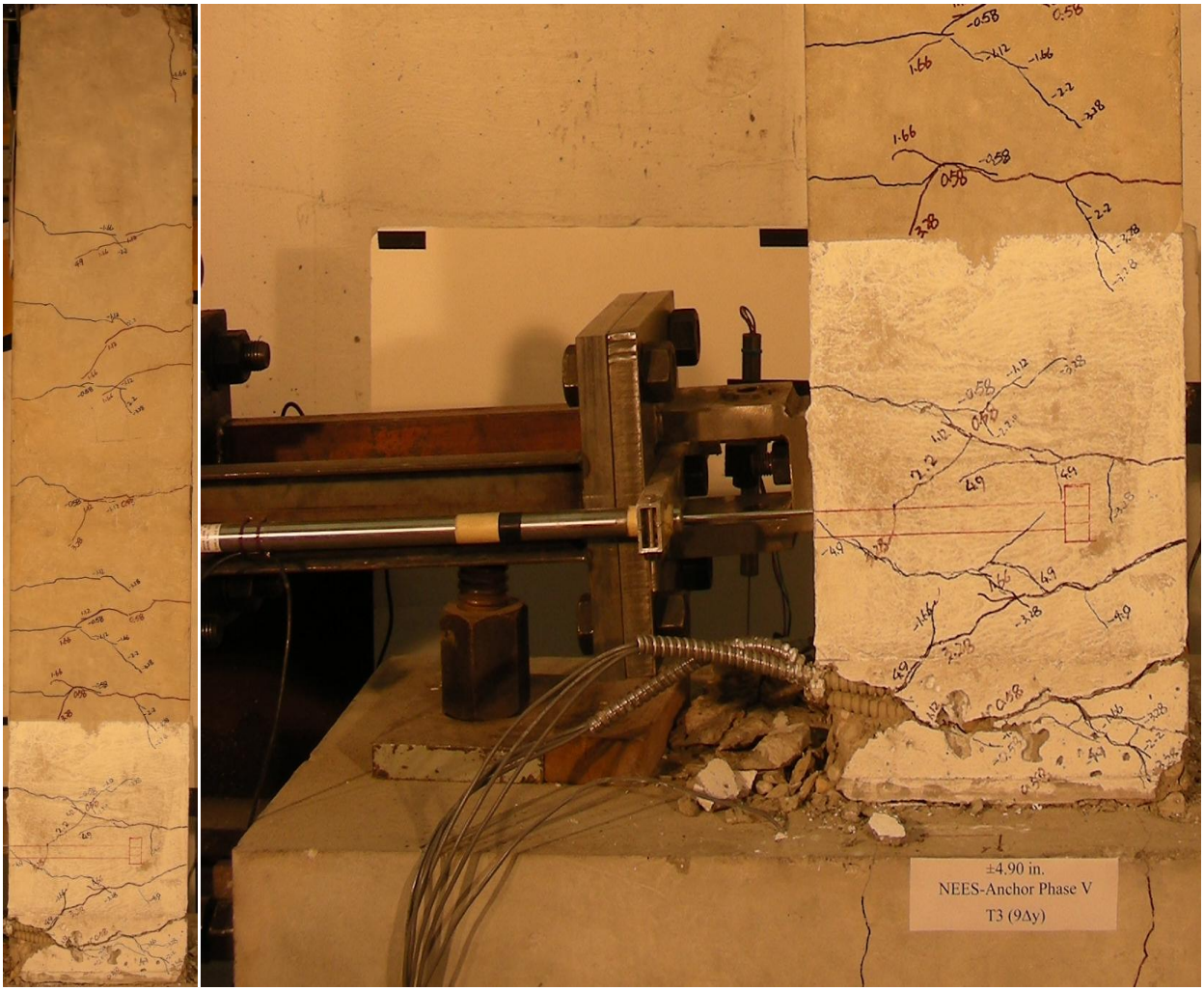

(a) Column crack pattern **(b) local cracking pattern**

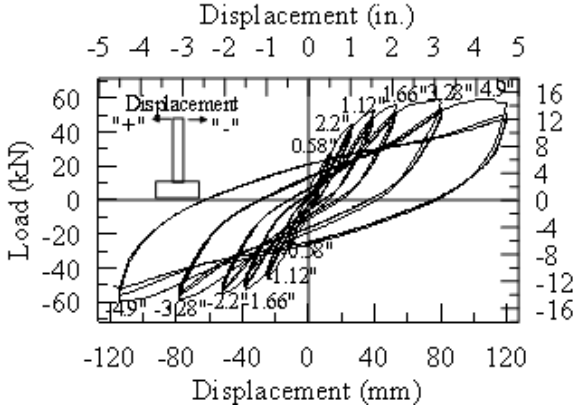

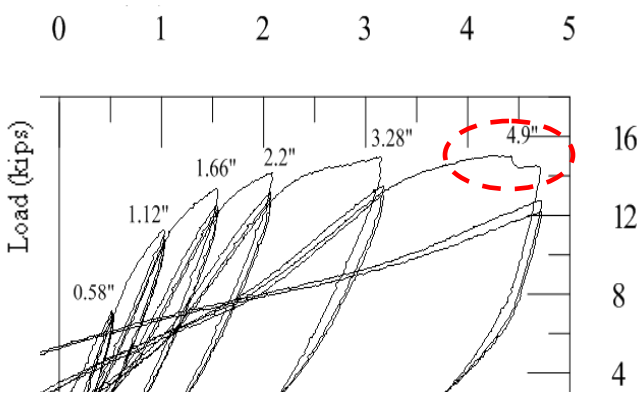

(c) Load vs. displacement **(d) local load drop near 4.9 in.**

Figure A.13-T3 after loading at ±4.9 in.

(a) ±0.58 in. (b) ±1.12 in. (c) ±1.66 in. (d) ±2.20 in. (e) ±3.28 in. (f) ±4.9 in.

Figure A.14-Crack map under various loading cycles (T3)

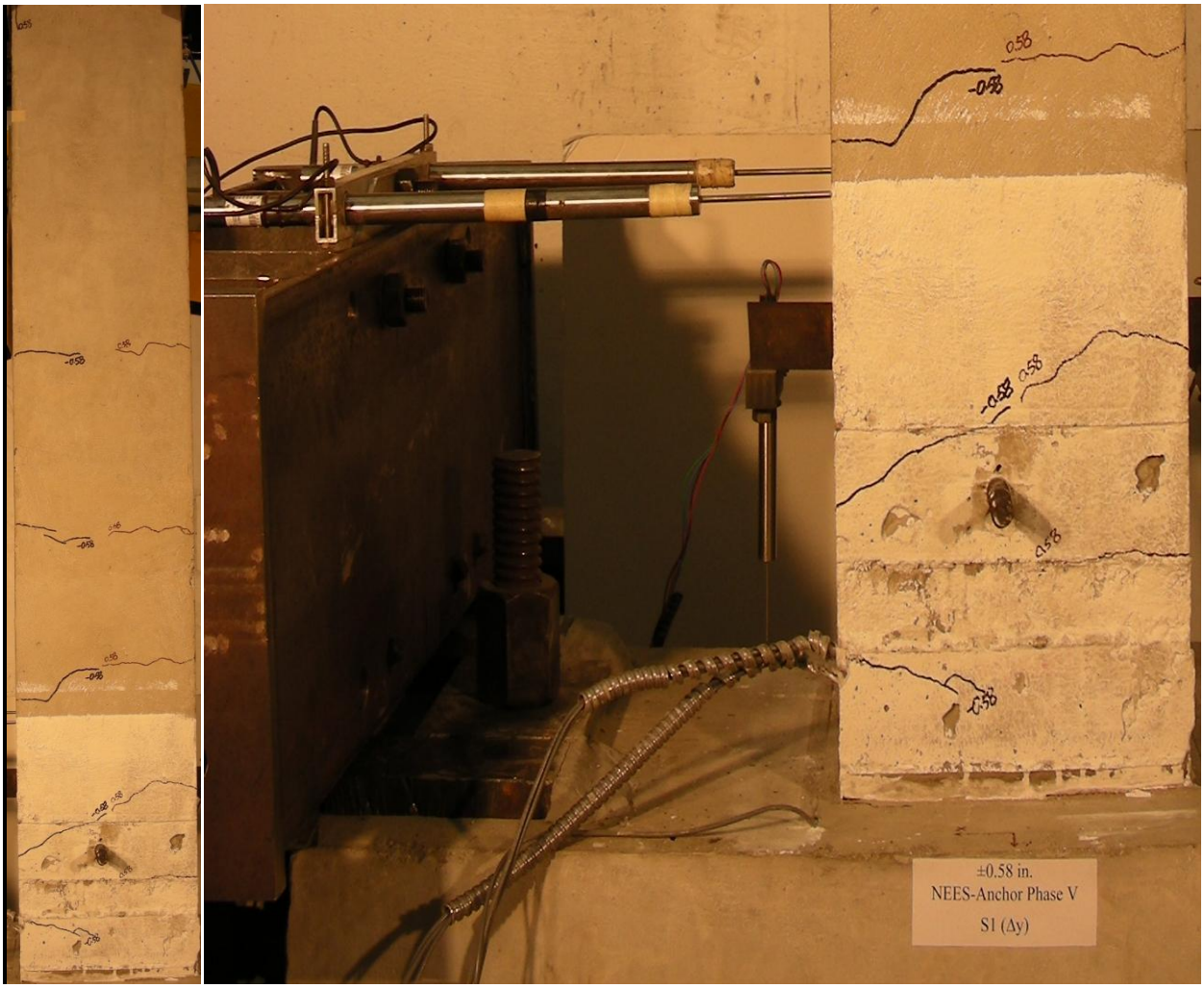

(a) Column crack pattern **(b) local cracking pattern**

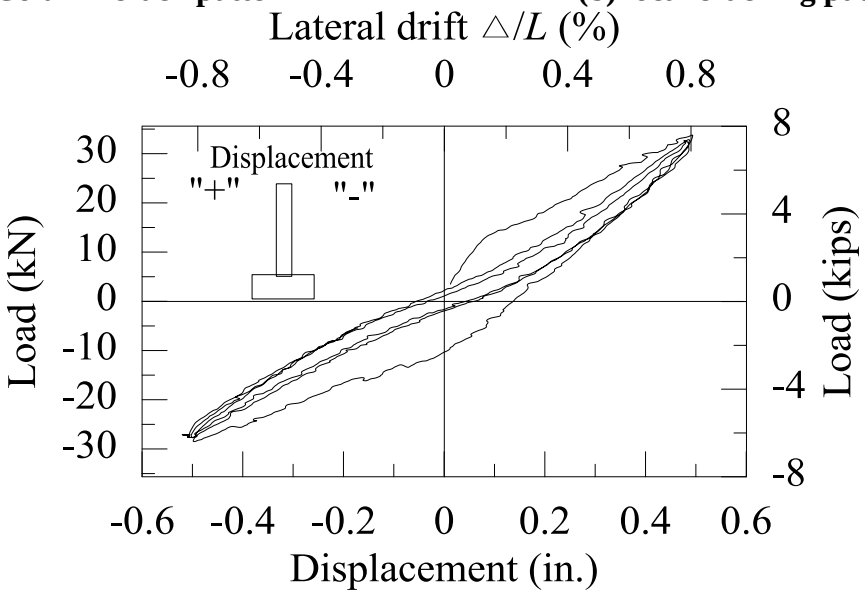

(c) Hysteresis loop

Figure A.15- S1 after loading at ±0.58 in.

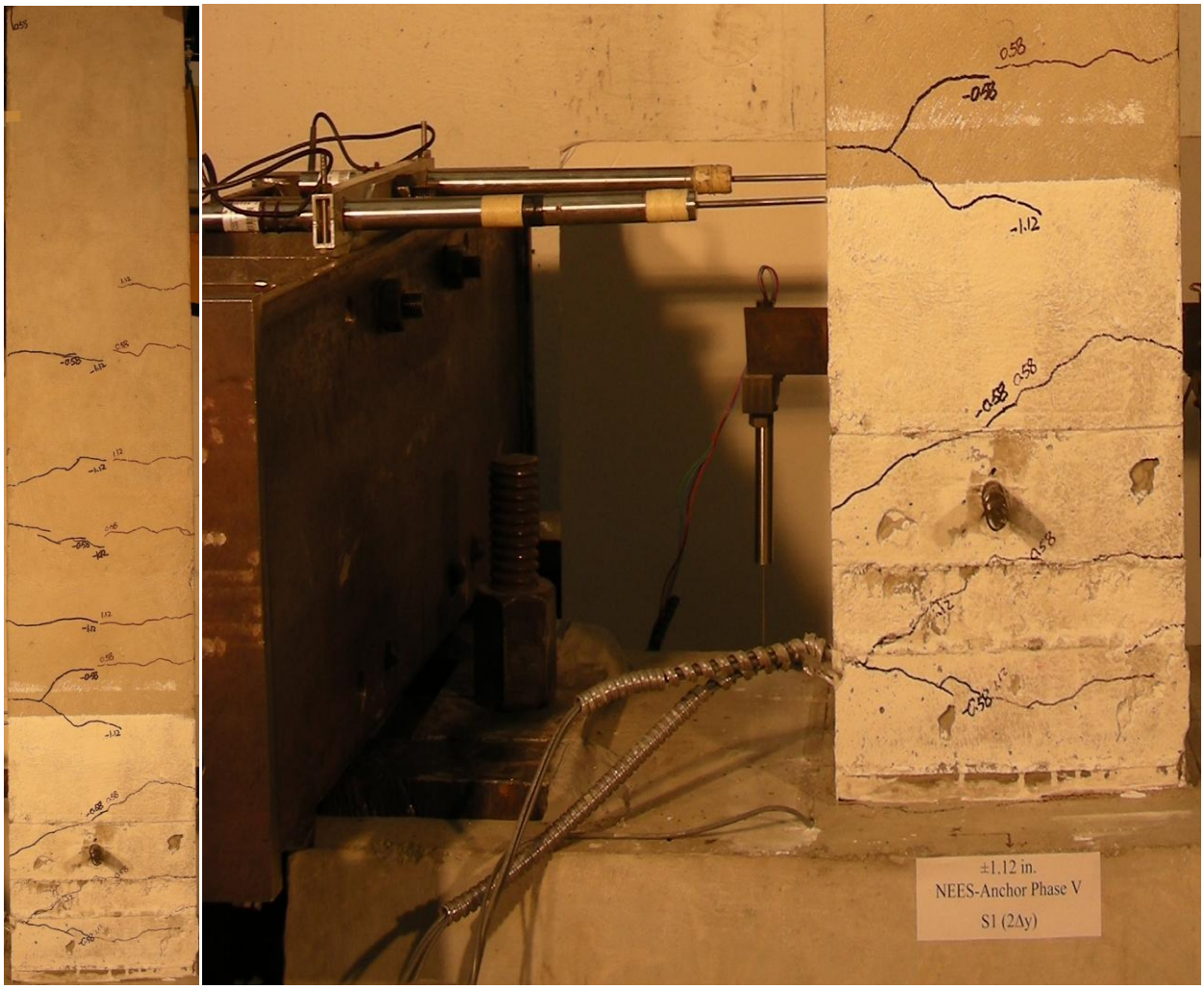

(a) Column crack pattern **(b) local cracking pattern**

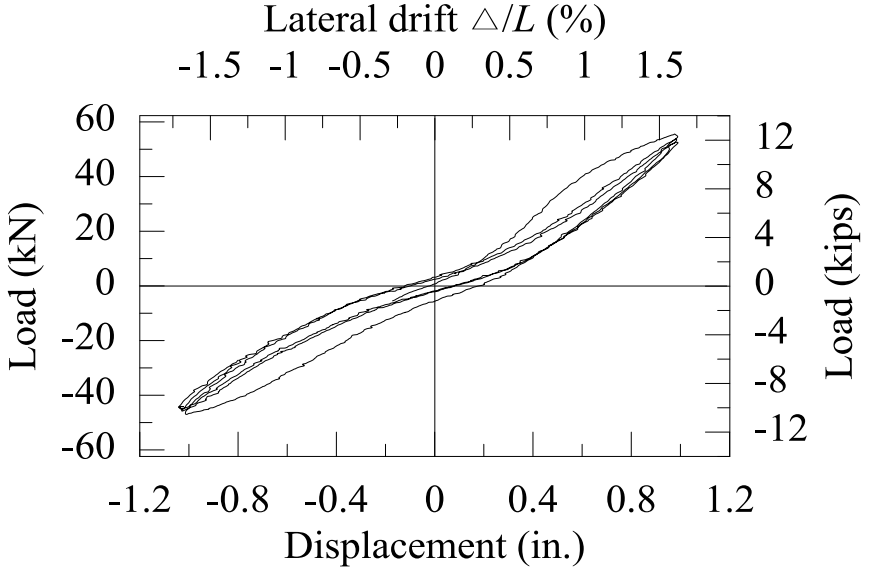

(c) Hysteresis loop

Figure A.16-S1 after loading at ±1.12 in

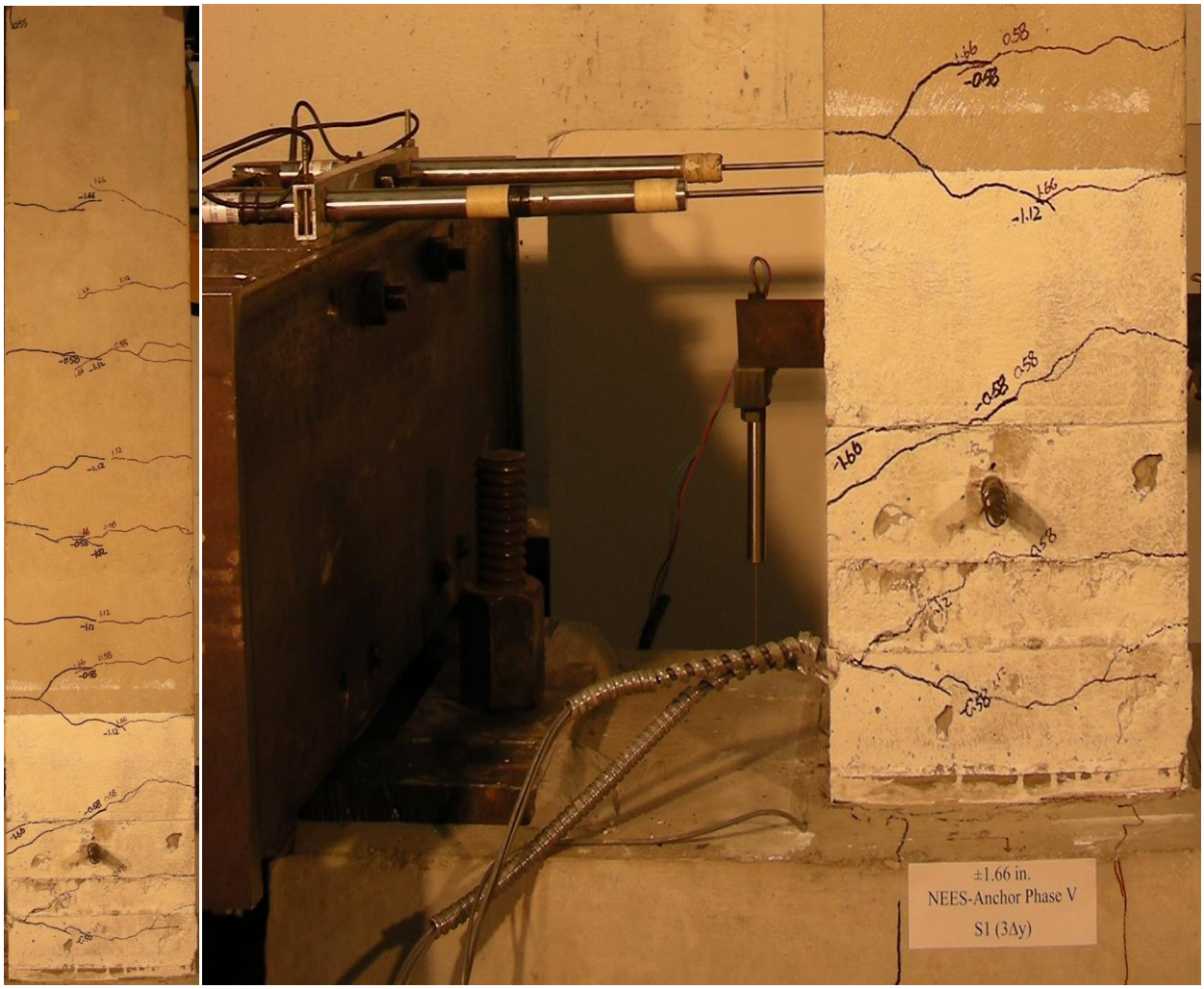

(a) Column crack pattern **(b) local cracking pattern**

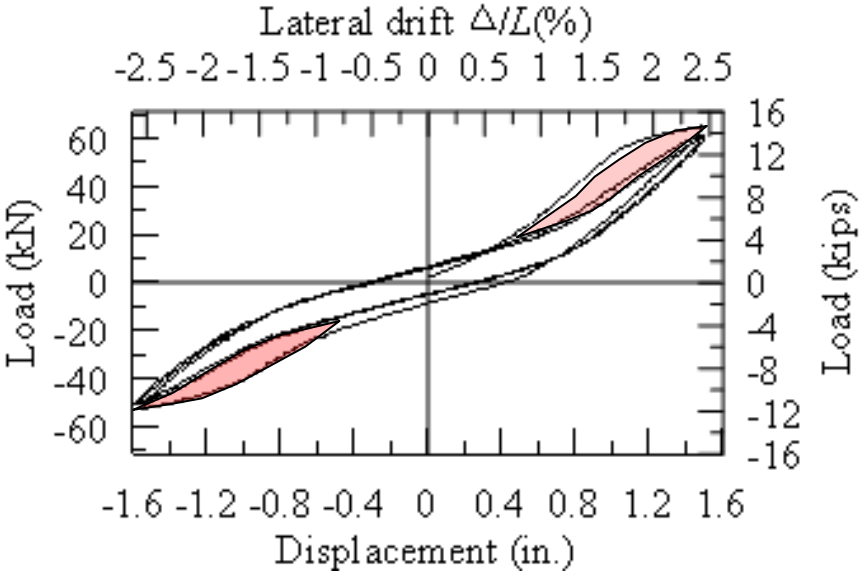

(c) Hysteresis loop

Figure A.17- S1 after loading at ±1.66 in.

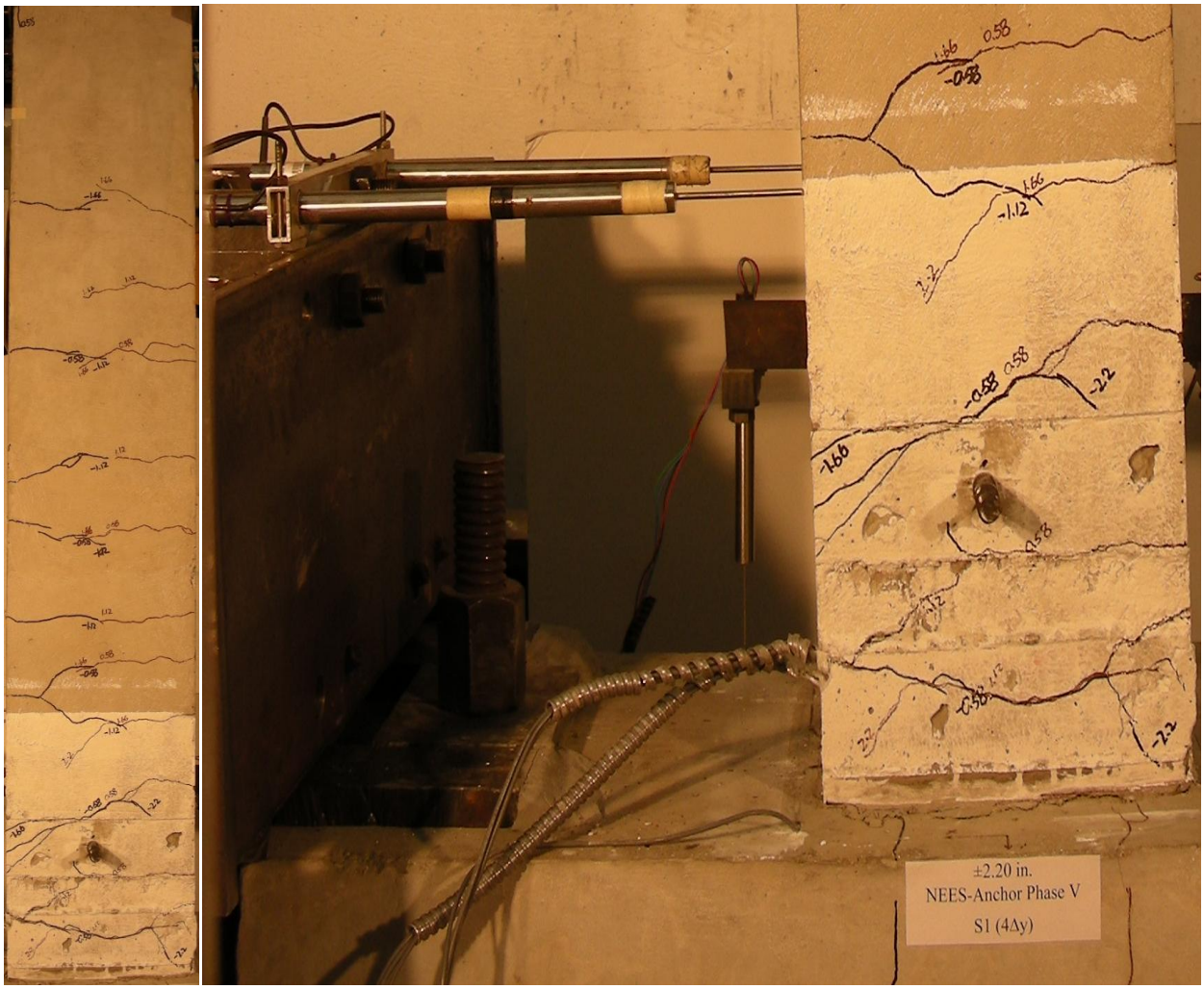

(a) Column crack pattern **(b) local cracking pattern**

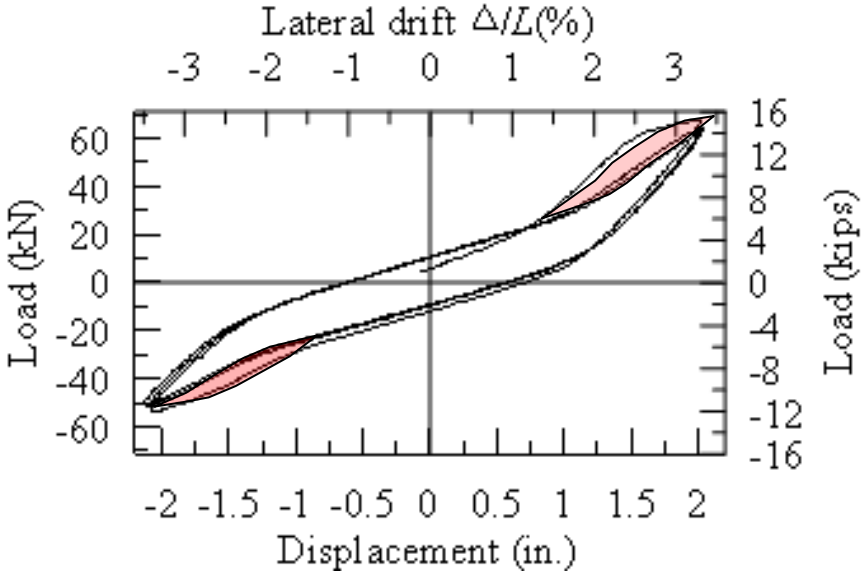

(c) Hysteresis loop

Figure A.18- S1 after loading at ±2.2 in.

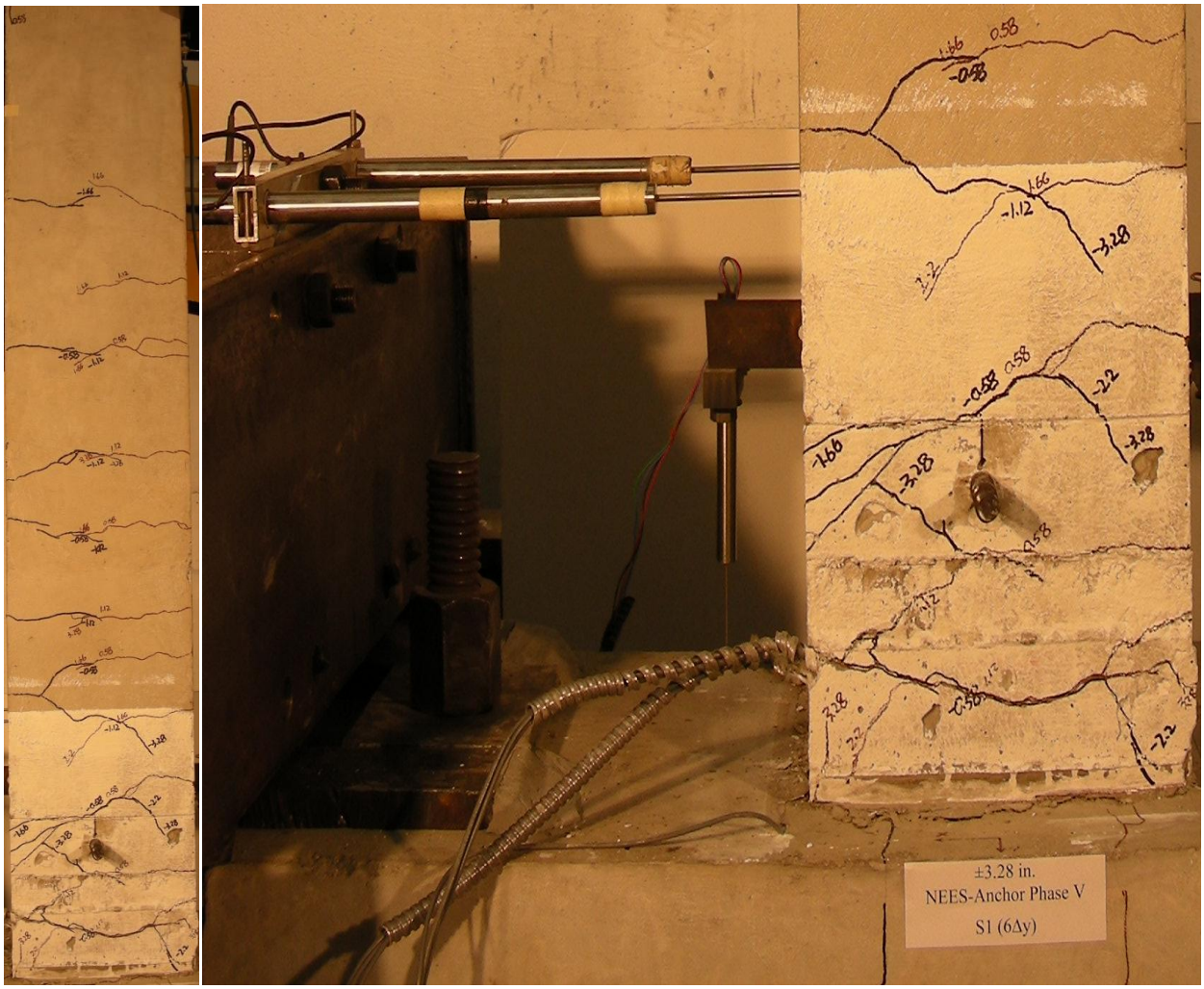

(a) Column crack pattern **(b) local cracking pattern**

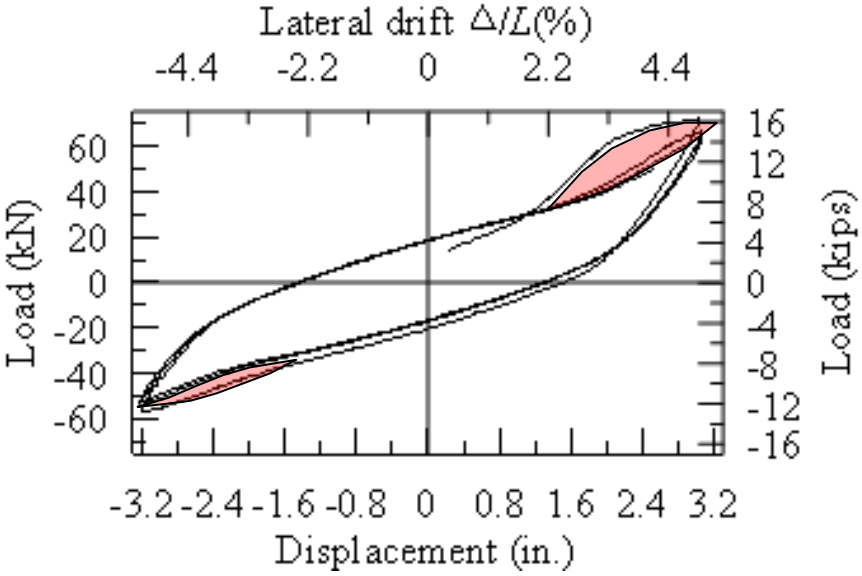

(c) Hysteresis loop

Figure A.19- S1 after loading at ±3.28 in.

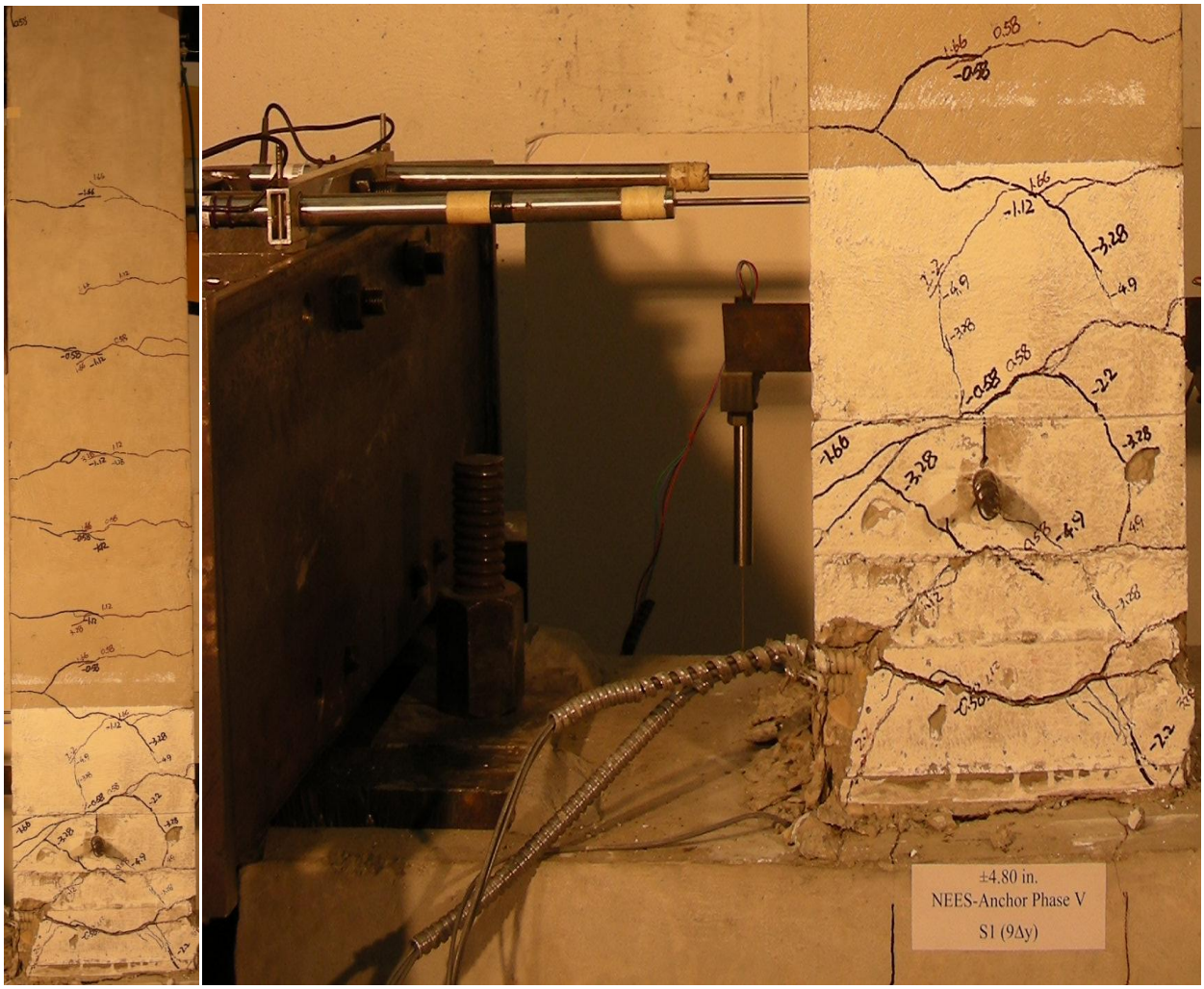

(a) Column crack pattern **(b) local cracking pattern**

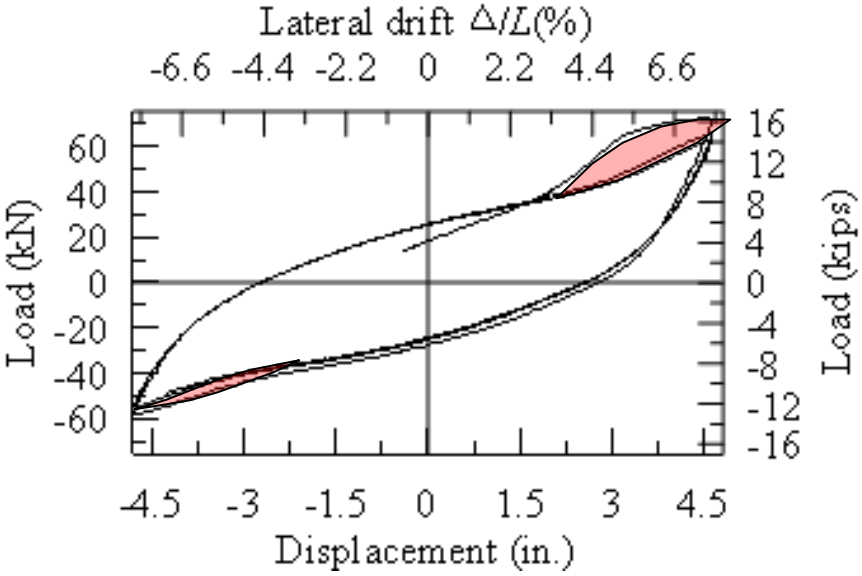

(c) Hysteresis loop

Figure A.20-S1 after loading at ±4.8 in.

(a) ±0.58 in. (b) ±1.12 in. (c) ±1.66 in. (d) ±2.20 in. (e) ±3.28 in. (f) ±4.8 in.

Figure A.21-Crack map under various loading cycles (S1)

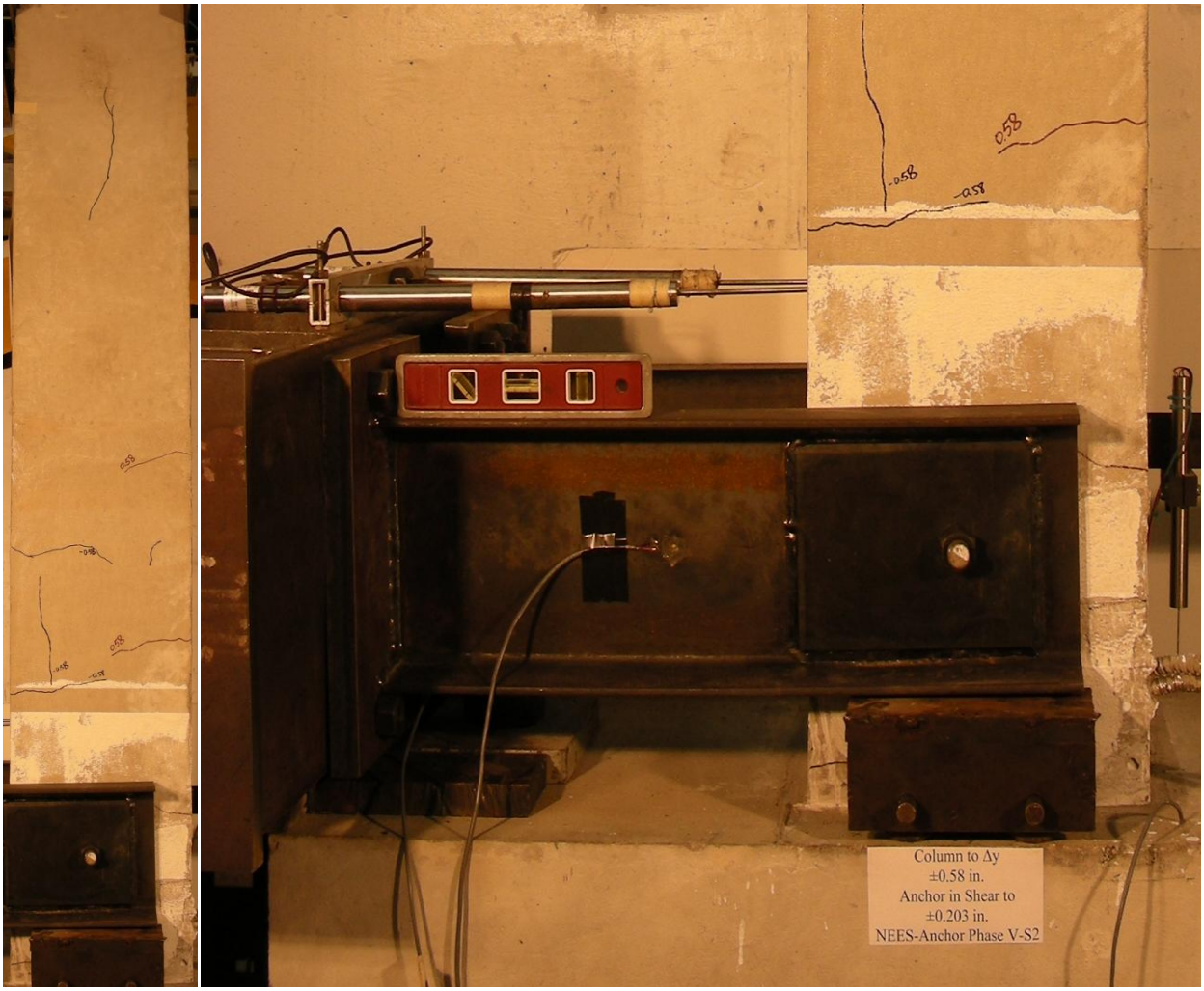

(a) Column crack pattern **(b) local cracking pattern**

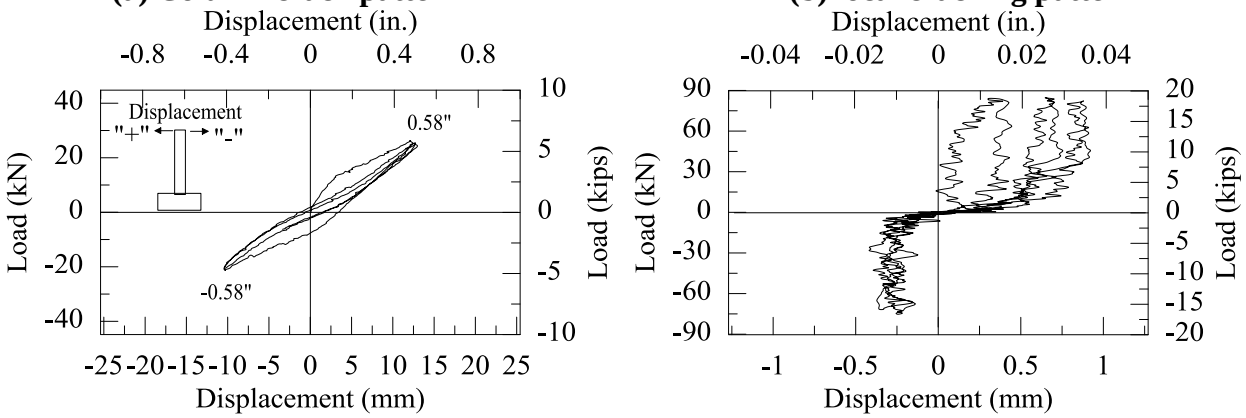

(c) Column hysteresis behavior **(d) Anchor load vs. anchor displacement**

Figure A.22-S2 after column loading at ±0.58 in. and anchor at ±0.203 in.

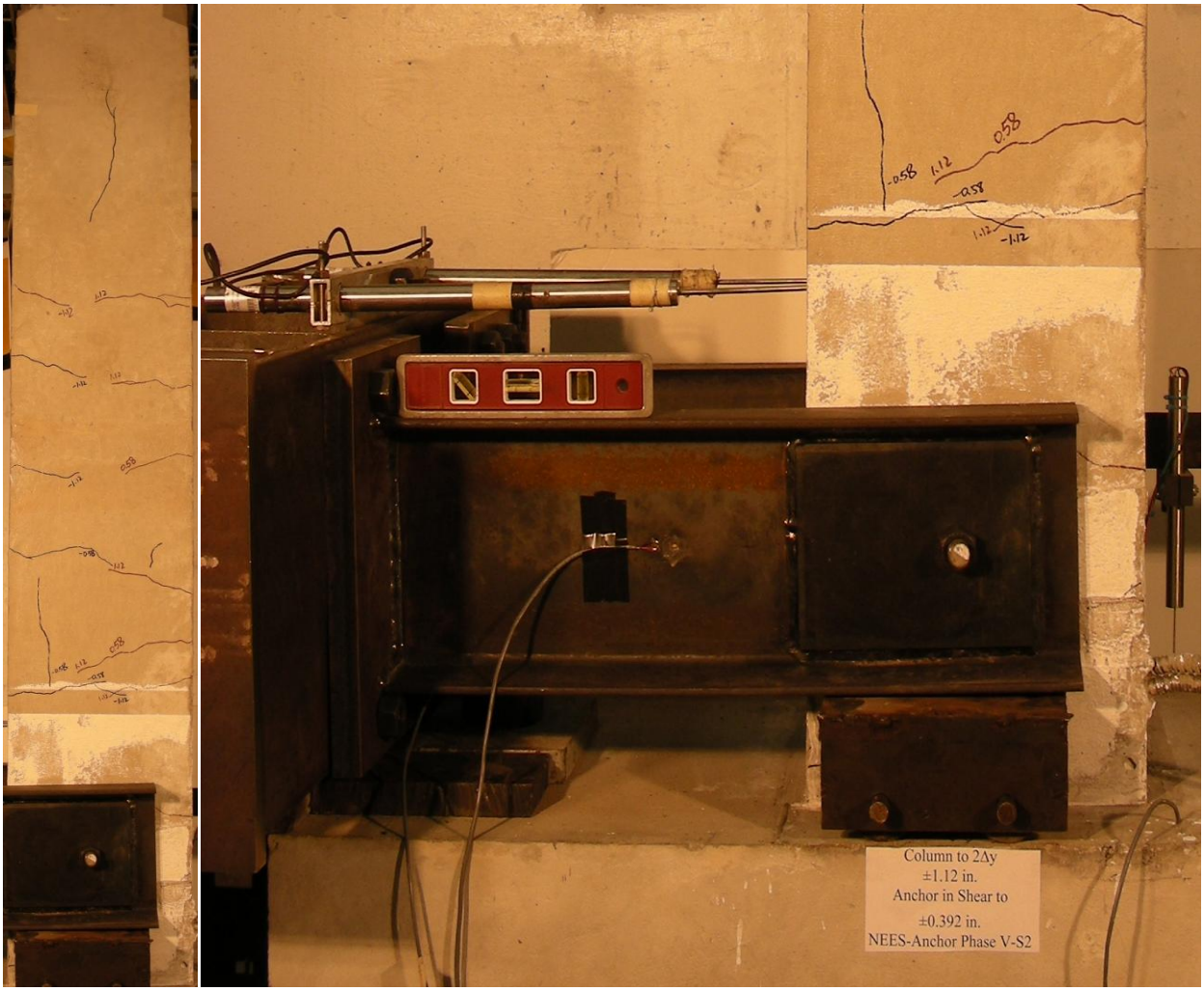

(a) Column crack pattern **(b) local cracking pattern**

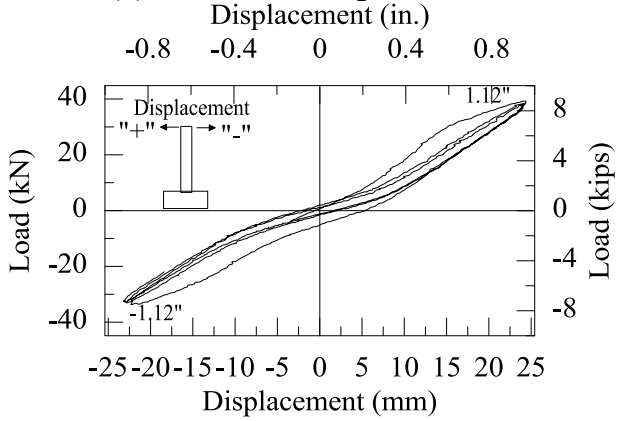

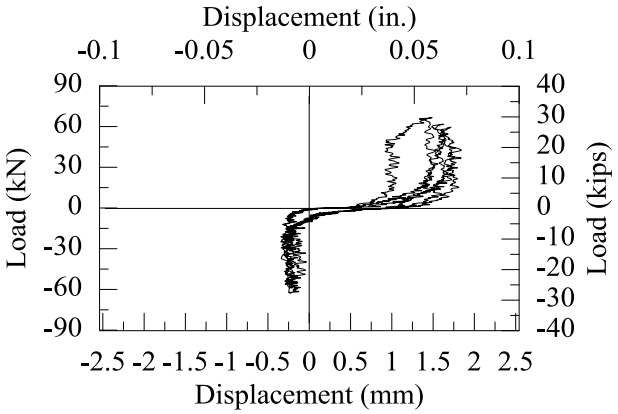

(c) Column hysteresis behavior **(d) Anchor load vs. anchor displacement**

Figure A.23-S2 after column loading at ±1.12 in. and anchor to ±0.392 in.

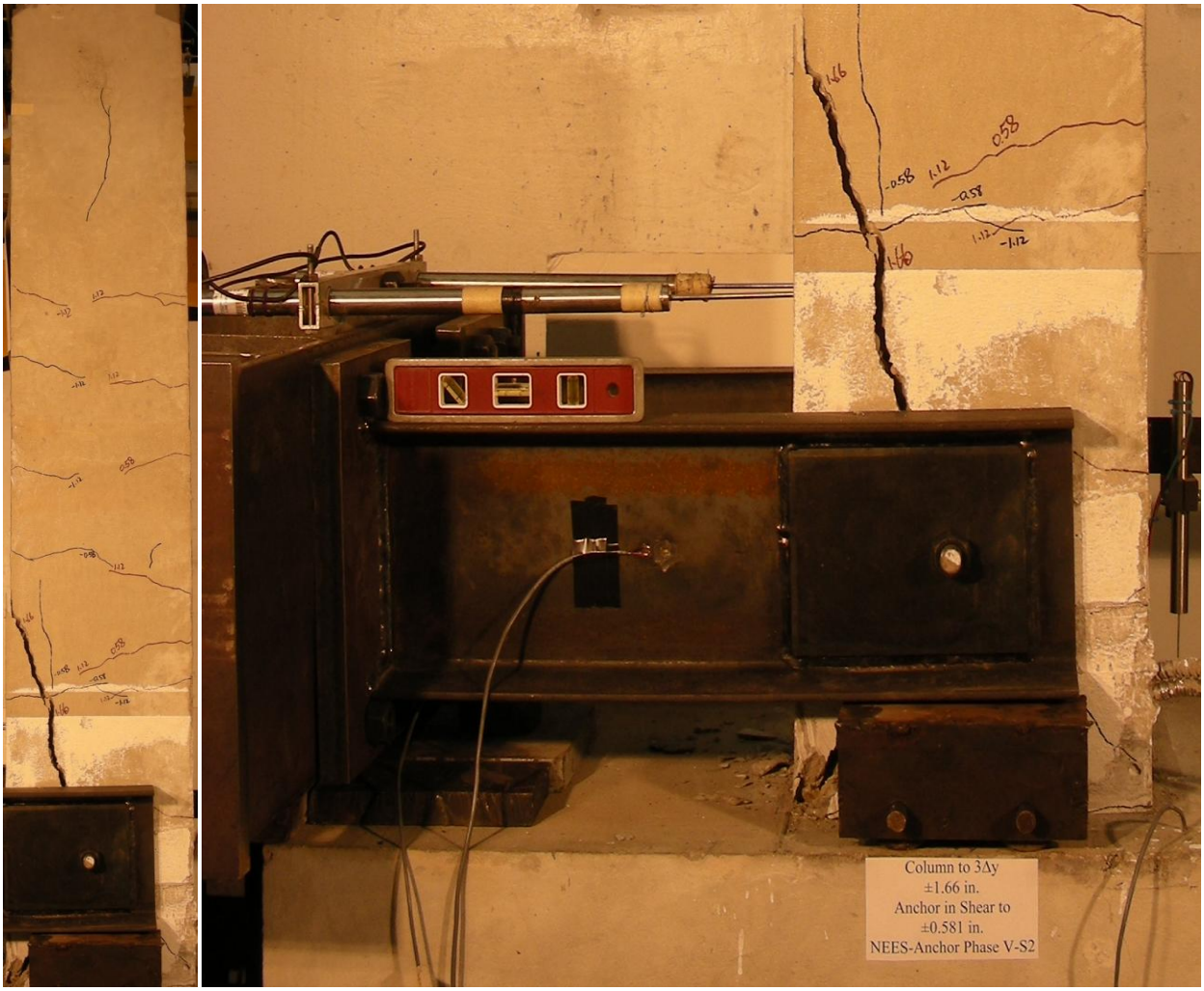

(a) Column crack pattern **(b) local cracking pattern**

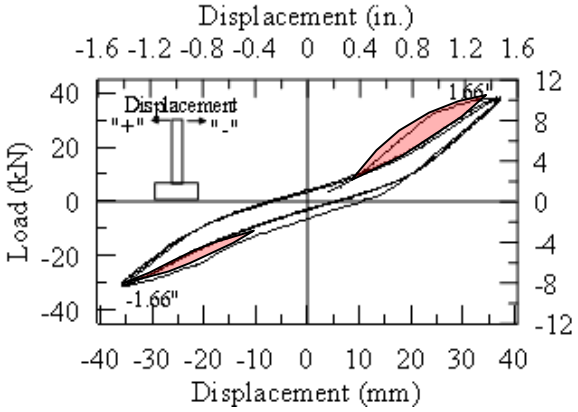

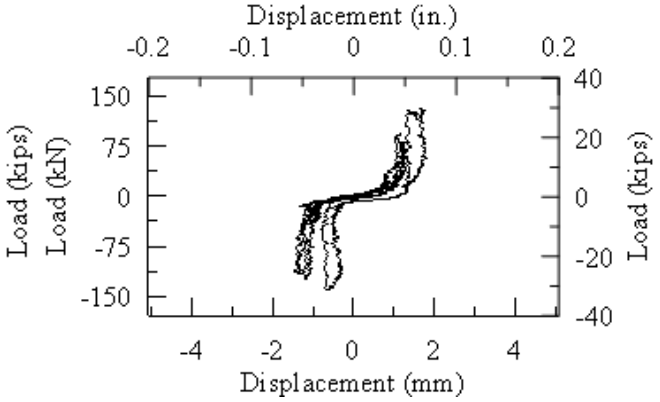

(c) Column hysteresis loop **(d) Anchor load vs. anchor displacement**

Figure A.24- S2 after column loading at ±1.66 in. and anchor to ±0.581 in.

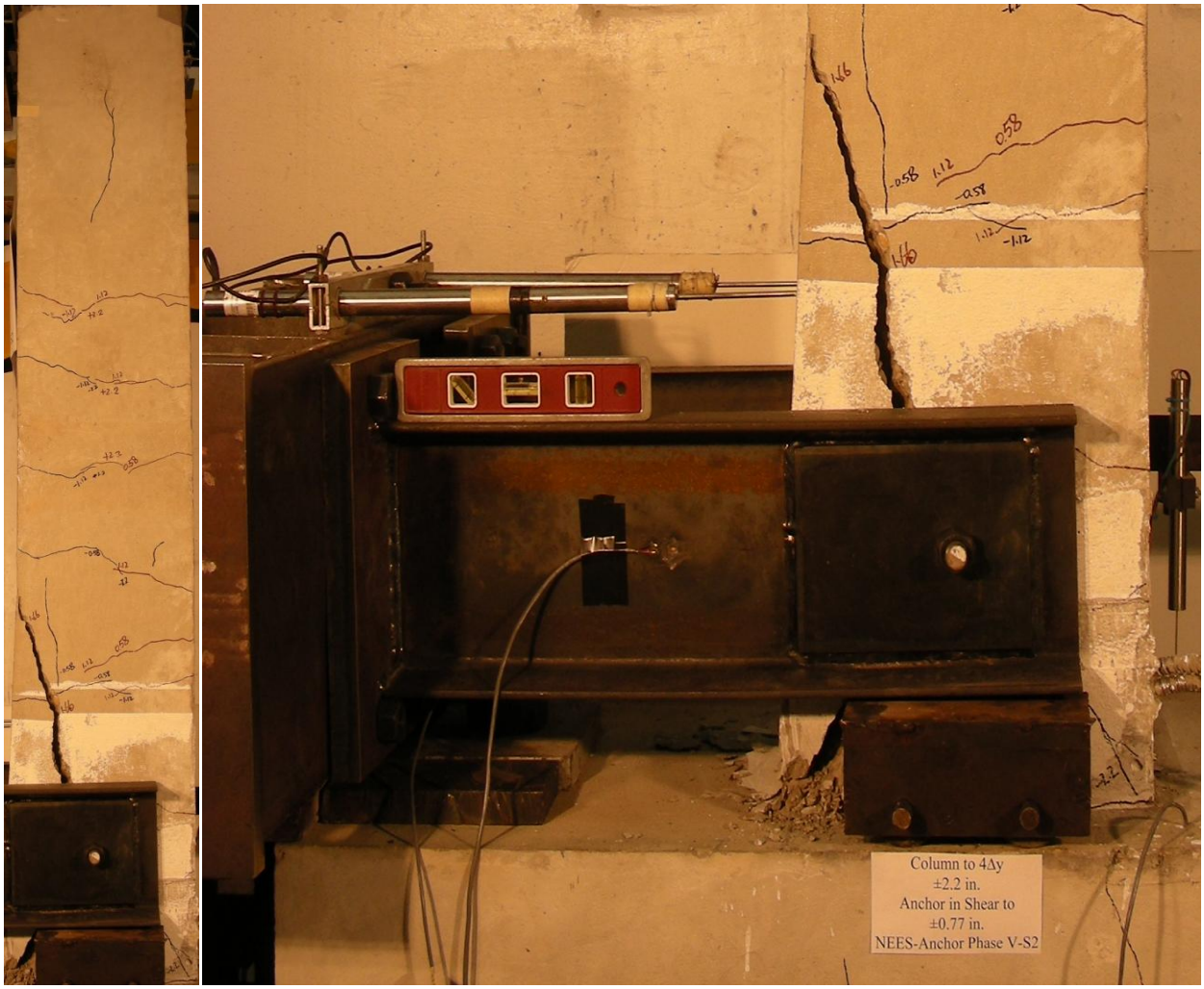

(a) Column crack pattern **(b) local cracking pattern**

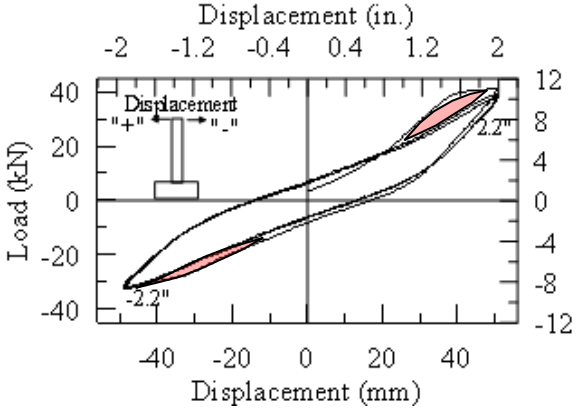

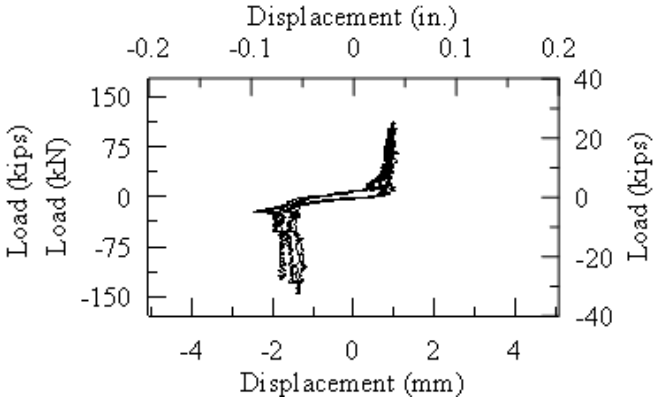

(c) Column hysteresis loop **(d) Anchor load vs. anchor displacement**

Figure A.25- S2 after column loading at ±2.2 in. and anchor to ±0.77 in.

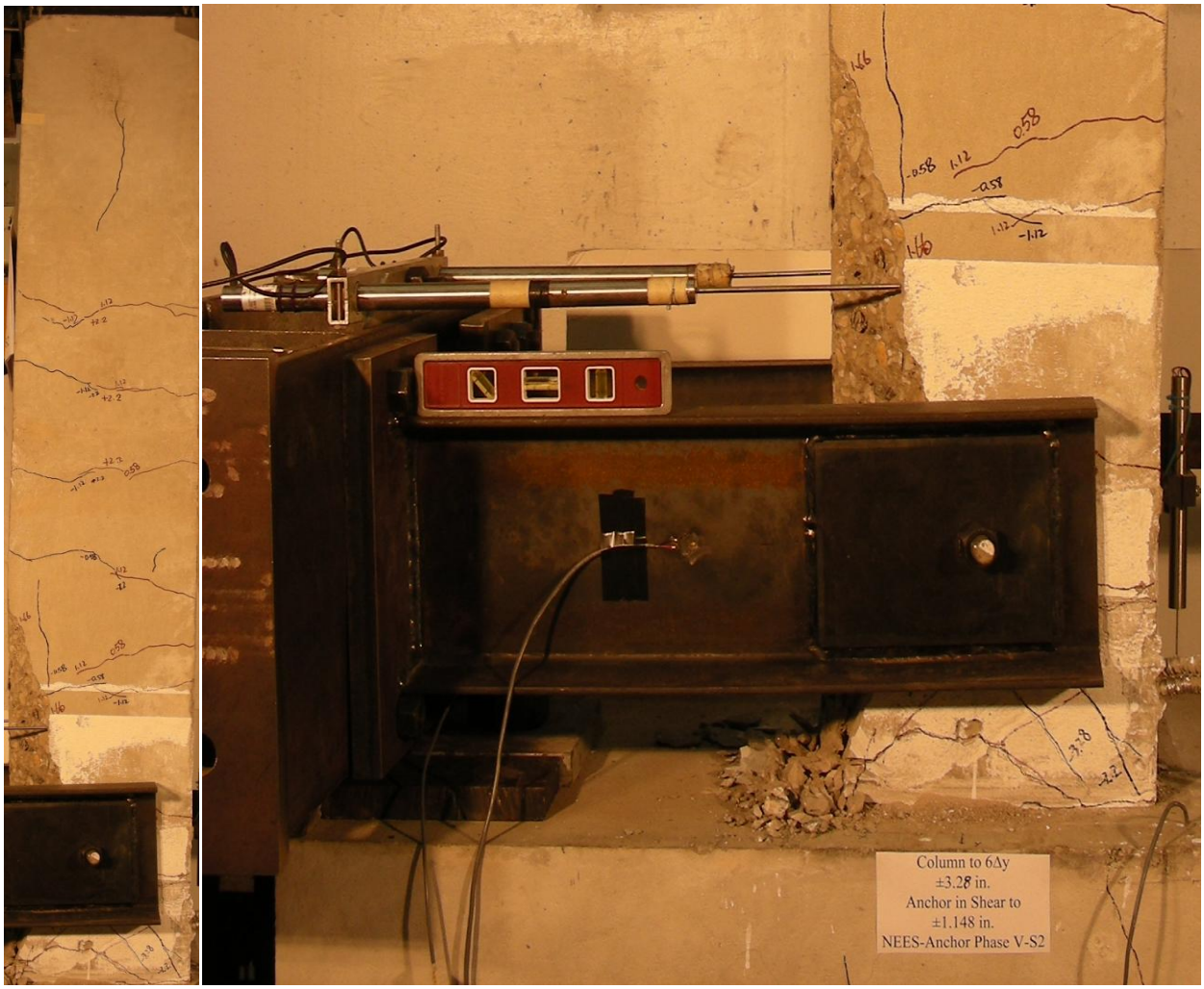

(a) Column crack pattern **(b) local cracking pattern**

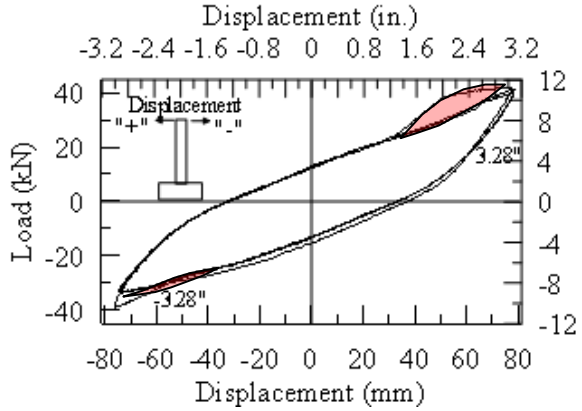

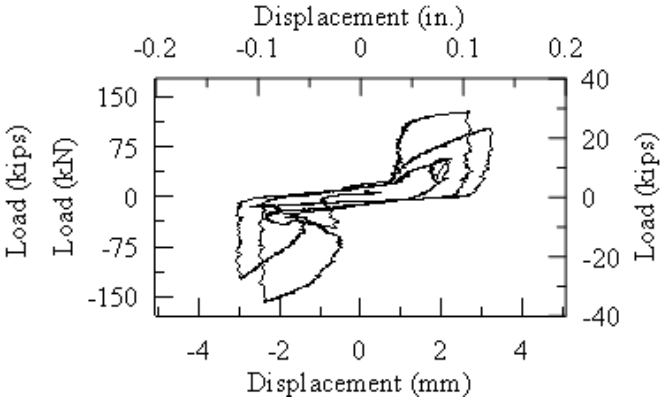

(c) Column hysteresis loop **(d) Anchor load vs. anchor displacement**

Figure A.26-S2 after column loading at ±3.28 in. and anchor to ±1.148 in.

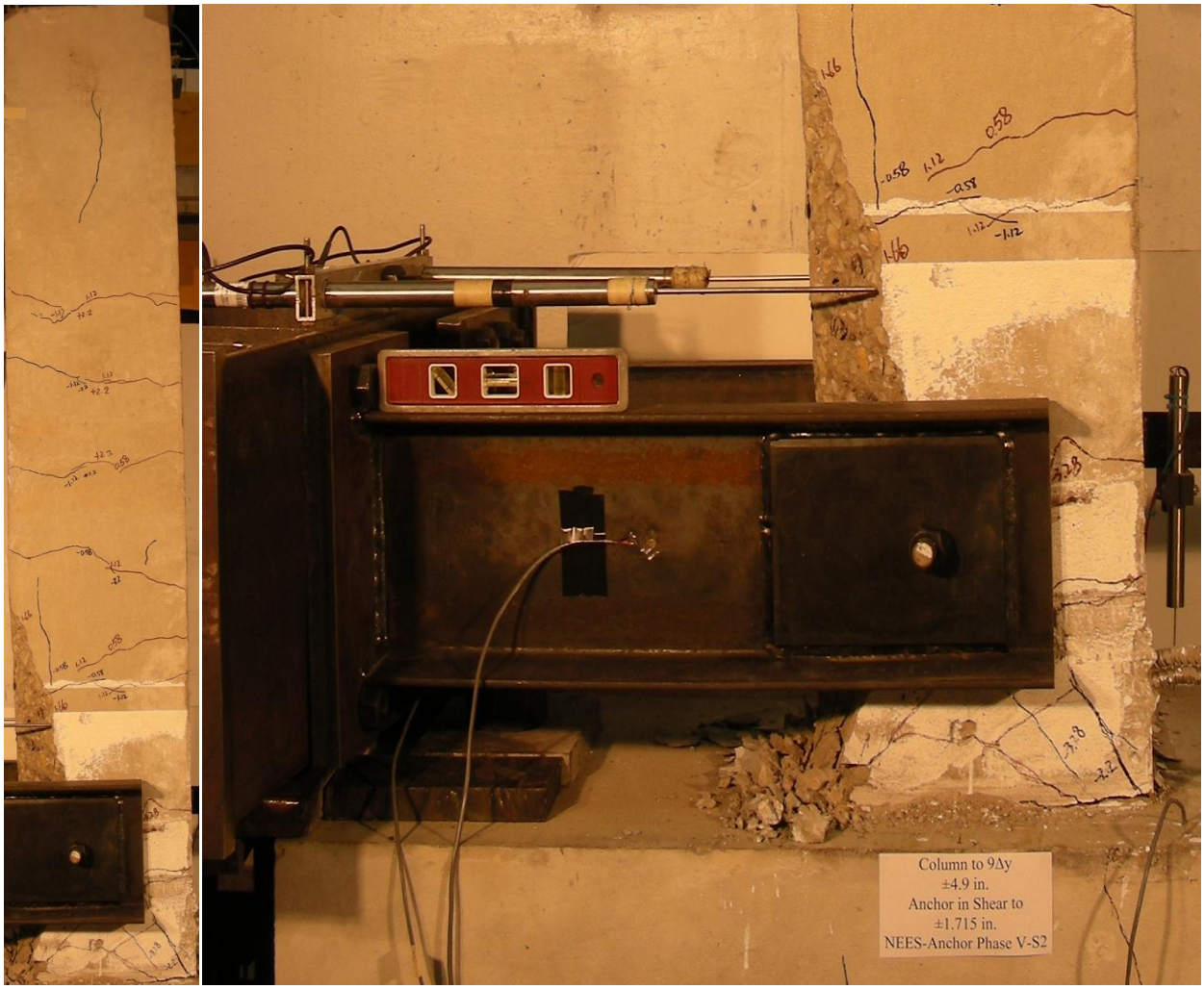

(a) Column crack pattern **(b) local cracking pattern**

FigureA.27-Loading column to ±4.9 in. and anchor to ±1.715 in.

(a) ±0.58 in. (b) ±1.12 in. (c) ±1.66 in. (d) ±2.20 in. (e) ±3.28 in. (f) ±4.9 in.

Figure A.28-Crack map of S2 under various loading cycles

APPENDIX B Preliminary Investigation (Phase IV)

B.1: ETABS Model

Table B.1: Summary of beams used in ETABS model

Location	Exterior E-W	Interior E-W	Exterior N-S		Interior N-S	
			20-ft. span	30-ft. span	40-ft. span	30-ft. span
Roof	W12x14	W14x22	W12x14	W16x26	W21x50	W16x31
Floors	W12x19	W12x16	W12x16	W16x26	W24x55	W18x35

Table B.2: Summary of Columns used in ETABS model

Column Line (*)	Story Number														
	15	14	13	12	11	10	9	8	7	6	5	4	3	2	1
1-A	W14x43			W14x43			W14x43			W14x61			W14x74		
1-B	W14x43			W14x43			W14x61			W14x68			W14x90		
1-C	W14x43			W14x48			W14x61			W14x82			W14x99		
2-A	W14x43			W14x61			W14x90			W14x109			W14x145		
2-C	W14x43			W14x82			W14x109			W14x145			W14x193		
3-A	W14x43			W14x61			W14x90			W14x109			W14x145		
4-A	W14x43			W14x61			W14x90			W14x109			W14x145		

B.2. Wall Calculations

Longitudinal Reinforcing Design

The wall was designed such that the wall would be at or close to flexural capacity when the anchors reached their capacities. Therefore the longitudinal reinforcing was designed using the XTRACT software (See Section B.3). XTRACT allows the user to build a wall cross-section configuration similar to Figure B.2-1. The software would output moment-curvature plots as well as output rebar strains for each corresponding cross-section. A free body diagram was used to determine the wall forces and moments at theoretical flexural wall failure determined by XTRACT(see Figure B.2-2). The longitudinal reinforcing was designed such that the flexural capacity moment of the wall would be close to the moment induced on the wall at connection failure.

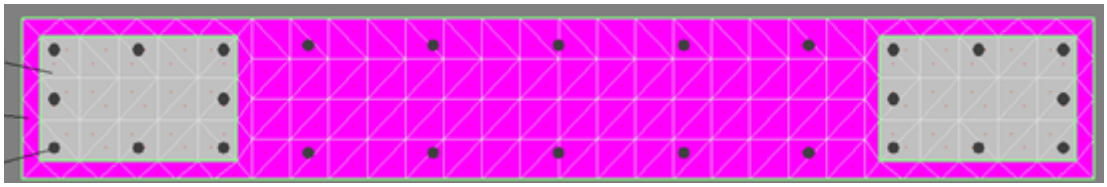

Figure B.2-1: XTRACT Cross-Section Configuration

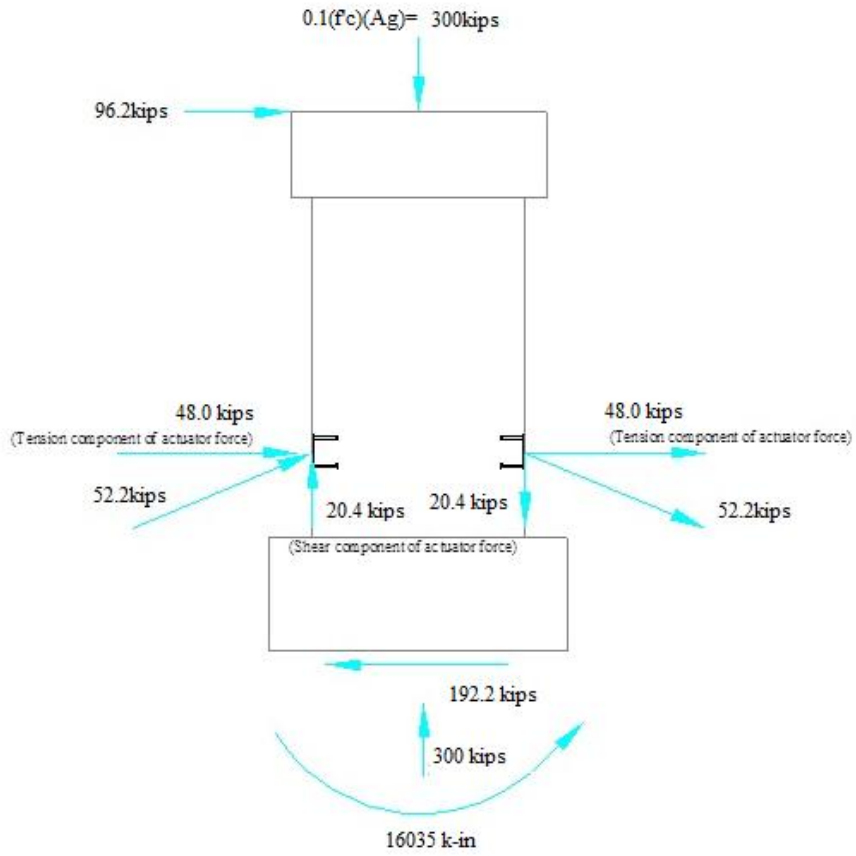

Figure B.2-2: Free Body Diagram at Expected Wall Failure.

Web Horizontal Reinforcing Design

After the longitudinal reinforcing was designed provision from ACI 11.9.9 were used to design the reinforcing.

Web Vertical Reinforcing Design

The vertical web reinforcing was used in XTRACT to calculate the wall's flexural capacity, but provisions from ACI 11.9.9 were also checked.

B.3. Expected Capacity of Wall from XTRACT Software

The plot shows the XTRACT output which corresponds applied moment in the plane of the wall versus the steel strain of the outer-most longitudinal steel in the wall. The tabulated data of the XTRACT output can be found in Table B.3.

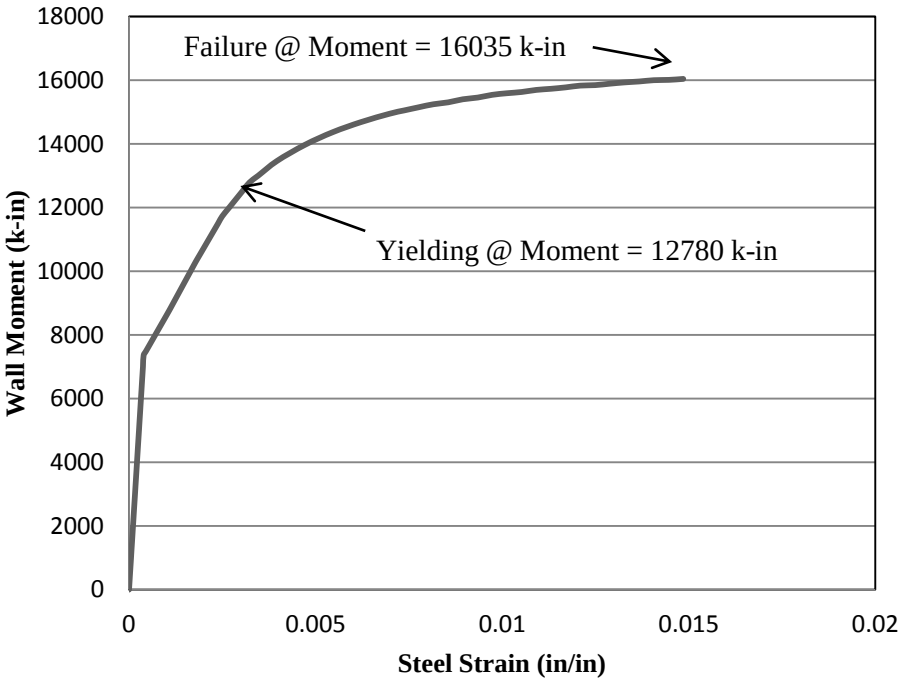

Figure B.3-1: Expected Wall Moment vs. Steel Strain

Table B.3: XTRACT Output of Expected Wall Performance

Avg. Wall Moment (k-in) XTRACT	Avg. Strain (in/in) XTRACT	Avg. Stress (ksi) XTRACT	Actuator Load, F (kips)	Fh (kips)	Fv (kips)
0	0	0	0.0	0.0	0.0
500	2.66202E-05	0.79	1.6	1.5	0.3
1000	5.32405E-05	1.57	3.3	3.0	0.6
1500	7.98607E-05	2.36	4.9	4.5	0.8
2000	0.000106481	3.15	6.5	6.0	1.1
2500	0.000133101	3.93	8.1	7.5	1.4
3000	0.000159721	4.72	9.8	9.0	1.7
3500	0.000186342	5.50	11.4	10.5	2.0
4000	0.000212962	6.29	13.0	12.0	2.3
4500	0.000239582	7.08	14.6	13.5	2.5
5000	0.000266202	7.86	16.3	15.0	2.8
5500	0.000292823	8.65	17.9	16.5	3.1
6000	0.000319443	9.44	19.5	18.0	3.4
6500	0.000346063	10.22	21.1	19.5	3.7
7000	0.000372683	11.01	22.8	21.0	4.0
7360	0.00039	11.58	23.9	22.1	4.2
7500	0.000460122	13.39	24.4	22.5	4.2
8000	0.000703952	19.86	26.0	24.0	4.5
8500	0.000947782	26.33	27.7	25.5	4.8
8766	0.00108	29.78	28.5	26.3	5.0
9000	0.001186132	32.68	29.3	27.0	5.1
9500	0.001418251	38.90	30.9	28.5	5.4
10000	0.001650371	45.11	32.5	30.0	5.6
10290	0.00179	48.72	33.5	30.9	5.8
10500	0.001889341	50.96	34.2	31.5	5.9
11000	0.002137774	56.28	35.8	33.0	6.2
11500	0.002386206	61.61	37.4	34.5	6.5
11725	0.00250	64.01	38.1	35.2	6.6
12000	0.002687242	65.92	39.0	36.0	6.8
12500	0.003031318	69.40	40.7	37.5	7.1
12780	0.00322	71.36	41.6	38.4	7.2
13000	0.003463735	72.11	42.3	39.0	7.3
13460	0.00397	73.69	43.8	40.4	7.6
13965	0.00471	75.92	45.4	41.9	7.9
14365	0.00546	78.16	46.7	43.1	8.1
14680	0.00622	79.84	47.8	44.1	8.3
14940	0.00697	80.80	48.6	44.8	8.4

15045	0.00737	81.20	48.9	45.2	8.5
15145	0.00776	81.56	49.3	45.5	8.6
15240	0.00816	82.01	49.6	45.7	8.6
15300	0.00855	82.32	49.8	45.9	8.6
15395	0.00894	82.67	50.1	46.2	8.7
15450	0.00934	83.08	50.3	46.4	8.7
15535	0.00973	83.39	50.5	46.6	8.8
15585	0.01013	83.69	50.7	46.8	8.8
15625	0.01052	83.96	50.8	46.9	8.8
15690	0.01092	84.27	51.0	47.1	8.9
15725	0.01131	84.51	51.2	47.2	8.9
15770	0.01170	84.74	51.3	47.3	8.9
15825	0.01209	85.00	51.5	47.5	8.9
15840	0.01249	85.29	51.5	47.5	8.9
15885	0.01289	85.62	51.7	47.7	9.0
15925	0.01328	85.90	51.8	47.8	9.0
15955	0.01367	86.11	51.9	47.9	9.0
15995	0.01406	86.33	52.0	48.0	9.0
16005	0.01447	86.61	52.1	48.0	9.0
16035	0.01485	86.87	52.2	48.1	9.1

APPENDIX C Test Specimen CAD Drawings and Test Specimen Pictures

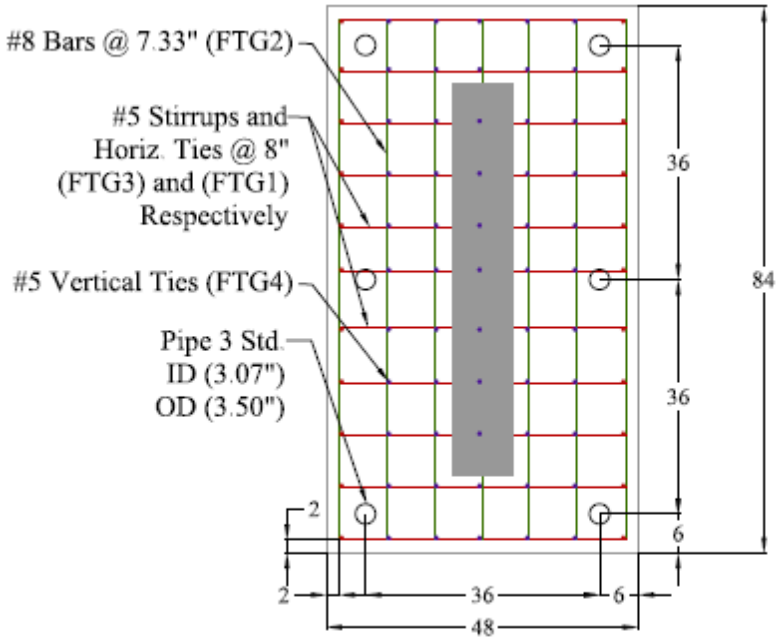

TOP VIEW OF THE WALL PEDESTAL

Figure C.1: CAD Drawing of Reinforcing of Wall Footing

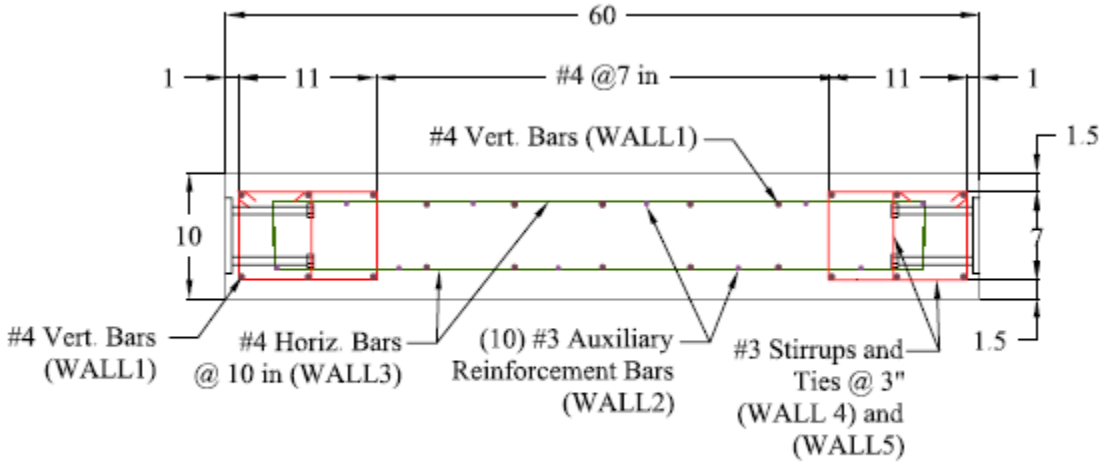

SECTION A-A

Figure C.2: CAD Drawing of Reinforcing of Wall Cross-Section

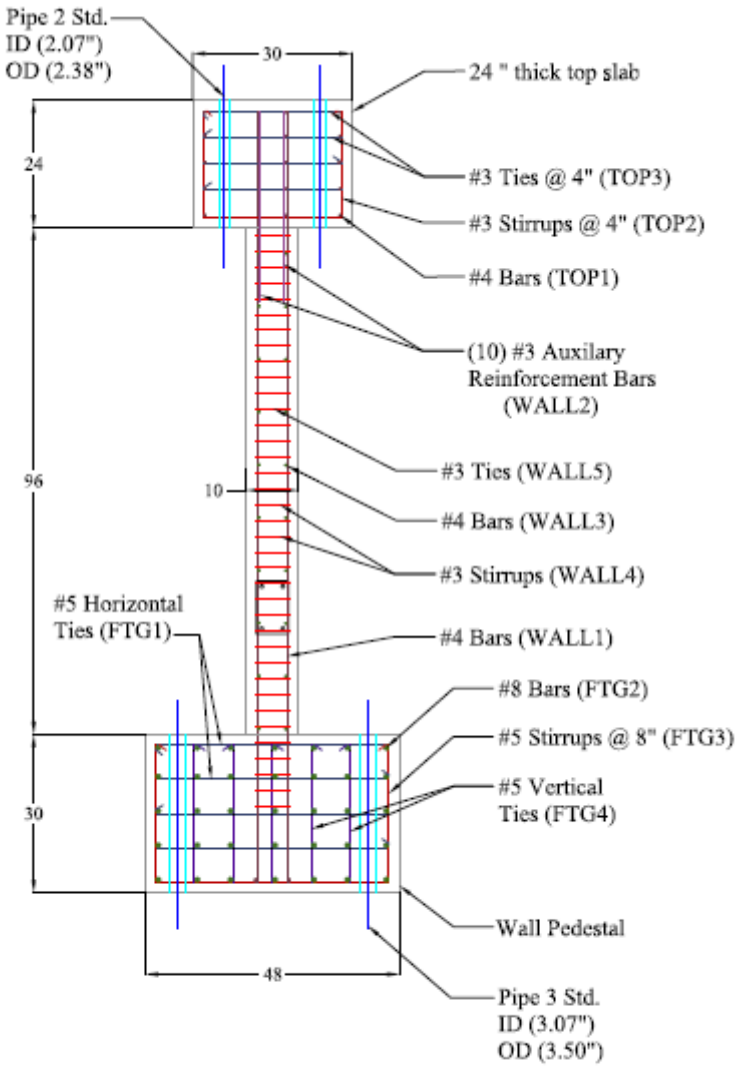

FRONT VIEW OF THE RECTANGULAR WALL

Figure C.3: CAD Drawing of Front View of Wall Reinforcing

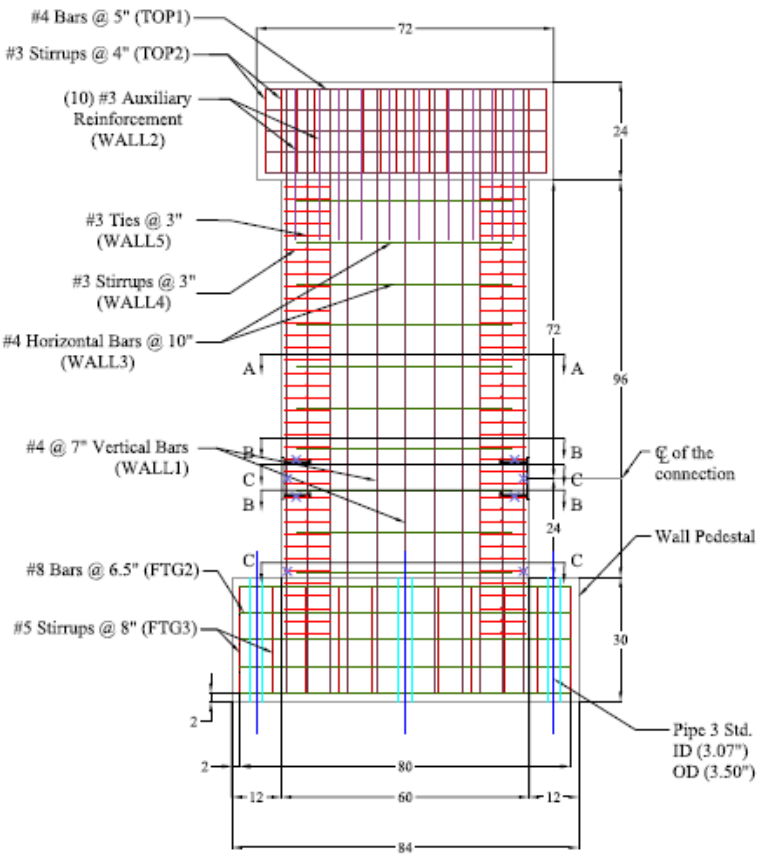

SIDE VIEW OF THE RECTANGULAR WALL

Figure C.4: CAD Drawing of Side View of Wall Reinforcing

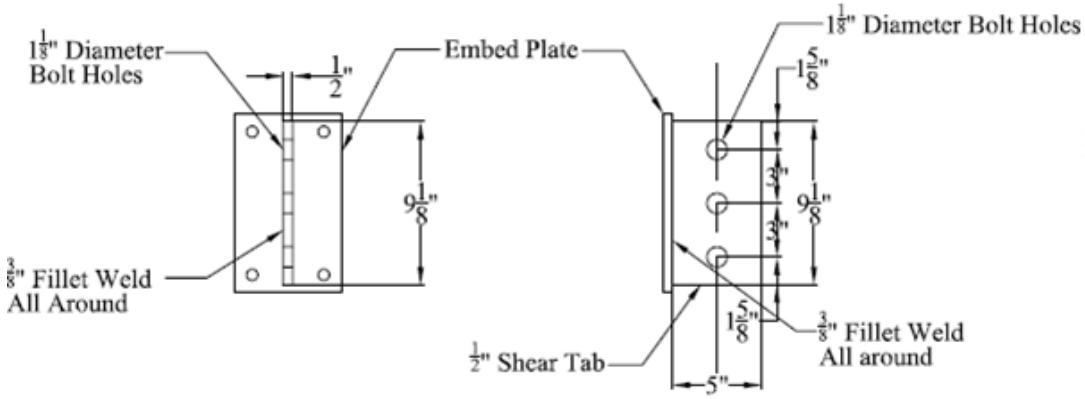

Figure C.5: CAD Drawing of Shear Tab and Weld Size

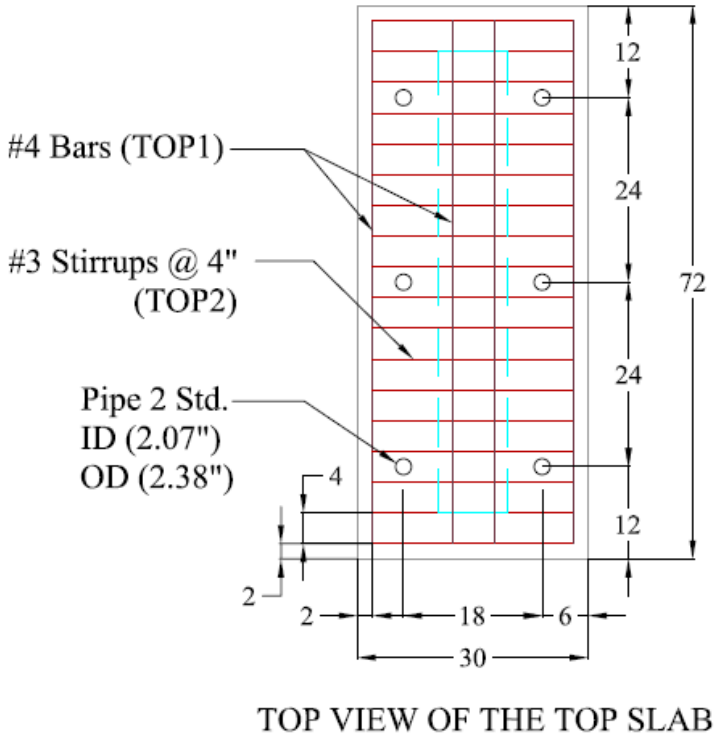

Figure C.6: CAD Drawing of Reinforcing of Top Loading Slab

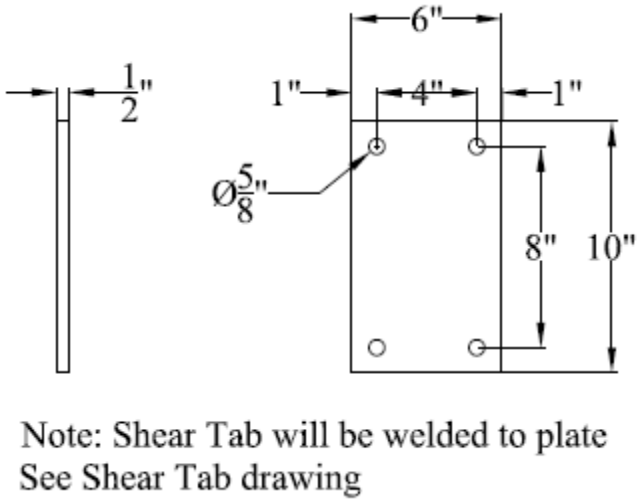

Figure C.7: CAD Drawing of Dimension of Embed Plate

Figure C.8: Photo of Wall Specimen Right Before Concrete Placement

Figure C.9: Photo of Wall Specimen Right After Concrete Placement

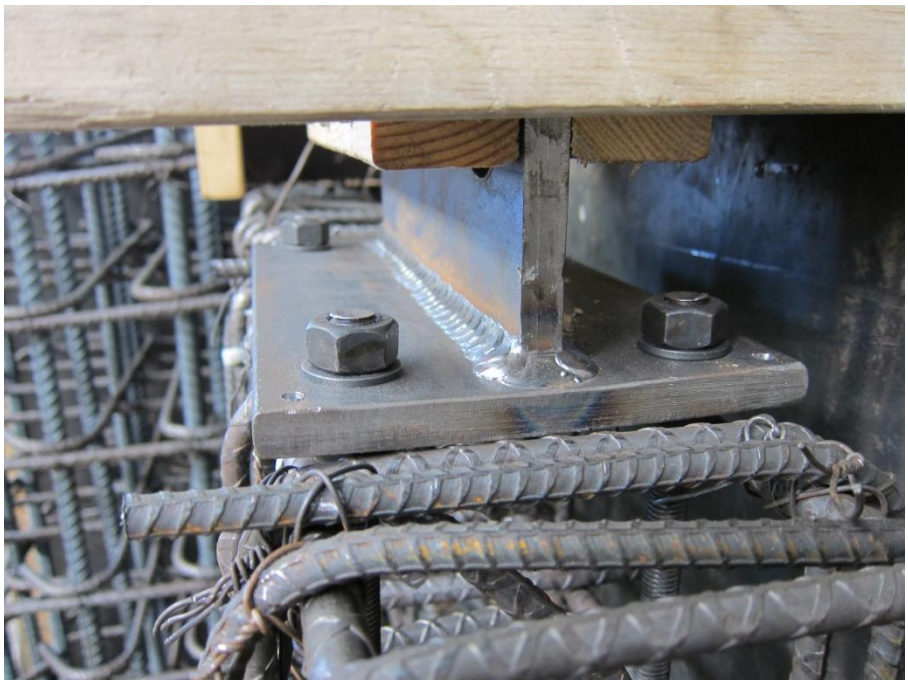

Figure C.10: Photo of Embedded Connection in Formwork

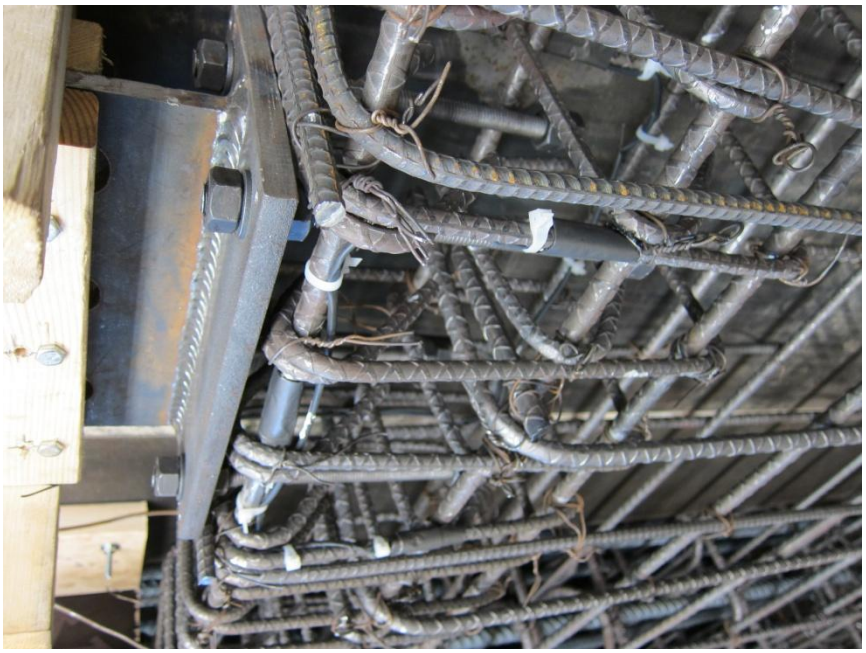

Figure C.11: Photo of Embedded Connection and Boundary Element

Figure C.12: Photo of Wall Specimen Reinforcing

Figure C.13: Photo of Shear Tab

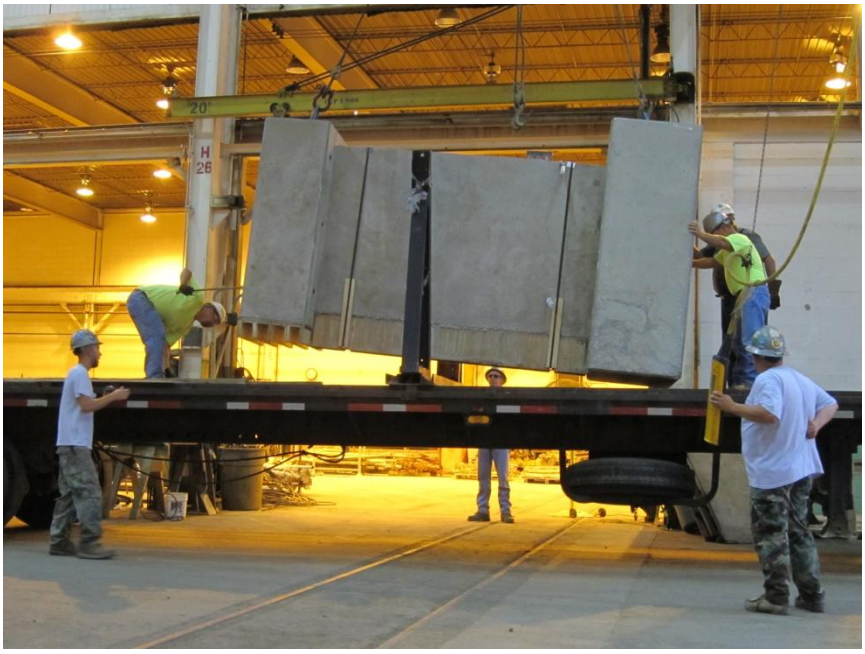

Figure C.14: Photo of Wall Specimen to be Transported to UIUC

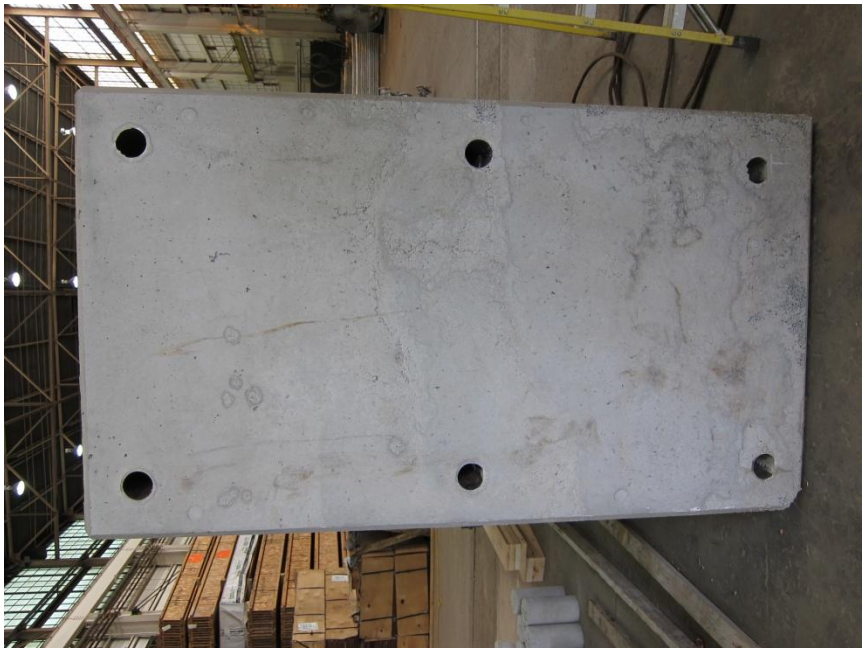

Figure C.15: Photo of Wall Footing and Floor Post-tensioning Holes

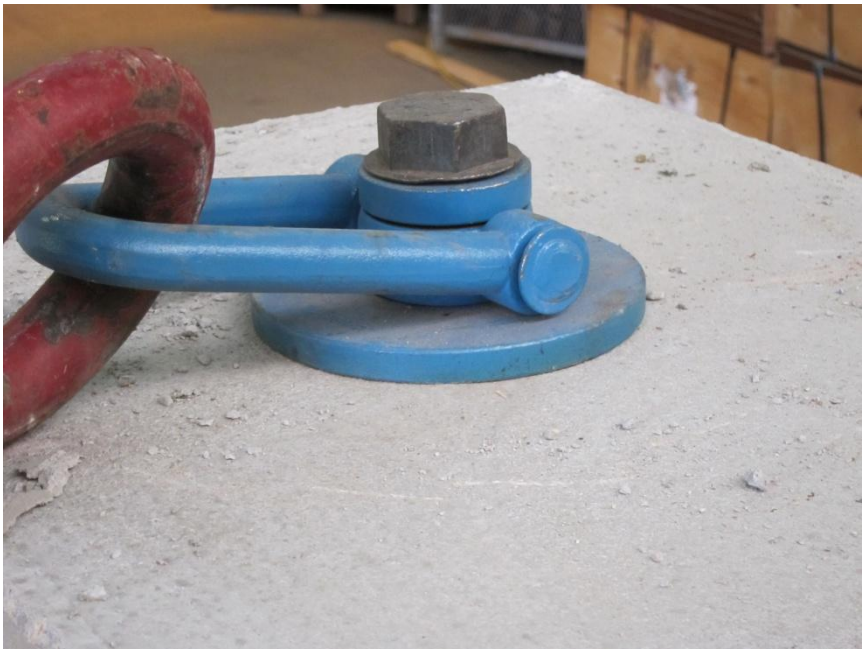

Figure C.16: Photo of Lift Point on Structural wall

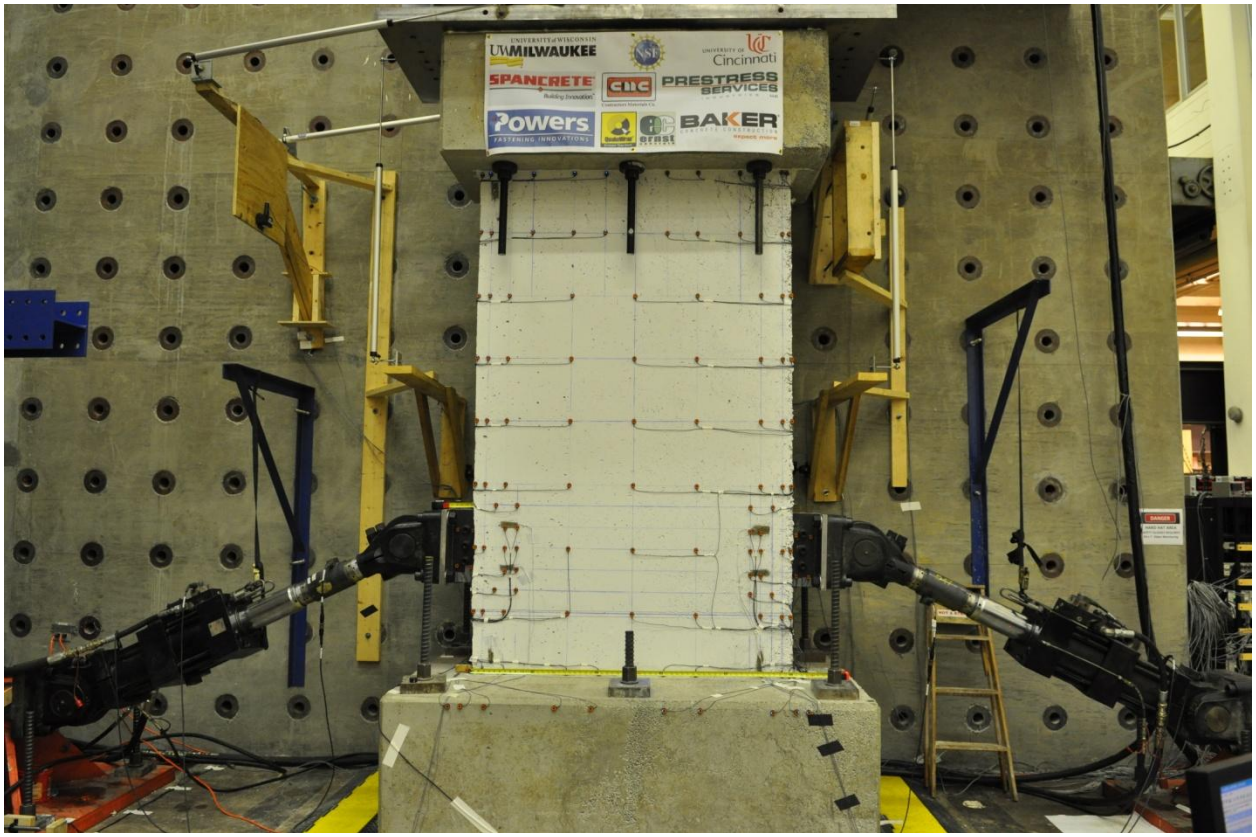

Figure C.17: Photo of Wall Specimen in Loading Apparatus at the NEES Lab at UIUC

APPENDIX D Instrumentation Plan (Phase IV)

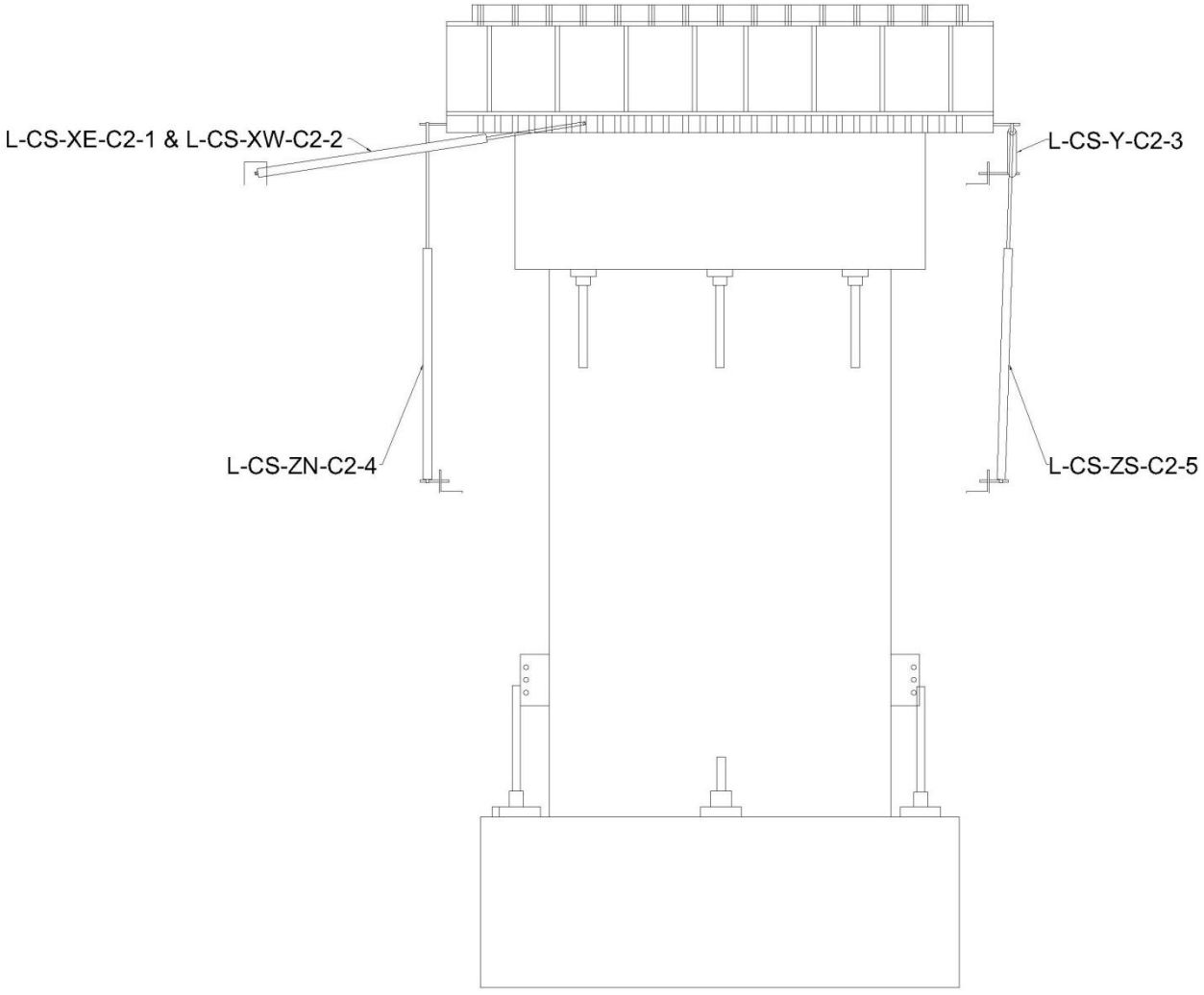

Figure D.1 Control sensors for the wall in Phase IV tests (front view)

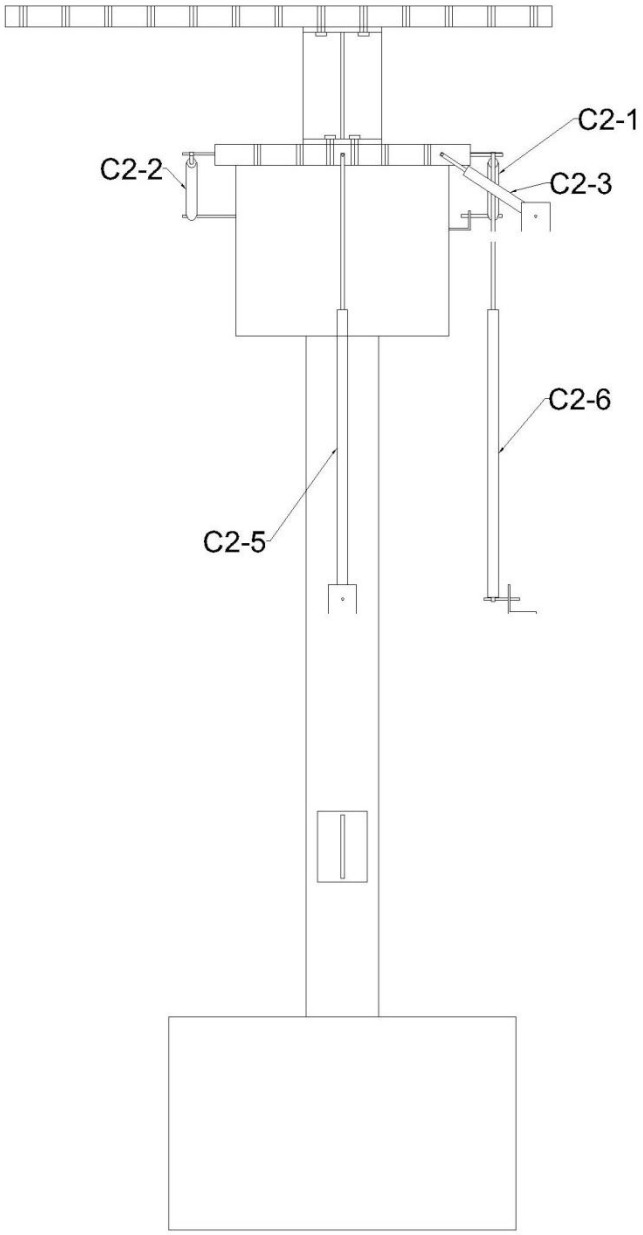

Figure D.2: Control sensors for the wall in Phase IV tests (side view)

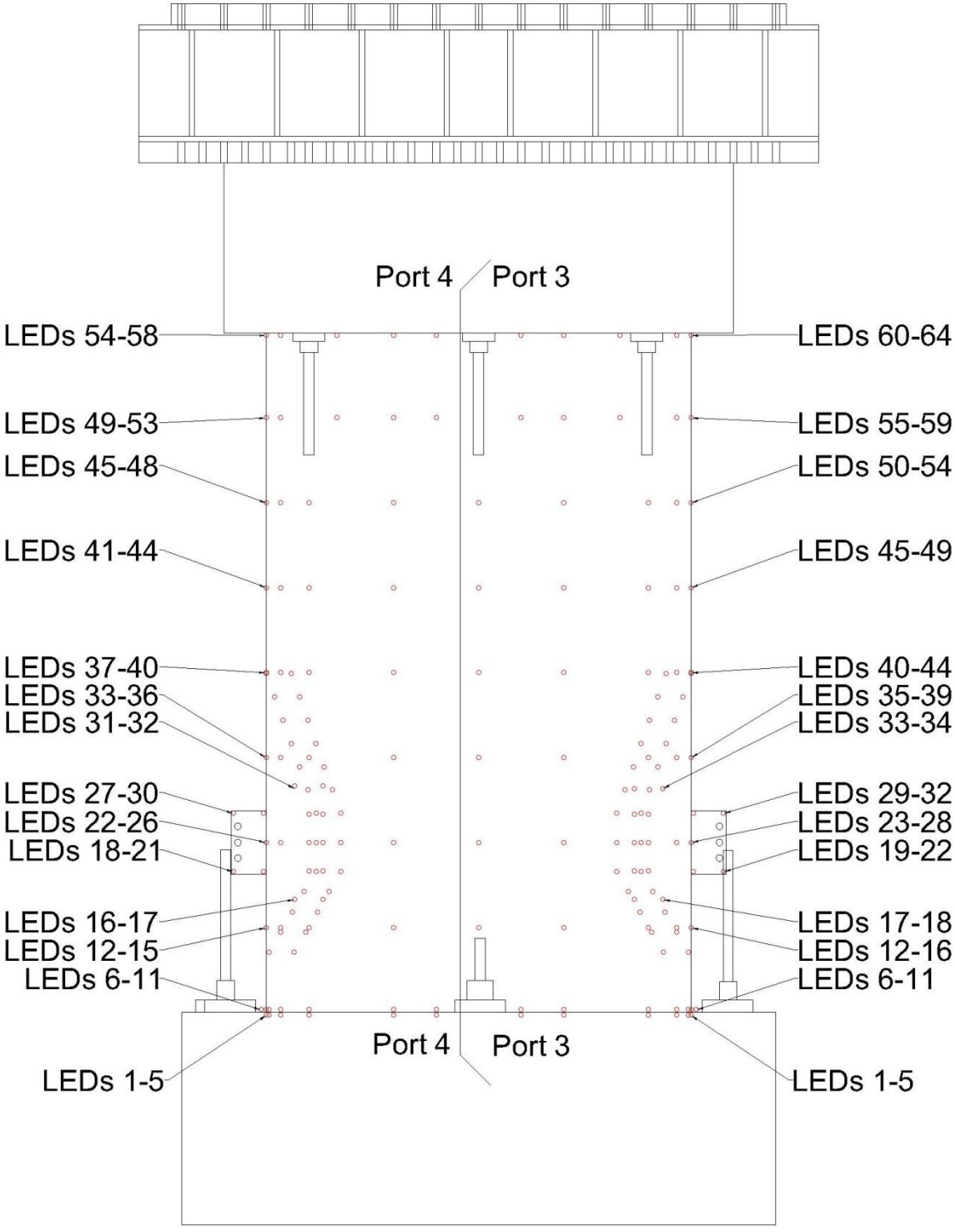

Figure D.3: LED sensors for the wall in Phase IV tests (front view)

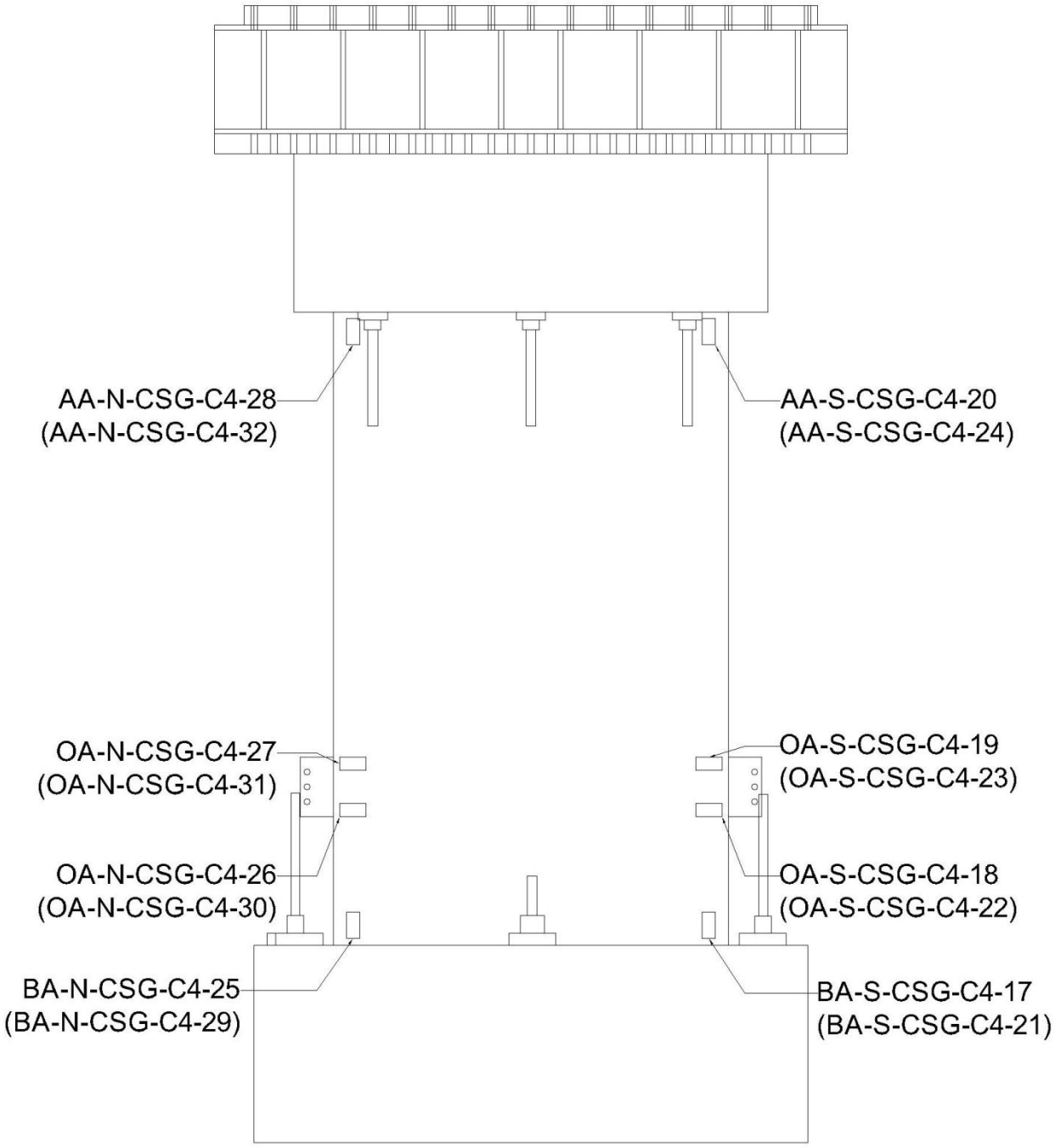

Figure D.4: Concrete strain gages for the wall in Phase IV tests (front view)

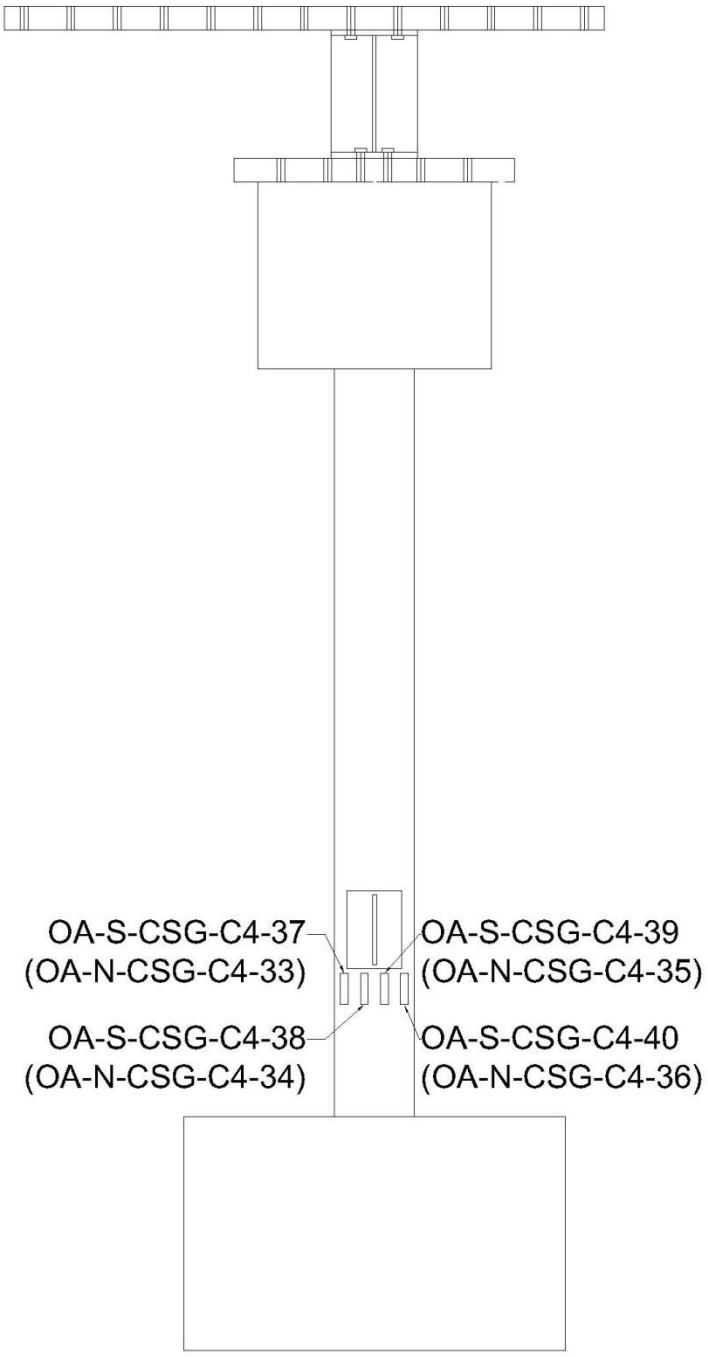

Figure D.5: Concrete strain gages for the wall in Phase IV tests (side view)

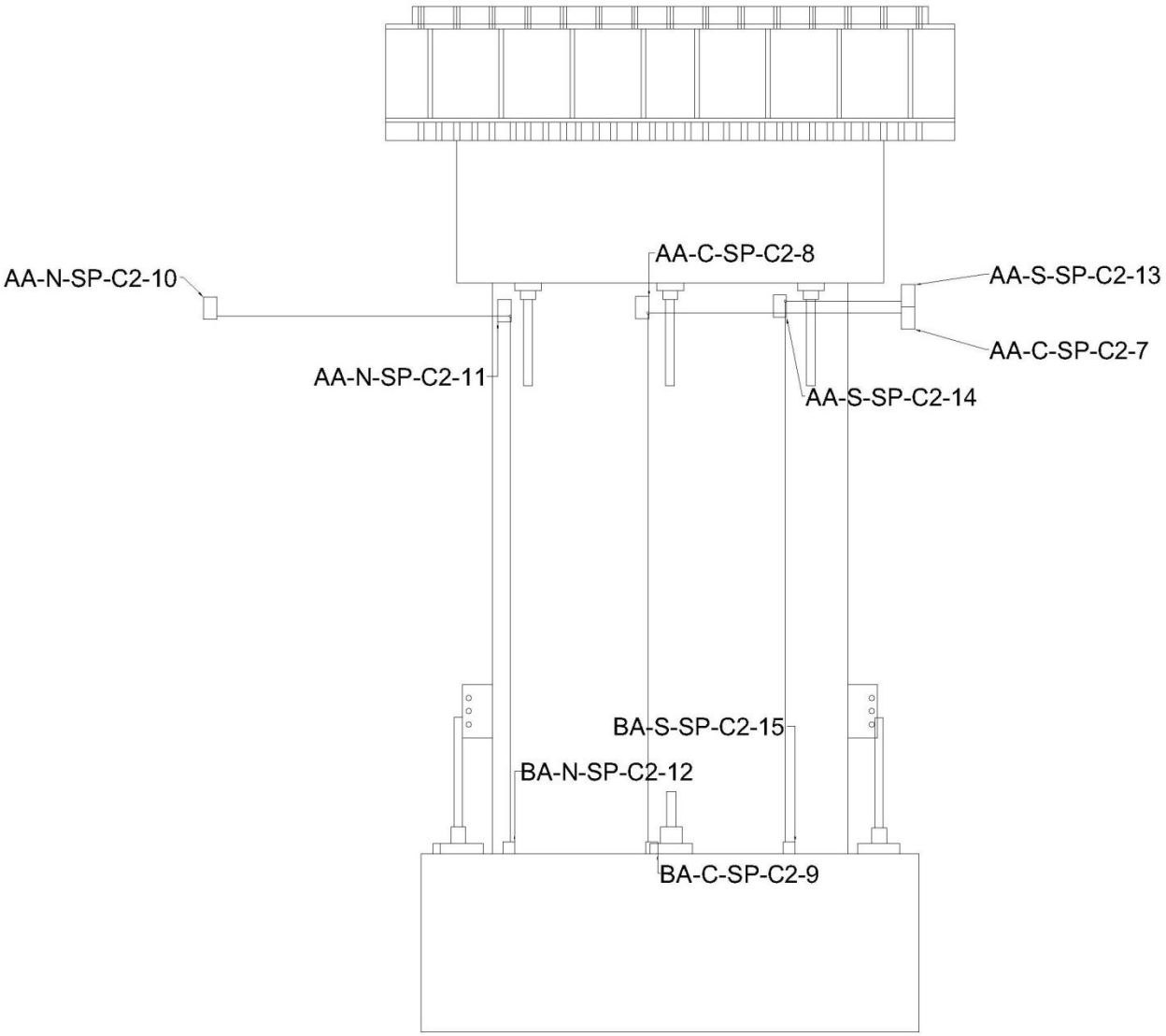

Figure D.6: String pots for the wall in Phase IV tests (front view)

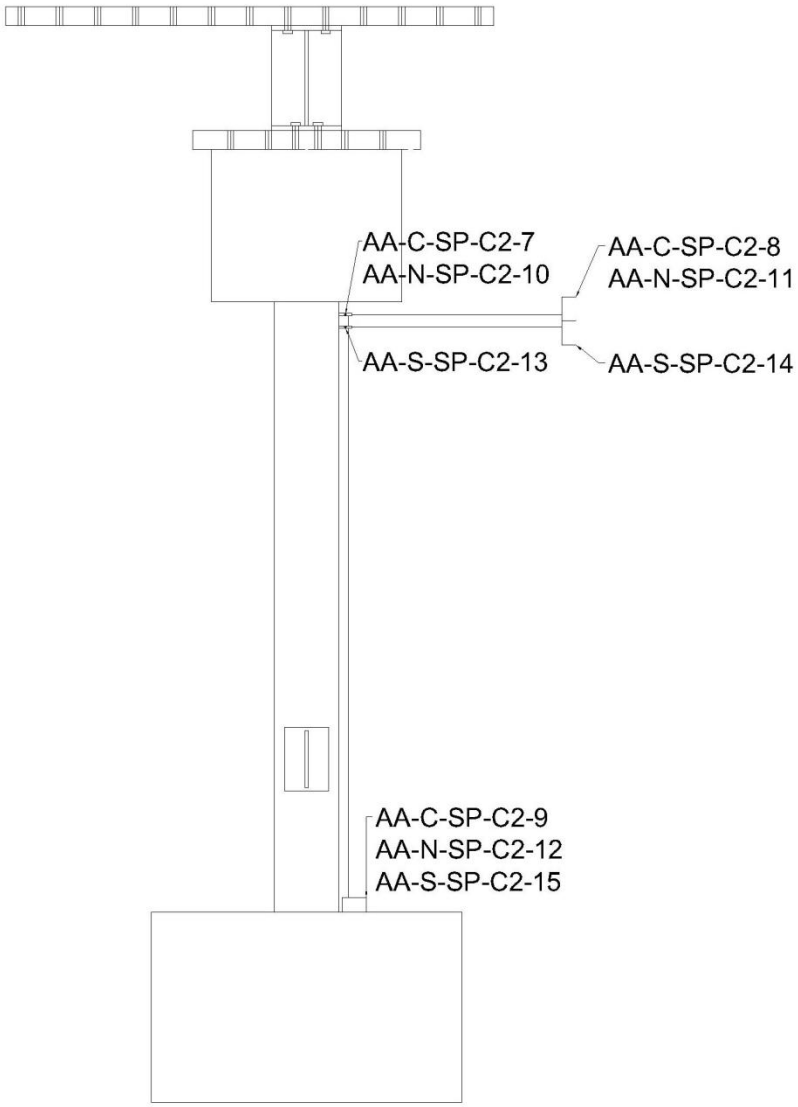

Figure D.7: String pots for the wall in Phase IV tests (side view)

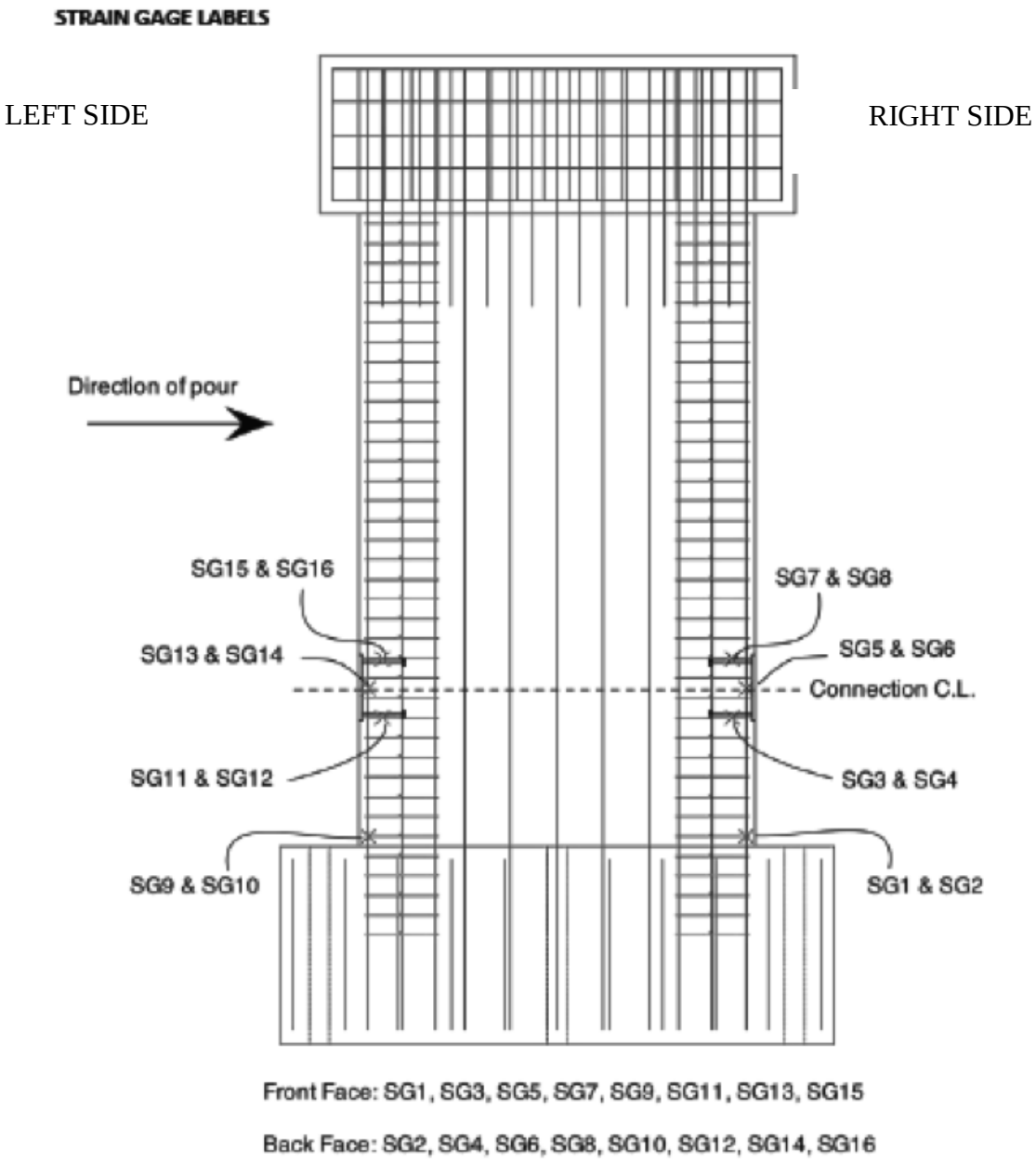

Figure D.8: Strain gage on bars for the wall in Phase IV tests (front view)